WARWICK
THE UNIVERSITY OF WARWICK

A Thesis Submitted for the Degree of PhD at the University of Warwick

Permanent WRAP URL:

http://wrap.warwick.ac.uk/163996

Copyright and reuse:
This thesis is made available online and is protected by original copyright.
Please scroll down to view the document itself.
Please refer to the repository record for this item for information to help you to cite it.
Our policy information is available from the repository home page.

For more information, please contact the WRAP Team at: wrap@warwick.ac.uk

warwick.ac.uk/lib-publications

Spectral and dynamical signatures of localization in many-body systems

by

Leonardo Benini

Thesis

Submitted to the University of Warwick

for the degree of

Doctor of Philosophy

Department of Physics

June 2021

A Norma.
1929 - 2021

Abstract

The interplay between strong interactions and disorder is at the core of one of the most exciting and active fields of modern quantum condensed matter physics. In the last two decades, attempts to characterize interacting disordered quantum systems in terms of both static and dynamic properties have been the focus of much attention, mainly due to experimental advancements in quantum simulation techniques. In this Thesis, we explore aspects of disorder-induced localization in different models and setups, ranging from strongly interacting spin chains to free models of spinful fermions. Firstly, we study the emergence of local conserved quantities (l-bits) in paradigmatic models of localization through the lens of the quench dynamics of the survival probability. We discuss the appearance of periodic cusp singularities in the unitary evolution of the survival probability as a new signature of localization, which can be exactly captured and predicted by an effective model of two-level systems undergoing collective Rabi oscillations. We then test the sensitivity of many-body localized (MBL) systems to global perturbations by studying the decay of the fidelity between quantum states in different disorder regimes. Our numerical results unveil a rich decay structure and a direct connection to spectral measures of localization, suggestive of promising directions for the experimental probing of eigenstate fractality. Lastly, we turn our attention towards localization effects in non-interacting models, investigating the stability of spin-polarized transport in a linear chain of atoms grafted onto a magnetic substrate. We demonstrate the robustness of spin-filtering effects against weak disorder, confirming the proposed system as a good candidate model for realizations of spin-selective transport devices.

Acknowledgments

Firstly, I would like to acknowledge the extreme pleasure that working under the supervision of Prof. Rudolf Römer has been during the last four years. He has been an invaluable source of guidance and advice, helping me to get through the hardest moments of this PhD with immense calm and patience. He gave me enormous freedom in pursuing my own ideas, always backing me up along unknown and difficult paths. His never-ending curiosity and perseverance have made me realize what it means to be a true scientist. Also, I feel extremely grateful to all past and present members of the DisQS group, who concurred to create a stimulating research environment that has been crucial for the pursue of my PhD. More broadly, I would like to acknowledge all the special moments I shared with my fellow colleagues at Warwick. Thanking them all would be impossible. A special mention goes to Benoit, Duncan, Samuele, Eva, Jamie, Matteo, Irene, and all the others who have enriched me with memories that I will carry for the rest of my life.

I have been lucky enough to work with some amazing collaborators throughout these years. On a chronological order, I express my gratitude to Prof. Arunava Chakrabarti and Amrita Mukherjee for their crucial help and contribution to the first project I embarked upon during my first year, and for their extraordinary hospitality during my visits to Kolkata. I am especially grateful to Prof. Tommaso Roscilde for the kindness and dedication he demonstrated towards our projects together in the last two years. He has been an incredible guide and inspiring mentor, and his physical intuition has been pivotal for the realization of part of this Thesis. A great thank you also to Fabio, Tommaso, and all other members

of the Theory of Quantum Matter group in Lyon, who warmly welcomed me twice during last year. Last but not least, a big thank you to Piero Naldesi, who has been guiding me since my MSc time in Bologna and who I consider a dear friend. His help and support have been invaluable in the last few years.

If I stand here, on the verge of the greatest accomplishment of my academic life, I owe it for the most part to my family. They never fail to remind me how proud they are of my achievements and of what I have become, but I know at the bottom of my heart that I will never be able to repay them in full. Nevertheless, I will keep trying. Thank you.

Lastly, a special thank you to Leti. I feel nothing but lucky for everyday we spend together, and words cannot express what our continuous and unconditional reciprocal support means to me. I look forward to the next chapters of our lives, and I cannot wait to share every moment of them with you.

Declarations

This thesis is submitted to the University of Warwick as part of my application for the degree of Doctor of Philosophy in Physics. It contains work composed by myself and my collaborators and has not been submitted in any previous application for any degree or other university. I declare that this thesis is my own work except where indicated.

Part of the work presented in this thesis is based on the following publications:

- Chapter 4 is based upon
  - (Benini et al. 2021a). "Loschmidt echo singularities as dynamical signatures of strongly localized phases", *New Journal of Physics*, 23 023030
  - (Benini et al. 2021b). "Quench dynamics of quasi-periodic systems exhibiting Rabi oscillations of two-level integrals of motion", *Annals of Physics*, 168545
- Chapter 6 is based upon
  - (Benini et al. 2019). "Spin-polarized localization in a magnetized chain.", *Scientific Reports* 9 5930

Contents

List of Abbreviations

2LS *2-level systems*. 57

3LS *3-level systems*. 57

AA *Aubry-André*. 33

AL *Anderson localization*. 27

BEC *Bose-Einstein condensate*. 35

CDW *charge density wave*. 57

ED *Exact Diagonalization*. 39

EE *Von Neumann entanglement entropy*. 8

ETH *Eigenstate Thermalization Hypothesis*. 11

FR *fully random*. 58

GOE *Gaussian Orthogonal Ensemble*. 40

IID *interaction-induced dephasing*. 72

IPR *inverse participation ratios*. 42

JW *Jordan-Wigner transformations*. 18

LDOS *local density of states*. 103

LIOMS *local integrals of motion*. 50

MBL *Many-body localization*. 11

MBME *many-body mobility edge*. 39

QP *quasi-periodic*. 58

RDM *reduced density matrix*. 7

RMT *Random Matrix Theory*. 40

TMM *Transfer Matrix Method*. 99

List of Figures

Part I

Background material

1

Introduction

Hard as it may be, we as human beings are accustomed to deal with the inherent imperfections of our lives on a daily basis. Such a trivial observation gains a further practical meaning for those who try to understand and model the weirdness of quantum reality. The scientific paradigm of reducing physical phenomena to the study of the behavior of individual constituents has led to tremendous progress in our description of the world, starting from Newton's classical mechanics to the birth and formulation of quantum theory and general relativity. In doing so, scientists needed to strip reality of its most inconvenient aspects to focus on the search for fundamental laws, often relying on neglecting a very plain fact: matter around us is not perfect. Disorder and randomness are ubiquitously present in every material we create or study, no matter how hard we try to smooth out the defects.

In (Anderson 1958), Phillip Warren Anderson provided a first attempt of incorporating the unavoidable existence of disorder in quantum materials, discussing a model of random lattices where the "hopping" of particles across the system was inhibited by destructive quantum interference with impurities. Anderson's argument followed by initializing a single electron at a specific position i of the lattice, and computing the probability amplitude of finding the particle anywhere else after a certain amount of time. Its main finding, i.e. the *exponential localization* of this probability around the initial position for a strong enough disorder, inspired a plethora of works in the following decades (Kramer et al. 1993; Brandes et al. 2003; Abrahams 2010), including the present thesis.

The scope of this Introduction is to lay the foundations for the following Chapters: we will briefly review a certain set of basic facts about quantum and statistical mechanics, and the description of out-of-equilibrium dynamics in

many-body systems, that represent the bulk of background knowledge underlying this work.

1.1 Quantum theory in a nutshell

1.1.1 Pure and mixed states

Quantum mechanics assigns a certain probability distribution for each possible outcome of a measurement, that depends on the state of the system under examination (Messiah 2014). Such a quantum state is described as a complex vector $|\psi\rangle$ in a Hilbert space $\mathbb{H}$ of dimension $\mathcal{D}$. Quantum states are normalized, ensuring that

$$\langle\psi|\psi\rangle = 1, \tag{1.1}$$

where we introduced $\langle\psi| = (|\psi\rangle)^\dagger$ as the state Hermitian conjugate. A *pure state* is a vector of unit norm that cannot be written as a mixture of other states, and it represents a ray in $\mathbb{H}$ over the complex numbers. The set of all pure states thus corresponds to the unit sphere in $\mathbb{H}$. If a basis $\{|\alpha_i\rangle\}$ is selected for $\mathbb{H}$, any state can be expanded as a *superposition* of basis states,

$$|\psi\rangle = \sum_i c_i \, |\alpha_i\rangle \, , \tag{1.2}$$

with the complex coefficients given by $c_i = \langle\alpha_i|\psi\rangle$ if we choose an orthonormal basis. Following from the normalization condition (1.1) we have that $\sum_i |c_i|^2 = 1$.

A state expressed as statistical mixture of pure states is called a *mixed* state. The description of a mixed state is usually attained by means of the associated *density matrix*, ρ[1] expressed in terms of an ensemble of pure states $\{|\psi\rangle_i\}$ and associated probabilities p_i as

$$\rho = \sum_i p_i \, |\psi_i\rangle \, \langle\psi_i| \, . \tag{1.3}$$

Formally, ρ is a linear, positive semi-definite Hermitian operator of trace one acting on $\mathbb{H}$, of dimension $\mathcal{D} \times \mathcal{D}$. One could recover the simple case of a pure state by maximizing a single $p_i = 1$, that leads to $\rho = |\psi\rangle \, \langle\psi|$, i.e. a rank one projector with $\rho^2 = \rho$.

[1]Throughout this thesis, we will refrain from using the usual "hat" notation for operators, unless specifically required for clarity.

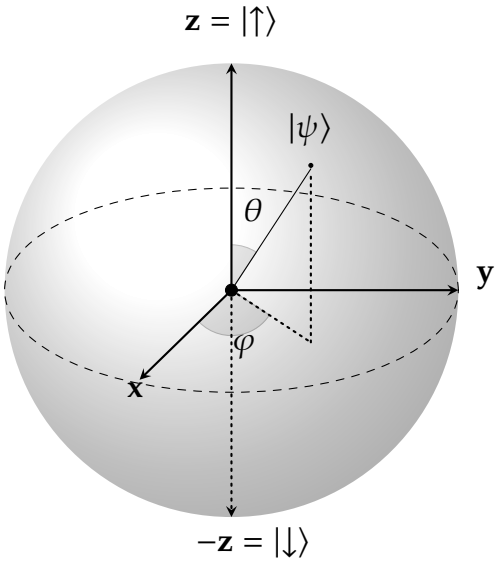

Figure 1.1. *Bloch sphere representation of a pure state of a* 2*-level system* (*qubit*).

Example: Spin-1/2 particle

For a system comprising of a single spin-1/2 particle, whose possible states are $\{|\uparrow\rangle, |\downarrow\rangle\}$, the density operator is a 2×2 matrix usually written as a linear combination of the identity $\mathbb{1}$ and the Pauli matrices

$$\sigma^x = \begin{pmatrix} 0 & 1 \\ 1 & 0 \end{pmatrix}, \quad \sigma^y = \begin{pmatrix} 0 & -i \\ i & 0 \end{pmatrix}, \quad \sigma^z = \begin{pmatrix} 1 & 0 \\ 0 & -1 \end{pmatrix}, \tag{1.4}$$

as

$$\rho = \frac{1}{2}(\mathbb{1} + \vec{\kappa}\boldsymbol{\sigma}), \qquad \boldsymbol{\sigma} = (\alpha\sigma^x, \beta\sigma^y, \gamma\sigma^z). \tag{1.5}$$

The vector $\vec{\kappa} \in \mathbb{R}^3$ is called *Bloch vector*, and it is particularly useful for a geometric representation of a generic spin-1/2 system. Indeed, all spin-1/2 states lie on or within the surface of a unit radius sphere called *Bloch sphere* (see Fig.1.1), and the length of $\vec{\kappa}$ helps to characterize the mixedness of the given state. Following from $\rho^2 = \rho$ for pure states, one obtains that $||\vec{\kappa}|| = 1$, i.e. pure states lie on the surface of the Bloch sphere; on the other hand, as $\rho^2 \neq \rho$ in the case of mixed states, such states lie in the bulk of the Bloch sphere, i.e. $||\vec{\kappa}|| < 1$.

1.1.2 Observables

Following the most common interpretation of quantum mechanics that goes under the name of Copenhagen interpretation (Heisenberg 1949), a quantum

state does not possess any definite properties prior to measurements. Quantum mechanics offers a way of computing the probability that a measurement will yield a certain outcome, and the measuring act itself will make the system "collapse" towards one of the eigenstates of the operator representing the physical observable. Indeed, physical quantities that can be measured appear in a quantum theory formalism as linear self-adjoint operators, $A = A^\dagger$ on $\mathbb{H}$, whose eigenvectors form an orthonormal basis for $\mathbb{H}$. The expectation value of an operator A on a state $|\psi\rangle$ is given by

$$\langle A \rangle = \langle \psi | A | \psi \rangle . \tag{1.6}$$

If A has a discrete spectrum, the possible outcomes of measurements correspond to eigenvalues of A, i.e. the probability $p(a_n)$ of obtaining a certain outcome a_n from the measurement of A is given by the square modulus of the projection of $|\psi\rangle$ on the relative eigenvector $|\phi_n\rangle$,

$$p(a_n) = |\langle \phi_n | \psi \rangle|^2, \tag{1.7}$$

given that $A|\phi_n\rangle = a_n |\phi_n\rangle$. In the density matrix picture, an operator expectation value is obtained with $\langle O \rangle = \mathrm{Tr}[\rho O]$.

1.1.3 Time evolution

The mathematical formulation of quantum mechanics offers different ways of conceiving the evolution of a system, mainly dependent on a basis change in relation to time-dependency. In the work presented in this thesis, we will employ the so-called Schrödinger picture, where the time-dependency is attached to states rather than to operators. An evolving quantum state is obtained in this framework by integrating the Schrödinger equation

$$\mathrm{i}\hbar \frac{\partial}{\partial t} |\psi(t)\rangle = \mathcal{H} |\psi(t)\rangle , \tag{1.8}$$

where i is the imaginary unit, $\hbar$ is the reduced Planck constant and $\mathcal{H}$ is a time-independent Hamiltonian operator corresponding to the total energy of the system. A general form for the solution of (1.8) is

$$|\psi(t)\rangle = U(t, t_0) |\psi(t_0)\rangle , \tag{1.9}$$

expressed in terms of the time-evolution operator $U(t, t_0)$ acting on the state at time t_0 to yield the state at time t, given by

$$U(t, t_0) = \mathrm{e}^{-\frac{\mathrm{i}}{\hbar}\mathcal{H}(t-t_0)}\,. \tag{1.10}$$

As we demand the norm of a quantum state to be constant, U must be a unitary operator, i.e. $U^\dagger U = \mathbb{1}$, yielding

$$\langle\psi(t)|\psi(t)\rangle = \langle\psi(t_0)|U^\dagger(t, t_0)U(t, t_0)|\psi(t_0)\rangle = \langle\psi(t_0)|\psi(t_0)\rangle\,. \tag{1.11}$$

Suppose that at time $t_0 = 0$ the system is in an eigenstate of $\mathcal{H}$, we can see that the state simply acquires a phase during time evolution,

$$|\psi(t)\rangle = \mathrm{e}^{-\frac{\mathrm{i}}{\hbar}\mathcal{H}t}\,|\psi(0)\rangle = \mathrm{e}^{-\frac{\mathrm{i}}{\hbar}Et}\,|\psi(0)\rangle\,, \tag{1.12}$$

with $\mathcal{H}\,|\psi(0)\rangle = E\,|\psi(0)\rangle$. Hence, eigenstates are *stationary states*, as physical measurements will not be able to distinguish between the state of the system at any point in time, as

$$\langle A(t)\rangle = \langle\psi(0)|\,\mathrm{e}^{\frac{\mathrm{i}}{\hbar}Et}\,A\,\mathrm{e}^{-\frac{\mathrm{i}}{\hbar}Et}\,|\psi(0)\rangle = \langle A(0)\rangle\,. \tag{1.13}$$

To describe how a density operator evolves in time, the Schrödinger equation can be recast into the Von Neumann equation,

$$\mathrm{i}\,\hbar\frac{\partial}{\partial t}\rho = [\mathcal{H}, \rho], \tag{1.14}$$

where the square brackets denote the commutator $[\mathcal{H}, \rho] = \mathcal{H}\,\rho - \rho\,\mathcal{H}$. If the Hamiltonian is time-independent, (1.14) yields the solution

$$\rho(t) = \mathrm{e}^{-\mathrm{i}\,\mathcal{H}\,t/\hbar}\,\rho\,\mathrm{e}^{\mathrm{i}\,\mathcal{H}\,t/\hbar}\,. \tag{1.15}$$

1.1.4 Composite systems and entanglement

Entanglement is one of the most defining features of quantum mechanics. It quantifies the "lack of independence" between the degrees of freedom composing a system, i.e. the impossibility of describing their individual behavior separately. In order to properly introduce the concept of quantum entanglement, let us consider a system $\mathcal{S}$ initialized in a pure state $|\psi\rangle$ in a finite size Hilbert space $\mathbb{H}_\mathcal{S}$. If we choose to partition $\mathcal{S}$ into two spatial sub-regions A and B, a postulate of quantum mechanics (Nielsen et al. 2010) states that $\mathbb{H}_\mathcal{S}$ is given by the tensor

product of the local Hilbert spaces of A and B, $\mathbb{H}_{\mathcal{S}} = \mathbb{H}_A \otimes \mathbb{H}_B$. Selecting $|i\rangle_A$ and $|j\rangle_B$ as basis for A and B respectively, every state of $\mathcal{S}$ can be represented as

$$|\psi\rangle_{\mathcal{S}} = \sum_{i}^{N_A} \sum_{j}^{N_B} a_{ij} |i\rangle_A \otimes |j\rangle_B , \tag{1.16}$$

where N_A, N_B are the number of sites in A and B respectively. We can perform a singular value decomposition (SVD) on the $N_A \times N_B$ matrix of coefficients a_{ij} in order to bring it in a diagonal form,

$$a_{ij} = \sum_{\alpha} U_{i\alpha} S_{\alpha\alpha} V^{\dagger}_{\alpha j} \tag{1.17}$$

with S a diagonal matrix with non-negative entries Λ_α and U and V are complex unitary matrices. This leads to the *Schmidt decomposition* of the state (Nielsen et al. 2010),

$$|\psi\rangle_{\mathcal{S}} = \sum_{\alpha=1}^{N_{min}} \Lambda_\alpha |\alpha\rangle_A \otimes |\alpha\rangle_B , \tag{1.18}$$

where the state $|\alpha\rangle_{A,B}$ form an orthonormal set for $\mathrm{H}_{A,B}$ and $N_{min} = \min(N_A, N_B)$. The Schmidt values $\Lambda_\alpha \geq 0$ for a normalized state satisfy $\sum_\alpha \Lambda_\alpha = 1$, and the number of non-zero Λ_α, called *Schmidt number*, serves as an indicator of the level of entanglement between A and B. A state with no entanglement, called a *separable state*, can be written as a simple product state in the Schmidt basis and thus has a Schmidt number of one, i.e. only a single Schmidt value is different from zero. On the contrary, for an entangled state we have a set of Schmidt values $\{\alpha^* | \Lambda_\alpha \neq 0 \text{ for } \alpha = \alpha^*\}$.

The framework of density operators is particularly suited to the description of subsystem properties. Let consider again the system $\mathcal{S}$ cut in the same bipartition $A|B$. Given $\rho^{\mathcal{S}}$ as the state of $\mathcal{S}$, we can describe the state of A as the *reduced density matrix* (RDM) of A, given by

$$\rho^A = \mathrm{Tr}_B \left[\rho^{\mathcal{S}}\right] = \mathrm{Tr}_B \left[|\psi\rangle_{\mathcal{S}} \langle\psi|_{\mathcal{S}}\right] = \sum_{\alpha} \Lambda_\alpha^2 |\alpha\rangle_A \langle\alpha|_A , \tag{1.19}$$

where Tr_B is a generalization of the trace operator called *partial trace*, defined as

$$\mathrm{Tr}_B \left[\rho^{\mathcal{S}}\right] = \rho^A \mathrm{Tr} \left[\rho^B\right] . \tag{1.20}$$

We are now equipped with all the information needed for the definition of the

Von Neumann entanglement entropy (EE) of subsystem A,

$$S(\rho^A) = -\operatorname{Tr}\left[\rho^A \log\left(\rho^A\right)\right] = -\sum_{\alpha}^{N_{min}} \Lambda_\alpha^2 \log \Lambda_\alpha^2 = S\left(\rho^B\right), \tag{1.21}$$

which is one most widely employed entanglement quantifiers. From the above expression we note that the entropy varies from 0 for a separable state to $\log N_{min}$ for a maximally entangled state in which all Schmidt values are equal. As an example, if we are dealing with a chain of spin-1/2 particles of length L, the maximal EE for a bipartition of size $L/2$ is

$$S \propto L \log 2, \tag{1.22}$$

since $N_{min} = 2^{L/2}$. The result is that the maximal entropy of entanglement scales extensively with the volume of the sub-region, similarly to the macroscopic thermodynamic entropy. In one-dimensional systems, this essentially means that entanglement scales linearly with the size of the partition. Such scaling behavior, described by the general form

$$S(\rho^A) = O(|L|), \tag{1.23}$$

has been dubbed *volume law*, and it characterizes "typical"[2] thermal states (Eisert et al. 2010). Interestingly, specific classes of quantum states display a different scaling law for the EE, which scales with the area of the boundary between the partition, i.e.

$$S(\rho^A) = O(\partial|L|). \tag{1.24}$$

The *area law* for the EE scaling appears, for instance, in a small low-energy subset and particularly in typical ground-states of local gapped Hamiltonians (Hastings 2007), as well as for the entire eigenspectrum of many-body systems in the presence of strong disorder (A. Pal et al. 2010), a case of interest for the present work. Indeed, as we will discuss later, the crossover between the area-law and the volume-law for the EE of Hamiltonian eigenstates is a well-known signature of the localization effects induced by disorder in quantum systems.

[2] By "typical" we refer here to a quantum state randomly picked from the spectrum of a generic local Hamiltonian on a lattice.

1.2 Non-equilibrium dynamics in many-body systems

Non-equilibrium processes in quantum systems may assume various forms: one could imagine to slowly drive a system with an external force in such a way that at every instant in time an equilibrium description is still possible, or tend towards the extreme limit where a massive perturbation induces a dynamical behavior that defies such possibility. The main question that non-equilibrium scenarios lead to can be formulated in terms of what steady state, if any, will be reached by the system at very long times, and how to characterize it. Thus, it may not come as a surprise that exploring steady state properties of quantum systems requires the ability of maintaining for very long a high degree of control on the system under study, in order to delay dissipating processes induced by the coupling with the external environment. New promising candidates for the solution of such an experimental challenge came in the form of what have now been labelled *quantum simulation platforms*, quantum technology platforms allowing to realize interacting quantum many-body systems isolated from external baths with a high degree of tunability on the system parameters. Ultra-cold atoms loaded in optical lattices (Bloch et al. 2008), for instance, have become an extremely powerful tool to study exotic phenomena in minimal prototypical models of strongly correlated physics. Textbook Hamiltonians like the Fermi-Hubbard and the Bose-Hubbard models, the Ising and Heisenberg spin models, and many more, are nowadays an exciting experimental playground rather than only theoretical abstractions. As a result, the capability of simulating the dynamics of closed interacting systems has propelled a massive surge of theoretical effort in exploring a plethora of non-equilibrium phenomena related to long-standing fundamental issues such as quantum ergodicity and chaos, equilibration and thermalization mechanisms and their failures, driven only by pure quantum unitary dynamics.

1.2.1 Ergodicity and thermalization

Although the problem of *quantum thermalization* and its violations will be the main focus of the next Chapter, it is useful to briefly introduce the basic concepts here. The term "thermalization" usually refers to the dynamical process by which a generic many-body system approaches thermal equilibrium at long times. It is a fairly accepted notion in statistical mechanics that it is a typical be-

havior of generic[3] macroscopic systems to evolve into a thermal state after being brought out-of-equilibrium and let free to evolve. What we mean by thermal equilibrium is not a trivial issue, but let us start from the probabilistic interpretation put forward by Ludwig Boltzmann (Sharp et al. 2015): given a *a priori equal probability* to all possible microscopic configurations under eventual constraints (e.g. fixed energy and particle number), the equilibrium state for a generic macroscopic system corresponds to the macrostate with maximum probability. Such probabilistic arguments built the foundation of statistical mechanics as developed by (Gibbs 1902), which represents one of the pillars of modern physics. From a classical point of view, the probability of each possible macrostate is derived by the equal probability principle, as proportional to the phase-space volume occupied by a set of microstates compatible with the given macroscopic configuration. Alternatively, one could imagine a different way of defining such probabilities: observing a system evolving for a certain time period T, with τ being the fraction of time the system spend in a specific macrostate, the fraction τ/T gives the probability assigned to that macrostate. The attempt of proving the equality of the above definitions originated the so-called *ergodic hypothesis*, that ensures the equivalence between the long-time average of a generic observable

$$\overline{O}(t) = \frac{1}{T}\int_0^T d\tau O(\tau), \tag{1.25}$$

and the statistical ensemble average $\langle O \rangle$, i.e.

$$\overline{O} = \langle O \rangle\,, \tag{1.26}$$

for $T \to \infty$. Here, $\langle \cdots \rangle$ denotes an average over microcanonical, canonical or grandcanonical ensembles. Ergodicity has straightforward implications from a dynamical perspective: Eq. (1.26) means that a generic system evolves over time exploring all accessible microstates.

A first notable exception to the ergodic hypothesis came in the form of numerical simulations of anharmonic perturbations on a simple system of masses connected by springs (Fermi et al. 1955), that showed an unexpected recurrence in the energy distribution of harmonic modes, incompatible with the assumption of ergodicity. This result, known as the Fermi-Pasta-Ulam problem, proved crucial for the development of chaos theory and its relation to thermalization,

[3] By "generic" we mean here the absence of fine-tuning and thus of integrability. The case of integrable systems, that defy the thermalization paradigm discussed here, will be briefly covered in Chapter 2.

leading to important discovery such as the KAM theorem (Kolmogorov 1954; Moser 1962; Arnol'd 1963) and solitons (Zabusky et al. 1965). [4]

A quantum version of the ergodic hypothesis first appeared in (Neumann 1929), in which Von Neumann provided an argument for the thermalization of quantum system as a typical phenomenon. His quantum ergodic theorem states that for a finite family of commuting macroscopic observables, every wave function, starting from an initial microcanonical energy shell, evolves so that for most times in the long run, the probability distribution of these observables obtained from the unitarily time-evolved wave function is close to their microcanonical distribution (Goldstein et al. 2010). The extension of this seminal result led decades later to the current understanding of quantum thermalization in isolated many-body systems in terms of individual energy eigenstates encoding thermal expectation values of local observables, a framework that goes under the name of *Eigenstate Thermalization Hypothesis* (ETH) (Deutsch 1991; Srednicki 1994). In systems fulfilling the ETH, the local correlations encoded in specific initial states get "washed out", or *scrambled* between all degrees of freedom due to the growth of entanglement between separate regions of the system. The last few years have been characterized by a large research effort in describing systems that defy the ETH and fail to thermalize even at long times, maintaining "memory" of the initial conditions. Amongst all exotic phenomena identified, what is now considered to be the most general mechanism to avoid quantum thermalization has been dubbed *Many-body localization* (MBL) (R. Nandkishore et al. 2015), which is the extension of Anderson localization to interacting systems. On a historical note, it is worth remembering that already in (Anderson 1958), Anderson mentioned that part of the motivation for studying the problem of disorder in quantum systems was to study its implications for dynamical behavior. Indeed, a non-interacting system with localized single-particle eigenstates represents a minimal example of a non-thermalizing quantum system.

1.2.2 Quantum quenches

The simplest non-equilibrium protocol consists in preparing a many-body system in a specific non-equilibrium state and monitoring its evolution under the action of the system Hamiltonian. A general protocol of this kind is called

[4] The difference between the concepts of ergodicity and thermalization is a subtle issue, and the two terms are often used interchangeably, see e.g. (A. Pal et al. 2010). This follows from the still unsettled debate around the definition of ergodicity in the context of quantum many-body dynamics. Classically, one considers thermalization, and thus the validity of the predictions of statistical mechanics, as arising from the ergodicity of a given dynamical system.

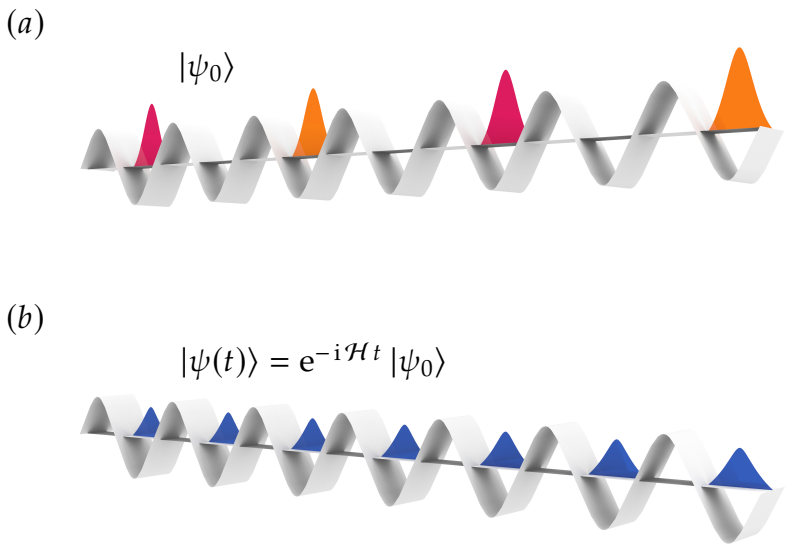

Figure 1.2. *Scheme of a typical quench experiment.* (*a*) *The system is initially prepared in an experimentally relevant state such as* $|\psi_0\rangle$*, with particle density distributed only on odd sites* (*red and orange bell-shaped distributions*). (*b*) *After letting the system free to evolve under the action of* $\mathcal{H}$*, we reach a thermal state in which the particle density is spatially homogeneous and equally distributes among all lattice sites* (*blue bell-shaped distributions*).

a *quantum quench* (Calabrese et al. 2004), pictorially represented in Fig. 1.2. In a slightly more formal way, let us consider a generic local Hamiltonian $\mathcal{H}(\lambda)$ depending on some tunable parameter λ and let the system be initialized in the ground-state $|\psi_0\rangle$ of $\mathcal{H}(\lambda_i)$. A quench is realized at a time $t \geq 0$ by an abrupt change $\lambda_i \to \lambda_f$, leading to non-trivial dynamics guided by $\mathcal{H}(\lambda_f)$, [5]

$$|\psi(t)\rangle = e^{-i\mathcal{H}(\lambda_f)t}|\psi_0\rangle\,, \tag{1.27}$$

provided that the evolved state is not an eigenstate of $\mathcal{H}(\lambda_f)$ and thus a stationary state (see (1.13). Depending on the fraction of degrees of freedom involved during the process, quantum quenches can be classified as *global*, when an extensive amount of work is peformed on the system, or *local*, affecting only small sub-regions and yielding non-extensive average work. Quench protocols are

[5] From now on, we will employ natural units setting, e.g., $\hbar = 1$.

nowadays a central tool in quantum simulators: in ultra-cold gases experiments, for instance, one can suddenly change the depth of the optical lattice (Greiner et al. 2002; Will et al. 2010; Trotzky et al. 2012; Will et al. 2015) to enhance or suppress hopping, displace the center of the trapping potential (Ott et al. 2004; Fertig et al. 2005; Strohmaier et al. 2007), or turn off a trapping potential while keeping the optical lattice on (Schneider et al. 2012; Ronzheimer et al. 2013; Xia et al. 2015). Quantum quenches allow the exploration of a wide range of basic phenomena, especially related to relaxation and equilibration mechanisms in many-body systems. The final asymptotic state induced by a quench experiment can be characterized through appropriate observables to experimentally probe fundamental assumptions of statistical mechanics.

1.3 Irreversibility

We conclude this Chapter with a review of a few concepts related to irreversibility and time reversal procedures that are necessary to introduce some of the main quantities involved in the results presented in this Thesis. Time reversal symmetry is a basic feature of most microscopic theories in physics. There is no apparent reason in the way classical laws of motion were formulated that prohibits an object to follow the same trajectory in one direction of time or the other. Gravity provides an intuitive and visual example: looking at a ball thrown up in the air, reaching a certain height and then falling back, we have no difficulty in imagining the same object following the trajectory backward. On the other hand, thermodynamics establishes a clear asymmetry on the arrow of time through its Second Law, stating that spontaneous evolution of an isolated system always tends towards a state with higher entropy. The implications of the Second Law translate quite easily to our perception of the flow of time. Imagine adding a milk foam layer to a cup of coffee to prepare a delicious cappuccino: inevitably, the two layers will start to mix after some time, leaving an indistinguishable mixture of coffee and milk at the end. Contrary to the simple motion of classical objects, the inverse process, i.e. cappuccino spontaneously separating back into layers of milk and coffee, seems utterly unrealistic. Indeed, the cappuccino state has a higher entropy than the perfectly ordered layers of milk and coffee. Furthermore, it is immediately noticeable that it is impossible to retrieve the information encoded in the initial conditions just by looking at the final mixture. Someone not knowing how a cappuccino is prepared would not be able to point out that some moments before, the initial state comprised two

separate layers of two different substances. In the language introduced in 1.2.1, the system evolution has scrambled such information, making it inaccessible after the thermalization process.

In 1872, while trying to develop its microscopic theory of thermodynamics, Boltzmann provided the proof that in a nearly-ideal gas of colliding molecules the entropy always increases in time (Boltzmann 1872),

$$\frac{dS}{dt} > 0. \tag{1.28}$$

This seminal result, known as *H-theorem*, was one of the first demonstrations of how statistical mechanics could justify the existence of irreversible processes and the emergence of the Second Law starting from the reversible mechanics of elementary particles. Nonetheless, a few years later, Johann Josef Loschmidt proposed a paradox that challenged Boltzmann derivation (Loschmidt 1876), based on the time reversal symmetry of classical mechanics. Loschmidt suggested that inverting all the momenta of the particles constituting the gas would in fact invert the dynamics, bringing the system back to its initial configuration and thus decreasing the total entropy in evident violation of the Second Law. In response, Boltzmann argued that such a *gedankenexperiment* would be effectively impossible to reproduce in practice, laying the grounds of the statistical interpretation of thermodynamics that characterized his following research efforts. The impossibility of the time-reversal process put forward by Loschmidt is today understood as a consequence of deterministic chaos (Lorenz 1963). Since typical many-body systems are chaotic, their dynamics is exponentially sensitive to small variations of the initial conditions or of the equations of motion, with a set of *Lyapunov exponents* governing the divergence of nearby trajectories. Hence, trying to manipulate a chaotic system in order to reverse the particle velocities would bring the system toward a state which is exponentially far from the desired initial state, given any arbitrarily small imperfections in the experimental procedure.

1.3.1 Fidelity decay in chaotic and regular dynamics

Moving away from the classical world, quantum mechanics offers a radically different picture. Classical chaos emerges from the non-linearity of the equations of motion, while Eq. (1.8), describing quantum evolution, is inherently linear. Moreover, as shown in (1.11), the unitarity of the time evolution operator preserves the overlap between two states during the dynamics. This

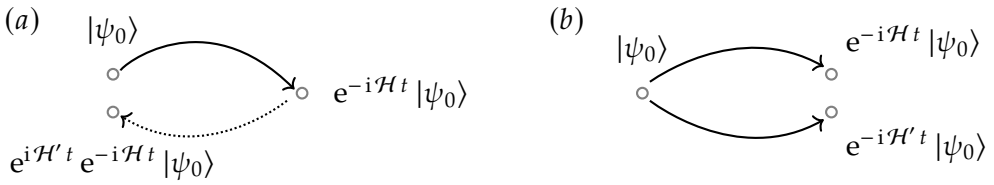

Figure 1.3. *Depiction of the dual view of a Loschmidt echo protocol. (a) The initial state is first evolved forward (thick line) under $\mathcal{H}$ and then evolved backward under perturbed Hamiltonian $\mathcal{H}$ (dotted line). (b) The initial state is evolved forward with both $\mathcal{H}$ and $\mathcal{H}'$ and the two final states are compared.*

seems a rather solid obstacle to the translation of chaos concepts in quantum terms: not only quantum overlaps, i.e. the similarity between quantum states, do not diverge exponentially, but they do not diverge at all. Indeed, numerical tests implemented to probe the reversibility and to expose the chaotic behavior of classical dynamics, show instead the perfect stability of quantum motion when applied to the hydrogen atom (Casati et al. 1986). It is thus unclear what "irreversibility" even means in quantum terms.

Nonetheless, (Peres 1984) proposed an insightful signature able to mark the manifestation of classical chaos in quantum dynamics. Following the historical suggestion of Loschmidt, Peres presented a quantum time-reversal procedure, obtained in the quantum formalism through a sign change of the Hamiltonian describing some generic quantum system, $\mathcal{H} \rightarrow -\mathcal{H}$. As we stressed above, inevitable imperfections in the preparation of the time-reversal protocol appear as arbitrary perturbations in the evolution. Such perturbative terms can be integrated in a quantum time-reversal protocol by imagining the following scenario: a first forward evolution of an initial state $|\psi_0\rangle$ governed by $\mathcal{H}$, followed by a backward evolution driven by a perturbed Hamiltonian $\mathcal{H}' = \mathcal{H} - \epsilon V$, where ϵ is the strength of the perturbation and V is some bounded hermitian operator. The central object of Peres proposal was the *fidelity* between the initial state and the time-evolved state,

$$\mathcal{L}(t) = |\langle\psi_0|\psi(t)\rangle|^2 = |\langle\psi_0| e^{i(\mathcal{H}-\epsilon V)t} e^{-i\mathcal{H}t} |\psi_0\rangle|^2, \tag{1.29}$$

later termed *Loschmidt echo*. Alternatively, one could simply imagine evolving the same initial state with both $\mathcal{H}$ and $\mathcal{H}'$ and computing the overlap between the two obtained states, as sketched in Fig.1.3. Peres original intuition was that in quantum systems possessing a classical chaotic counterpart, the fidelity $\mathcal{L}(t)$ should decay exponentially, reminiscent of the exponential divergence of

classical trajectories. Since Peres early works, several works have refined the study of the fidelity decay in quantum systems, highlighting a rich behavior and different decay regimes, depending on the underlying classical dynamics and on the perturbation strength. The current understanding is that the typical decay of the Loschmidt echo in chaotic systems is mainly composed of three time regimes (Goussev et al. 2012):

A. An initial parabolic decay, $\mathcal{L}(t) \sim 1 - \eta^2 t^2$, where η is the dispersion of the perturbation operator V on the initial state, i.e.

$$\eta = \epsilon \sqrt{\overline{\langle \psi_0 | V^2 | \psi_0 \rangle} - \overline{\langle \psi_0 | V | \psi_0 \rangle}^2}. \tag{1.30}$$

B. An asymptotic regime dependent on the perturbation strength ϵ. For weak perturbations $\epsilon \to 0$, the decay is Gaussian, $\mathcal{L}(t) \sim \exp(-\eta t)^2$. For stronger perturbations the fidelity decays exponentially as $\mathcal{L}(t) \sim \exp(-\Gamma(\epsilon)t)$. For *global* perturbations affectting all the degrees of freedom of the system, the parameter Γ is independent of ϵ above a critical strength ϵ_c (*Lyapunov regime*), while it shows a Gaussian dependence $\Gamma \sim \epsilon^2$ for $\epsilon < \epsilon_c$ (*Fermi-golden-rule regime*).

C. The fidelity eventually saturates as $\mathcal{L}(t) \sim 1/\mathcal{N}$, with $\mathcal{N} = \dim(\mathbb{H})$ being the dimension of the effective Hilbert space.

A schematic diagram of the typical stages of the fidelity decay in chaotic systems is shown in Fig. 1.4.

On the other hand, a full classification of the fidelity decay regimes in non-chaotic systems, such as system with an integrable classical limit and regular dynamics in phase-space, is still a challenge in the field. Interestingly, a series of works (Prosen 2002; Prosen et al. 2002; Prosen et al. 2003; Znidaric et al. 2003) developed a linear response theory approach to extract the Loschmidt echo behavior in the limit of weak enough perturbations. The main finding that we would like to stress here is that this approach suggests that increasing the chaoticity of the underlying classical dynamics actually *stabilizes* the quantum dynamics. In other words, contrary to what one could expect, quantum fidelity can decay faster in non-ergodic systems than in chaotic ones. Indeed, the *average* fidelity $\overline{\mathcal{L}(t)}$, where the average is performed over a fixed pure state or over the ensemble of all possible states, was found to exhibit a Gaussian decay in the asymptotic regime on a time scale $t_I \sim \epsilon^{-1}$ for integrable systems, as opposed to an exponential decay on a time scale $t_E \sim \epsilon^{-2}$ for ergodic systems (Prosen

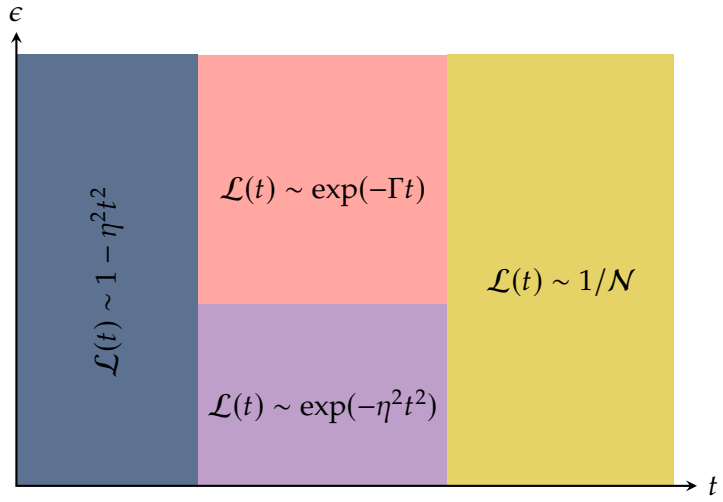

Figure 1.4. *Decay regimes of the Loschmidt echo in quantum systems with a classical chaotic limit.*

2002). In particular, such behavior is expected when the perturbation is small enough that the fidelity decay time is longer than other typical relaxation time scales such as the Ehrenfest time t_E for wave packets in systems with a chaotic classical limit. In the case of stronger perturbations, $\overline{\mathcal{L}}(t)$ displays a crossover into a slower algebraic decay $\overline{\mathcal{L}(t)} \sim t^{-\alpha}$, with $\alpha = 3d/2$ depending only on the dimension of the system (Jacquod et al. 2003).

1.4 Organization of this work

This Thesis is organized in three parts. The rest of the background material includes Ch. 2, which contains a basic introduction to the concept of thermalization in quantum systems with particular focus on the ETH and its violations, and Ch. 3, which presents a (non-exhaustive) review of the many features of Many-Body Localization (MBL), the main phenomenon explored in this work. The second and third parts of the Thesis contain original results on different aspects of disorder-induced localization: Chap. 4 presents a novel signature of localization in the short-time dynamics of one-dimensional systems in the presence of both disorder and interactions, while Chap. 5 explores the sensitivity of MBL systems to global perturbations via the study of the Loschmidt echo (1.29). Lastly, Ch. 6 focus is on the effects of disorder on spin-polarized transport, in the form of the interplay between Anderson localization and spin-filtering effects in simple tight-binding models of magnetic atoms.

2

Quantum thermalization

This chapter contains an expanded description of the thermalization phenomenon in closed quantum many-body systems, briefly introduced in 1.2.1. We will first review the paradigm that is today accepted as an explanation of thermalizing behavior in a large number of generic many-body systems, the ETH, and we will then describe some of the recent developments regarding its failures. Particularly, we will focus on localized systems, both in single-particle and interacting scenarios, reviewing notable models in which a certain number of localization hallmarks have been discussed.

2.1 Quantum chaos and thermalization

Let consider a many-body system $\mathcal{S}$ containing N two-state systems decoupled from any external reservoir or any measurement apparatus. We well refer to the individual constituents as either 1/2-spins or particles (fermions) interchangeably throughout this discussion, unless specified.[1] The spins are arranged over a regular lattice $\mathcal{L}$ and have a local state space $\mathbb{H}_i = \mathbb{C}^2$ of dimension $\dim \mathbb{H}_i = 2$ comprising two pure states and their linear combinations. As introduced in 1.1.2 when discussing the example of a single spin-1/2 particle, there are four linear operators that can act on each spin, i.e.
the Pauli matrices $\sigma_i^x, \sigma_i^y, \sigma_i^z$ in eq. (1.4) acting on site i and the identity operator $\mathbb{1}$. A generic state of a spin is represented by a linear combination of these 2×2 matrices, as in eq. (1.5). To represent the many-body state of the full system it

[1] The equivalence between spin and fermion language can be made formally precise through the use of *Jordan-Wigner transformations* (JW) (Jordan et al. 1928), see Appendix A. Please note that the JW mapping is not complete as fermionic anticommuting properties leads to non-local strings at the end of the transformation.

is convenient to choose as a basis the set formed by the 2^N eigenstates of all the $\{\sigma_i^z\}$. The Hilbert space of the total system is thus given by the tensor product of N local Hilbert spaces

$$\mathbb{H} \equiv \bigotimes_{i=1}^{N} \mathbb{H}_i, \tag{2.1}$$

with a total dimension $\dim \mathbb{H} = 2^N$. A complete basis for the whole system can be given as a sequence of outer-products between local spin operators and identities, e.g.

$$\sigma_1^z \otimes \sigma_2^y \otimes \cdots \otimes \mathbb{1}_{N-1} \otimes \sigma_N^x. \tag{2.2}$$

In this thesis, we will assume to work with *local* Hamiltonians, defined as sums of local operators of the form

$$\mathcal{H} = \sum_i h_i, \tag{2.3}$$

where the locality refers to the fact that all h_i are few-body operators that act on a bounded subset of sites around site i.[2] In practice, we will always consider operators located on the sites of $\mathcal{L}$ and on their nearest-neighbors.

Working in the Schrödinger representation, we consider the system to be in some initial pure state $\rho_0 = |\psi_0\rangle\langle\psi_0|$ and evolving in time according to (1.14). As mentioned in 1.2.1, the concept of thermalization in closed systems, i.e. the process of relaxation towards a thermal equilibrium state, is closely related to the ergodic hypothesis: if a system is ergodic, we can equate the long-time behavior of a system with a thermal density operator $\langle\rho\rangle$ which depends only on a few macroscopic thermodynamic parameters, one for each extensive conserved quantity. For simplicity, let us choose a closed system with only energy as a conserved quantity. In this example, if the system thermalizes we can write

$$\overline{\rho} \equiv \lim_{T\to\infty} \lim_{N\to\infty} \int_0^T dt\, \rho(t) = \frac{1}{Z} e^{-\beta \mathcal{H}} \equiv \langle\rho\rangle^c, \tag{2.4}$$

where we expressed $\langle\rho\rangle^c$ in the canonical ensemble form with $Z = \mathrm{Tr}[e^{-\beta\mathcal{H}}]$ and β the (inverse) temperature $\beta = 1/k_B\mathcal{T}$, with k_B the Boltzmann constant and $\mathcal{T}$ the temperature.[3] It is worth noting that the two limits in (2.4) must be taken

[2] More formally, one could define the degree of locality of an operator of the form (2.2) by counting the number of sites K upon which the operator acts non-trivially. In other works, a K-local operator containes K entries that are different from the identity $\mathbb{1}$. The two extremes are represented by *global* and *local* operators, with $K = N$ and $K = 1$ respectively.

[3] It is important to note that without an external bath through which the system is able to exchange energy, the concept of temperature itself is not well-defined (Vázquez et al. 2003).

simultaneously, as for finite systems the dynamics is quasi-periodic and thus it is not possible to take an infinite time limit, and at finite times conserved quantities get transported only at finite distances, making thermalization unreachable. Crucially, as we already stressed, the state $\rho(t) = U\rho_0 U^\dagger$ will remain a pure state during time evolution, due to the unitarity of the evolution operator $U = \mathrm{e}^{-\mathrm{i}\mathcal{H}t}$. This represents one of the most puzzling questions of our thermalization discussion. How can the information stored in a pure state and a rank-1 projector "vanish" when we look at the unitarily evolved state at long times, which will converge to an equilibrium density operator with rank larger than one? To answer these questions, we must take a "closer" look at the system, i.e. we need to study how individual subsystems thermalize. Let us partition the total system $\mathcal{S}$ into A and B, along the same lines as in Sec. 1.1.4. We consider A as the subsystem of interest and B as the environment, and we take the thermodynamic limit in B ($N_B \to \infty$), so that the number N_A of degrees of freedom in A goes to zero. To study the properties of A, we take the partial trace as defined in (1.20) at each time t and obtain

$$\rho_A(t) = \mathrm{Tr}_B[\rho(t)], \tag{2.5}$$

which is not a pure state in general. For a given equilibrium temperature T, the system thermalizes if

$$\begin{aligned}\overline{\rho_A} &\equiv \lim_{T\to\infty}\lim_{N_B\to\infty}\int_0^T dt\,\rho_A(t) = \lim_{T\to\infty}\lim_{N_B\to\infty}\int_0^T dt\,\mathrm{Tr}_B[\rho(t)] \\ &= \mathrm{Tr}_B\left[\lim_{T\to\infty}\lim_{N_B\to\infty}\int_0^T dt\,\rho(t)\right] = \mathrm{Tr}_B\left[\frac{1}{Z}\,\mathrm{e}^{-\beta\mathcal{H}}\right] = \mathrm{Tr}_B[\langle\rho\rangle^c] \equiv \langle\rho\rangle_A^c\end{aligned} \tag{2.6}$$

for all subsystems A. Thus, a closed system is able to thermalize if it can act *as its own thermal bath* (R. Nandkishore et al. 2015).

Let us be more transparent in the formulation of the explicit requirements of thermalization. We denote the eigenstates of $\mathcal{H}$ by $\{|E_\alpha\rangle\}$, corresponding to the eigenvalues $\{E_\alpha\}$, given by $\hat{H}\,|E_\alpha\rangle = E_\alpha\,|E_\alpha\rangle$. The initial pure state $|\psi_0\rangle$ and its well-defined mean energy can be written as

$$|\psi_0\rangle = \sum_\alpha c_\alpha\,|E_\alpha\rangle\,, \qquad E_0 = \langle\psi_0|\hat{H}|\psi_0\rangle = \sum_\alpha |c_\alpha|^2 E_\alpha, \tag{2.7}$$

with the coefficients $c_\alpha = \langle E_\alpha|\psi_0\rangle$ resulting from the overlap between the initial state and the Hamiltonian eigenstates. The overlaps c_α encode all the information about the initial condition and the probability of having the system in the α-th

eigenstate is given by $p_\alpha = |c_\alpha|^2$. The time-evolving state is

$$|\psi(t)\rangle = \sum_\alpha c_\alpha \, \mathrm{e}^{-\mathrm{i}E_\alpha t} \, |E_\alpha\rangle \, . \tag{2.8}$$

Let us look now at the time evolution of some observable of interest O, which we expand in the eigenbasis $\{E_\alpha\}$ as

$$\begin{aligned} O(t) \equiv \langle\psi(t)|O|\psi(t)\rangle &= \sum_{\alpha,\beta} c_\alpha^* c_\beta \, \mathrm{e}^{i(E_\alpha - E_\beta)t} \, O_{\alpha\beta} \\ &= \sum_\alpha |c_\alpha|^2 O_{\alpha\alpha} + \sum_{\alpha\neq\beta} c_\alpha^* c_\beta \, \mathrm{e}^{i(E_\alpha - E_\beta)t} \, O_{\alpha\beta}, \end{aligned} \tag{2.9}$$

where $O_{\alpha\beta} = \langle E_\alpha|A|E_\beta\rangle$. Taking the infinite time-average one thus gets

$$\lim_{T\to\infty} \frac{1}{T} \int_0^T dt O(t) = \sum_\alpha p_\alpha O_{\alpha\alpha} \equiv \langle O\rangle^{DE} \, , \tag{2.10}$$

which is often referred to as the *diagonal ensemble* prediction (Rigol et al. 2007; Rigol et al. 2008; Rigol 2009a). Looking back to (1.26), the requirement for thermalizing dynamics is the agreement between the long-time average $\overline{O}$ of the given observable with its micro-canonical prediction $\langle O\rangle$; unfortunately, such a condition presents some difficulties in reconciling with (2.9). Indeed, since in the long-time average we are left with the sum of the diagonal elements of O weighted by p_α, which are conserved in time, how is it possible for $\overline{O}$ to agree with the micro-canonical prediction? A second issue concerns the time-scales required to reach thermalization: as the energy eigenvalues separation decays exponentially in many-body systems as one increases the size of the system, to make sure that the second sum in (2.9) effectively sum to 0 one may wait for an exponentially long time, which could potentialy exceed the age of our universe even for rather small systems. This is of course in open contrast with our daily experience and measurements, that prove that even large systems thermalize over time scales much shorter than the age of the universe. In the following, we will try to describe a solution of this apparent paradoxes.

2.1.1 Eigenstate thermalization hypothesis

It is instructive to start considering the very simple case in which a system is initialized in one eigenstate $|E_\alpha\rangle$ of $\mathcal{H}$. As eigenstates are stationary quantum states (see (1.12)), time evolution is then trivially given by $|\psi(t)\rangle = \mathrm{e}^{-\mathrm{i}E_0 t} \, |\psi_0\rangle$.

As this is true for all eigenstates, a first intuition is that thermalization implies that the whole eigenspectrum of $\mathcal{H}$ comprises thermal states. Sadly, eigenstates do not constitute a set of experimentally relevant states, as their preparation in a laboratory is nearly impossible. Although unrealistic, such a simple example returns the flavor of the paradigm underlying the current description of thermalization in closed interacting systems, i.e. the ETH, developed in the 1990s by (Deutsch 1991) and (Srednicki 1994).

As we derived in the previous section, the problem of thermalization reduces to demanding that the diagonal ensemble (2.10) and the appropriate statistical ensemble give the same expected values for the expected value of a generic local observable O. For instance, let us consider the micro-canonical ensemble average

$$\langle O \rangle^{mc} \equiv \frac{1}{N_{E_0,\Delta E}} \sum_{|E_\alpha - E_0| < \Delta E} O_{\alpha\alpha}, \tag{2.11}$$

where E_0 is the initial state mean energy given in (2.7), ΔE is the half-width of a chosen energy window around E_0 and $N_{E_0,\Delta E}$ is the number of states contained in such energy window. The thermalization condition then leads to the equation

$$\sum_\alpha p_\alpha O_{\alpha\alpha} = \frac{1}{N_{E_0,\Delta E}} \sum_{|E_\alpha - E_0| < \Delta E} O_{\alpha\alpha}, \tag{2.12}$$

where the left hand term contains the initial state information, encoded in p_α, and the right hand term depends only on the choice of the total energy. Equation (2.12) contains so-called *thermodynamic universality* (Rigol et al. 2008), as it does not depend on the choice of particular initial conditions, but it applies for a large class of initial states. The ETH provides the necessary ingredients to explain this universality, in the form of the following ansatz for the statistical properties of matrix elements of O,

$$O_{\alpha\beta} = O(\overline{E})\delta_{\alpha\beta} + \mathrm{e}^{-S(\overline{E}/2)} f_O(\overline{E}, \omega) R_{\alpha\beta}, \tag{2.13}$$

where $\overline{E} = (E_\alpha + E_\beta)/2$, $\omega = E_\alpha - E_\beta$, and $S(E)$ is the thermodynamic entropy at energy E. $O(\overline{E})$ is equal to (2.11) at energy $\overline{E}$ and $R_{\alpha\beta}$ is a random (real or complex) number with zero mean value and unit variance. Lastly, both $O(\overline{E}$ and f_O are smooth functions of their arguments. One can thus see that, so long as the energy fluctuations δE in the diagonal ensemble, i.e.

$$\delta E \equiv \sqrt{\langle \psi_0 | \mathcal{H}^2 | \psi_0 \rangle - \langle \psi_0 | \mathcal{H} | \psi_0 \rangle^2} \tag{2.14}$$

are small, the ETH leads to

$$\overline{O} \simeq \langle O \rangle^{DE} \simeq \langle O \rangle^{mc} . \tag{2.15}$$

More explicitly, the ETH ansatz provides a way to quantify the difference between the predictions of the given ensembles, without any assumption on the distribution of p_α. Indeed, we can expand $O_{\alpha\alpha}$ around the mean energy E_0 as

$$O_{\alpha\alpha} \approx \langle O \rangle^{DE} + (E_\alpha - E_0) \frac{dO}{dE}\bigg|_{E_0} + \frac{1}{2}(E_\alpha - E_0)^2 \frac{d^2O}{dE^2}\bigg|_{E_0}, \tag{2.16}$$

and the long-time average expectation value of O thus reads

$$\overline{O} \approx \langle O \rangle^{DE} + \frac{1}{2}(\delta E)^2 O''(E_0) \approx \langle O \rangle^{mc} + \frac{1}{2}[(\delta E)^2 - (\delta E_{mc})^2] O''(E_0), \tag{2.17}$$

where δE_{mc} are the subextensive energy fluctuations in the micro-canonical ensemble. Hence, so long as δE are subextensive too, [4] the second term of the last expression in (2.17) gives only a small correction to $\langle O \rangle^{mc}$, which is suppressed for large sizes. Furthermore, the ansatz (2.13) also offers a solution to the problem of the time required for equilibration, formally scaling with the system size as $t_{therm} \sim e^N$. In fact, a key property of the ETH is that off-diagonal elements are exponentially small in the system size compared to diagonal ones. One can thus compute the long-time average of the fluctuations of the observable O as (D'Alessio et al. 2016)

$$\sigma_O^2 \equiv \lim_{T\to\infty} \frac{1}{T} \int_0^t dt \left[O(t)^2 - \overline{O}^2 \right] \leq \max |O_{\alpha\beta}|^2 \propto e^{-S(\overline{E})}, \tag{2.18}$$

and as the diagonal terms cancel in the subtraction the temporal fluctuations σ_O^2 indeed vanish in the thermodynamic limit. This ensures that the time average in (2.10) actually stays close to the predicted average.

At this point, it is not clear to what kind of observables does the ETH successfully apply to, and one can imagine a counter-example in a rather simple way. Indeed, any function $f(\mathcal{H})$ chosen as the observable of interest would commute with $\mathcal{H}$ and yield $O_{\alpha\alpha} = f(E_\alpha)$. If $f(E_\alpha)$ is not a smooth function, e.g. a δ-function, this will result in a clear violation of the ETH. The current understanding is that the ETH works well for operators that, contrary to the presented

[4] Note that this is the case for generic systems described by local Hamiltonians, as discussed for example in Sec. 4.3.2 of (D'Alessio et al. 2016).

counter-example, act on a relatively small subset of degrees of freedom, i.e. for local operators. Indeed, the ETH has been numerically verified in a variety of non-integrable lattice models in fields including hard-core bosons, interacting spin systems and fermionic models (Rigol et al. 2008; Rigol 2009a; Rigol 2009b; Rigol et al. 2010; Santos et al. 2010; Neuenhahn et al. 2012; Khatami et al. 2013; Steinigeweg et al. 2013; Beugeling et al. 2014; Kim et al. 2014; Steinigeweg et al. 2014). Nonetheless, the exact limits of validity of the ETH are still an active research issue.

2.1.2 Integrability and the violation of ETH

Despite being accepted as the thermalization paradigm in isolated many-body systems, the ETH fails for a number of systems that are known to avoid thermalization in the sense we have discussed so far, i.e.

$$\overline{O} = \lim_{T\to\infty} \int_0^T dt O(t) \neq \langle O \rangle^{ensemble} . \tag{2.19}$$

The most well-known example, deeply rooted in classical mechanics, is represented by *integrable* systems. A classical dynamical system described by an Hamiltonian $H(\boldsymbol{p}, \boldsymbol{q})$, with canonical coordinates and momenta $\boldsymbol{q} = (q_1, \cdots, q_N)$, $\boldsymbol{p} = (p_1, \cdots, p_N)$, is integrable if it has a set of N independent conserved quantities $\{I_i\}$, called *integrals of motion*, in involution, i.e.

$$\{I_i, H\} = 0, \quad \{I_i, I_j\} = 0, \tag{2.20}$$

where $\{\cdot, \cdot\}$ are Poisson brackets. Classical integrable systems are often solved by a canonical transformation $(p, q) \to (I, \theta)$ to so-called *action-angle* variables (Vogtmann et al. 1997), such that $H(p, q) = H(I)$. After the transformation, one could integrate the simplified equations of motion obtaining solutions that describe periodic motion on tori in phase-space, clearly defying the concept of ergodicity introduced in 1.2.1, i.e. the dense exploration of phase-space during time evolution. It follows from the definition that we provided that to get a crossover between regular and chaotic motion, one usually needs a number of conserved quantities in involution which is smaller than the total number of degrees of freedom of the system.

Once again, the translation of classical concepts to quantum mechanics has proven to be challenging, and the definition of quantum integrability is still a debated problem (Caux et al. 2011). Albeit naive, the most widely employed defi-

nition of quantum integrability directly relate to its classical counterpart through a word-to-word translation, substituting the Poisson brackets with commutators. Hence, a quantum system is integrable if one can define an extensive set of operators $\{I_\alpha\}$, $\alpha = \{1, \ldots, \dim(\mathcal{H})\}$, that commute with themselves and with the Hamiltonian $\mathcal{H}$. The problem with such a definition is clear: it is always possible to find a trivial set of such operators for any Hamiltonian, i.e. the set of projectors $I_\alpha = |\psi_\alpha\rangle \langle\psi_\alpha|$ to the Hamiltonian eigenstates, that can be obtained after diagonalizing $\mathcal{H}$. Obviously, this has no defining consequence on the system dynamical structure and it is thus not particularly useful for partitioning quantum systems into distinct dynamical classes. A more general definition, often encountered in the literature, refers to integrable systems as quantum systems that can be solved exactly, i.e. if one could explicitly construct the full set of eigenstates of the Hamiltonian of interest. Notable examples in this regard include Bethe-Ansatz solvable models (Bethe 1931; Sutherland 2004; Essler et al. 2005) and non-interacting (quadratic) Hamiltonians (Lieb et al. 1961). Moreover, further definitions have been put forward and extensively discussed, specifically linking integrability to spectral properties such as Poisson level statistics (Berry et al. 1977; Montambaux et al. 1993; Poilblanc et al. 1993; Relaño et al. 2004; Brandino et al. 2010) and presence of energy level crossing (Yuzbashyan et al. 2002; Stepanov et al. 2008), i.e. absence of level repulsion. Despite being aware of the flaws of the different notions of quantum integrability presented so far, we will not touch upon the matter anymore, and simply refer to integrability in quantum systems as to the existence of an extensive number of non-trivial local operators (or sums of local operators) that independently commute with the Hamiltonian. Moreover, the relation between integrability and level statistics will be explored further in Sec. 3.2.1 in the context of MBL.

Despite the presence of an extensive number of conserved quantities, quantum integrable systems are still expected to relax to steady values in the long-time limit, albeit not agreeing with statistical ensemble predictions. The quest for a generalized ensemble able to describe the relaxation of integrable systems, sparked from the intuition that during unitary evolution the dynamics must be constrained by a subset of eigenstates that are selected by the choice of the initial state, and that provide the major contribution to the overall dynamics. In (Rigol et al. 2007), the study of long-time relaxation in a model of hard-core bosons led to the proposition of the *generalized Gibbs ensemble* (GGE) as a natural extension of the grand-canonical ensemble including the existence of integrals of motion.

The GGE density operator is defined as

$$\langle \rho \rangle^{GGE} = \frac{e^{-\sum_\alpha \lambda_\alpha I_\alpha}}{Z^{GGE}}, \tag{2.21}$$

where $Z^{GGE} = \mathrm{Tr}[\exp(-\lambda_\alpha I_\alpha)]$ is the GGE partition function and λ_α are Lagrangian multipliers, obtained by imposing that, for all α,

$$\langle I_\alpha \rangle^{GGE} = \mathrm{Tr}[\rho^{GGE} I_\alpha] = \langle I_\alpha \rangle^{t=0}. \tag{2.22}$$

It should be noted that for a generic system, the ensemble (2.21) reduces to the usual grand-canonical ensemble (and by equivalence of statistical ensembles also to the micro-canonical and canonical), where the only conserved quantities are the total energy and the number of particles. The correct description of the relaxation of local observables to the values prescribed by the GGE has been numerically or analytically established in several integrable models (Rigol et al. 2007; Calabrese et al. 2011; Cassidy et al. 2011; Collura et al. 2013; Caux et al. 2013; Fagotti et al. 2013; Fagotti et al. 2014; Wright et al. 2014; Vidmar et al. 2016); nonetheless, other works have pointed out the dependence of the relaxation values on the initial state choice, that could lead to almost thermal expectation values in integrable systems (Cramer et al. 2008; Chung et al. 2012; He et al. 2013; Torres-Herrera et al. 2013).

We would like to conclude this brief overview of quantum integrability and ETH violations mentioning a recently discovered mechanism of *weak* ergodicity breaking. In 2017, an experiment on a Rydberg-atom quantum simulator provided evidence of non-thermalizing behavior in a system without any conserved quantities: despite most initial states relaxed to thermal expectation values, a small subset of states exhibited persistent oscillations. A series of subsequent works have tried to solve the puzzle of such so-called *revivals*, leading to the birth of the concept of *quantum many-body scars* (Turner et al. 2018b; Turner et al. 2018a; Moudgalya et al. 2018; W. W. Ho et al. 2019; Lin et al. 2019; Khemani et al. 2019; S. Choi et al. 2019; Moudgalya et al. 2020; Bull et al. 2020). The term "scars", reminiscent of studies of unstable periodic orbits in classically chaotic systems (Heller 1984), refers to the existence of a fraction of non-thermal eigenstates immersed in the rest of the thermalizing eigenspectrum. The violation of the ETH is "weak" in the sense that albeit non-thermal, such special eigenstates occupy a vanishing small portion of the Hilbert space when taking the large size limit. Nevertheless, it is surprising how such a small number of scarred eigen-

states can effectively provide a dominant contribution to the system real-time dynamics, as observed in the periodic revivals in (Bernien et al. 2017). The influence of scarred eigenstates is embodied by the fact that they have a particularly large overlap, compared to the rest of the spectrum, with physically relevant states such as product states, which are often the preferred choice for the initial configuration of quantum simulation setups.

2.2 Robust ergodicity breaking: localized systems

Anderson localization (AL) is a wave interference phenomenon that leads to the suppression of transport in non-interacting systems in the presence of an uncorrelated disorder potential (Anderson 1958). We already mentioned in 1.2.1 that P. W. Anderson himself pointed out the intriguing possibility that disorder may help escaping thermalization. Indeed, he wrote in his seminal 1958 paper that a localized system would provide *"an example of a real physical system with an infinite number of degrees of freedom, having no obvious oversimplification, in which the approach to equilibrium is simply impossible"*. Interestingly, Anderson study was motivated by some unexplained experimental observations made by Fletcher and Feher at Bell Laboratories, in which they measured anomalously long relaxation times for electron spins in semiconductor samples doped with a large injection of impurities (Feher et al. 1955; Feher et al. 1959). The failure of thermalization is intuitively clear: as particle wavefunctions are localized on specific points in real space, every single-particle occupation number is a non-trivial integral of motion (Modak et al. 2016). Particles are not able to freely explore either real nor momentum space, clearly violating ergodicity. The scope of this section is to review the main ideas underlying the phenomenon of localization in non-interacting systems and to prepare the ground for a discussion on the recent extension of AL to the many-body scenario, which constitutes the main object of investigation of this thesis.

2.2.1 Anderson model of localization

The model considered by Anderson consisted in a tight-binding Hamiltonian with spinless free fermions hopping on a lattice with random onsite potentials. The Hamiltonian of the Anderson model reads

$$\mathcal{H}_{AL} = \sum_i \epsilon_i c_i^\dagger c_i - J \sum_{\langle ij \rangle} \left(c_i^\dagger c_j + h.c. \right), \tag{2.23}$$

where $c_i^\dagger$, c_i are the usual fermionic creation and annihilation operators on site i, J is the nearest-neighbor hopping term and ϵ_i are onsite energies, taken as random variables within a uniform distribution $[-W, W]$. [5] The half-width W is a parameter conventionally dubbed *disorder strength*. The Hamiltonian (2.23) is quadratic in the fermionic operators, and conserves the number of particles since it commutes with the total number of fermions, i.e. $[\mathcal{H}, \mathcal{N}] = 0$, with $\mathcal{N} = \sum_i c_i^\dagger c_i$. One can thus restrict the analysis to one of the subspaces of the total Fock space $\mathbb{F}$, spanned by the action of the fermionic creation/annihilation operators operators on the vacuum state. Working in the one-particle sector $\mathbb{F}_1$, the model (2.23) reduces to

$$\mathcal{H}_{AL} = \sum_i \epsilon_i |i\rangle \langle i| - J \sum_{\langle ij \rangle} \left(|i\rangle \langle j| + |j\rangle \langle i| \right), \tag{2.24}$$

where $|i\rangle$ is $\bigotimes_{j \neq i} |0\rangle_j \otimes |1\rangle_i$, i.e. denotes the particle being located on the i-th site. For any state $|\psi\rangle$ in $\mathbb{F}_1$, it is possible to define the wavefunction $\psi(i)$ as $\langle i|\psi\rangle$.

Following Anderson's initial formulation of the problem, we would like to ask what is the probability that a particle initially located at the origin ($i = 0$ at time $t = 0$) eventually visits again the same position during the unitary evolution driven by (2.24). The main observable is thus the *return probability* (or *survival probability*), defined as

$$P(t) \equiv |\psi(t, 0)|^2, \tag{2.25}$$

with $\psi(0, i) = \delta_{0,i}$. We note that, in general, the survival probability (2.25) can be conceived as a particular case of the Loschmidt echo defined in (1.29), where $|\psi_0\rangle$ is chosen such that $\mathcal{H}' |\psi_0\rangle = 0$, where $\mathcal{H}'$ is the Hamiltonian governing the backward evolution in the echo procedure, i.e.

$$P(t) = \mathcal{L}(t) = |\langle \psi_0 | \, \mathrm{e}^{-\mathrm{i}\mathcal{H}t} \, |\psi_0\rangle|^2. \tag{2.26}$$

It is instructive to proceed by considering two extreme limits (Scardicchio et al. 2017) before focusing on the most general formulation of the problem.

Zero disorder ($J/W \to 0$)

In the limit of vanishing disorder, the model (2.24) is the textbook translationally invariant tight-binding model, which conserves crystalline momentum

[5] Localization effects induced by different disorder distributions, such as Gaussian correlated disorder, have also been extensively studied. An early but exhaustive summary can be found in (Kramer et al. 1993).

(Ashcroft et al. 1976). In case of a lattice of size L with periodic boundary conditions, the eigenstates of (2.24) are Bloch-type plane waves

$$\phi_k(i) = \frac{1}{\sqrt{L^d}} \mathrm{e}^{\mathrm{i}\, k i}, \qquad k = \frac{2\pi}{L}(n_1, \ldots, n_d), \tag{2.27}$$

with the dispersion relation

$$E_k = -2J \sum_{n+1}^{d} \cos(k_n), \tag{2.28}$$

where d is the dimensionality of the lattice. The time evolved wavefunction is the superposition of all Bloch-type eigenstates

$$\psi(t, i) = \frac{1}{L^d} \sum_k \mathrm{e}^{[\mathrm{i}\, k i + 2\,\mathrm{i}\, t \sum_n \cos(k_n)]}, \tag{2.29}$$

and it is a periodic function with a period that scales as the size L. Thus, revivals bring the particle back at the origin persistently during the dynamics. In the thermodynamic limit $L \to \infty$ one can show that for a fixed time t the evolved wavefunction converges to

$$\psi(t, i) = \int_0^{2\pi} \frac{d^d k}{(2\pi)^d} \mathrm{e}^{[\mathrm{i}\, k i + 2\,\mathrm{i}\, t \sum_n \cos(k_n)]} = \mathrm{i}^d \prod_{n=1}^{d} \mathcal{J}_{i_n}(2Jt), \tag{2.30}$$

where we restricted into the first Brillouin zone and $\mathcal{J}_\alpha(x)$ is the α-th Bessel function of the first kind (Abramowitz et al. 1964). At this point, noting that Bessel functions decay asymptotically to $1/\sqrt{x}$ for $x \to \infty$, the return probability for the clean case can be computed as

$$P(t) \equiv |\psi(t, 0)|^2 \sim \frac{1}{t^{d/2}}, \tag{2.31}$$

thus decaying to 0 in the long-time limit. Furthermore, one could also consider the mean-square displacement of the wavepacket

$$\Delta^2(t) \equiv \langle \psi(t, i) | X^2 | \psi(t, i) \rangle - \langle \psi(t, i) | X^2 | \psi(t, i) \rangle^2 = \sum_i i^2 |\psi(t, i)|^2, \tag{2.32}$$

where X is the position operator, and obtain (Scardicchio et al. 2017)

$$\Delta^2(t) = 2dJ^2 t^2. \tag{2.33}$$

Thus, the wavefunction spreads ballistically starting from its initial position, as each Bloch wavefunction spreads ballistically in every available direction.

Infinite disorder ($J/W \to \infty$)

The large disorder limit is considerably simpler, as the eigenstates coincide with the position basis of the system, i.e. $\mathcal{H}_{AL} |i\rangle = \epsilon_i |i\rangle$. Hence, they represent stationary states and the Hamiltonian dose not generate any non-trivial dynamics:

$$|\psi(t,0)\rangle = \mathrm{e}^{-\mathrm{i}\epsilon_0 t} |0\rangle . \tag{2.34}$$

As a consequence, the survival probability stays at $P(t) = P(0) = 1$ and the expansion of the wavepacket is suppressed, leading to perfect localization.

Intermediate disorder

In the most general case of intermediate disorder, one could first look at the problem from a classical perspective, imagining the time evolution as a sequence of elastic scattering events between the particle and the impurities of the medium. In such a picture, reminiscent of the well-known scenario of a random walk, the motion is diffusive and the mean-square displacement is

$$\Delta^2(t) \approx Dt, \tag{2.35}$$

where $D = v^2\tau > 0$ is the diffusion constant and t must be larger than the scattering time τ. Also, a diffusive behavior implies a decay of the survival probability as

$$P(t) = \frac{1}{(Dt)^{d/2}}, \tag{2.36}$$

strongly dependent on the specific form of the diffusion coefficient D. One could expect that D must clearly depend on the strength of disorder W (in classical terms, on the density of scattering impurities). This is indeed the case, as one can show with a perturbative calculation employing the Fermi golden rule to obtain the scattering rate (Dirac et al. 1927)

$$\Gamma_k = \frac{1}{\tau} = \pi |\langle k|V|k'\rangle|^2 \delta(E_k - E_{k'}), \tag{2.37}$$

where $V = \sum_i \epsilon_i |i\rangle \langle i|$ is the onsite potential, which is treated as a small perturbation. Briefly sketching the calculation, one could split the sum in (2.37) into diagonal and off-diagonal terms and performing a disorder average, obtaining

(Scardicchio et al. 2017)

$$\begin{aligned}\Gamma_k &= \pi \sum_{k'} \left(\sum_i \epsilon_i^2 \frac{1}{L^{2d}} + \sum_{i \neq i'} \epsilon_i \epsilon_{i'} \frac{e^{i(k-k')(i-i')}}{L^{2d}} \right) \delta(E_k - E_{k'}) \\ &= \pi \sum_{k'} \frac{W^2}{3L^d} \delta(E_k - E_{k'}) \\ &= \pi \int \frac{d^d k'}{(2\pi)^d} \frac{W^2}{3} \delta(E_k - E_{k'}) \\ &= \pi \int dE' \rho(E') \frac{W^2}{3} \delta(E_k - E_{k'}) \\ &= \frac{\pi W^2}{12} \rho(E_k),\end{aligned} \tag{2.38}$$

where ρ is the density of states and we used the fact that the variance of a uniform distribution of width $2W$ is equal to $(2W)^2/12 = W^2/3$. Inserting (2.38) into $D = v^2\tau$ and taking $v_g \sim \partial E_k/\partial k$ as the group velocity, one gets

$$D \sim \frac{v_g^3}{W^2}. \tag{2.39}$$

It is worth noting that the expression above predicts that D always remains finite for every $W \neq 0$. However, Anderson predicts D to strictly equal 0 for a disorder strength greater than a critical value $W > W_c$, [6] thus imagining a transition between a diffusive and an insulating localized phase that is now known as Anderson transition or localization-delocalization transition.

2.2.2 Eigenstate localization and the role of dimensionality

The persistence of a finite $P(t)$ at strong disorder and the absence of transport with a vanishing conductivity $\sigma \sim 0$ represent the most defining feature of the localized phase. In such a phase, the eigenstates of (2.23) resemble the infinite disorder case that we examined above, decaying exponentially with the distance from a localization centre i_0 with the asymptotic form

$$|\phi(i)|^2 \sim e^{\frac{-|i-i_0|}{\xi}}, \tag{2.40}$$

where ξ is the *localization length* (Kramer et al. 1993).

Following Anderson's seminal result, several works explored the role of the dimensionality d on the onset of localization and the existence of a delocaliza-

[6] As we will see shortly, W_c is finite only for $d \geq 3$.

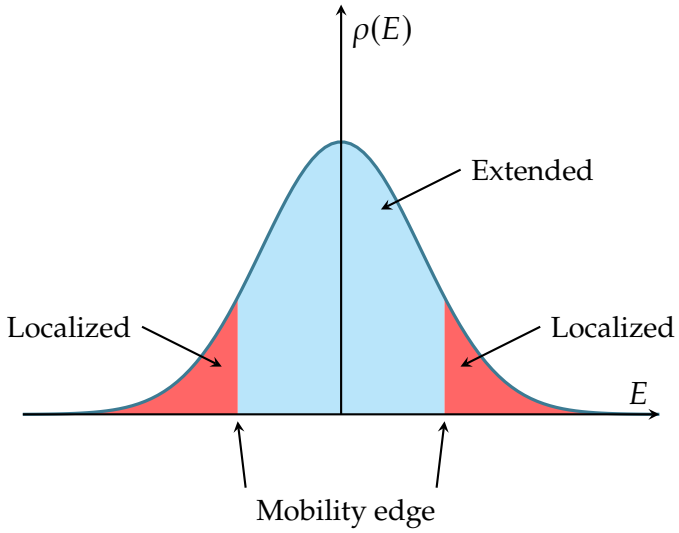

Figure 2.1. *Sketch of the density of states $\rho(E)$ of the Anderson model in $d = 3$. The extended part of the spectrum (light blue) is separated from the localized tails (light red) by the mobility edge.*

tion transition. In $d = 1$ the full localization of the whole eigenspectrum for any disorder strength $W > 0$ has been rigorously proven, with a localization length decaying with the disorder strength as $\xi \sim 1/W^2$ (Kramer et al. 1993). Similarly, the influential paper of the "Gang of four" (Abrahams et al. 1979) went on to provide scaling arguments supporting the absence of diffusion in $d \leq 2$ for any $W > 0$. A true phase transition at a finite value $W_c > 0$ is expected for $d = 2 + \epsilon$ for $\epsilon > 0$ (Kramer et al. 1993), where the eigenspectrum becomes fully localized for $W > W_c$. Below the critical disorder strength, Mott introduced the crucial concept of *mobility edge* (Mott 1967), describing the non-simultaneuous localization of the Hamiltonian spectrum: at weak disorder, eigenstates become rapidly localized at tails of the spectrum (Kramer et al. 1993), while the remaining states are delocalized; as one increases W, the delocalized portion of the spectrum shrinks until vanishing at $W = W_c$. A more detailed discussion of the scaling theory of localization, and its implications in terms of the role of dimensionality, is provided in App. B.

2.2.3 Quasi-periodic systems

We present here an alternative pathway to eigenstate localization, that is of particular importance for experimental reasons and that is often employed in this thesis. In 1980, Aubry and André proved that localization can appear in a peculiar class of systems without relying on the presence of "true" disorder

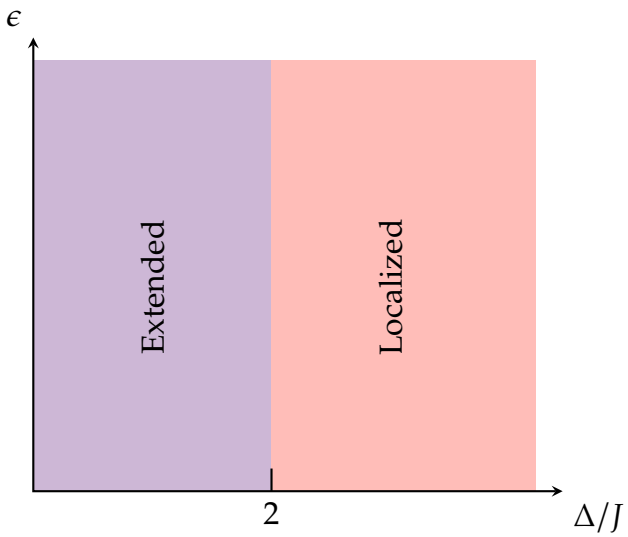

Figure 2.2. *Typical phase diagram of the AA model (2.41), where ϵ labels the energy eigenvalues and Δ/J the dimensionless parameter driving the transition at $\Delta/J = 2$.*

(Harper 1955; Aubry et al. 1980), studying a thight-binding model of the form

$$\mathcal{H}_{AA} = -J \sum_{\langle nm \rangle} \left(c_n^\dagger c_m + h.c. \right) + \Delta \sum_n \cos\left(2\pi\beta n + \phi\right) c_n^\dagger c_n, \tag{2.41}$$

where the random onsite potential term in (2.23) is replaced by a *quasi-periodic* potential, with β an irrational number ensuring the incommensurability of the potential profile with respect to the lattice and ϕ a random phase comprised in $[0, 2\pi]$. The main point of interest in studying model (2.41), besides the higher experimental feasibility (Lye et al. 2007; Roati et al. 2008), is that it hosts a delocalization transition in $d = 1$ without the presence of a mobility edge. The lack of a mobility edge arises from the *self-duality* of the *Aubry-André* (AA) model at $\phi = 0$, that can be appreciated by transforming the hopping term to reciprocal space with

$$c_n = \frac{1}{\sqrt{L}} \sum_k \mathrm{e}^{\mathrm{i}\, 2\pi\beta k n}\, c_k, \tag{2.42}$$

leading after substitution to

$$\mathcal{H}_{AA} = 2J \sum_k \cos(2\pi\beta k) c_k^\dagger c_k + \Delta \sum_n \cos(2\pi\beta n) c_n^\dagger c_n. \tag{2.43}$$

The Hamiltonian (2.43) is evidently self-dual, in the sense that extended k modes in Fourier space correspond to localized n modes in real space and they switch

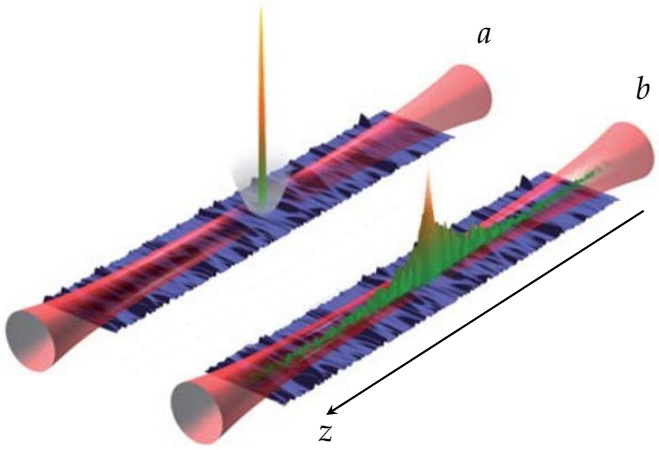

Figure 2.3. *Experimental observation of AL of matter waves in an expanding BEC in an optical trap. The BEC is initially confined longitudinally by a combination of optical wave-guides and magnetic traps (a) and subsequently left free to expand lifting the trap (b). Adapted from* (*Billy et al.* 2008).

roles at the critical point $\Delta_c = 2J$. Indeed, it was shown that in the thermodynamic limit the AA model displays a transition at Δ_c for any value of the irrational number β (Thouless et al. 1983). Moreover, such self-duality property is independent of energy, meaning that all the eigenstates localize at the same critical point. This can be easily seen also by solving the integral

$$\frac{1}{\xi(E)} = \int_{-\infty}^{\infty} \ln|E-\epsilon|\rho(\epsilon), \tag{2.44}$$

that describes the dependence of the localization length on the energy (Thouless 1972a). Indeed, solving (2.44) in the AA model yields an energy independent value of $\xi = d/\ln(\Delta/2J)$ (Modugno 2010), implying that all the eigenstates share the same localization length.

2.2.4 Experimental progress on single-particle localization

The phenomenon of Anderson localization has attracted experimental curiosity since its very birth, and traces of localization have been reported in a wide variety of wave media and solid-state systems in the following decades (Cutler et al. 1969; P. A. Lee et al. 1985; Weaver 1990; Dalichaouch et al. 1991; Wiersma et al. 1997; Stoytchev et al. 1997; Störzer et al. 2006; Schwartz et al. 2007; Hu et al.

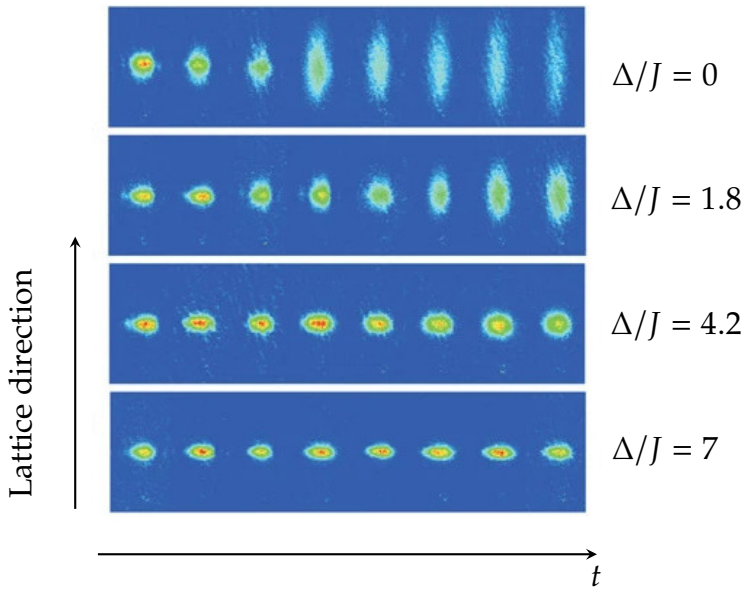

Figure 2.4. *Absorption images showing the BEC diffusion across an optical quasi-periodic lattice. Increasing the potential amplitude Δ/J results in the localization of the atomic cloud around the initial position. Adapted from* (*Roati et al.* 2008).

2008; Chabé et al. 2008; Sperling et al. 2013; Lopez et al. 2012; Manai et al. 2015; Ying et al. 2016). Recent progress in the manipulation of cold-atoms platforms have provided new ways for the exploration of AL in a more controlled and tunable environment. An experimental breakthrough appeared in (Billy et al. 2008), where the exponential localization of a *Bose-Einstein condensate* (BEC) was observed after releasing a cloud of ^{87}Rb atoms in the presence of uncorrelated disorder created by a laser speckle. The realization scheme is depicted in Fig. 2.3 The atoms are brought into a BEC state by combining a strong confinement in the transverse direction by means of a horizontal optical waveguide, and a loose magnetic trap in the longitudinal direction. After super-imposing a weakly disordered optical potential via laser speckle the BEC is left free to expand by switching off the longitudinal confinement. By direct imaging of the fluorescence of the atoms irradiated by a resonant probe, the BEC rapidly stops to diffuse and remains localized around the starting position.

Surprisingly, a second experiment (Roati et al. 2008) was published on the same day as (Billy et al. 2008), reporting a similar localization observation in a BEC of ^{39}K atoms in the presence of an incommensurate potential, thus effectively realizing the AA model (2.41). The absorption images collected during the expansion of the atomic cloud after releasing the confinement are reported

in Fig. 2.4 for different values of the potential amplitude Δ/J. In the clean case ($\Delta/J = 0$) the gas expands ballistically as expected, but displays no expansion in the strong potential regime ($\Delta/J = 7$), as the BEC is a superposition of exponentially localized eigenstates. At intermediate potential strengths, the authors observe a gradual speed reduction of the ballistic expansion.

In the last decade, a series of new experiments managed to extend the results we briefly presented here to the realm of many-body systems, inspired by the perspective of the survival of localization in the presence of particle interactions. Such a fascinating phenomenon is the focus of the next Chapter.

3

Many-body localization

The question of whether particle interactions would lead to the destroying of localization has been long debated. In an early work, (Fleishman et al. 1980) argued in favor of localization survival in the presence of weak, short-ranged interactions, paving the way for the application of renormalization group methods for the study of localization. On the same line, an extension of the scaling theory of localization taking into account the interplay of disorder and interactions appeared in (Finkelstein 1983) and (Giamarchi et al. 1988) developed a renormalization group method to describe 1D interacting quantum liquids at zero temperature. Over the last fifteen years, a picture of a localized phase of matter including local interactions and surviving at *non-zero temperatures* has emerged, firstly reported in (Gornyi et al. 2005; Basko et al. 2006). Such a perfect insulator at finite energy densities represents the so-called MBL phase, that *robustly* violates the ETH. Compared to the case of integrable systems, that can be thought as highly fine-tuned points in parameter space and thus highly sensitive to weak perturbations, MBL is expected to be a robust mechanism against thermalization, not requiring any fine-tuning but only the presence of strong enough disorder. It is worth stressing the fact that MBL is a dynamical phenomenon in the sense that it involves the properties of eigenstates at finite energy densities (or equivalently, at high temperatures); one can establish MBL only by probing that highly excited eigenstates are localized. On the other hand, the single-particle localization at zero temperature, discussed in 2.2, requires the localization of a finite number of excitations; indeed, probing the localization of the ground-state usually suffices to demonstrate Anderson localization.

MBL is currently the object of intense research both on the theoretical and on the experimental side, as evidenced by recent comprehensive reviews such

as (R. Nandkishore et al. 2015; Alet et al. 2018; Parameswaran et al. 2018; Abanin et al. 2019). As much as fundamental issues related to the violation of ETH and statistical mechanics foundations appeal to theoreticians, experimentalists have been attracted by the intriguing implications of MBL properties in the development of quantum memories. Indeed, exploiting the failure of thermalization, a MBL system can store information regarding its initial configuration even after long times, avoiding relaxation towards thermal states and the scrambling of such information across the system. For instance, the signature of initially uneven particle/spin imbalance will remain finite instead of decaying to zero, leading to measurable *memory effects*.

3.1 The paradigmatic model of MBL

We will develop our discussion focusing on the paradigmatic model in MBL studies, i.e. the 1D XXZ model [1] with a random external magnetic field for L sites described by the Hamiltonian

$$\mathcal{H} = J \sum_{\langle ij \rangle}^{L} \left(S_i^x S_j^x + S_i^y S_j^y \right) + J_z \sum_{\langle ij \rangle} S_i^z S_j^z + \sum_{i}^{L} h_i S_i^z , \tag{3.1}$$

where $S_i^\alpha = \sigma_i^\alpha / 2$ is the spin operator at site i and σ_i^α are the usual Pauli matrices (1.4). The random transverse field amplitudes are randomly picked from a box distribution $[-W, W]$. The model (3.1) can be mapped to a 1D interacting fermion model by means of Jordan-Wigner transformations (Jordan et al. 1928) as shown in App. A, leading up to irrelevant constants, to

$$\mathcal{H} = \frac{J}{2} \sum_{\langle ij \rangle}^{L} \left(c_i^\dagger c_j + h.c. \right) + J_z \sum_{\langle ij \rangle} n_i n_j + \sum_i h_i n_i , \tag{3.2}$$

with the number operator defined as $n_i = c_i^\dagger c_i$. In the fermion picture, it is easy to appreciate how the $S_i^z S_j^z$ term in (3.1) corresponds to effective nearest-neighbor particle interactions with strength J_z, and the random magnetic fields h_i map onto random onsite energies, reminiscent of the original AL Hamiltonian (2.23). Indeed, in the limit $J_z \to 0$, the model (3.2) reduces to the non-interacting Anderson problem and all eigenstates are localized for any $W > 0$.

The first numerical evidence of localization at high temperatures came from

[1] In the most general case of completely anisotropic couplings between $S_i^\alpha S_j^\alpha$ terms, the model is known as the 1D XYZ model.

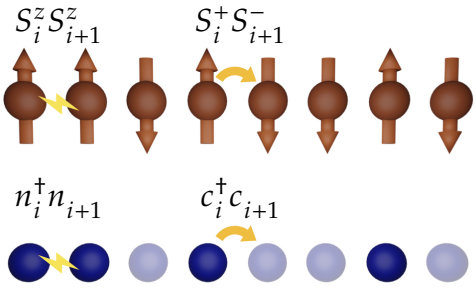

Figure 3.1. *Sketch of two common models in MBL studies.* (*a*) *The Heisenberg spin chain* (3.1) *and* (*b*) *a spinless fermion chain with nearest neighbor interaction* (3.2).

(Oganesyan et al. 2007) with an *Exact Diagonalization* (ED) study of a fermionic model similar to (3.2), with the addition of long-range hopping. In the following years, extensive numerical studies of (3.1) showed that increasing the interactions above a certain value J_z^c may lead to delocalization for a fixed (not too large) W (Žnidarič et al. 2008; A. Pal et al. 2010; Luitz et al. 2015; Serbyn et al. 2015). Alternatively, one could trigger the transition into the MBL phase by increasing the disorder W above a certain critical value W_c at a fixed interaction strength. Moreover, multiple works based on ED simulations detected the presence of a *many-body mobility edge* (MBME) across the many-body spectrum of (3.1), separating extended from localized states at $W < W_c$. The exact value of W_c is currently an object of debate. The early works (Luitz et al. 2015; Serbyn et al. 2015) were based on ED techniques and thus restricted to small system sizes ($L \sim 20$), where the analysis of spectral signatures (see Sec. 3.2) yielded estimates of a critical disorder $W_c \approx 3.5 \pm 1.0$ for $J = 1$. However, recent works employing tensor network methods have been able to reach larger system sizes ($L \sim 100$), suggesting a drift of the critical disorder to larger values $W_c \approx 5.5$ (Doggen et al. 2018; Doggen et al. 2019; Doggen et al. 2021). Further theoretical debate concerns whether the appearance of a MBME is actually possible in the thermodynamic limit. The authors of (De Roeck et al. 2016; De Roeck et al. 2017) argued, though perturbative calculations, that even for strong disorders a local fluctuation with a higher energy density than the background (a *hot bubble*) may lead to the thermalization of neighboring regions, destabilizing the MBL phase with an avalanche effect that would eventually destroy it, forbidding the existence of an MBME in the large L limit.

In the following, we review the main signatures of the MBL transition

obtained by numerical simulations, constituting an overview of the main features of the MBL phase.

3.2 Hallmarks of the MBL phase

3.2.1 Level statistics

A convenient metric to distinguish between ergodic and localized phases, commonly known as *level statistics*, lies in the spectral properties of the Hamiltonian. Such a measure was first introduced in the context of *Random Matrix Theory* (RMT), a framework first developed by (Wigner 1955; Wigner 1958) and (Dyson 1962) to describe the properties of heavy atomic nuclei. The basic idea was to provide an ansatz for the spectrum of such complex system, for which the direct analysis of the Hamiltonian would be intractable, following the spacing between the eigenvalues of random matrices, only depending on the underlying symmetry properties of the system. The main quantities of interest in MBL studies are the simple gaps δ_n between adjacent energy levels and the so called gap-ratio parameter r_n, given by

$$\delta_n = E_n - E_{n-1}, \qquad r_n = \frac{\min(\delta_n, \delta_{n-1})}{\max(\delta_n, \delta_{n-1})}. \tag{3.3}$$

The parameter r_n, introduced by (Oganesyan et al. 2007), is a compact measure that avoids the notable problem of the *unfolding* of the spectrum, i.e. the dependence of δ_n on the density of states, that often leads to finite-size issues in many-body systems (Gomez et al. 2002; Avishai et al. 2002; Serbyn et al. 2016). The distribution of the level spacing for an ergodic system is expected to follow the prediction for random matrices belonging to the same symmetry class. For instance, real random Hamiltonians with time reversal symmetry belong to the so-called *Gaussian Orthogonal Ensemble* (GOE)[2], and the distribution of level spacings thus the so-called Wigner-Dyson "surmise"

$$P_{GOE}(\delta) = \alpha\delta\, \mathrm{e}^{-\beta\delta^2}, \tag{3.4}$$

[2]A quantum systems without time-reversal symmetry is instead described by the *Gaussian Unitary Ensemble* (GUE).

with α and β constants. The probability distribution for the gap-ratio r_n can be generally obtained by computing the joint probability

$$P(r) = \int P(\delta_1, \delta_2)\delta\left(r - \frac{\delta_1}{\delta_2}\right) d\delta_1 d\delta_2. \tag{3.5}$$

In the case of the GOE distribution (3.4), (Atas et al. 2013) showed that the joint distribution is well described by

$$P_{GOE}(r) \sim \frac{r + r^2}{(1 + r + r^2)^{5/2}}. \tag{3.6}$$

It is convenient to consider only the average value of $P_{GOE}(r)$, which can be computed as $\overline{r}_{GOE} \approx 0.5307$. Thus, in the ETH phase, model (3.1) is expected to follow the above prediction. On the other hand, in the MBL phase, eigenvalues are uncorrelated random variables described by a Poisson distribution

$$P_{Poisson}(\delta) = \frac{1}{\gamma} \mathrm{e}^{-\delta/\gamma}, \qquad P_{Poisson}(r) = \frac{2}{(1 + r)^2}, \tag{3.7}$$

with mean value $\overline{r}_{Poisson} = 2\ln(2) - 1 \approx 0.386$ (Oganesyan et al. 2007).

Level statistics provides an accessible signatures of localization when the full eigenspectrum (or significant portions of it) is directly accessible, such as in ED studies like the example reported in Fig. 3.2, where increasing the disorder strength W results in a crossover between $\overline{r}_{GOE}$ and $\overline{r}_{Poisson}$. Moreover, the curves for different system sizes L cross each other in the vicinity of $W_c \approx 3.7$, suggesting the presence of a phase transition. A finite size scaling analysis with the simple form $f[L^{1/\nu(W-W_c)}]$, makes the data collapse and allows the extraction of the critical value $W_c = 3.72(6)$ with $\nu = 0.91(7)$.

The physical intuition behind level statistics is related to the concept of *level repulsion*, a feature commonly associated with ergodic systems and thus Wigner-Dyson statistics. Indeed, it is the general belief for generic many-body systems that the probability of having two consecutive levels at the same energy, i.e. the probability of degeneracies, is vanishing. This is due to the low number of conserved quantities in ergodic systems, which are responsible for the characteristic level crossing of integrable systems. As we will discuss in Sec. 3.3, MBL systems represent a sort of intermediate scenario between full integrability and ergodicity. As such, integrability signatures like the absence of level repulsion appear as spectral properties of MBL systems, and they have been exploited so far in a variety of numerical works (Laumann et al. 2014; Kjäll et al. 2014; Agarwal et al.

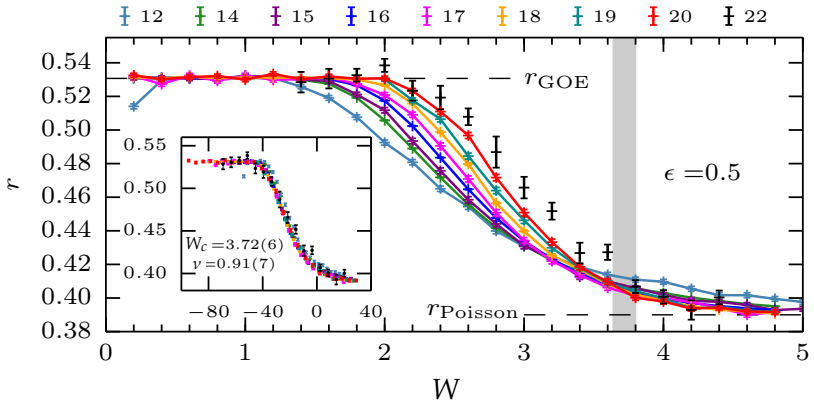

Figure 3.2. *Gap ratio r in the random Heisenberg chain (3.1) as a function of disorder strength W for different system sizes $L \in [12, 22]$. The level statistics follows the GOE prediction at weak disorders, while it becomes Poissonian at stronger disorders. The inset displays the data collapse obtained with the simple finite size scaling form $L^{1/\nu(W-W_c)}$. Adapted from (Luitz et al. 2015).*

2015; Bar Lev et al. 2015; Luitz et al. 2015; Pekker et al. 2017a; Serbyn et al. 2017; Stagraczyński et al. 2017).

3.2.2 Participation ratios and multifractality

Another widely employed spectral measure of localization is given by the *inverse participation ratios* (IPR), generally defined as

$$\mathrm{IPR}_q^\alpha = \sum_n^{\mathcal{N}} \left|\langle\phi_n|\psi_\alpha\rangle\right|^{2q}, \tag{3.8}$$

with $|\psi_\alpha\rangle$ the α-th eigenstate of the system and the sum running over all the $\mathcal{N}$ basis states $\{|\phi_n\rangle\}$. The IPRs provide information about the structure of the eigenstates $|\psi_\alpha\rangle = \sum_n c_n^\alpha |\phi_n\rangle$ in the chosen basis, with $c_n^\alpha = |\langle\phi_n|\psi_\alpha\rangle|$. For instance, let us choose $\{|\phi_n\rangle\}$ as the position basis $\{|x\rangle\}$ in the non-interacting AL case. The IPRs (3.8) then quantify the number of lattice sites over which the α-th eigenstate is spread, i.e. the eigenstate *support*. Thus, an intuitive expectation is that if a state is localized in the chosen basis then its support remains approximately constant as a function of $\mathcal{N}$ and $\mathrm{IPR}_q^\alpha \sim$ constant as long as the system size L is larger than the localization length. On the other hand, an extended state is expected to have a support that samples most of the Hilbert space, and the GOE predicted scaling for $q = 2$ is $\mathrm{IPR}_2^\alpha \sim 1/\mathcal{N}$ (Zelevinsky et al. 1996; Torres-Herrera

et al. 2016; Torres-Herrera et al. 2017). [3] At the AL transition, the overlaps c_n^α are known to display large fluctuations and the IPR_q^α show anomalous *multifractal* scaling with the system size, i.e.

$$\mathrm{IPR}_n^\alpha \sim \mathcal{N}^{D_q(1-q)}. \tag{3.9}$$

The exponent D_q is called the generalized fractal dimension and multifractality manifests itself in a nonlinear dependence of D_q on q close to criticality. For fully ergodic states $D_q = 1$ in 1D systems, while it approaches zero in the fully localized regime, $D_q = 0$. Interestingly, an intermediate case of a delocalized but non-chaotic eigenstate leads to $D_q \sim N^{-D_q}$, with a fractal dimension $0 < D_q < 1$.

The multifractal nature of localized eigenstates is a widely explored topic in the AL field (Schreiber 1985; Ono et al. 1989; Schreiber et al. 1991; Brandes et al. 1996; Parshin et al. 1999; Mildenberger et al. 2002; Rodriguez et al. 2009; Rodriguez et al. 2011; Tarquini et al. 2017; Lindinger et al. 2017; Krishna et al. 2018; Torres-Herrera et al. 2019), and it has been very recently at the center of renewed interest in MBL studies (Torres-Herrera et al. 2015; Serbyn et al. 2017; Macé et al. 2019; Luitz et al. 2020a; Torres-Herrera et al. 2020; Solórzano et al. 2021; Pietracaprina et al. 2021). Furthermore, we would like to mention that experimental observations of multifractality have been carried out in disordered semiconductors (Richardella et al. 2010) and in cold-atoms platforms (Lemarié et al. 2010; Sagi et al. 2012).

Lastly, a few works unveiled an intriguing connection between the fractal dimension D_q and the dynamical properties of AL systems. Indeed, quantities such as the Loschmidt echo (1.29) and the survival probability (2.25) display a characteristic power-law decay in the vicinity of the transition, with an exponent equal to the fractal dimension D_q (Huckestein et al. 1994; Huckestein et al. 1999; Ng et al. 2006). We will return to such considerations in Chapter 5, when we will present new results on the relation between the Loschmidt echo and the fractality of eigenstates in a MBL scenario.

3.2.3 Area law entanglement

In Sec. 1.1.4, we provided a brief overview of the concept of entanglement in composite quantum systems, anticipating that the eigenstates of thermalizing systems typically follow a volume law scaling of the EE, i.e. $S(\rho^A) = O(|L|)$,

[3] In the literature, the nomenclature *inverse participation ratio* is usually reserved for the specific case $q = 2$.

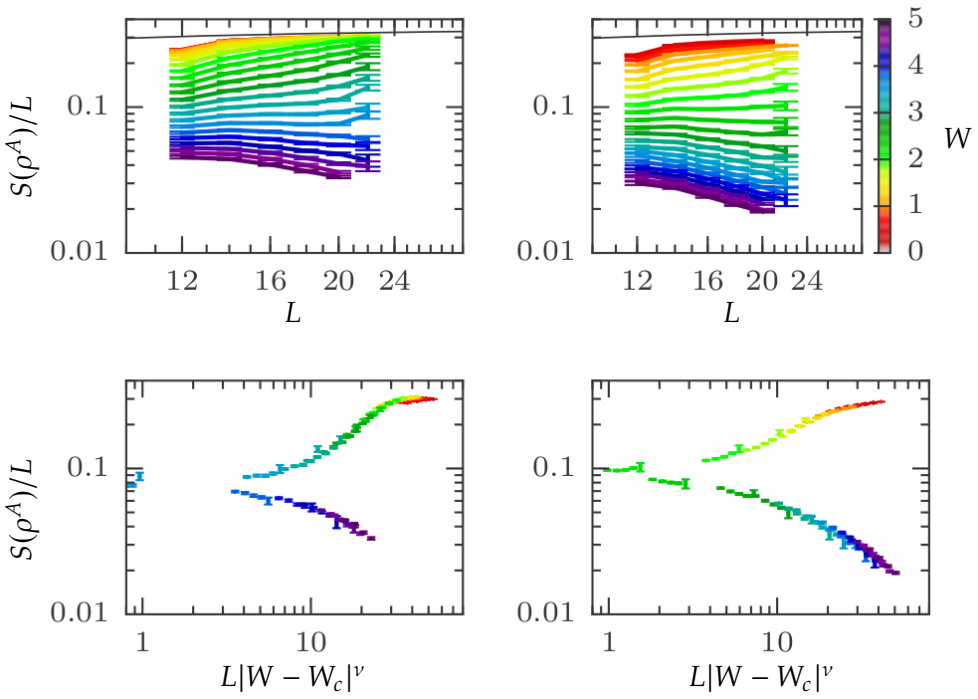

Figure 3.3. *EE per site S^E/L as a function of system size L for various disorder strength values h for the Hamiltonian (3.1). The left panels are obtained from eigenstates in the middle of the spectrum while the right panels from eigenstates located in the upper sector. The volume law scaling leading to a constant $S(\rho^A)/L$ for weak disorder is opposed to the area law at larger disorder, detected by the decrease of $S(\rho^A)/L$. Adapted from (Luitz et al. 2015).*

with A being a subsystem and L the size of the whole system. A highly excited eigenstate on the ergodic side of the MBL transition can be thought as a thermalizing state at finite temperature, and it is thus expected to follow the same extensive scaling. The alternative picture is represented by ground-states of local gapped Hamiltonians (Hastings 2007), that display an area law scaling as $S(\rho^A) = O(\delta|L|)$, thus growing with the area of the boundary between the given subregions. In the case of a 1D system, the area-law simply predicts a constant scaling for the EE $S(\rho^A) \sim$ constant. The eigenstates in the MBL phase possess drastically lower EE compared to the ergodic phase, and an area law scaling for the entire eigenspectrum at strong disorders has been confirmed by several numerical studies in models such as (3.1) and (3.2) (Bauer et al. 2013; Kjäll et al. 2014; Luitz et al. 2015; Lim et al. 2016; Khemani et al. 2017a). As an example, we report in Fig. 3.3 the results of ED simulations of model (3.1) obtained in (Luitz

et al. 2015), that show a very clear difference in the scaling of the EE density $S(\rho^A)/L$ for a bipartition of the chain at different disorder strengths $W \in [0, 5]$. For $W < W_c$, the EE density $S(\rho^A)/L$ scales as a constant as a function of L, while for $W > W_c$ it decreases for larger L, implying a sub-extensive scaling which is in contrast with the prediction for ergodic systems. The finite size scaling ansatz $f[L^{1/\nu}(W - W_c)]$ leads to a data collapse similar to what can be obtained for the level statistics (Fig.(3.2)), allowing the estimate of W_c and of the critical exponent ν. Moreover, the fluctuations of the EE have been used as a succesful diagnostic tool for the location of the MBL transition, as they display a peak at W_c (Kjäll et al. 2014; Luitz et al. 2015). Such a peak results from the high sensitivity of the entanglement properties of the system in the vicinity of the critical point, as small variations of the disorder strength select contributions coming either from extended or localized states. Thus, the variance of the EE will diverge close to criticality, providing a reliable hallmark of the MBL transition.

We would like to summarize the list of spectral measures that we discussed so far by showing the complete phase diagram of the random field Heisenberg model (3.1), obtained combining some of the diagnostics covered in this subsection. The diagram in Fig.3.4 illustrates the separation between extended and MBL eigenstates as a function of the normalized energy density $\epsilon = (E - E_0)/(E_M - E_0)$, with E_0 (E_M) the ground-state (maximum) energy in the spectrum of the Hamiltonian. The MBME separating the two phases was obtained in (Luitz et al. 2015) by an analysis of the level statistics (gap-ratio r), EE scaling (volume-law vs area-law) and its fluctuations (σ_S), as well as through other measures like the spin density correlations decay and the fluctuations of the half-chain magnetization (not presented here). The color scheme can be understood through the relation between the IPRs (3.8) and the so-called *participation (or Renyi) entropies* (Bell 1972; F. Wegner 1980; Rodriguez et al. 2011; Luitz et al. 2014b; Luitz et al. 2014a; Macé et al. 2019), defined as

$$S_q^\alpha = \frac{1}{1-q} \ln \left(\mathrm{IPR}_q^\alpha \right) \sim D_q \ln \mathcal{N}. \tag{3.10}$$

The limit $q \to 1$ returns the *Shannon entropy*

$$S_1^\alpha = \lim_{q \to 1} S_q^\alpha = - \sum_n |\langle \phi_n | \psi_\alpha \rangle|^2 \ln \left(|\langle \phi_n | \psi_\alpha \rangle|^2 \right), \tag{3.11}$$

which allows the calculation of the fractal dimension D_1, plotted in Fig 3.4, and the relative different scaling in the two regimes. Indeed, a leading scaling $S_1^\alpha =$

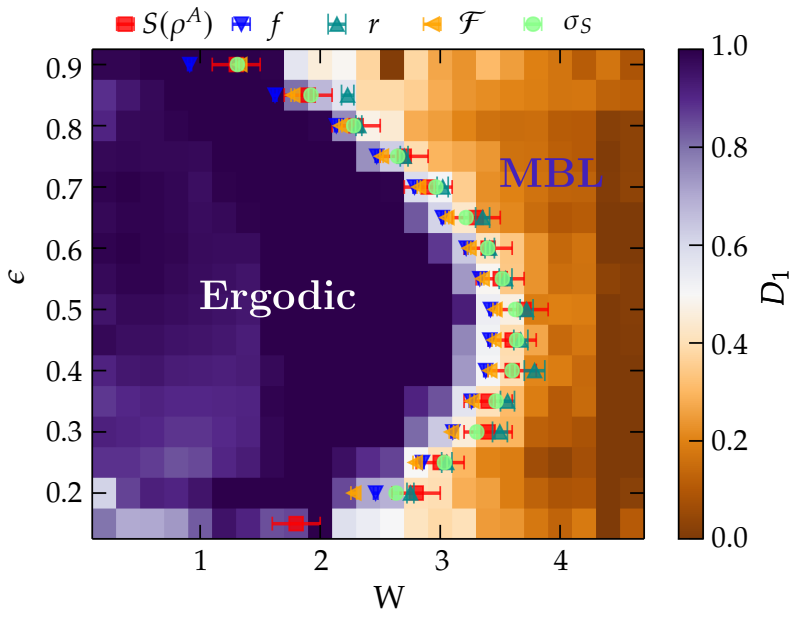

Figure 3.4. *Phase diagram of the random field XXZ Heisenberg model in* 1*D, obtained as a function of the energy density* ϵ*, normalized between* 0 *and* 1*, and the disorder strength* W*. The diagram was obtained in* (Luitz et al. 2015) *by exact diagonalization of chains of up to* $L = 22$ *spins, using different markers of the MBL transition (top symbols): the bipartite entanglement entropy (red squares), the bipartite fluctuations of the magnetization (yellow triangles) per site (blue triangles), level statistics (light blue triangles) and the entanglement entropy variance (green circles). The color scheme corresponds to the scaling of the fractal dimension* D_1*. Adapted from* (Luitz et al. 2015).

$D_1 \ln \mathcal{N}$ with $D_1 = 1$ was found in the ergodic regime, while the participation entropies grow much slower with $D_1 < 1$ at intermediate disorder strengths, ultimately reaching $D_1 = 0$ deep in the MBL phase.

3.2.4 Anomalous transport in the thermal regime

Similarly to its non-interacting counterpart, the absence of transport is a defining feature of the MBL phase, numerically established in a series of works reviewed in (Prelovšek et al. 2017; Luitz et al. 2017). The main quantity of interest in such studies is the frequency dependent conductivity

$$\sigma(\omega) = \frac{1 - \mathrm{e}^{-\beta\omega}}{2\omega} \Re\mathrm{e} \left[\int_{\infty}^{\infty} dt\, \mathrm{e}^{\mathrm{i}\,\omega t} \langle \mathcal{J}(t) J(0) \rangle \right], \tag{3.12}$$

where the spin current $\mathcal{J}$ is defines as the spin current operator for model (3.1)

$$\mathcal{J} = \frac{1}{L} \sum_{\langle ij \rangle} \left(S_i^x S_j^y - S_j^x S_i^y \right). \tag{3.13}$$

The dc part $\sigma_{dc} = \sigma(\omega \to 0)$ of the conductivity (3.12) was found to vanish at any finite temperature T in the MBL phase, $\sigma_{dc} = 0$. On the other hand, the transport scenario in the ETH phase has proven to be considerably richer than what was expected, and it is still the subject of intense debate. Indeed, the expectation in the case of a pure ergodic phase is a finite dc conductivity $\sigma_{dc} > 0$ and diffusive behavior. Surprisingly, several works instead found evidence of anomalous transport in the region preceding the MBL transition, with *subdiffusive* spin (or particle) transport (Bar Lev et al. 2014; Luitz 2016; Luitz et al. 2016b; Žnidarič et al. 2016; Schulz et al. 2018; Schulz et al. 2020). In particular, (Žnidarič et al. 2016) found that the subdiffusive behavior dominates at any finite disorder strength for strong interactions $J_z > 1$, while a transition between subdiffusive and diffusive transport appears in the regime $J_z < 1$. The boundaries of the subdiffusive regime are still disputed (Agarwal et al. 2015; Luitz et al. 2016a; Barišič et al. 2016; Khait et al. 2016), and (Bera et al. 2017) put forward the possibility that such behavior might be transient and related to finite-size effects. The origin of such anomalous transport properties has been attributed to the effects of rare spatial regions with unusually strong disorder, which act as "bottlenecks" for the transport of energy/particles (Agarwal et al. 2015). In fact, such rare regions have been first described by (R. B. Griffiths 1969; McCoy 1969) in the context of random spin systems, and are now known as *Griffiths regions*. Griffiths effects are indeed responsible for the broadening of relaxation times in thermal phases of 1D systems (Agarwal et al. 2017), as confirmed also by the phenomenological renormalization group approaches presented in (Vosk et al. 2015; Potter et al. 2015). Nonetheless, it is now clear that rare Griffiths effects may not be the only ones responsible for the slow transport on the ergodic side of the MBL transition, as evidence of subdiffusive behavior was found also in quasi-periodic systems (Naldesi et al. 2016; Lev et al. 2017; M. Lee et al. 2017), which are known to be devoid of such rare effects.

3.2.5 Quantum quenches and entanglement growth

A further clear distinction between the ergodic and the MBL phase, which concludes this overview, is found in the peculiar behavior of the EE after a

quantum quench (see Sec. 1.2.2). Despite being characterized by the absence of transport, MBL systems display a slow spreading of entanglement in time. The propagation of entanglement is one of the most notable hallmarks of MBL, as it represents a peculiar feature that is not shared with AL, and thus serves as a definite probe of the uniqueness of MBL systems. Let us imagine a general quench protocol: we initialize a 1D spin chain in a typical state $|\psi_0\rangle$, such as a product state in the S^z basis, and we monitor unitary dynamics generated by the Hamiltonian (3.1). In the ETH regime, the state is expected to reach thermal equilibrium, with a temperature dependent on the energy of $|\psi_0\rangle$. As we mentioned in 1.2.1, thermalization is accompanied by a rapid scrambling of the information encoded in the structure of $|\psi_0\rangle$. Consider for example the Neel state $|\psi_0\rangle = |\uparrow,\downarrow,\uparrow,\downarrow,\ldots\rangle$, which has a maximum value of the staggered magnetization, or *spin imbalance*,

$$I(t=0) = \frac{2}{L}\sum_i (-1)^i \langle\psi_0|S_i^z|\psi_0\rangle = 1. \tag{3.14}$$

In the limit of long times, the state will evolve towards a thermal state $\psi(\infty)$ and the imbalance will tend to its thermal expectation value, i.e. $I(t\to\infty)$=0. The ergodic regime is further characterized by ballistic growth of the bipartite EE of the evolved state $|\psi(t)\rangle$, i.e. $S(t) \sim t$ (Kim et al. 2013), eventually leading to a saturation value $S(\infty) \sim L + O(\frac{\ln L}{L})$ (Page 1993), thus following a volume-law scaling. If, on the other hand, the disorder is sufficiently strong to enter the MBL phase, local observables such as $I(t)$ are expected to decay to steady values that are not predicted by any statistical ensemble. Thus, the imbalance $I(t)$ may preserve part of the initial structure by saturating to finite values $I(\infty) > 0$ (Serbyn et al. 2014), as also observed in cold-atoms experiments (M. Schreiber et al. 2015). The failure of thermalization in MBL systems is marked by a characteristic logarithmic growth of the EE in time, $S(t) \sim \ln t$ (Žnidarič et al. 2008; Bardarson et al. 2012; Serbyn et al. 2013a; Andraschko et al. 2014). The non-interacting AL case is instead characterized by an early saturation of the EE and the absence of further propagation, $S(t) \sim$ constant. Moreover, the saturation value $S(\infty)$ in the MBL phase is still scaling with L as in the ETH case, but with a *smaller* pre-factor, thus reaching lower values than the ones expected in the extended phase (Bardarson et al. 2012).

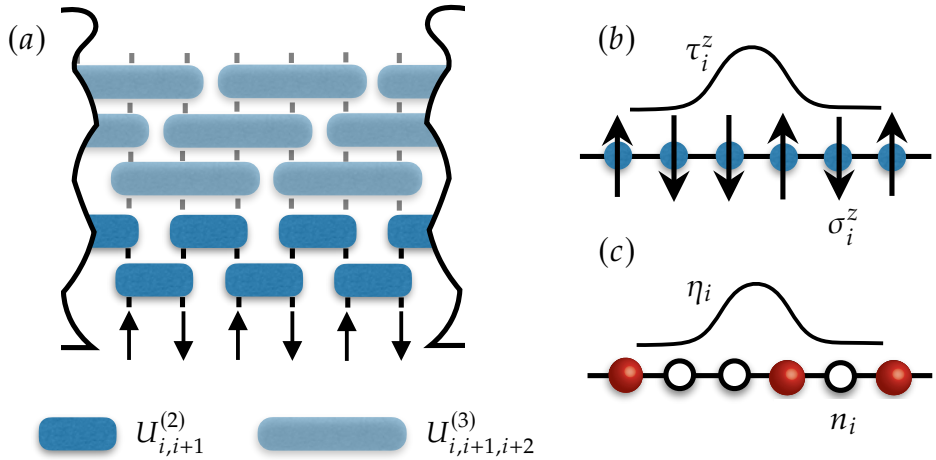

Figure 3.5. (*a*) *An initial product state is rotated applying a sequence of quasi-local unitary transformations.* (*b*) *The original spin operators* σ_i^z *are transformed into quasi-local operators (l-bits)* τ_i^z*, acting as effective local integrals of motion.* (*c*) *Same as* (*b*) *in fermion language*: *the number operators* n_i *are mapped onto the dressed operators* η_i*. Adapted from* (*Abanin et al.* 2019).

3.3 Phenomenology of MBL systems

We present here the description of an effective theory for the MBL phase that represents a unifying framework able to explain most of the phenomenology presented in the previous discussion. The basic intuition stems from the low entanglement structure of eigenstates in the MBL phase, characterized by the area-law discussed Sec. 3.2. As MBL eigenstates possess a very low degree of entanglement, they can be connected to product states by a sequence of *quasi-local* unitary transformations (Serbyn et al. 2013b), that are able to diagonalize the Hamiltonian of the system in a given basis made of product states. [4] Let us consider a simplified version of (3.1) deep in the MBL phase ($W \gg W_c$) in the limit $J \to 0$,

$$\mathcal{H}_0 = J_z \sum_{\langle ij \rangle} \sigma_i^z \sigma_j^z + \sum_i h_i \sigma_i^z. \tag{3.15}$$

Such a model is trivially integrable as the Hamiltonian commutes with σ_i^z

[4] We remind the reader that product states are non-entangled states, defined in Sec. 1.1.4

for each site, and the eigenstates are simple product states of the form

$$\{|\sigma\rangle\} = |\sigma_1, \sigma_2, \ldots, \sigma_{\mathcal{N}}\rangle\,, \tag{3.16}$$

with $\sigma_i = \{\uparrow, \downarrow\}$ and $\mathcal{N} = 2^L$. Turning on a weak spin-flip (hopping) term J leads to the Hamiltonian not being diagonal in the $\{|\sigma\rangle\}$ basis anymore. Nonetheless, one could define a quasi-local unitary transformation U with a finite spatial support that can be factorized into a sequence of unitary operators as

$$U = \prod_i \ldots U^{(3)}_{i,i+1,i+2} U^{(2)}_{i,i+1}, \tag{3.17}$$

through which the new eigenstates can be obtained starting from the product states (3.16) (see Fig. 3.5 for a schematic illustration). The quasi-locality is induced by the peculiar area-law structure of the MBL eigenstates: for a thermalizing systems, the transformation U becomes highly non-local, rotating the product states into volume-law eigenstates. Applying U to the product states (3.16) leads to the definition of the so-called *local integrals of motion* (LIOMS) (also known as *l-bits)*

$$\tau^z_i = U \sigma^z_i U^\dagger, \tag{3.18}$$

which form a complete set of independent and commuting operators, i.e. $[\tau^z_i, \tau^z_j] = 0$ and $\left[\tau^z_i, \mathcal{H}\right] = 0$. The l-bits have a finite overlap with the original spin operators σ^z_i, decaying exponentially with the distance from the original sites. In other words, the τ^z_i can be written as

$$\tau^z_i = A_i \sigma^z_i + \sum_{i \neq j} C_{i+j} \sigma^z_j, \tag{3.19}$$

with $A_i < 0$ and the terms C, decaying exponentially as $C_{i+j} \sim e^{-|j|/\xi_\tau}$ with a certain localization length ξ_τ. The τ^z_i operators can thus be viewed as a "dressed" version of the underlying spin operators, or as *pseudo-spin* degrees of freedom, which are particularly useful for the description of MBL systems. [5] Indeed, a general MBL Hamiltonian can be expressed in terms of the l-bits in the general form (Serbyn et al. 2013b; Huse et al. 2014)

$$\mathcal{H}_{MBL} = \sum_i \tilde{h}^z_i \tau^z_i + \sum_{i>j} J_{ij} \tau^z_i \tau^z_j + \sum_{i>j>k} J_{ijk} \tau^z_i \tau^z_j \tau^z_k + \ldots, \tag{3.20}$$

[5] One could, of course, define similar τ^z_i operators also in the case of thermalizing systems; however, the resulting operators would be highly non-local and hence not particularly useful.

with the coupling terms $J_{ijk\ldots}$ decaying exponentially with the separation between the l-bits as

$$J_{ijk\ldots l} \sim \mathrm{e}^{-|i-l|/\xi_{MBL}}, \tag{3.21}$$

where the localization length ξ_{MBL} is not necessarily equal to ξ_τ. The interaction terms $J_{ijk\ldots}$ are important in distinguishing between the many-body and the non-interacting scenarios, as the AL case is exactly recovered in the case of vanishing couplings.

The quasi-locality of the unitary U, and thus the validity of the universal form (3.20), was a central result of the (so-far) only rigorous proof of the existence of the MBL phase, obtained by (Imbrie 2016) for a strongly disordered Ising model with transverse and longitudinal fields.[6] From the l-bits framework, one can recover all the properties of the MBL phase that we discussed in this Chapter. For instance, the area-law for the MBL eigenstates and the Poisson level statistics emerge naturally by the simple labelling of the eigenstates of (3.20) given by the set of eigenvalues ± 1 for each τ_i^z, e.g., $|1, 1, -1, \ldots\rangle$. Memory effects in the out-of-equilibrium dynamics, as well as the long-time relaxation of local observables to non-thermal values, can be deduced from the finite overlap of such observables with the conserved operators τ_i^z. The interactions between l-bits intervene crucially in the dynamics, marking the difference with the AL case, as they provide a mechanism for dephasing. Indeed, each l-bit precesses around the z-axis at a rate set by its interactions with all other τ_i^z, producing entanglement at long distances and thus dephasing. Such dephasing process is peculiarly slow, and the logarithmic growth of entanglement, characteristic of MBL, is induced by the exponentially weak interactions between the l-bits.

The existence of a set of local integrals of motion built as dressed versions of physical degrees of freedom is a central feature of MBL systems, from which all the major static and dynamical properties of the MBL phase originate naturally. The explicit construction of the relevant set of l-bits is in general model dependent; an approximate method for the construction of l-bits in arbitrary dimensions has been proposed in (Ros et al. 2015), employing perturbative techniques similar to the self-consistent approximation used in the seminal work of (Basko et al. 2006). Further advancements came in the form of numerically constructed sets of local integrals of motion (Chandran et al. 2015; O'Brien et al. 2016; Rademaker et al. 2016; Pekker et al. 2017b; Thomson et al. 2018). In the next Chapter, we will build an explicit set of approximate l-bits in the

[6] It is worth noting that the proof relies on minimal assumptions on the energy level statistics of the system Hamiltonian, limiting the attraction between neighboring eigenenergies.

strong disorder regime of localized systems in the presence of both fully random or quasi-periodic potentials, building an effective model able to provide *exact* quantitative predictions for a variety of dynamical probes of localization.

3.4 Experimental realizations of MBL

The main experimental challenge in realizing MBL regards the requirement of maintaining the system under study isolated from the environment. As we mentioned already in 1.2, the progress in the field of quantum simulators based on cold atoms and ions has allowed the exploration of non-equilibrium phenomenon with almost perfect isolation and very small coupling with the environment. Indeed, the first successful attempts of observing MBL at high energy densities appeared in cold atoms platforms (M. Schreiber et al. 2015), where quantum quench protocols of the type described in 1.2.2 led to the observation of nonthermal relaxation of local observables, thus probing the failure of ETH. In particular, (M. Schreiber et al. 2015) realized a generalization of the AA model (2.41) with 1d Fermi-Hubbard chains of interacting spin mixtures in the presence of a quasi-periodic potential landscape, obtained by super-imposing an optical lattice with incommensurate spacing with respect to the lattice hosting the particles. The Fesbach resonances between the different atomic spin states allow one to tune the interaction coupling between the particles (Bloch et al. 2008). The resulting Hamiltonian can be described as

$$\mathcal{H} = -J \sum_{\langle ij \rangle} \left(c^{\dagger}_{i,\sigma} c_{j,\sigma} + h.c. \right) + \Delta \sum_{i} \cos\left(2\pi\beta i + \phi\right) n_{i,\sigma} + U \sum_{i} n_{i,\uparrow} n_{i,\downarrow}, \quad (3.22)$$

where $c^{\dagger}_{i,\sigma}$ ($c_{i,\sigma}$) is the creation (annihilation) fermionic operator at site i with spin state $\sigma = \{\uparrow, \downarrow\}$, U is the onsite interaction strength and Δ is the quasi-periodic potential amplitude. The system was then initialized in a density wave state with particles occupying mostly even sites. [7] The main observable employed in the study was the particle imbalance

$$I(t) = \frac{1}{L} \sum_{i} (-1)^{i} (2[\langle n_i \rangle]_{\text{av}} - 1) \,, \quad (3.23)$$

where the notation $[\dots]_{av}$ indicates an average over different realizations of the potential. The imbalance clearly saturates to a value close to 1 in a configuration

[7] This configuration corresponds to an almost perfect antiferromagnetic arrangement in spin language.

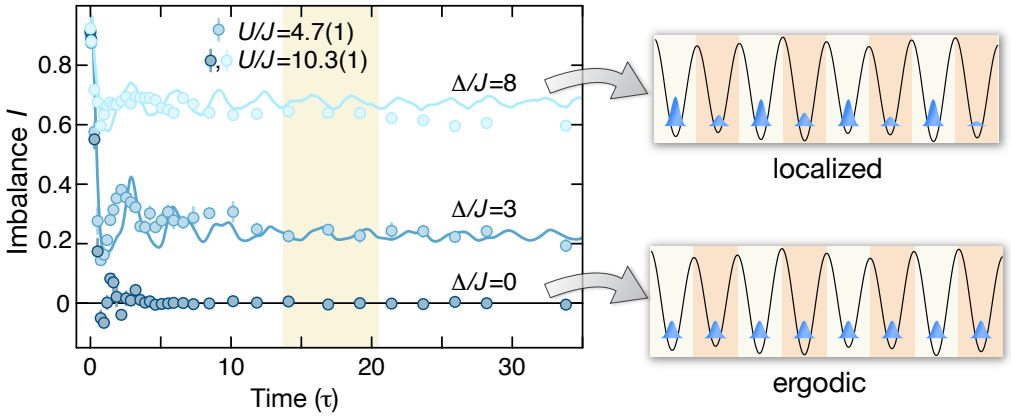

Figure 3.6. *Non-equilibrium dynamics of a density wave state in the presence of a quasi-periodic potential of strength Δ. The dots are experimental measurements of $I(t)$ obtained at different values of Δ and at different time stamps. Solid lines are DMRG simulations. Adapted from (M. Schreiber et al. 2015).*

such as the chosen density wave state. By monitoring the evolution driven by (3.22) and measuring $I(t)$ one can thus keep track of the evolution of the density profile, obtaining clearly different behaviors for weak or strong Δ, as shown in 3.6. Indeed, for weak potential strengths $\Delta \to 0$, the imbalance rapidly decays towards zero, as expected in the case of relaxation towards a thermal state in which the particles occupy even and odd sites with equal probability. Increasing Δ leads to the saturation of $I(t)$ to finite non-vanishing values, marking the crossover to a non-thermalizing regime which was reported as the manifestation of MBL.

Following experimental efforts enriched the overall picture. For instance, (Bordia et al. 2016) probed the delocalization effects induced by the coupling of several 1d quasi-periodic chains. In (J. Y. Choi et al. 2016), the persistence of a wall-domain in a 2d boson gas subject to a random laser pattern suggested the existence of MBL in two dimensions, a possibility which is still debated from a theoretical perspective. Furthermore, a remarkable work by (Lukin et al. 2019) presented the first observation of the logarithmic spreading of entanglement discussed in 3.2.5 in small quasi-periodic Bose-Hubbard chains. Experiments with other quantum simulation platforms provided further evidence. A disordered quantum Ising Hamiltonian was realized in (Smith et al. 2016) with trapped ions, encoding effective spin-1/2 particles in hyperfine states of the atoms. Measurements of the evolution of single-site magnetization, starting from a Neél state $|\psi_0\rangle = |\uparrow,\downarrow,\uparrow,\downarrow,\ldots\rangle$ exhibited stationary values over a certain critical disorder

strength, a memory signature associated with MBL. Interestingly, trapped ions quantum simulators present the capability of tuning the interaction or hopping range, thus allowing the exploration of localization effects in long-range models, which represent an active field of research. In fact, the question of whether sufficiently long-range hopping (or interactions) is sufficient to destroy localization is a long-standing question both in AL (Anderson 1958; Levitov 1990) and MBL (Yao et al. 2014; Burin 2015; Li et al. 2016; R. M. Nandkishore et al. 2017) studies. Superconducting circuits have emerged as another powerful tool in the study of tunable quantum many-body systems (Houck et al. 2012). In the context of MBL, (Roushan et al. 2017) developed a novel spectroscopy techniques to obtain information of the eigenenergies and thus on the level statistics of the simulated Hamiltonian, showing clear differences in the disordered vs the clean case already at the level of two-particles. Very recently, (Q. Guo et al. 2021) explored MBL using a 19-qubit programmable superconducting processor, reporting the observation of a MBL transition in an energy-resolved fashion, paving the way for the experimental investigation of MBMEs.

Part II

Signatures of localization via quantum quenches

4

Singularities in strongly localized dynamics

As we discussed in Chapters 3 and 2, localized phases are generally characterized in the negative (absence of transport, of long-range order, of level repulsion, etc.), while positive characterizations are typically elusive. A crucial aspect of localization is the persistence of initial conditions, which, in the case of AL of non-interacting particles, is related to the conservation of populations in the localized single-particle eigenstates of the Hamiltonian. In the case of MBL, the analog phenomenon would be the appearance of the l-bits presented in Sec. 3.3, whose existence directly explains much of the phenomenology of MBL dynamics. Yet observing direct effects of the existence of l-bits is an arduous task, given that their expression is highly disorder-dependent (and generally unknown even in theory), and would require high-precision measurements of local observables in different local bases. An even more ambitious task for experiments is the one of probing directly the existence of interactions among l-bits, which is a defining feature distinguishing MBL from AL. Measuring the consequences of such interactions on correlation and entanglement dynamics is currently the focus of a considerable experimental effort based on state-of-the-art quantum simulation platforms (Rispoli et al. 2019; Lukin et al. 2019; Chiaro et al. 2020). The purpose of this work is to show that, in the case of strongly localized phases, both in the presence and absence of many-body interactions, the existence of l-bits can offer striking signatures in the dynamics of the survival probability (2.25). More precisely, we will focus on the logarithm of the survival probability with respect

to the initial state $|\psi_0\rangle$, i.e.

$$\lambda(t) = -\frac{1}{L}\left[\log|\langle\psi_0|e^{-i\mathcal{H}t}|\psi_0\rangle|^2\right]_{\text{av}} . \tag{4.1}$$

Here $\mathcal{H}$ is the system's Hamiltonian and L the lattice size; $[...]_{\text{av}}$ indicates the disorder average. When $|\psi_0\rangle$ has a simple factorized form, and in the case of strong disorder, we will show that the survival probability displays periodic singularities, decaying very slowly in amplitude – as illustrated using a model of disordered spinless fermions in 1d (corresponding to the $S = 1/2$ XXZ model in a fully random or quasi-periodic field) initialized in a *charge density wave* (CDW) state. The singularities in the survival probability are very well explained quantitatively by a simple model of a collection of localized *2-level systems* (2LS) undergoing independent Rabi oscillations (D. J. Griffiths et al. 2018), and approximating strongly localized l-bits. The same minimal model captures quantitatively the dynamics of the entanglement entropy at short times as well as of the number entropy at longer times; and the dynamics of the density imbalance characterizing the initial state.

At longer times the deviation of the exact results for the MBL dynamics from the predictions of the 2LS ensemble offers direct evidence of the interactions among the l-bits in the form of a faster decay of the Loschmidt-echo singularities and imbalance oscillations. As the survival probability and the imbalance are generally accessible to quantum simulators, either measuring individual degrees of freedom (Gärttner et al. 2017; Jurcevic et al. 2017) or even global ones (M. Schreiber et al. 2015; Bordia et al. 2016; Lüschen et al. 2017), our results show that strong direct signatures of l-bits dynamics and interactions are within the immediate reach of state-of-the-art experiments on disordered quantum systems. The structure of the paper is as follows: section 4.1 introduces the XXZ model in a random/quasi-periodic field; section 4.2 discusses the observation of survival probability singularities in the exact dynamics and their quantitative understanding via a model of 2LS as well as *3-level systems* (3LS); section 4.5 discusses the dynamics of imbalance, and the comparison with the prediction of the 2LS and 3LS model; section 4.6 discusses the departure of the exact data (for the survival probability and imbalance dynamics) from the 2LS/3LS predictions as a signature of l-bit interactions; section 4.7 shows that the 2LS/3LS models capture quantitatively the entanglement dynamics at short time, and of the number entropy at longer times; conclusions are drawn in section 4.9.

4.1 Model

Our platform for the investigation of the return probability dynamics is given by the paradigmatic models (3.1) and (3.2), that we rewrite here in both spin and fermion language as

$$\begin{aligned}\mathcal{H} &= \sum_{i=1}^{L-1}\left[-\frac{J}{2}\left(S_i^+S_{i+1}^- + \text{h.c.}\right) + J_z S_i^z S_{i+1}^z\right] - \sum_{i=1}^{L} h_i S_i^z \\ &= \sum_{i=1}^{L-1}\left[-\frac{J}{2}\left(c_i^\dagger c_{i+1} + \text{h.c.}\right) + J_z n_i n_{i+1}\right] - \sum_{i=1}^{L} h_i n_i,\end{aligned} \tag{4.2}$$

where h_i is taken to be either a *quasi-periodic* (QP) potential (Schuster et al. 2002; Iyer et al. 2013), namely $h_i = \Delta\cos(2\pi\beta i + \phi)$ with $\beta = 0.721$ (inspired by experiments on bichromatic optical lattices (M. Schreiber et al. 2015; Kohlert et al. 2019)) and ϕ a random phase [1]; or to be *fully random* (FR) and uniformly distributed in the interval $[-\Delta, \Delta]$. The QP case represents the many-body extension of the AA model (2.43). We consider chains of length L (up to $L = 22$) with open boundaries, and we average our results over $\sim 10^3$ realizations of the random phase (QP) or of the full random potential (FR). All the unitary evolutions considered in this study are obtained using exact diagonalization (ED), and they start from the charge-density wave state $|\psi_0\rangle = |1010101...\rangle$, corresponding to a Néel state for the spins. We shall focus on the case of interacting fermions $J_z = J$ (corresponding to an SU(2) invariant spin-spin interaction) and contrast it with the limit of free fermions $J_z = 0$. In the latter case, the QP potential leads to a transition to fully localized single-particle eigenstates for $\Delta \geq J$, with an energy independent localization length $\xi = 1/\log(\Delta/J)$; while the FR potential leads to AL of the whole spectrum at any infinitesimal value of disorder. In the interacting case, instead, a QP potential of strength $\Delta \gtrsim 4J$ (Naldesi et al. 2016) and a FR potential of strength $\Delta \gtrsim 3.5J$ (Luitz et al. 2015; Devakul et al. 2015; Khemani et al. 2017b; Doggen et al. 2018; Doggen et al. 2019; Weiner et al. 2019; Sierant et al. 2020; Laflorencie et al. 2020) are numerically found to lead to MBL.

In the following sections we shall generally start our discussion from the case of the QP potential, which has a simpler spatial structure devoid of rare regions, leading to stronger localization effects; and we shall later discuss how to enrich the picture in the case of the FR potential, in order to account for the existence of rare regions.

[1] The quasi-periodicity is assured by the fact that the systems studied here are of finite size.

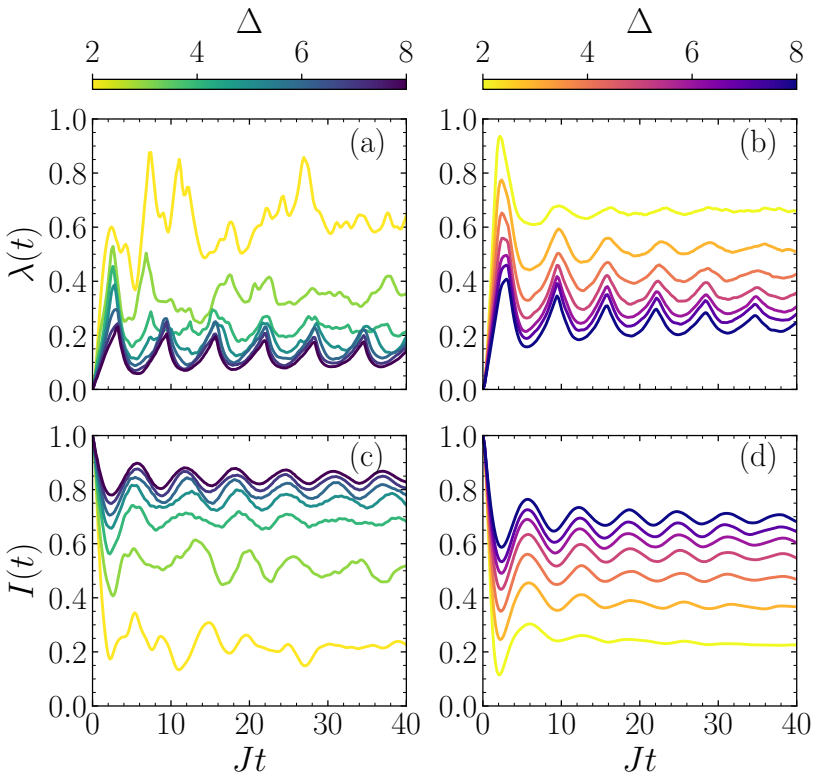

Figure 4.1. *Survival probability and imbalance dynamics for an $L = 22$ chain with QP potential (a-c) and FR potential (b-d), for various disorder strengths $\Delta = 2, \ldots, 8$ as indicated by the colors.*

4.2 Survival probability singularities and imbalance oscillations

Figure 4.1 shows the dynamics of the survival probability $\lambda(t)$ (4.1), along with that of the imbalance (3.23). The latter saturates to its maximum value of 1 in the initial state and probes the persistence of the initial density/spin pattern (M. Schreiber et al. 2015; Bordia et al. 2016; Lüschen et al. 2017). We observe that for both the QP and FR potentials, and for disorder strengths compatible with the onset of the MBL regime, the survival probability displays a sequence of periodic cusp-like peaks at times $t_m = (2m + 1)\pi/J$ ($m = 0, 1, 2, \ldots$). These times correspond almost exactly to minima in the imbalance, as the system reaches instantaneous configurations which are the farthest from the initial spin/density pattern. A closer inspection shows that, for sufficiently strong disorder, all the peaks become sharp cusps, namely they represent genuine non-analyticities of the survival probability. They are rather remarkable given that they survive

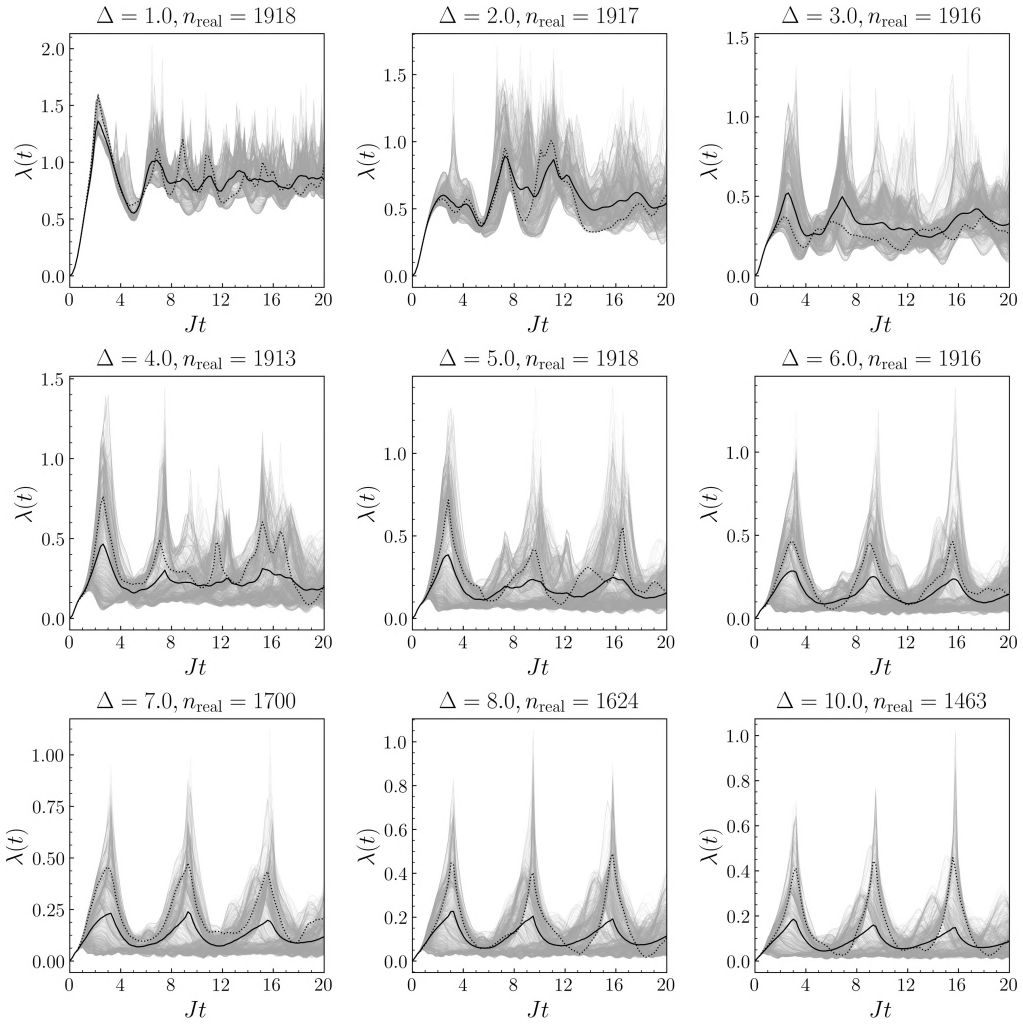

Figure 4.2. *Averaged $\lambda(t)$ (black line) at different disorder strengths $\Delta = 1, \ldots, 10$ for a chain of $L = 22$ sites in a QP, plotted along with all the realizations (n_{real} is the number of realizations) used for the averaging procedure (grey lines). The dotted line represents a typical individual realization exhibiting singular behavior.*

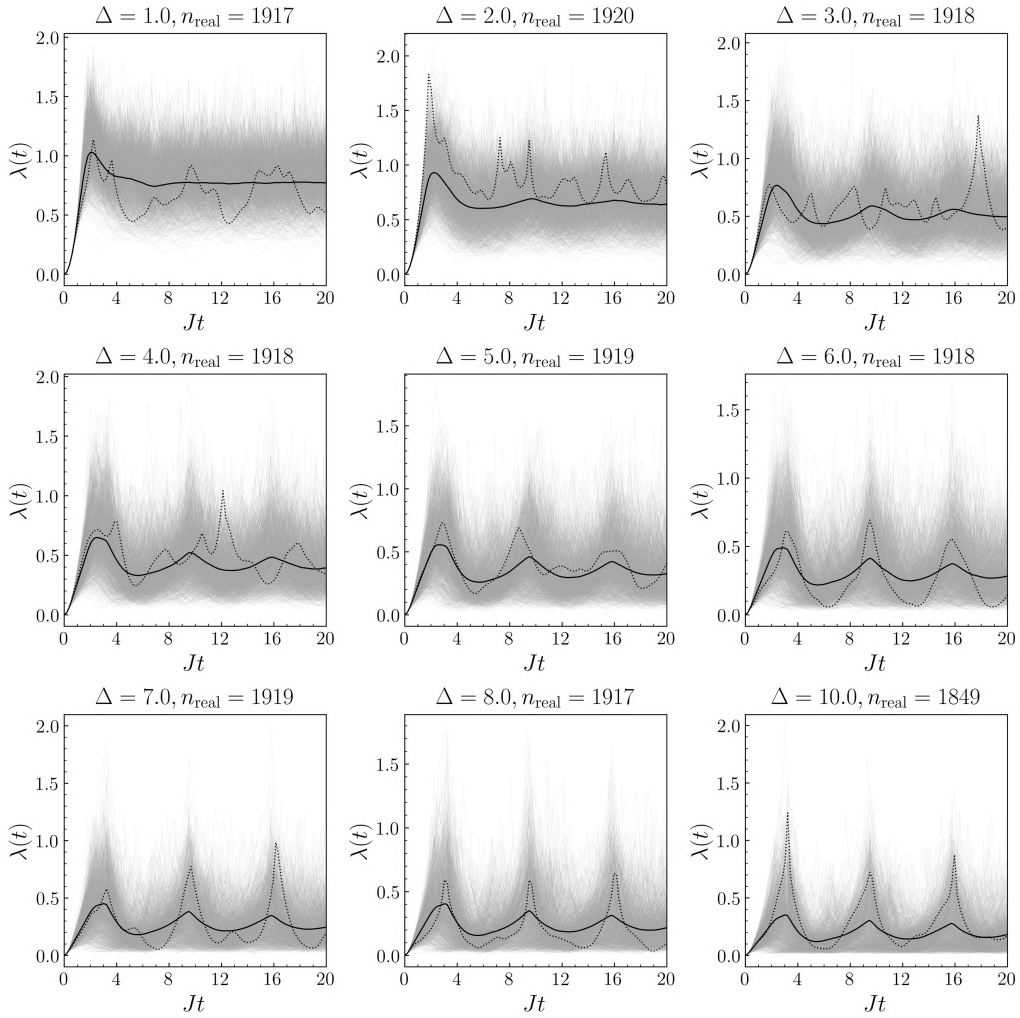

Figure 4.3. *Averaged $\lambda(t)$ (black line) at different disorder strengths $\Delta = 1, \ldots, 10$ for a chain of $L = 22$ sites in a FR potential, plotted along with all the realizations (n_{real} is the number of realizations) used for the averaging procedure (grey lines). The dotted line represents a typical individual realization exhibiting singular behavior.*

disorder averaging, and they appear in a finite fraction of disorder realizations that does not vanish as we increase the number of realizations, signalling the robustness of the phenomenon; and in particular they decay very slowly in time, as we shall discuss in detail later on. Indeed, Figs. 4.2 and 4.3 show the disorder average of the Loschmidt echo for a chain of $L = 22$ sites, along with all the disorder realizations ($\sim O(10^3)$) contributing the average, for various strengths ($\Delta/J = 1, 2, ..., 10$) of the QP and FR potential, respectively. We observe that sharp cusp singularities are exhibited by a signification portion of the disorder realizations, and that for sufficiently strong disorder these realizations are a finite fraction of the disorder statistics (in the asymptotic limit), so that cusp singularities persist in the disorder-averaged results as well. These plots also suggest the fact that cusp singularities can be observed with a limited disorder statistics, under realistic experimental conditions.

The rest of this Chapter will be devoted to developing a quantitative understanding of the dynamics of Loschmidt-echo singularities and imbalance oscillations as signatures of the existence of l-bits and of their interacting nature.

4.3 Quantitative modeling of the survival probability singularities

All the essential details of the short-time evolution of the survival probability can be captured with a surprisingly simple, yet rather insightful model. This model is best understood (and justified) in the case of the QP potential, as illustrated in figure 4.4. In the case of strong amplitude Δ, the fastest dynamics in the system starting from a Fock state will be offered by those particles that sit on a site i which is nearly resonant with its unoccupied neighbor (say $i + 1$), because the hopping $J/2$ is either larger than the energy offset $\delta_i = h_{i+1} - h_i$ (in the non-interacting case) or larger than the screened offset $\delta_i - J_z$ (in the presence of nearest-neighbor repulsion). These 2-site clusters, representing nearly resonant 2LS, have the property of being spatially isolated in the QP potential, because of the strong anticorrelation among two consecutive energy offsets (δ_i and $\delta_{i\pm1}$ – see 4.4). As a consequence, a nearly resonant 2-site system will be generally surrounded by highly non-resonant pairs of sites, which can be considered as nearly frozen to the initial state.

Let us isolate a two-site system $(i, i+1)$ hosting one particle in the fermionic

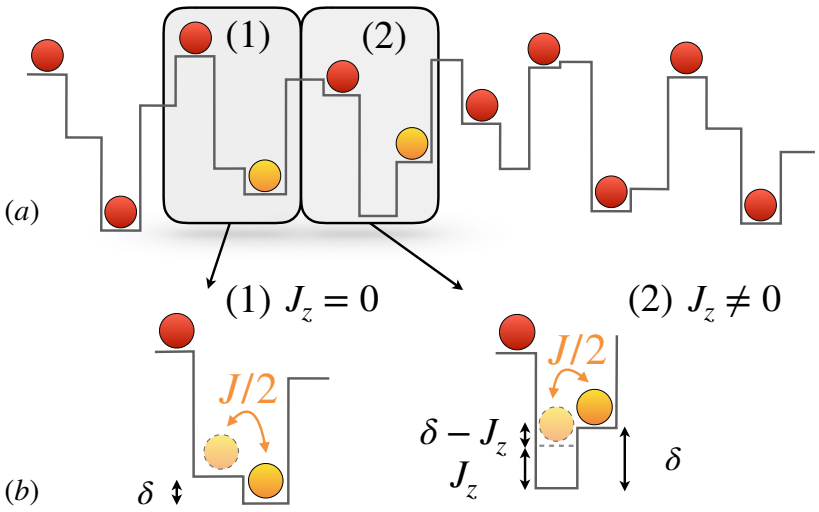

Figure 4.4. (*a*) *Example of a* $L = 22$ *chain in a QP potential* (*lines*) *in the initial CDW state* $|1010\ldots\rangle$. *Particles are denoted as coloured balls.* (*b*) *Zoom on two quasi-resonant regions* (*shaded areas*): *in the case of non-interacting particles* ($J_z = 0$) *the region* (1) *presents a pair of quasi-resonant sites for the particle in orange; in the case of interacting particles, region* (2) *shows two quasi-resonant sites for the orange particle, thanks to the partial screening of disorder offered by the interaction with the red particle.*

chain, with Hamiltonian

$$\mathcal{H}_{2-\text{site}} = -\frac{J}{2}\left(c_i^\dagger c_{i+1} + c_{i+1}^\dagger c_i\right) + h_i n_i + (h_{i+1} + J_z) n_{i+1}, \tag{4.3}$$

where we assume that the site $i+2$ is occupied by a (pinned) particle, while size $i-1$ is empty (or occupied by a pinned hole). Introducing the spin operators

$$\begin{aligned} \sigma^z &= n_i - n_{i+1}, \\ \sigma^x &= c_i^\dagger c_{i+1} + c_{i+1}^\dagger, c_i, \end{aligned} \tag{4.4}$$

the Hamiltonian becomes simply

$$\mathcal{H}_{2-\text{site}} = -\frac{J}{2}\sigma^x + \frac{\delta}{2}\sigma^z + \text{const.}, \tag{4.5}$$

namely, a 2LS with splitting δ and Rabi frequency J. If the system starts from the $|10\rangle$ state, the return probability is given by the well-known formula for the probability of persistence in the initial state during Rabi oscillations (Scully et al.

1997), namely $1 - p(\delta; t)$, which in our case is

$$p(\delta; t) = \frac{1}{1 + (\delta/J)^2} \sin^2\left(\frac{\sqrt{1 + (\delta/J)^2}}{2} tJ\right) . \tag{4.6}$$

The above discussion invites us to write for the evolved state a 2LS Ansatz

$$|\psi(t)\rangle \approx \left(\otimes_p |\psi_{2LS}^{(p)}(t)\rangle\right) \otimes \left(\otimes_i' |\psi_{0,i}\rangle\right) , \tag{4.7}$$

where the first tensor product $\otimes_p$ runs over the nearly resonant 2LS, while the second tensor product $\otimes_i'$ runs over the leftover sites (we have taken the freedom of reordering the sites arbitrarily in the tensor product). [2] $|\psi_{2LS}^{(p)}(t)\rangle$ is the evolved state of the p-th (isolated) 2LS system, corresponding to two states split by an energy difference $\delta_p' = \delta_p - J_z$ and connected by a Rabi coupling J; while $|\psi_{0,i}\rangle$ is the (persistent) initial state of the site i belonging to the remainder of the system. The survival probability for such a system is readily calculated as

$$\lambda(t) = -\frac{1}{L} \sum_p \log\left[1 - p(\delta_p', J, t)\right] , \tag{4.8}$$

with $p(\delta, \Omega, t) = (\Omega/\Omega')^2 \sin^2(\Omega' t/2)$ (and $\Omega' = \sqrt{\Omega^2 + \delta^2}$) the probability of finding the 2LS in the state orthogonal to the initial one while performing Rabi oscillations with frequency Ω (Scully et al. 1997). When averaging Eq. (4.8) over disorder, it is immediate to obtain the following simple expression

$$\lambda_{2LS}(t) = -\int d\delta' P(\delta' + J_z) \log\left[1 - p(\delta'; J, t)\right] , \tag{4.9}$$

where $P(x)$ is the probability that the energy offset between two neighboring sites takes the value x. Going from Eq. (4.8) to Eq. (4.9) implies that we in fact count all of the L pairs of sites in a chain as nearly resonant 2LS, thereby counting twice every site. The mistake that one makes in doing this is minor, though, because the non-resonant pairs of sites give a very small contribution to the survival probability; and, if neighboring pairs of sites are not simultaneously resonant, a site will not be counted twice in practice. Eq. (4.9) is an analytical integral formula which depends uniquely on the (known) statistics of the disorder potential via

[2] See (Sierant et al. 2017a; Sierant et al. 2017b; Janarek et al. 2018) for a similar Ansatz to study the long-time dynamics

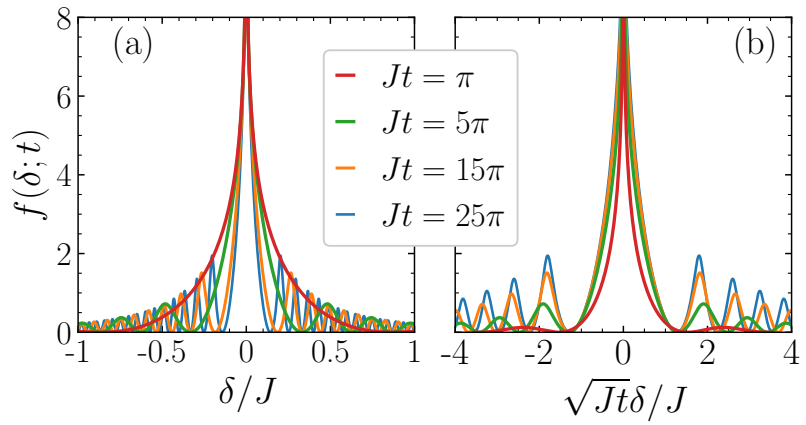

Figure 4.5. *Function $f(\delta;t)$ vs. δ at different singularity times $t_m J = (2m+1)\pi$; as shown in the right panel, for large t_m the width of the central peak becomes time-independent when f is plotted as a function of $\sqrt{t}\,\delta$.*

the P distribution. In the case of the QP potential

$$P(x) = \frac{[1-(x/\tilde{\Delta})^2]^{-1/2}}{\pi\tilde{\Delta}} \tag{4.10}$$

with $\tilde{\Delta} = \Delta\sin(\pi\beta)$ (Guarrera et al. 2007); while for the FR potential $P(x)$ is the normalized triangular distribution defined on the $[-2\Delta, 2\Delta]$ interval.

The cusp singularities in $\lambda(t)$ at times $t_m J = (2m+1)\pi$, $m = 0, 1, 2, \ldots$, descend from the fact that the integrand function $f(\delta;t_m) = \log[1-p(\delta, J, t_m)]$, seen as a function of δ, develops a logarithmic singularity at $\delta = 0$, as shown in figure 4.5, while it is fully regular at any other time. The singular peak centered at $\delta = 0$ has a support shrinking with t_m as $t_m^{-1/2}$ – as seen in figure 4.5 when plotting the function $f(\delta;t_m)$ vs $\delta\sqrt{t_m}$. This leads to a collapse of the peak widths at different times (when $m \gg 1$). The integral of the f function outside the peak contributes to the regular part of the survival probability, while the integral of the peak dictates fundamentally the height of the cusps above the regular background (estimated as the long-time average $\bar{\lambda}$), namely the quantity $\lambda_P(t_m) = \lambda(t_m) - \bar{\lambda}$. The decay of the height of these cusps as $t_m^{-1/2}$ will be verified numerically in section 4.6. Figure 4.6(a-b) shows that, for the case of the QP potential, Eq. (4.9) is able to predict with high accuracy the ED results deep in the MBL phase without *any* adjustable parameter. In particular the cusp singularities of the ED results are easily explained as descending from the divergent singularity of the survival probability for a fully resonant 2LS with $\Omega = \Omega' = J$, reaching a state orthogonal to the initial one after odd multiples

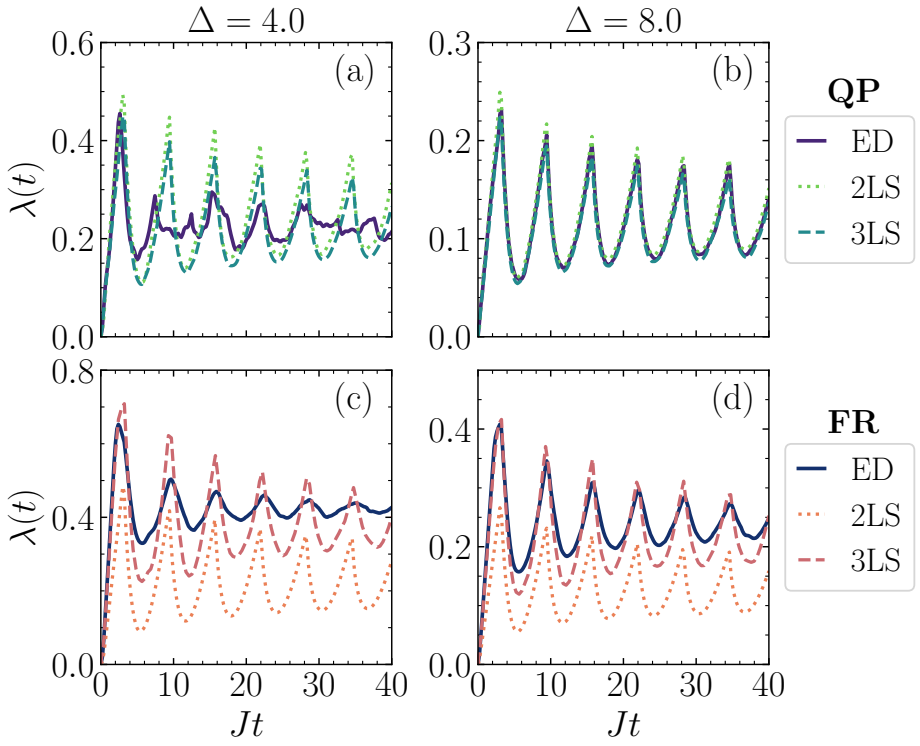

Figure 4.6. *Comparison between the LE $\lambda(t)$ for a $L = 22$ chain and the predictions of the 2LS and 3LS models*: (*a-b*) *QP potential*; (*c-d*) *FR potential.*

of half a Rabi oscillation $t_m = (2m+1)\pi/\Omega$. These divergences are smoothened into cusp singularities due to the fact that such resonant 2LSs are a set of zero measure in the disorder statistics. This result has important consequences. Indeed the nearly resonant 2LSs captured by the model are clearly an ensemble of approximate l-bits with Hamiltonian

$$\mathcal{H} \approx \sum_p K_p \tau_p, \tag{4.11}$$

where $\tau_p = \delta'_p/K_p \sigma^z_p - J/K_p \sigma^x_p$ is a Pauli matrix expressed as a rotation of the Pauli operators $\sigma^z_p = S^z_{i+1} - S^z_i$ (when projected onto the subspace with $S^z_i + S^z_{i+1} = 0$) and $\sigma^x = S^+_i S^-_{i+1} + \text{h.c.}$, built from the original spin operators for the pair $p = (i, i+1)$; and $K_p = \sqrt{\delta^2_p + J^2}$ is the l-bit splitting. Hence the return probability singularities are a striking manifestation of the existence of such (nearly free) l-bits, to be found in the short-time dynamics of the system.

4.3.1 Relationship to dynamical quantum phase transitions

It is worthwhile to mention at this point that the existence of singularities in the quench dynamics of the survival probability is currently the subject of several theoretical and experimental investigations, as they represent the main signature of so-called dynamical quantum phase transitions, studied both in non-random systems (Heyl et al. 2013; Heyl 2014; Jurcevic et al. 2017; Heyl 2018; X.-Y. Guo et al. 2019) as well as in disordered quantum systems (Yang et al. 2017; Yin et al. 2018; Halimeh et al. 2019). Nonetheless our observation of Loschmidt-echo singularities is fully explained by a model of individual 2LS, without the need of any many-body effect. Therefore we shall refrain from associating them to any form of time-dependent transitions.

4.4 Spatial correlations in the quasi-periodic vs. fully random potential

A fundamental assumption of the 2LS model described in the main text is that quasi-resonant two-site systems are spatially isolated in a (quasi)-disordered chain – namely, if a pair of sites $(i, i+1)$ is quasi-resonant for the motion of a particle, the two adjacent pairs of sites $(i-1, i)$ and $(i+1, i+2)$ are not resonant. Defining $\delta_1 = h_{i+1} - h_i$ as the energy difference of the two sites in question, and $\delta_2 = h_{i+2} - h_{i+1}$ as that of the following pairs of sites, in the case of non-interacting fermions, the above condition requires that the two energy differences do not vanish simultaneously.

Such a form of correlation is indeed observed in the case of QP potential: figure 4.7(a) shows the joint probability $P(\delta_1, \delta_2)$ for two adjacent energy differences, displaying a dip for $\delta_1 = \delta_2 = 0$ – an aspect which prevents two successive pairs of sites from being resonant simultaneously. In the case of interacting fermions, on the other hand, the above condition requires that if, *e.g.* $J_z \pm \delta_1 \approx 0$, then $J_z \mp \delta_2$ is non-zero, or vice versa – this prevents a state of the type $|101\rangle$ on the sites $(i, i+1, i+2)$ from being simultaneously (quasi-)resonant with $|110\rangle$ and $|011\rangle$, or, similarly, the state $|010\rangle$ from being quasi-resonant with $|100\rangle$ and $|001\rangle$. This is indeed guaranteed by the fact that $P(\delta, -\delta)$ is nearly vanishing for any finite δ, except for $\delta \approx 1.25\Delta$ – but the latter situation does not lead to consecutive resonances when $\Delta > 1.25J$, which is always the case in our study.

On the other hand the uniform potential has no correlations between two consecutive energy differences, and the $P(\delta_1, \delta_2)$ distribution is the product

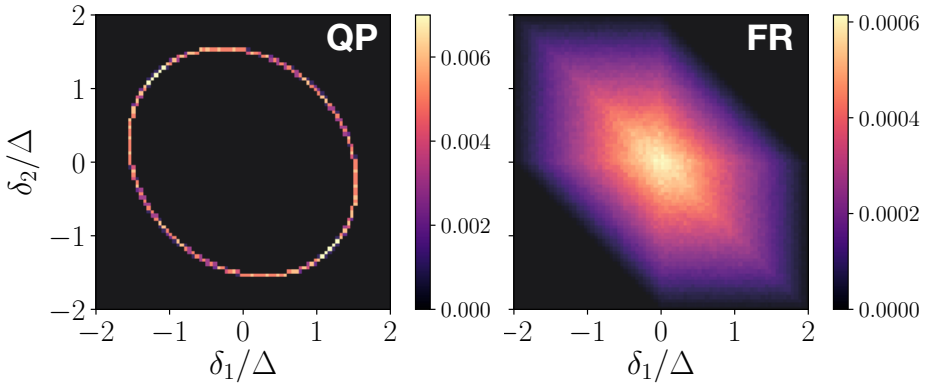

Figure 4.7. *Numerically sampled probability distribution $P(\delta_1, \delta_2)$ for two energy differences δ_1 and δ_2 on contiguous pairs of sites. Left panel: QP potential; Right panel: FR potential.*

of two triangular distributions for δ_1 and δ_2 – shown in figure 4.7(b). This implies that a fundamental assumption behind the 2LS model description is not guaranteed to be satisfied – while it is more likely to have two adjacent pairs of sites with different energy offsets than with similar ones, one cannot exclude the existence of "rare" regions with consecutive nearly resonant pairs. This requires to improve the 2LS model to a three-site (three-level) one, as detailed in section 4.4.1.

4.4.1 From two-level systems to three-level ones

Figure 4.6 (c-d) shows that, in the case of the FR potential, the 2LS model of (4.9) still predicts the correct frequency of the survival probability singularities, but not the correct height; and it also misses a global offset. This is not surprising, as in the case of the FR potential the assumption of anti-correlation between the energy offset of contiguous pairs is no longer valid, namely the potential can host "rare" regions in which contiguous pairs of sites – $(i-1, i)$ and $(i, i+1)$ – are nearly resonant at the same time. To take those regions into account (at least partially) one can easily promote the 2LS model to a model of 3-site systems (amounting to effective three-level systems – 3LS), and approximate the evolved state as that of a collection of independent 3LS. The Hamiltonian of a three-site system $(i, i+1, i+2)$ containing two interacting fermions in an initial $|101\rangle$ state

is explicitly given by

$$\begin{aligned}\mathcal{H}_{101} = &-\frac{J}{2}\left(c_i^\dagger c_{i+1} + c_{i+1}^\dagger c_{i+2} + \text{h.c.}\right) \\ &+ \delta_i n_{i+1} + (\delta_{i+1} + \delta_i) n_{i+2} \\ &+ J_z\left(n_i n_{i+1} + n_{i+1} n_{i+2}\right) + \text{const.}\end{aligned} \tag{4.12}$$

Here all single-site energies are referred to the energy of site i, and $\delta_i = h_{i+1} - h_i$. The above Hamiltonian assumes that the sites $i-1$ and $i+3$ remain empty during the time evolution. The Hilbert space of the 3-site system is restricted to the three states $|101\rangle$, $|110\rangle$ and $|011\rangle$, making of it a three-level system (3LS), with a generic time-dependent wavefunction

$$|\psi_{101}(t)\rangle = \alpha(t)\,|011\rangle + \beta(t)\,|101\rangle + \gamma(t)\,|110\rangle \ . \tag{4.13}$$

Its explicit form can be easily calculated numerically for any specific choice of the energy differences δ_i. A similar calculation can be done for a three-site system hosting a single particle, and starting from the $|010\rangle$ configuration, with Hamiltonian

$$\begin{aligned}\mathcal{H}_{010} = &-\frac{J}{2}\left(c_i^\dagger c_{i+1} + c_{i+1}^\dagger c_{i+2} + \text{h.c.}\right) \\ &+ J_z n_i + \delta_i n_{i+1} + (\delta_{i+1} + \delta_i + J_z) n_{i+2},\end{aligned} \tag{4.14}$$

which assumes that the sites $i-1$ and $i+3$ host two pinned particles. The Hilbert space $|100\rangle$, $|010\rangle$, $|001\rangle$ defines a 3LS, whose instantaneous state takes the generic form

$$|\psi_{010}(t)\rangle = \tilde{\alpha}(t)\,|100\rangle + \tilde{\beta}(t)\,|010\rangle + \tilde{\gamma}(t)\,|001\rangle \ . \tag{4.15}$$

For the two types of clusters the survival probability can be readily evaluated as

$$\lambda_{101}(t;\delta_i,\delta_{i+1}) = -\log|\beta(t)|^2 \tag{4.16}$$

$$\lambda_{010}(t;\delta_i,\delta_{i+1}) = -\log|\tilde{\beta}(t)|^2. \tag{4.17}$$

We can then model a chain in a QP or FR potential as an ensemble of independent 3LSs by generating sequences of energy offsets δ_i, δ_{i+1} between adjacent site pairs according to the distribution $P(\delta_i, \delta_{i+1})$. The 3LS prediction for the survival

probability of the ensemble is

$$\lambda_{3\mathrm{LS}} = \frac{1}{2}\int d\delta_1 d\delta_2\, P(\delta_1,\delta_2)\left[\lambda_{101}(t;\delta_1,\delta_2)+\lambda_{010}(t;\delta_1,\delta_2)\right]\,. \tag{4.18}$$

In practice, the above integral can be sampled numerically by averaging over a large number of different realizations of the potential on 3-site systems, such as those offered by a very long chain, namely

$$\lambda_{3\mathrm{LS}}(t) \approx \frac{1}{L}\sum_{i=1}^{L} \lambda_{\alpha_i}(t;\delta_i,\delta_{i+1}), \tag{4.19}$$

where $\alpha_i = 101$ if i is odd and 010 if i is even, and $L \gg 1$.

Eq. (4.19) for the survival probability has the apparent drawback of triple-counting each site. Nonetheless, similarly to what was argued for the 2LS case, it seems fair to assume (and it can be numerically tested) that, out of the three clusters containing each site, only one at most will contribute significantly to the survival probability. As a consequence the triple counting has only a mild effect on the final result. One could avoid triple counting by thoughtfully decomposing a chain into non-overlapping clusters of up to 3 sites, in such a way as to maximize the survival probability; yet this procedure introduces significant complications which are not justified a posteriori, given the quality of the results offered already by the naive ensemble average. As shown by figure 4.6(c-d), the improvement offered by the 3LS model for the FR potential is substantial; these results can further be improved by moving to 4-site clusters etc., albeit at an exponential cost.

4.5 Imbalance dynamics

The 2LS model prediction for the imbalance is very similar to that of the survival probability, as the imbalance is related to the persistence probability of the initial state ($|10\rangle$ or $|01\rangle$) on the 2-site cluster – given that the orthogonal state contributes zero to the imbalance. Therefore the 2LS expression for the imbalance simply reads

$$I_{2LS}(t) = \int d\delta\; P(\delta)\;\left[1-p(\delta,t)\right]\,. \tag{4.20}$$

The times t_m giving cusp singularities in the survival probability correspond to dips in the imbalance, and these dips come from local dips in the $g(\delta;t) =$

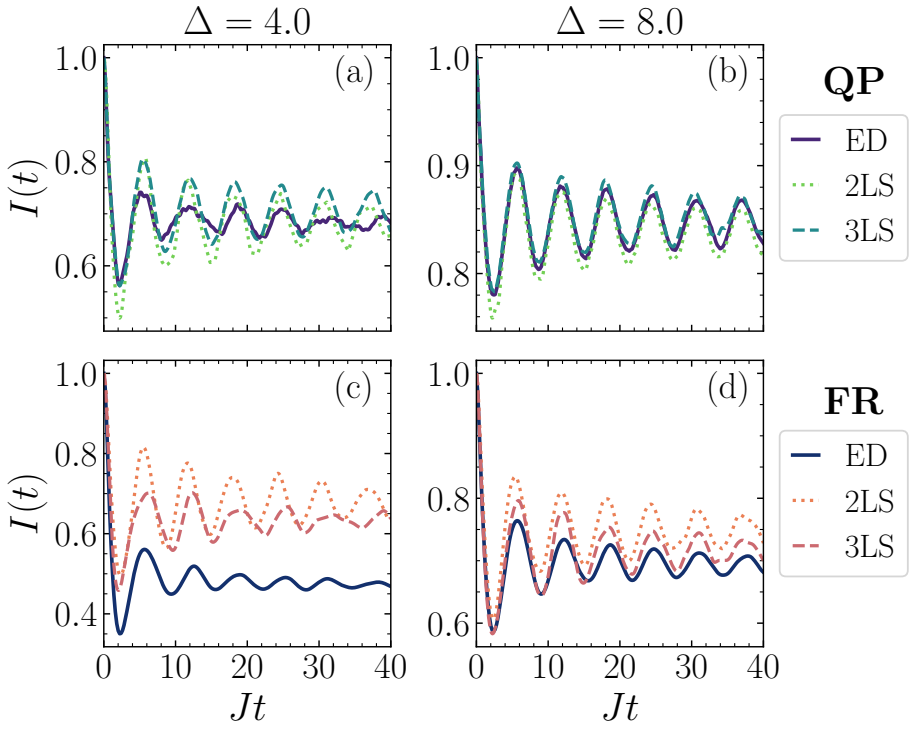

Figure 4.8. *Comparison between the imbalance $I(t)$ for a $L = 22$ chain and the predictions of the 2LS and 3LS models given by (4.20), (4.21): (a-c) QP potential; (d-f) FR potential.*

$1 - p(\delta, t)$ function centered around $\delta = 0$ and touching zero for $t = t_m$. The width of these dips is also shrinking in time as $t_m^{-1/2}$. Therefore one expects the depth of the minima in the fluctuations of the imbalance to decay to the long-time average as $t_m^{-1/2}$ as well – this prediction will be verified in section 4.6. Extending the 2LS model to 3LS, the imbalance can be calculated as

$$I_{3\mathrm{LS}}(t) \approx \frac{1}{3L} \sum_i \left(-|\alpha_i|^2 + 3|\beta_i|^2 - |\gamma_i|^2 \right) \tag{4.21}$$

with $\alpha_i, \beta_i, \gamma_i = \alpha(t), \beta(t), \gamma(t)$ or $\tilde{\alpha}(t), \tilde{\beta}(t), \tilde{\gamma}(t)$ depending on whether i is odd or even. Figure 4.8 shows the comparison between the ED results for the imbalance dynamics of interacting fermions immersed in a QP and FR potentials of variable strength, compared with the predictions of the 2LS and the 3LS models. For sufficiently strong disorder ($\Delta \gtrsim 6J$) the 2LS predictions are already rather accurate in the case of the QP potential, and the 3LS model offers further improvement. On the other hand in the case of the FR potential the 3LS model offers a more substantial improvement, fixing an overall offset (for sufficiently

strong disorder) which is seen in the 2LS predictions.

4.6 Dephasing in the survival probability and imbalance oscillations: evidence of l-bit interactions

A significant feature of the survival probability singularities is their slow decay in time – which is remarkable given that they result from the Rabi oscillations of a collection of 2LS with a distribution of frequencies that can be *a priori* expected to lead to fast dephasing. The reason behind the slow decay is also captured by the 2LS model, Eq. (4.9) – namely by the fact that the integral expressing the survival probability takes contributions from a small window of detunings δ' around zero that shrinks as the system evolves, as mentioned in section 4.3. When looking at the singularity times $t = t_m$, a direct inspection of the function $\log[1 - p(\delta', \Omega, t_m)]$ seen as a function of δ' shows that it has a large peak centered on $\delta' = 0$ with a width depending on time as $t_m^{-1/2}$. The singularity in the average survival probability comes from the integral of this peak, while the rest of the integral contributes essentially to the regular part of the survival probability; hence it is immediate to predict that the height of the cusp singularity should decay as the peak width, namely as $t_m^{-1/2}$.

Figure 4.9(a) shows the time evolution of singularity peaks in the survival probability for free as well as interacting fermions in the QP potential, compared to the prediction of the 2LS model (for the interacting case): we observe that the $t^{-1/2}$ decay is indeed confirmed by the ED data for free fermions, as well as by the ED data for interacting fermions at sufficiently short times ($tJ \lesssim t^* \approx 100$ for $\Delta = 8J$). On the other hand, at longer times the interacting data are found to display a strong deviation from the 2LS model prediction, exhibiting a much faster decay. This crossover to an *interaction-induced dephasing* (IID) regime clearly shows the limits of the 2LS model as a model of free l-bits and marks a fundamental difference between AL and MBL in the QP system. The faster decay of the survival probability must be related to the effect of l-bit interactions, which are a defining feature of MBL, and which add terms of the kind

$$\sum_{pq} U_{pq}\tau_p\tau_q + \sum_{pql} V_{pql}\tau_p\tau_q\tau_l + \ldots \tag{4.22}$$

to the effective l-bit Hamiltonian (4.11). Such terms are responsible for the persistent growth of entanglement entropy in the system (Serbyn et al. 2013b) as the logarithm of time, and indeed the onset of the $\log t$ growth of entanglement

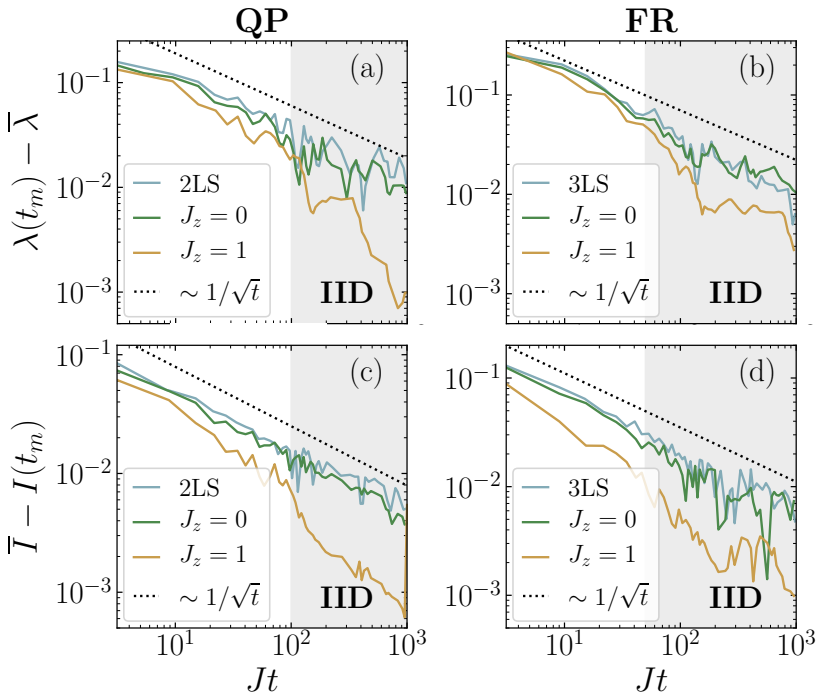

Figure 4.9. *(a-b) Decay of the peak heights of the survival probability, $\lambda(t_m) - \bar{\lambda}$ ($\bar{\lambda}$ stands for the time-averaged survival probability). (c-d) Decay of the depth of the imbalance minima $I(t_m)$ with respect to the average value $\bar{I}$. ED data in both absence ($J_z = 0$) and presence ($J_z = 1$) of interactions are compared with 2LS and 3LS predictions. The data are obtained for $\Delta = 8J$; the 2LS and 3LS predictions are for $J_z = J$. The grey-shaded area marks the interaction-induced dephasing (IID) regime exhibited by the exact data for $J_z = J$.*

occurs at a time compatible with t^* (see section 4.7 - figure 4.10). A similar crossover from a slow power-law decay of the Loschmidt-echo peak height to a faster decay, dictated by the presence of interactions, is also exhibited by the comparison between the ED data for interacting fermions in the FR potential with the same data for non-interacting fermions and for the 3LS model – as shown in figure 4.9(b).

The same crossover between the dynamics of effectively independent l-bits to a regime of interacting ones is observed in the decay of imbalance oscillations. Figure 4.9(c) shows the evolution of the depth of the minima of the imbalance at times $t = t_m$, taken with respect to the long-time average, namely the quantity $I_M(t_m) = \bar{I} - I(t_m)$. We observe that the predictions of the 2LS system for the fermionic chain immersed in the QP potential shows a clear, slow power-law decay at long times, compatible with $t^{-1/2}$, which is indeed reproduced in the case of non-interacting fermions. In the case of interacting fermions, on the

other hand, a crossover is observed at long times ($t \gtrsim t^* \approx 100$) to a faster decay, marking the IID regime. A similar picture is offered by the case of the FR potential. There the ED results are compared with the predictions from the 3LS model; the latter model predicts correctly the decay of the minima depth in the non-interacting case at all times, while the exact results for the interacting system show a clear crossover towards a faster decay for times $t \gtrsim t^* \approx 50$. For both kinds of disorder, the crossover time t^* is compatible both with what is observed in the decay of the survival probability as well as with the evolution of the entanglement entropy (see again figure 4.10 in the next section). Therefore we conclude that the crossover to the IID regime is a robust feature of MBL dynamics, clearly exposing the interactions among l-bits.

4.7 Entanglement dynamics

4.7.1 Entanglement entropy from the 2LS and 3LS model

If we partition the entire system into two adjacent parts A/B, the 2LS and 3LS models allow for a simple calculation of the EE (1.21) of A, which we consider here in a time-dependent fashion as

$$S_A(t) = -\mathrm{Tr}\left[\rho_A(t)\log\rho_A(t)\right]. \tag{4.23}$$

The evolving RDM $\rho_A(t) = \mathrm{Tr}_B|\psi(t)\rangle\langle\psi(t)|$ is obtained through the partial trace (1.19) over the degrees of freedom in B of the instantaneous pure-state density matrix associated with the evolved state $|\psi(t)\rangle$.

The entanglement associated with such a bipartition simply comes from the entanglement inside the 2-site or 3-site cluster which contains the cut defining the bipartition. In the case of the 2LS model the disorder-averaged entanglement entropy of a bipartition is predicted as the entropy of the reduced state of one site in the 2-site cluster, namely

$$S_A(t) = \int d\delta\, P(\delta)\, h[p(\delta;t)], \tag{4.24}$$

and $h[x] = -x\log x - (1-x)\log(1-x)$. Notice that, unlike for the formulas of the survival probability and of the imbalance, no-double counting is implied in the above formula, since the entanglement is referred to a cut of the chain, and there is one unique cut per 2-site cluster.

On the other hand a 3-site cluster can be cut in two different ways, that we

will indicate as $\circ\,|\,\circ\circ$ and $\circ\circ\,|\,\circ$ in the following (where $\circ$ stands for a site and $|$ stands for the cut). The reduced density matrices for the two cuts are readily obtained from the cluster wavefunctions described in section 4.4.1; e.g. for a "101" cluster the reduced density matrix associated with the $\circ\,|\,\circ\circ$ cut reads

$$\rho_{101}^{\circ|\circ\circ}(t) = \begin{pmatrix} |\alpha(t)|^2 & 0 \\ 0 & |\beta(t)|^2 + |\gamma(t)|^2 \end{pmatrix}, \tag{4.25}$$

with associated entanglement entropy

$$S_{101}^{\circ|\circ\circ} = -|\alpha(t)|^2 \log |\alpha(t)|^2 - \left(|\beta(t)|^2 + |\gamma(t)|^2\right) \log \left(|\beta(t)|^2 + |\gamma(t)|^2\right); \tag{4.26}$$

the one associated with the $\circ\circ\,|\,\circ$ cut reads

$$\rho_{101}^{\circ\circ|\circ}(t) = \begin{pmatrix} |\gamma(t)|^2 & 0 \\ 0 & |\alpha(t)|^2 + |\beta(t)|^2 \end{pmatrix}. \tag{4.27}$$

The density matrices $\rho_{010}^{\circ|\circ\circ}$ and $\rho_{010}^{\circ\circ|\circ}$ and related entropies associated with a "010" cluster can be calculated similarly. The disorder-averaged entanglement entropy of the whole system within the 3LS model is then given by

$$\mathcal{S}(t) = \frac{1}{2L} \sum_i S_i(t), \tag{4.28}$$

where

$$S_i = \begin{cases} S_{101}^{\circ|\circ\circ}(t) + S_{101}^{\circ\circ|\circ}(t) & \text{if } i \text{ odd}, \\ S_{010}^{\circ|\circ\circ}(t) + S_{010}^{\circ\circ|\circ}(t) & \text{if } i \text{ even}. \end{cases} \tag{4.29}$$

The factor $1/2$ in (4.28) comes from the double counting of each cut (which is contained both in a "101" cluster as well as in a "010" cluster).

Figure 4.10 shows a comparison between the entanglement entropy of interacting fermions in a QP potential and the 2LS prediction. We observe that at moderate disorder in the MBL phase ($\Delta = 8J$) the 2LS and 3LS models only capture the initial rise of the entanglement entropy and (partly) the first maximum; in particular the very existence of a maximum is explained by the models as the result of nearly resonant small clusters returning close to the initially factorized state – albeit at different times due to the inhomogeneously broadened local frequencies, which explains why the entanglement entropy does not come back to (nearly) zero. The 2LS and 3LS models on the other hand completely miss the

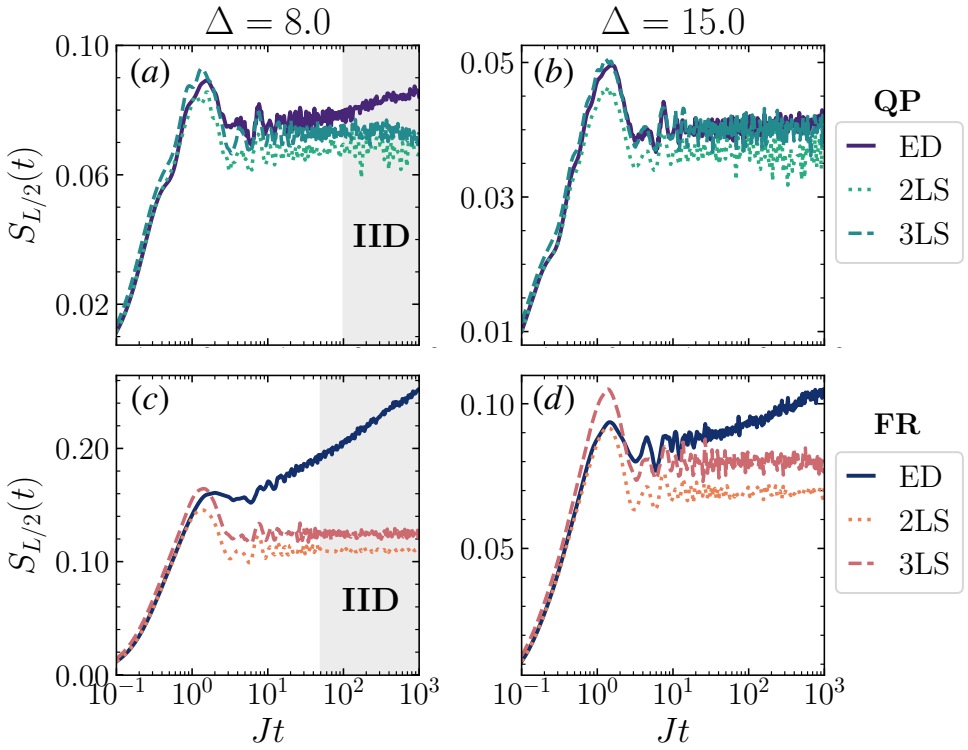

Figure 4.10. *Half-chain entanglement entropy of interacting fermions in a QP potential (a-b) and FR potential (c-d) for a chain of size $L = 16$, compared with the prediction for the 2LS/3LS models for two different disorder strengths ($\Delta/J = 8$ and 15).*

long-time logarithmic growth of the entanglement entropy – something which is fully expected, given that such a growth is the consequence of interactions between l-bits, not included in the 2LS and 3LS models by construction. On the other hand, at stronger disorder ($\Delta = 15J$) the interactions between l-bits are parametrically suppressed, and the 2LS and 3LS description of entanglement becomes accurate up to very long times.

4.7.2 Entanglement entropy vs. number entropy

The 2LS and 3LS models picture the entanglement between two adjacent subsystems as arising uniquely from the coherent motion of particles within the restricted size of the clusters they describe. When starting from a factorized state, this picture is certainly valid at short times. At long times it remains valid only if particles remain localized within the size of the clusters (namely if the localization length is smaller than the cluster size), and if this is a sufficient condition for entanglement not to spread any further. The latter aspect is true in the case of non-interacting fermions, for which the only mechanism behind

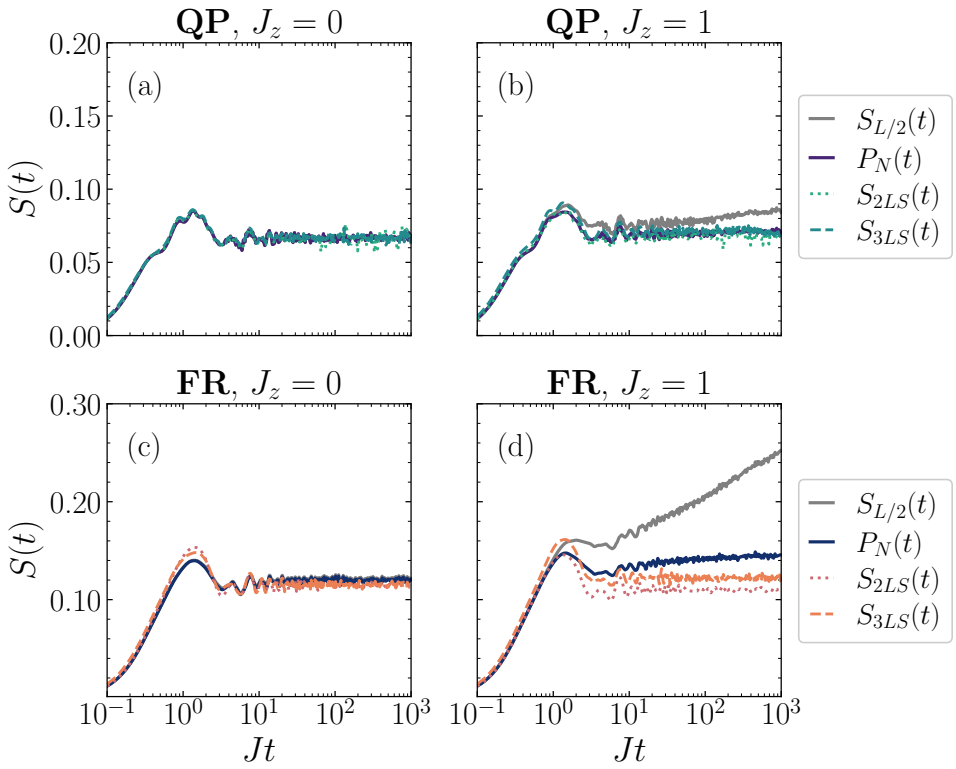

Figure 4.11. *Half-chain entanglement entropy and number entropy of free and interacting fermions on a $L = 16$ chain, compared with the 2LS and 3LS predictions*: (*a*) *non-interacting fermions in a QP potential*; (*b*) *interacting fermions* ($J_z = 1$) *in a QP potential*; (*c*) *non-interacting fermions in a FR potential*; (*d*) *interacting fermions* ($J_z = 1$) *in a FR potential. For all the panels the disorder strength is* $\Delta = 8J$.

entanglement of different spatial partitions is particle motion between them. On the other hand, in the case of interacting fermions in the MBL regime, entanglement keeps growing due to the interactions between l-bits, and distant degrees of freedom can become entangled even without any net particle exchange. In this context it is useful to decompose the entanglement entropy of a subsystem A into a *number entropy* contribution, and a remainder part called the *configurational entropy*, $S_A = S_{A,n} + S_{A,c}$ (Lukin et al. 2019; Kiefer-Emmanouilidis et al. 2020; Luitz et al. 2020b; Kiefer-Emmanouilidis et al. 2021) (see App.C for a short derivation). The number entropy is given by

$$S_{A,n} = -\sum_n p_n \log p_n, \tag{4.30}$$

where p_n is the probability of having n particles in subsystem A. Eq. (4.30) accounts for the particle number uncertainty appearing in subsystem A because

of the coherent exchange of particles with its complement B. On the other hand the configurational entropy accounts for correlations establishing between the particle arrangements in A and B once the partitioning of the particles between A and B has been fixed. The 2LS and 3LS models, completely lacking any form of correlations among the clusters, can only capture the number entropy contribution in systems with a localization length smaller than the cluster size. Nonetheless, this limited picture still offers a faithful description of entanglement in the MBL regime for short times (the longer the stronger disorder is), while it can describe entanglement at all times for strongly localized non-interacting particles. Thus, as suggested above, a more appropriate comparison with the entanglement entropies of the 2LS and 3LS models would involve the number entropy from the ED data – shown in figure 4.11. For non-interacting fermions in a QP potential of strength $\Delta = 8J$, $S_{A,N}$ is found to nearly coincide with the full entanglement entropy, and to be very well described by the 2LS prediction – see figure 4.11(a). When adding the interactions, the agreement between the number entropy and the 2LS entropy deteriorates mostly at long times, seemingly due to the $\sim \log\log t$ growth of the number entropy observed in the MBL phase (Kiefer-Emmanouilidis et al. 2020). Similar considerations can be made in the case of the FR potential, i.e. the 3LS models describe well the entropies in the non-interacting case, and they miss the slow long-time growth of the number entropy in the interacting case.

4.8 Energy selective quenches

We present here results obtained with an alternative quench protocol. The aim is to provide an energy-resolved method to study dynamical properties of MBL systems through the observation of the return probability, implementing a quantum-quench spectroscopy protocol (Naldesi et al. 2016). We prepare the system in the ground-state of (4.2) for a given initial potential amplitude Δ_i, and we trigger the quench by suddenly switching the QP potential to a fixed final value Δ_f. If one wants to study the behavior across the MBL transition, the natural choice of the parameter connecting the pre-quench and post-quench Hamiltonians is Δ. The sudden quench injects in the system a controlled amount of energy

$$\Delta E = \langle\psi_i|\mathcal{H}(\Delta_f)|\psi_i\rangle - \langle\psi_f|\mathcal{H}(\Delta_f)|\psi_f\rangle\,, \tag{4.31}$$

where $|\psi_{i(f)}\rangle$ is the ground state of $\mathcal{H}(\Delta_{i(f)})$. Thus, the eigenspectrum of the final Hamiltonian $\mathcal{H}(\Delta_f)$ can be explored by fixing the final disorder strength

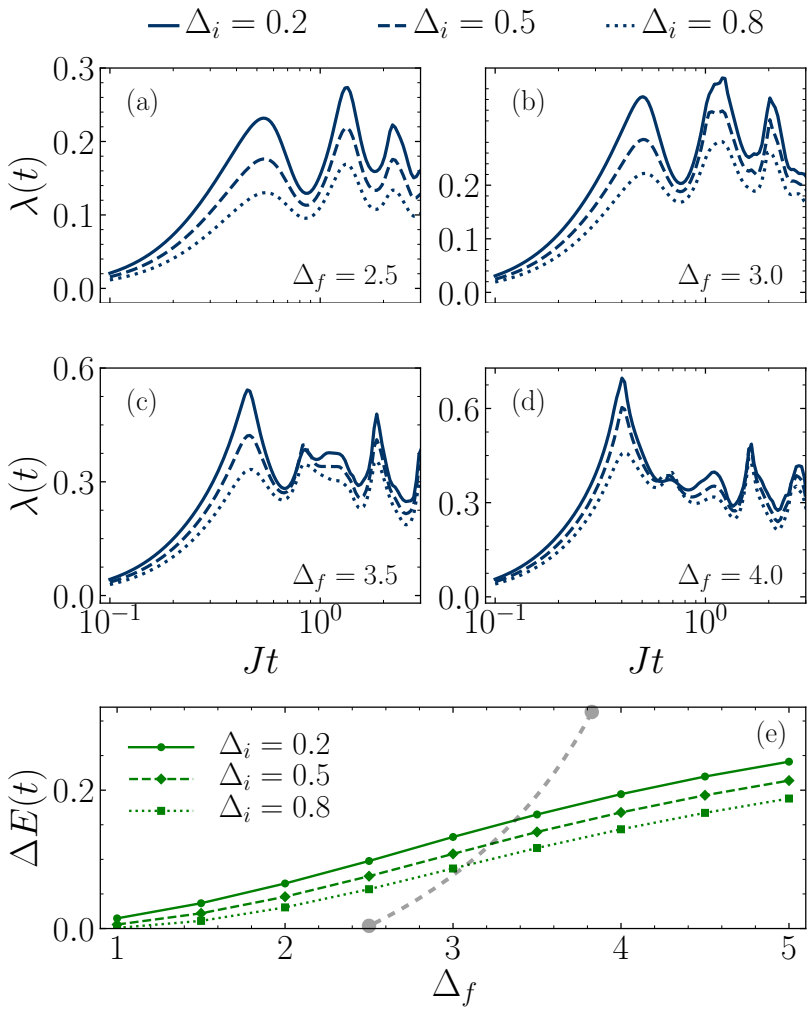

Figure 4.12. (*a-d*) $\lambda(t)$ *dynamics for the ground-state of Hamiltonian* 4.2 *for different initial QP potential strengths* $\Delta_i = (0.2, 0.5, 0.8)$. *The quench is realized at fixed final disorder values* $\Delta_f = (2.5, 3.0, 3.5, 4.0)$, *in proximity of the critical region separating extended from MBL phases.* (*e*) *Energy injected through the quench for different initial* Δ_i *as a function of* Δ_f. *The grey dashed line is a guide to the eye depicting the MBME at the relevant energy densities, from data adapted from* (Naldesi et al. 2016).

and continuously varying Δ_i. A wider quench in the disorder amplitude leads to eigenstates of the final Hamiltonian with parametrically higher energy density $\epsilon = \Delta E/W$, where W is the spectral width of $\mathcal{H}(\Delta_f)$.

At the ground-state level, model (4.2) is characterized by a quantum critical point separating a broad gapless Luttinger liquid phase and an Anderson glass phase, displaying exponentially decaying correlations (Naldesi et al. 2016). The critical disorder at which the system undergoes an MBL transition in our case is at $\Delta_c = 2.5$. With respect to the non-interacting AA case ($V = 0$), the critical point at $\Delta_c = J$ is shifted towards higher values of the disorder due to the screening effect of repulsive interactions for $V > 0$. Above the ground-state, the full eigenspectrum is separated with an energy-dependent boundary, i.e. a MBME (see Chap. 3), between an ETH and an MBL phase. At a fixed disorder strength Δ, the system is characterized by the coexistence of extended and localized states depending on the energy density.

We study the behavior $\lambda(t)$ following the quench-spectroscopy scheme described above. We prepare the system in the ground-state of $\mathcal{H}(\Delta_i)$ and we quench to final disorder strengths $\Delta_f > \Delta_i$, monitoring the out-of-equilibrium dynamics through the computation of $\lambda(t)$ and ΔE. The scope of the investigation is to determine whether the survival probability dynamics provide any robust signatures of the MBL transition, able to identify the MBME. As we will discuss in the following, our numerical results suggest not.

Figs. 4.12(a-d) illustrate the ED results of the quench obtained for three different values of the initial disorder $\Delta_i = 0.2, 0.5, 0.8$ at four fixed values of the quenching disorder $\Delta_f = 2.5, 3.0, 3.5, 4.0$, in a chain of $L = 20$ sites. The signature revealed by $\lambda(t)$ is again the emergence of a sharp singularity in the short-time dynamics as we cross the critical disorder Δ_c and we enter into the MBL regime. The critical region identified by the onset of the first non-analyticities is $\Delta_f \in [3.5, 4.0]$, which is consistent with the values predicted by the MBME at the energy density reached though our quenches, i.e. $\epsilon \sim 0.2$ (Naldesi et al. 2016). As can be seen in Fig. 4.12(e), the energy injected in the system at different Δ_f increases with the quench width separating Δ_i and Δ_f. At this stage, the qualitative analysis of the Loschmidt singularities does not provide a confirmation of the existence of an MBME. The shrinking of the peaks of $\lambda(t)$ leading to true singularities seems to be largely independent of the choice of Δ_i, and thus of the energy density injected through the quench. The non-analytic behavior emerges more evidently for *large* quenches, i.e. for increasing $\Delta_f - \Delta_i$. Intuitively, this is consistent with the interpretation of $\lambda(t)$ singularities as zeros

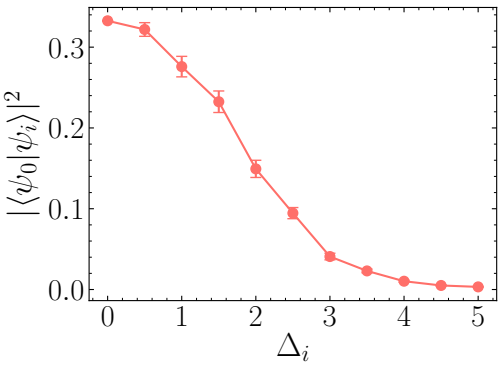

Figure 4.13. *Quantum overlap between the CDW state* $|\psi_0\rangle = |1010101...\rangle$ *and the ground-state* $|\psi_i\rangle$ *of* (4.2) *as a function of the initial potential strength* Δ_i.

of the survival probability: as the distance $\Delta_f - \Delta_i$ increases, the evolution driven by $\mathcal{H}_f$ brings the evolved state $|\psi(t)\rangle$ to be orthogonal to the ground-state of $\mathcal{H}_i$ more rapidly. On the other hand, the energy resolution reached through this series of quenches seems too low for a proper quantitative conclusion.

Furthermore, the 2LS framework described in Sec. 4.3 offers a qualitative explanation for the emergence of singularities in the dynamics of the LE. We recall that an essential ingredient underlying the construction of the 2LS model is the single particle occupation of each well of the quasi-periodic potential (whose quasi-period is between three and four sites). This is clearly satisfied by the choice of a CDW-like factorized state, which is precisely the case studied in Sec. 4.2. As $\Delta_i \to 0$, the ground-state of model (4.2) develops very strong long-range anti-correlations, with the main contributions coming equally from the basis states $|101010\ldots\rangle$ and $|010101\ldots\rangle$. Indeed, as can be seen in Fig. 4.13, the overlap between the ground-state $|\psi_i\rangle$ and the CDW state $|\psi_0\rangle = |1010101...\rangle$ is significant for very low Δ_i, being maximal in the extreme case $\Delta_i = 0$. Hence, the similarity of the initial ground-state for small Δ_i with $|\psi_0\rangle$ explains qualitatively the appearance of singularities in the return probability dynamics, albeit less pronounced than in the pure CDW case.

On the other hand, $|\langle\psi_0|\psi_i\rangle|^2$ has a fast decay as we increase Δ_i, becoming negligible for $\Delta_i \gtrsim 3$. An intuitive expectation is that evolving an initial ground-state already localized by a strong quasi-periodic potential, i.e. for high Δ_i, with an Hamiltonian with $\Delta_f < \Delta_i$, would not lead to singular behavior. This is indeed confirmed by the results presented in Fig. 4.14, in which we show a comparison between different choices of the initial ground-state. With a quench to quasi-periodic potential strengths $\Delta_f \in [1.0, 8.0]$, one observes the emergence

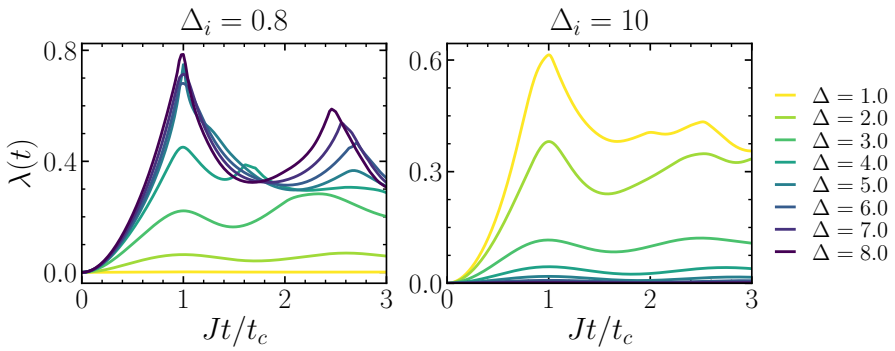

Figure 4.14. *Quench dynamics of $\lambda(t)$ starting from a low initial disorder $\Delta_i = 0.8$ (left) and a high initial disorder $\Delta_i = 10$. The time axis has been rescaled as $1/t_c$ to obtain disorder independence.*

of singularities for $\Delta_i = 0.8$ as we cross the ETH-MBL transition point, as discussed above. Moreover, the peaks become disorder-independent when the time axis is rescaled as $1/t_c$, where t_c is defined as the first relative maximum of $\lambda(t)$. Conversely, the LE evolution of the ground-state deep in the localized phase with $\Delta_i = 10$ displays a smooth behavior for all values of Δ_f.

4.9 Conclusions

In this Chapter, we have shown that sharp cusp-like singularities in the survival probability are a generic feature of the localized dynamics of an extended quantum system initialized in a factorized state. At strong disorder, these features can be fully explained by the dynamics of a simple model, describing an ensemble of effective independent two-level (or even three-level) systems, offering an explicit approximation to the conserved l-bits in the AL and MBL regime. Such a model predicts very accurately the survival probability singularities for strongly disordered systems as well as their decay, along with the imbalance oscillations. A faster decay in the survival probability and imbalance dynamics compared to that predicted by the model is a direct manifestation of the dephasing effect of interactions between the l-bits, and it intervenes at the same time as the onset of the logarithmic growth of entanglement entropy: hence it represents a distinct feature of MBL with respect to AL.

Let us comment briefly on the relation between the existence of cusps in the survival probability and the MBL-ETH transition. As extensively discussed throughout this Chapter, the sharp singularities in the survival probability arise from collective oscillations of an ensemble of free two-level systems. The iden-

tification of such independent two-site clusters as local integrals of motion appears exact only in the strong disorder regime and at short timescales, before interaction-induced dephasing kicks in. As such, our analysis suggests that such dynamical features can be used to identify *strongly* localized phases, whereas they are not reliable signatures of the MBL transition, which is supposed to happen at an intermediate disorder critical value. Nonetheless, the ground-state protocol described in Sec. 4.8 offers a more promising picture. Indeed, quenches from the ground-state of the system at low initial disorder strengths Δ_i to higher final values Δ_f shows the emergence of a cusp-like feature at Δ_f values that are comparable to the usual estimates of Δ_c for simulations of chains of similar sizes (Luitz et al. 2015). In order to establish the manifestation of such singularities as a reliable indicator of the transition, more refined numerical analyses are required to assess the extent of finite-size effects and to characterize more deeply the dependence on the initial Δ_i. We plan on proceeding along these lines in upcoming work.

Based on our results, we can conclude that experimental evidence of l-bit dynamics and of their interactions is readily accessible to state-of-the-art quantum simulators which have direct access to the survival probability and imbalance dynamics, such as *e.g.* trapped ions (Gärttner et al. 2017; Jurcevic et al. 2017), cold-atom simulators (M. Schreiber et al. 2015; Lüschen et al. 2017; Lukin et al. 2019) or superconducting circuits (Roushan et al. 2017; Chiaro et al. 2020).

5

Echo dynamics of localized systems

In this Chapter, we present an ongoing study of quench dynamics in MBL systems under the effect of parametrically small global perturbations. As we discussed in Sec. 1.3, the study of the sensitivity of many-body dynamical behavior to small perturbations is rooted in the inherent difference that separates quantum mechanics from classical chaotic motion. Indeed, classical chaos is a direct consequence of the non-linearity of the equation of motion, which leads to the exponential divergence of phase-space trajectories that were arbitrarily close to each other at the initial time. Unfortunately, attempting to follow the same line of reasoning in quantum mechanics turns out to be difficult. As shown by (1.11), the linearity of the Schrödinger equation guarantees the preservation of the dot product (i.e. the distance) between separate states, thus ruling out exponential sensitivity of slightly perturbed evolution. Nonetheless, the fidelity (1.29) [1] provides a significant measure of the degree of "chaoticity" of quantum dynamics, providing a rich decay structure summarized in Fig. 1.4 for systems with a classical chaotic limit. The main interest of the present Chapter is the exploration of the behavior of the Loschmidt echo decay in MBL systems, which represent a special class of systems that are not ergodic, being characterized by an extensive number of locally conserved quantities (see Sec. 3.3).

We consider the random 1d Heisenberg Hamiltonian already defined in (4.2),

[1] Throughout this Chapter, we will use the terms "fidelity" and "Loschmidt echo" interchangeably.

which we rewrite here as

$$\mathcal{H}_0 = J \sum_{\langle i,j\rangle,\alpha} S_i^\alpha S_j^\alpha + W \sum_i h_i S_i^z, \tag{5.1}$$

where $\alpha = \{x, y, z\}$, h_i are uniformly distributed random variables sampled in the window $[-1, 1]$, and W is the disorder strength. We initialize the system in a generic random product state, and we trigger the quench dynamics with a linearly perturbed Hamiltonian $\mathcal{H}_1(\epsilon)$ given as

$$\mathcal{H}_1 = \mathcal{H}_0 + \epsilon V, \tag{5.2}$$

with ϵ being the perturbation strength parameter, which is assumed to be independent of time. The main object of our analysis is the fidelity with respect to the unperturbed evolution driven solely by $\mathcal{H}_0$, defined via the Loschmidt echo (1.29)

$$\mathcal{L}(t) = |\langle\psi_0(t)|\psi_1(t)\rangle|^2 = |\langle\psi_0|e^{i\mathcal{H}_0 t}e^{-i\mathcal{H}_1 t}|\psi_0\rangle|^2. \tag{5.3}$$

As described in Sec. 3.3, most of the fundamental features of MBL systems, such as power-law decay of local observables and slow logarithmic spreading of entanglement, are now well understood as originating from an emergent form of integrability in the framework of l-bits, i.e. local integrals of motion built with a sequence of quasi-local unitary transformations acting on physical degrees of freedom. The present work is thus concerned with assessing whether this peculiar kind of local integrability similarly affects the decay of $\mathcal{L}(t)$ as well, providing new insights on the dynamical behavior on both sides of the transition. Moreover, we will show that the study of the Loschmidt echo saturation value at long times is directly connected to spectral signatures of localization, specifically allowing for the estimation of a dynamical version of the participation ratio (3.8) and the manifestation of the fractality of localized eigenstates. Before moving on to the results, we discuss an experimental proposal that allows the measurement of $\mathcal{L}(t)$ in cold-atoms platforms by means of recently developed many-body interferometric techniques.

5.1 Echo dynamics protocol for MBL systems

One can imagine an experimental quench protocol in the context of ultra cold-atoms that effectively returns the time-reversal dynamics probed by (5.3). Indeed, the overlap of the density matrices of two independently prepared $1d$

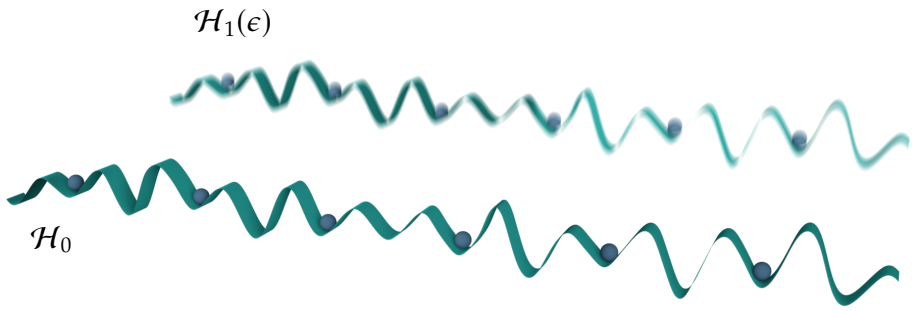

Figure 5.1. *Pictorial sketch of a viable experimental setup for the measurement of the Loschmidt echo, as described in Sec. 5.1. Blue spheres represent particles loaded into an optical lattice which is characterized by a random potential profile. The blur on the copy labelled by $\mathcal{H}_1(\epsilon)$ reflects the presence of noise in the preparation of the same disorder configuration as in $\mathcal{H}_0$.*

systems A and B, i.e. $P_{AB} = \mathrm{Tr}[\rho^{(A)}\rho^{(B)}]$, is now within reach, for instance, via many-body interferometric measurements (Islam et al. 2015). Before proceeding, it is thus instructive to briefly review the basic ideas of such a measurement scheme, which has been successfully applied in (Islam et al. 2015) for the direct measurement of the quantum purity, from which entanglement quantifiers such as Renyi entropies and mutual information can be derived.

5.1.1 Many-body interferometry

The estimation of quantities such as the quantum overlap (5.3), entanglement entropies, or the state purity $\mathrm{Tr}\,\rho^2$, formally requires the measurement of non-linear functionals of the density operator ρ. A conventional observable O, on the other hand, is obtained as a linear functional of ρ as $\langle O\rangle = \mathrm{Tr}\left[\rho O\right]$, which corresponds to a directly measurable object. A general protocol to quantify non-linear functionals of a quantum state, such as $\mathrm{Tr}\left[\rho^n\right]$, was introduced by (Ekert et al. 2002), based on the *swap operator*

$$\mathrm{SWAP}_n\left(|\psi_1\rangle\,|\psi_2\rangle\ldots|\psi_n\rangle\right) = |\psi_n\rangle\,|\psi_1\rangle\ldots|\psi_{n-1}\rangle\,, \tag{5.4}$$

acting on n copies of a many-body quantum system. Given n identical copies of ρ, we have that

$$\rho^{\otimes n} = \underbrace{\rho\otimes\rho\otimes\cdots\otimes\rho}_{n\text{ times}}, \tag{5.5}$$

and the SWAP operator is the cyclic permutation operator that permutes the n copies, i.e.

$$\mathrm{SWAP}_n = \sum_{i_1,i_2,\ldots i_n} |i_n\rangle\,|i_1\rangle \ldots |i_{n-1}\rangle\,\langle i_1|\,\langle i_2| \ldots \langle i_n|\,, \tag{5.6}$$

where $\{|i_j\rangle\}$ is the set of basis states for each copy. We note that two applications of the SWAP operator brings the system back to its initial configuration, i.e. $\mathrm{SWAP}_n^2 = \mathbb{1}$. In the simplest case $n = 2$ the operator SWAP_2 has thus eigenvalues ± 1, corresponding to subspaces of the system that are symmetric or antisymmetric after the exchange operation between the copies. It was shown in (Ekert et al. 2002) that $\mathrm{Tr}\left[\rho^n\right]$ can be written as

$$\mathrm{Tr}\left[\rho^n\right] = \mathrm{Tr}\left[\mathrm{SWAP}_n\,\rho^{\otimes n}\right] = \langle \mathrm{SWAP}_n \rangle\,, \tag{5.7}$$

thus reducing the measurement of quantities depending on $\mathrm{Tr}\left[\rho^n\right]$ to the determination of the expectation value of the swap operator acting on n copies of a given system. Let focus on the simplest case, which is also of interest here: we imagine two instances of the same 1d many-body system in two different states $\rho^{(1)}$ and $\rho^{(2)}$, and we aim to quantify their overlap $\mathrm{Tr}\left[\rho^{(1)}\rho^{(2)}\right]$. The action of a SWAP gate for any two pure states of the systems 1 and 2 is then defined as

$$\mathrm{SWAP}_2\,|\psi_1\rangle_1 \otimes |\psi_2\rangle_2 = |\psi_2\rangle_1 \otimes |\psi_1\rangle_2\,. \tag{5.8}$$

We can decompose the two states in the corresponding basis states for each copy as

$$\rho^{(1)} = \sum_{ij} \rho^{(1)}_{ij}\,|i\rangle\,\langle j|\,, \qquad \rho^{(2)} = \sum_{kl} \rho^{(2)}_{kl}\,|k\rangle\,\langle l|\,, \tag{5.9}$$

and it can be then easily seen that (Ekert et al. 2002; Islam et al. 2015)

$$\begin{aligned}
\mathrm{Tr}\left[\mathrm{SWAP}_2\left(\rho^{(1)}\otimes\rho^{(2)}\right)\right] &= \mathrm{Tr}\left(\mathrm{SWAP}_2 \sum_{ijkl} \rho^{(1)}_{ij}\rho^{(2)}_{kl}\,|i\rangle\,\langle j| \otimes |k\rangle\,\langle l|\right) \\
&= \mathrm{Tr}\left(\sum_{ijkl} \rho^{(1)}_{ij}\rho^{(2)}_{kl}\,|k\rangle\,\langle j| \otimes |i\rangle\,\langle l|\right) \\
&= \sum_{ijkl} \rho^{(1)}_{ij}\rho^{(2)}_{kl}\delta_{kj}\delta_{il} = \sum_{ik} \rho^{(1)}_{ik}\rho^{(2)}_{ki} \\
&= \mathrm{Tr}\left[\rho^{(1)}\rho^{(2)}\right],
\end{aligned} \tag{5.10}$$

which proves the equivalence between the expectation value of the swap operator acting on the product space of the two states and their overlap. It is clear that if the two copies are prepared in the same state, i.e. $\rho^{(1)} = \rho^{(2)} = \rho$, the measurement of the swap operator gives the quantum purity $\mathrm{Tr}\,\rho^2$. Crucially, (Daley et al. 2012) proved that the measurement of the swap operator expectation value amounts, for indistinguishable bosons, to a parity measurement of the site-resolved occupation number in each site and copy of the system, after the bosons on corresponding sites are made to interfere exploiting the Hong-Ou-Mandel effect (Hong et al. 1987). Such a measurement is an easily attainable procedure with state-of-the-art quantum gas microscopy techniques (Bakr et al. 2009). Let us briefly review the idea behind the correspondence of $\langle \mathrm{SWAP}_2 \rangle$ and a parity measurement. For simplicity, consider the case of two copies 1 and 2 in the same pure state ρ, such that $\mathrm{Tr}[\rho_1 \rho_2] = \mathrm{Tr}[\mathrm{SWAP}_2(\rho \otimes \rho)] = \mathrm{Tr}[\rho^2] = 1$. If we consider the case of indistinguishable bosons, the state of the two-copy system can be written in the basis

$$\prod_{ij} (a^\dagger_{1,i} - a^\dagger_{2,i})^{2p_i} (a^\dagger_{1,j} + a^\dagger_{2,j})^{q_j} \, |0\rangle \,, \tag{5.11}$$

where $p, q = 0, 1, 2, \ldots$ and $a^\dagger_{n,i}$ creates a boson mode i in the n-th copy. At this point, a discrete Fourier transform on the two copies of the form

$$a^\dagger_{1(2),i} \to \frac{\left(a^\dagger_{1,i} \pm a^\dagger_{2,i}\right)}{\sqrt{2}} \tag{5.12}$$

amounts to a beam-splitter operation that can be experimentally implemented by lowering the potential barrer between the copies and allowing a controlled tunnelling between them (Daley et al. 2012). It is easy to see that following this transformation the basis states (5.11) become (dropping the mode index)

$$\prod_i (a^\dagger_{2,i})^{2p_i} (a^\dagger_{1,i})^q_i \, |0\rangle \,, \tag{5.13}$$

with states having $2p_i$ particles in mode i of copy 2. Thus, following the transformation (5.12), a symmetric state will always have an even number of particles in copy 2. Similar steps can be applied to antisymmetric states and annihilation operators $a_{n,i}$, leading to a beam-splitter operation that leaves only an odd number of particles in copy 2. Thus, the expectation value $\langle \mathrm{SWAP}_2 \rangle$ can be computed as $(-1)^{\sum_i n_{i,2}}$, i.e. by observing the total particle number in copy 2 after the mea-

surement and determining whether it is even or odd (Daley et al. 2012). This scheme was directly implemented by (Islam et al. 2015) to probe entanglement in an optical lattice through atom-resolved microscope techniques.

Our proposal, inspired by the ideas discussed so far, consists in monitoring and recording over time the overlap between two 1d atomic chains, loaded in an optical lattice with the addition of a random potential. In experiments on large cold-atoms chains, the realization of a random potential pattern can be carried out by means of, e.g. a laser speckle field (Clément et al. 2006), typically generated by transmission of a laser beam through a ground glass plate (Goodman 2007), imposed on both copies. In experiments with quantum gas microscopes, a random potential pattern can also be obtained via a digital micro-mirror device which allows to expose atoms to programmable potentials on the scale of the wavelength of light (J. Y. Choi et al. 2016). An echo-dynamic protocol can thus be implemented *naturally* by considering experimental difficulties in duplicating exactly the same random potential pattern. Following this idea, we imagine a perturbation in the form of a systematic variation of the amplitude of the potential profile in one of the two prepared copies, explicitly describing the perturbed Hamiltonian (5.2) as

$$\mathcal{H}_1(\epsilon) = \mathcal{H}_0 + \epsilon V = \mathcal{H}_0 + \epsilon W \sum_i h_i S_i^z, \tag{5.14}$$

where h_i are the same random numbers that enter in $\mathcal{H}_0$. By initializing both chains in the same initial state ρ_0 and simultaneously evolving them under the action of $\mathcal{H}_0$ and $\mathcal{H}_1$ respectively, a measurement of the fidelity (5.10) at different times would allow to reconstruct the echo dynamics.

5.1.2 Perturbative expansion

Before presenting the numerical results of our ED simulations, we present a simple perturbative analysis that allows to extract useful insights regarding the behavior of $\mathcal{L}(t)$ in the limit of weak perturbation strength ϵ. Most of the following stems from the original formulation of the Loschmidt echo that can be found in (Peres 1984). We define the unperturbed (perturbed) eigenergies and eigenvectors as $E_n^{(0)}$, $|\phi_n^{(0)}\rangle$ ($E_n^{(1)}$, $|\phi_n^{(1)}\rangle$), given by

$$\mathcal{H}_0|\phi_n^{(0)}\rangle = E_n^{(0)}|\phi_n^{(0)}\rangle \qquad \mathcal{H}_1|\phi_n^{(1)}\rangle = E_n^{(1)}|\phi_n^{(1)}\rangle \ , \tag{5.15}$$

and, with a first-order perturbation expansion

$$\begin{aligned} E_n^{(1)} =& E_n^{(0)} + \epsilon \langle \phi_n^{(0)} | V | \phi_n^{(0)} \rangle + O(\epsilon^2), \\ |\phi_n^{(1)}\rangle =& |\phi_n^{(0)}\rangle + \epsilon \sum_{m \neq n} \frac{\langle \phi_m^{(0)} | V | \phi_n^{(0)} \rangle}{E_n^{(0)} - E_m^{(0)}} |\phi_m^{(0)}\rangle + O(\epsilon^2) \, . \end{aligned} \tag{5.16}$$

As a consequence the overlap between the state $|\psi_0\rangle$ evolved with the two Hamiltonians reads

$$\begin{aligned} \mathcal{L}(t) =& \left| \langle \psi_0 | e^{i\mathcal{H}_0 t} e^{-i\mathcal{H}_1 t} | \psi_0 \rangle \right|^2 \\ =& \Bigg| \sum_m e^{-i(E_m^{(1)} - E_m^{(0)})t} \left(|\langle \psi_0 | \phi_m^{(0)} \rangle|^2 + \epsilon \langle \psi_0 | \phi_m^{(0)} \rangle \sum_{p \neq m} \frac{\langle \phi_m^{(0)} | V | \phi_p^{(0)} \rangle}{E_m^{(0)} - E_p^{(0)}} \langle \phi_p^{(0)} | \psi_0 \rangle \right) \\ &+ \epsilon \sum_{mn} (1 - \delta_{nm}) e^{-i(E_n^{(1)} - E_m^{(0)})t} \langle \psi_0 | \phi_m^{(0)} \rangle \langle \phi_n^{(0)} | \psi_0 \rangle \frac{\langle \phi_m^{(0)} | V | \phi_n^{(0)} \rangle}{E_m^{(0)} - E_n^{(0)}} + O(\epsilon^2) \Bigg|^2 , \end{aligned} \tag{5.17}$$

where the ϵ expansion is only taken at the level of the Hamiltonian eigenstates, but not at the level of the eigenvalues appearing in the phase terms. Hence, the dominant term is given by

$$\mathcal{L}(t) = \left| \sum_n |\langle \psi_0 | \phi_n^{(0)} \rangle|^2 e^{-i\epsilon \langle \phi_n^{(0)} | V | \phi_n^{(0)} \rangle t} + O(\epsilon) \right|^2 . \tag{5.18}$$

5.2 Loschmidt echo decay

We perform ED simulations to obtain the evolution of the Loschmidt echo in different perturbation regimes and for varying disorder strengths W. We start initializing both chains in a random product state $|\psi_0\rangle = \bigotimes_i |m_i\rangle$ with $m_i \in \{|\uparrow\rangle, |\downarrow\rangle\}$, which corresponds to a single-site vector in the computational basis. We then compare the quench dynamics generated by evolving $|\psi_0\rangle$ with both $\mathcal{H}_0$ and $\mathcal{H}_1$., i.e. we compute the overlap between $|\psi_0(t)\rangle = \mathrm{e}^{-\mathrm{i}\mathcal{H}_0 t} |\psi_0\rangle$ and $|\psi_1(t)\rangle = \mathrm{e}^{-\mathrm{i}H_1 t} |\psi_0\rangle$. The results are obtained after averaging over $O(10^3)$ realizations of the random potential and the random initial states are sampled from an ensemble of $50 \sim 100$ possible configurations. The energy scale is set by $J = 1$. The results we present for the short-time regime (up to $t \sim 20$) are obtained for chains of $L = 20$ spins, while for long times ($t \sim 10^3$) we proceed by full diagonalization and we restrict ourselves to a maximum size of $L = 18$.

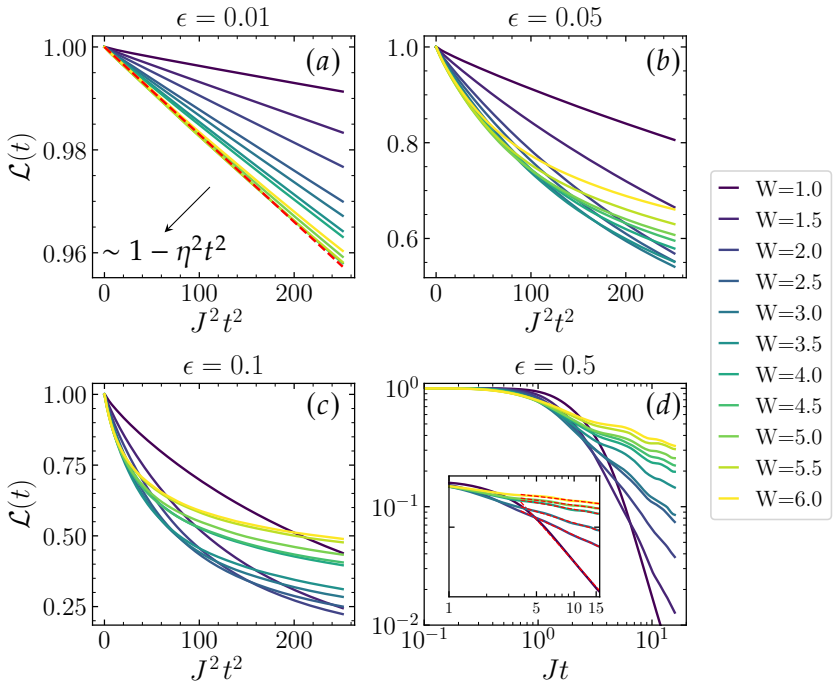

Figure 5.2. *Overlap $\mathcal{L}(t)$ vs. t^2 (a–c) and vs. t (d) averaged over 10^3 disorder realizations. The results are obtained for chains of length $L = 20$ at different disorder strengths and different values of the perturbation parameter ϵ. The red dashed line in (a) is a parabolic fit of the form $1 - \eta^2 t^2$ for the $W = 6$ data. Inset of (d): zoom of data for $t \geq 1$ with power-law fits (red dashed lines) for W=1.0, 2.0, 3.0, 4.0, 5.0, 6.0 from top to bottom.*

5.2.1 Short-time regime

In Fig. 5.2 (a-d) we report the results of ED simulations ($L = 20$) for different values of the perturbation strength ($\epsilon = 0.01, 0.05, 0.1, 0.5$) and for $W \in [1.0, \ldots, 6.0]$. For each ϵ, we find that $\mathcal{L}(t)$ displays an initial parabolic decay of the form $\mathcal{L}(t) \sim 1 - \eta^2 t^2$, which is a universal behavior expected at short times (see Sec. 1.3 and references therein), with η given by the dispersion of the perturbation operator V given by (1.30). The parabolic decay lasts up to a crossover time t_{par}, before which one can approximate the evolution operators with a second-order Taylor expansion, i.e.

$$e^{-i\mathcal{H}_\alpha t} \approx 1 - i\mathcal{H}_\alpha t - \frac{1}{2}(\mathcal{H}_\alpha t)^2, \tag{5.19}$$

with $\alpha = 0, 1$. We find the initial quadratic decay to be faster for growing disorder strength W, as shown in Fig. 5.2 (a) for weak perturbations $\epsilon = 0.01$. Moreover, t_{par} appears strongly dependent on both the perturbation strength ϵ

and W. At intermediate perturbation strength $\epsilon = 0.05$ (Fig. 5.2 (b)), the fidelity for $W = 1$ is still decaying quadratically at the maximum time reached in our simulations ($t \sim 16$), while the data for stronger W clearly show a different behavior at the same time scale. Thus, the parabolic regime persists longer in the putative ETH regime, i.e. at weak disorders. As we increase ϵ, the time spent in the parabolic regime shrinks into a vanishing time window, before developing a power-law decay with exponent ≤ 1, that decreases as we increase W. This can be appreciated in Fig. 5.2 (d) (please note the log-log scale used in this panel), where we report the Loschmidt dynamics at strong perturbations ($\epsilon = 0.5$). For $W = 1$, the initial parabolic regime holds up to $t_{\text{par}} \sim 4$, after which the systems starts decaying as a power-law (see the zoom in for $t \geq t_{\text{par}}$ in the inset). Increasing the disorder strength W results in a progressive reduction of t_{par} for $W < 4$, while for $W \geq 4$ the crossover time seems independent of the disorder strength with $t_{\text{par}} \sim 0.4$. The power-law decay at strong disorders is accompanied by oscillations that characterize the approach towards saturation values $\mathcal{L}_\infty$. The estimation of $\mathcal{L}_\infty$ will be the focus of the next section.

Before moving on, we would like to stress again the importance of the perturbation parameter ϵ. From an experimental point of view, the possibility of tuning ϵ results in the capability of manipulating the time-scales involved in the quench dynamics. Depending on the decay regime one decides to focus on, and on the coherence times of the specific experimental setup, decreasing ϵ, namely reducing the noise on the second copy of the system, allows one to access the initial fast parabolic regime up to long times t_{par}. Assuming that tuning ϵ does not impact the inherent coherence time of the system, one could instead increase ϵ to observe the power-law decay shown in Fig. 5.2 (d).

5.2.2 Long-time regime

We discuss now the connection between the fidelity dynamics and some well-known spectral measure of localization, already discussed in 3.2.2. Specifically, we will show how the study of the decay of $\mathcal{L}(t)$, experimentally attainable, yields the possibility of extracting information regarding the fractal nature of eigenstates in the MBL phase, a feature which has been the object of studies of AL since the early '90s (Janssen 1994; Evers et al. 2008).

The concept of multifractality, introduced originally by (Mandelbrot 1974), characterizes systems whose dynamics can not be described by a single critical exponent (called fractal dimension); instead, multifractal systems possess a infinite spectrum of critical exponents that describes the scaling of the moments of

some relevant distribution. In the case of an Anderson problem, for instance, a relevant measure is given by the wavefunction amplitude, and the corresponding moments are given by the IPRs

$$\mathrm{IPR}_q^\alpha = \sum_n^{\mathcal{N}} \left|\langle\phi_n|\psi_\alpha\rangle\right|^{2q}, \tag{5.20}$$

already introduced in Sec. 3.2.2, which act as an indicator of how spread the eigenstate $|\psi_\alpha\rangle$ is over the chosen basis $\{\phi_n\}$. Multifractality manifests more prominently in the vicinity of the critical AL transition, where IPR_q^α display the anomalous scaling (3.9), dependent on the so-called generalized fractal dimension D_q.

As anticipated in Sec. 3.2.2, a few works discussed the connection between the multifractal properties of localized eigenstates and the dynamics of quantities such as the survival probability $p(t) = |\langle\psi(0)|\psi(t)\rangle|^2$, a central object of this thesis. For instance, in the context of the quantum Hall effect, (Huckestein et al. 1994) studied the temporal decay of wavepackets built from states near the metal-insulator transition in the lowest Landau band, finding that $p(t)$ decays in time as $p(t) \sim t^{D_2/2}$, with D_2 being the generalized fractal dimension of the second moment of the wavefunction, i.e. the critical exponent of IPR_2^α. This result was later extended to higher dimensions in (Huckestein et al. 1999), that found the general scaling $p(t) \sim t^{D_2/d}$ for the survival probability, with d the dimensionality of the system.

In non-equilibrium studies, such as the one presented here, one usually deals with the participation ratio associated with the chosen initial state $|\psi_0\rangle$, that we define as

$$\mathrm{IPR}_0 = \sum_n \left|\langle\psi_0|\phi_n\rangle\right|^4. \tag{5.21}$$

The scaling of IPR_0 was found to scale similarly to (3.9) as $\mathrm{IPR}_0 \sim \mathcal{N}^{-\tilde{D}_2}$, with an exponent that was shown to be related to D_2 as $\tilde{D}_2 = dD_2$ (Huckestein et al. 1997) [2]. In the context of MBL, (Torres-Herrera et al. 2015) extended these results to interacting systems in the presence of disorder. Through extensive numerical calculations of $p(t)$ in a 1d system initialized in a highly excited non-equilibrium state, the authors found the survival probability to decay fast at short times, behaving similarly to clean systems, while developing a power-law decay at later times, with an exponent again given by D_2. In the weak perturbation

[2] As we work with systems with $d = 1$, we will drop the notation $\tilde{D}_2$ and speak directly of D_2.

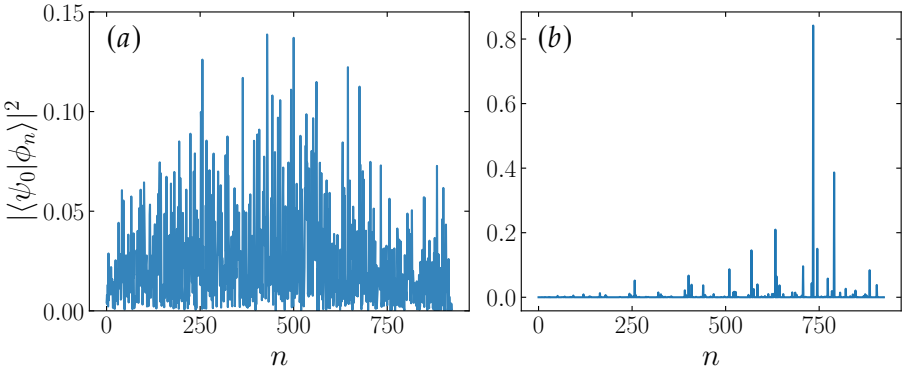

Figure 5.3. *Overlap coefficients* $|\langle\psi_0|n\rangle|^2$ *for a single realization of the disorder potential and a single random product state* $|\psi_0\rangle$. (*a*) *is for a single shot at disorder strength* $W = 1$, (*b*) *for* $W = 5$. *The results are obtained for a chain of* $L = 12$ *spins.*

regime, such as the one we are operating in, the saturation value $\mathcal{L}_\infty$ at long times can be easily obtained from the infinite time average of (5.18) as

$$\mathcal{L}_\infty = \overline{\mathcal{L}(t)} \sim \sum_n \left|\langle\psi_0|\phi_n\rangle\right|^4 = \mathrm{IPR}_0 \,. \tag{5.22}$$

Indeed, it was noted early on (Peres 1984) that for integrable Hamiltonian dynamics, most of the overlaps $\langle\psi_0|\phi_n\rangle$ are vanishing or very small, and only a few of them are significantly large. Thus, $\overline{\mathcal{L}(t)}$ oscillates with a high amplitude and the time average yields (5.22). On the other hand, for ergodic dynamics, one usually finds many small overlap coefficients that contribute equally to the fidelity decay, which ultimately results in a very small saturation value of the order $O(1/\mathcal{N})$, with $\mathcal{N}$ the dimension of the Hilbert space (Peres 1984). This conjectures can be easily tested numerically by fully diagonalizing the Hamiltonian and computing the overlap between the eigenstates and a chosen initial state $|\psi_0\rangle$. In Fig. 5.3 we show the overlaps $\langle\psi_0|\phi_n\rangle$ as a function of the eigenstate index n for a small chain of $L = 12$ sites at two different disorder strengths, $W = 1$ (a) and $W = 5$ (b). Even at the level of a single disorder realization, we find that for $W = 1$, $|\psi_0\rangle$ has a small but finite overlap with most of the ϕ_n, while the main contribution in the case of $W = 5$ clearly comes from few isolated "peaks".

In Fig. 5.4 (a), we show ED simulations of the evolution of $\mathcal{L}(t)$ in a chain of $L = 18$ spins for disorder strength $W \in [1.0, \ldots, 5.0]$ up to times $t = 10^3$. The curves shown are the result of averaging over $O(10^3)$ disorder realizations and 50 random initial product states. The perturbation strength is set at $\epsilon = 0.06$.

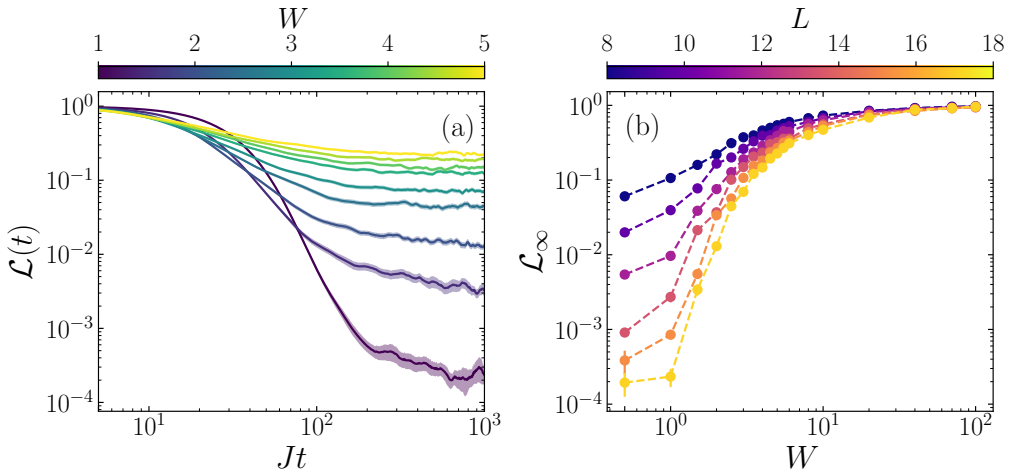

Figure 5.4. *Long-time decay of $\mathcal{L}(t)$ (a) and scaling of the saturation value $\mathcal{L}_\infty$ vs. disorder strength W (b). Data shown in (a) are obtained from long-time simulations of the dynamics of a chain of $L = 18$ sites for different values of W (color bar). The data in (b) are the result of an average over 100 data points at $t \gtrsim 10^3$ for system sizes $L = 8, 10, 12, 14, 16, 18$ (color bar). Results obtained for $\epsilon = 0.05$.*

As already discussed in Sec. 5.2.1, we find the Loschmidt echo to start decaying earlier for strong disorders, ultimately reaching a steady saturation value $\mathcal{L}_\infty$ at $t_{\text{sat}} \sim 10^2$. The decay towards $\mathcal{L}_\infty$ is steeper for low disorder strengths W, but its onset is again delayed with respect to the strong disorder case. As a result, the fidelity for $W = 1$ is still decaying at $t \sim 10^2$, before reaching $\mathcal{L}_\infty$ at $t_\infty \gtrsim 10^3$. Thus, there is approximately an order of magnitude of difference between the saturation times in the cases of weak ($W = 1$) and strong ($W = 5$) disorder. To obtain the saturation value $\mathcal{L}_\infty$, corresponding to IPR_0 as in (5.22), we consider 100 time points for $t \gtrsim 10^3$ and we compute their average $\overline{\mathcal{L}(t)}$ for different disorder strengths and systems sizes L. As suggested by the short-time results at stronger perturbation strengths (see Fig. 5.2.1 (a)), we find the value of $\mathcal{L}_\infty$ to increase with system size L for all disorder strengths W, as shown in Fig. 5.4 (b). Interestingly, the saturation value seems to stabilize at low disorders as we increase the system size: for $L = 18$, $\mathcal{L}_\infty$ appears almost constant for $W = 0.5$ and $W = 1$, before displaying a steep increase for $W > 1$. We provide further analysis on the scaling of $\mathcal{L}_\infty$ with the Hilbert space dimension $\mathcal{N}$ in Fig. 5.5. The saturation value $\mathcal{L}_\infty$ effectively follows the expected scaling for the IPR, i.e. $\mathcal{L}_\infty \sim \mathcal{N}^{-D_2}$, with the fractal dimension D_2 that can be extracted as the slope of a linear fit of $\ln \mathcal{L}_\infty$ vs. $\mathcal{N}$ (see Fig. 5.5 (b)). At weak disorders ($W = 0.5, 1$), the fit yields an exponent $D_2 \approx 1$, as expected in the case of a perfectly delocalized

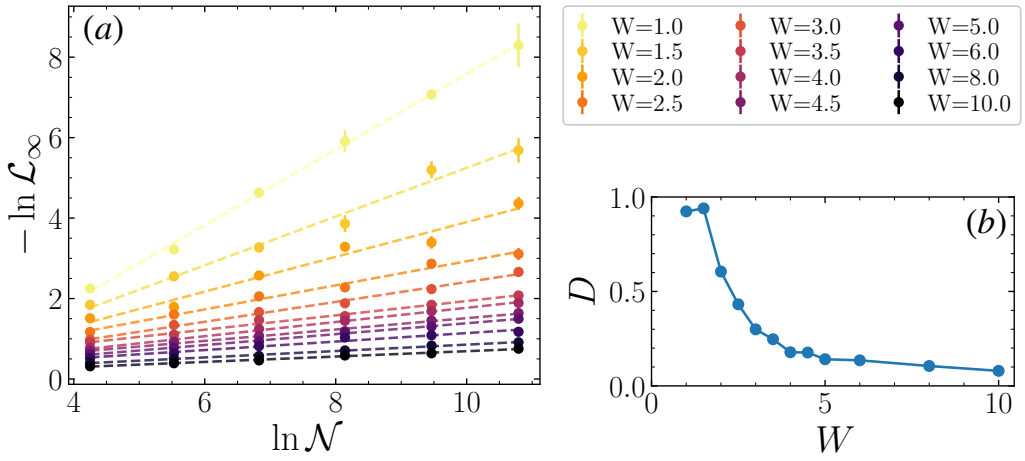

Figure 5.5. (*a*) *Scaling data of the disorder averaged* $-\ln \mathcal{L}_\infty$ *with the Hilbert space dimension of the system* $\ln \mathcal{N}$. *Dashed lines are a linear fit of the form* $D_2 \ln \mathcal{N}$. (*b*) *Fractal dimension* D_2 *extracted from the linear fit.*

state (Zelevinsky et al. 1996; Torres-Herrera et al. 2016; Torres-Herrera et al. 2017; Macé et al. 2019). As we increase $W > 1$, the data suggest that the eigenstates are delocalized but not fully ergodic, with the fractal dimension decreasing quickly for $1 < W \lesssim 3.5$. We suggest that this finding might be related to the existence of an MBME across the spectrum: contributions to the dynamics come from eigenstates both at the edges (localized) and the middle (extended) of the band. In particular, we confirm a crossover point at $W \gtrsim 1$ marking the start of the decay of D_2, as recently found in (Solórzano et al. 2021). At higher disorders D_2 starts slowly collapsing towards 0, marking the full localization of the many-body eigenstates, similarly to what is expected in the AL picture.

5.3 Conclusions and future work

In this Chapter, we presented preliminary results of an ongoing work about fidelity decay and sensitivity to global perturbations in MBL systems. We developed a non-equilibrium protocol through which one can study the fidelity dynamics as the evolving overlap between the states of two duplicates of a linear many-body system, with the only difference being a small parametric noise-like perturbation on one of the copies. Our protocol can be implemented with state-of-the art quantum simulation techniques, based on quantum many-body interferometry. We performed ED simulations focusing on both short and the long-time scales. The short-time decay of the Loschmidt echo suggests that

MBL systems are more sensitive to the effects of global perturbations at strong disorder, decaying more rapidly that in the ergodic regime of weak disorder. Nonetheless, the fidelity approaches higher saturation values at strong disorders, while decaying to values $\mathcal{L} \sim 1/\mathcal{N}$ in the delocalized regime. Tuning the strength of the perturbation results in the possibility of controlling the different time scales involved in the dynamics: decreasing the perturbation parameter delays the onset of the decay and the long-time saturation time.

In the long-time regime, we focused on the study of the steady saturation values $\mathcal{L}_\infty$. We found that the fidelity saturation value follows the same scaling expected for the IPR, confirming the predictions of perturbative analysis. The fractal dimension D_2 extracted from the scaling fit clearly identifies separate behaviors depending on the disorder strength. At weak disorders, D_2 is close to 1, as predicted for fully delocalized states, before decaying at intermediate disorder strengths towards very small values. We thus find a multifractal regime preceding the ETH-MBL transition, as also found in (Luitz et al. 2020a) and (Solórzano et al. 2021). On the other hand, large-scale numerics presented by (Macé et al. 2019) presents a scenario in which the fractal dimension is a sensitive probe of the MBL-ETH transition. Through an extensive scaling analysis in the vicinity of the critical point, they conclude that $D_2 = 1$ in the entire ETH phase and that it shows a discontinuous jump at the critical W_c to lower values. As we did not carry out a complete scaling analysis of this kind, which we intend to pursue in a future work, we cannot fully exclude the influence of finite-size effects in our simulations, with the multifractal regime shrinking towards the critical value, as suggested by (Macé et al. 2019).

The work presented in this Chapter provides a path to extract spectral features, such as IPR_0 and the fractal dimension D_2, via dynamical probes. Motivated by experimental considerations, we are looking forward to explore the role of the perturbation strength in more detail. Indeed, the possibility of tuning the time scales of the quench dynamics through the amplitude of the perturbation represents a novel feature of experimental interest. Nonetheless, one must find a delicate balance between the tuning of the perturbation strength and the possibility of exiting the perturbative regime, which ensures the correspondence between the participation ratios and the Loschmidt echo decay properties.

Part III

Spin-filtering robustness in the presence of disorder

6

Spin-filtering and localization

In the concluding part of this Thesis we take a step back from the interacting models we have been dealing with so far to focus on the effect of disorder on *spin transport* properties of some low dimensional free-particle structures. In particular, we will review a simple tight-binding framework able to describe the selective transmission of particles with arbitrary spin component, thus realizing a minimal design for spin filtering devices. After discussing the main numerical tool employed in this study, i.e. the *Transfer Matrix Method* (TMM), the central part of the Chapter will be devoted to the study of the robustness of spin-filtering effects in the presence of disorder-induced AL. Extensive numerical calculations of localization lengths reveal that, even in the presence of low to moderate disorder, different spin components can be selectively localized in different regimes of energy. While one spin component gets localized in a certain subband, the remaining ones can remain extended, at least within the system size considered. This implies that spin filtering can indeed be observed at different subsections of the 'energy bands', and such phenomenon can be assessed, via the TMM, to be robust even in the presence of randomness. The robustness of the phenomenon may be inspiring for experimentalists in designing quantum wires where a bit of disorder can creep in, and yet the system can act as a stable spin filter.

6.1 An overview of spin-polarized transport

The classical paradigm of charge transport in semiconductors, based on the propagation of electrons or holes, has been dressed, in recent years, with the novel concept of spin transport. The field of *spintronics* (Prinz 1998; Žutić

et al. 2004) evolved rapidly in the last few decades, bringing forward the idea of transporting information through the spin degrees of freedom of electrons, along with or even replacing the role of their charge. To allow such progress, a strong bond emerged between traditional solid state physics and materials science (Bercioux et al. 2015). Spintronics exploits the ability of conduction electrons to carry a spin-polarized current (Pareek et al. 2002), and relies heavily on long decoherence time and length scales, leading to elegant multi-functionality, increased data processing speed and less power consumption (Matityahu et al. 2013). Such a vast potential is definitely what puts the subject of spin-polarized transport at the forefront of contemporary solid state and materials science research, along with the pivotal role it plays in the development of quantum information technology (Awschalom et al. 2013).

Experiments in this direction have been inspiring, especially in the last two decades. The development of molecular wires and spin-polarized tunneling devices (Andres et al. 1996) helped to explore spin-polarized transport in low dimensional systems. Studies on the quantum confinement effect on electron transport (Goldhaber-Gordon et al. 1998; Cronenwett 1998; Yu et al. 2005), spin filtering and switching effects using ferromagnetic 'leads' and external fields (Frustaglia et al. 2001; Koga et al. 2002), precision maneuvering over spin currents (Lü et al. 2007) and other experiments on spin-polarized conductance in carbon nanotubes (Sahoo et al. 2005; Alam et al. 2015) have enriched the understanding and, at the same time, have brought the scope of this relatively recent field of spin transport into limelight. Besides, studies on the spin selective properties of chiral double-stranded DNA molecules (Göhler et al. 2011; Xie et al. 2011), on the spin filtering effect exhibited by chiral molecules (Mathew et al. 2014), and spin injection and spin transport in organic spin valves (Geng et al. 2016) have widened the horizon of the subject. Comprehensive theoretical knowledge also accumulated over the years, not only corroborating the experimental findings but also posing challenges concerning the design of new experimental setups. A simple quantum interferometer, designed in the shape of a single mode ring and threaded by a magnetic flux (Büttiker et al. 1984; Cheung et al. 1988), has proven to be a well-suited object to understand the interplay of a closed loop geometry and a trapped magnetic flux in terms of the path-breaking Aharonov-Bohm effect (Aharonov et al. 1959). Such a simple system with a two-terminal lead geometry was later exploited (Wang et al. 2008) to study the anisotropic spin transport in the presence of the Rashba and Dresselhaus spin-orbit interactions (Bychkov et al. 1984; Dresselhaus 1955). Earlier, a

model quantum ring with a side-coupled stub was proposed for potential spin filters with comprehensive control (M. Lee et al. 2006). Recently, an analytical tight binding model has been proposed to study the spin-polarized transport in DNA molecules as well (Varela et al. 2016).

In this context, it is worth pointing out that tight binding models of magnetic chains, acting as spin filters under various geometrical configurations, have provided a set of quite interesting tools in understanding certain subtle aspects of spin filtering. In this communication, we shall be focusing on such a model. A variety of such studies rely on describing a one-dimensional nano-wire by 'magnetic' atoms whose magnetic moments interact with the spin of the projectile that is incident on the system from one side (Shokri et al. 2005; Dey et al. 2011; Shokri et al. 2006; Mardaani et al. 2006).

Spin-polarized transport studies of higher-spin atoms have not yet received the same attention as more conventional spin-1/2 electronic transport. However, large-spin atomic gases have already been the subject of promising theoretical investigations since the end of the last century (T. L. Ho et al. 1999; Yip et al. 1999; Wu et al. 2003; Honerkamp et al. 2004), mainly inspired by the discovery of Bose-Einstein condensation in atomic gases and the search for superfluid phases in alkali atoms. Fermionic alkaline-earth atoms with large nuclear spin have also been considered for quantum information processing and as quantum simulators for many-body exotic phenomena (Gorshkov et al. 2010). In the last decade, the great experimental progress in the field of ultra-cold atoms in optical lattices, abundantly mentioned in previous Chapters, has made the realization of such systems possible. A far-from exhaustive list of examples include the study of quantum degeneracy in an ultracold gas of ^{87}Sr atoms (Desalvo et al. 2010), the realization of a 1D gas of fermions with tunable spin (Pagano et al. 2014), investigations on exotic forms of magnetism related to the SU(N) symmetry emerging in cold atoms with high-spin states (Zhang et al. 2014), and the gas mixture of two fermionic isotopes of Ytterbium, ^{1}71Yb (nuclear spin $I = 1/2$) and ^{1}73Yb (nuclear spin $I = 5/2$) (Taie et al. 2010). Theoretical (T. L. Ho 1998; Ciobanu et al. 2000; Zhou 2001; Demler et al. 2002; Kuhn et al. 2012) and experimental (Stenger et al. 1998; Stamper-Kurn et al. 1999; Leanhardt et al. 2003) efforts in the study of bosonic gases have been equally successful (Kawaguchi et al. 2012), attracting an increasing amount of attention due to a rich variety of phenomena.

6.1.1 Spin-filtering for arbitrary spins

A simple design for describing spin selective transport in a periodic array of magnetic atoms was introduced in (B. Pal et al. 2016b). The idea was later implemented to study the interplay of quasi-periodic arrangements and the topology of specific model networks comprising magnetic and non-magnetic atoms, having a minimal quasi-one dimensionality. It was shown how a hidden dimension in the linear chain of networks opened up, depending on the spin state of the incoming projectile (A. Mukherjee et al. 2018), which could be exploited to filter out any desired spin channel. The correlations between the parameters of the Hamiltonian and an external magnetic field were found crucial in delocalizing almost all the single particle states over continuous zones in the energy spectrum, thus obtaining a clean spin filtering.

The simple model proposed in (B. Pal et al. 2016b) is a linear array of magnetic atoms grafted onto a substrate. The substrate material is able to provide to each particle a magnetic moment $\vec{h} = (h_x, h_y, h_z)$, as depicted in Fig. 6.1 (a). A tight-binding Hamiltonian describing such a model reads (Shokri et al. 2005; Shokri et al. 2006; Mardaani et al. 2006; Dey et al. 2011)

$$\mathcal{H} = \sum_n \mathbf{c}_n^\dagger \left(\epsilon_n - \vec{h}_n \cdot \mathbf{S}_n\right) \mathbf{c}_n + \sum_{\langle n,m \rangle} \left(\mathbf{c}_n^\dagger \mathbf{t}_{n,m} \mathbf{c}_m + h.c.\right), \tag{6.1}$$

where each of the entries $\mathbf{c}_n^\dagger$, $\mathbf{c}_n$, ϵ_n, $\mathbf{t}_{n,m}$ and $\mathbf{S}_n$ are multi-component quantities expressed in terms of the spin projections $m_S = -S, -S+1, \cdots, S-1, S$, for a total of $2S+1$ components. In the spin-1/2 case, the only available components can be labelled as $\uparrow, \downarrow$ and subsequently we have

$$\mathbf{c}_n^\dagger = \left(c_{n,\uparrow}^\dagger c_{n,\downarrow}^\dagger\right), \quad \mathbf{c}_n = \left(c_{n,\uparrow} c_{n,\downarrow}\right), \quad \epsilon_n = \mathrm{diag}(\epsilon_{n,\uparrow}, \epsilon_{n,\downarrow}), \quad \mathbf{t}_{n,m} = \mathrm{diag}(t,t), \tag{6.2}$$

where $\mathbf{c}_n^\dagger(\mathbf{c}_n)$ is the spinful creation (annihilation) operator at site n, ϵ_n is the diagonal on-site potential and t is the spin-independent, uniform hopping integral along the chain. If a particle is injected in the system, its spin interacts with the local magnetic moment $\vec{h}_n$ at site n through the term $\vec{h}_n \cdot \mathbf{S}_n = h_{n,x}\boldsymbol{\sigma}_x + h_{n,y}\boldsymbol{\sigma}_y + h_{n,z}\boldsymbol{\sigma}_z$, where $\boldsymbol{\sigma}_x, \boldsymbol{\sigma}_y, \boldsymbol{\sigma}_z$ are the Pauli spin matrices (or the generalized Pauli matrices $\boldsymbol{\sigma}^{(S)}$ for higher spins). Explicitly, in the spin-1/2 case we have

$$\vec{h}_n \cdot \mathbf{S}_n = \begin{pmatrix} h_n \cos\theta_n & h_n \sin\theta_n e^{-i\phi_n} \\ h_n \sin\theta_n e^{i\phi_n} & -h_n \cos\theta_n \end{pmatrix}, \tag{6.3}$$

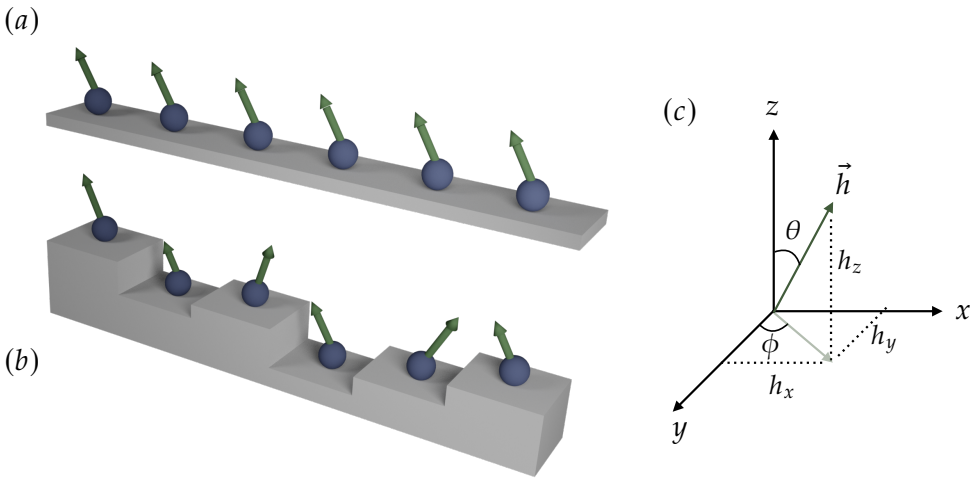

Figure 6.1. (*a*) *Schematic diagram of a linear magnetic chain grafted on a substrate* (*gray block*). *Each magnetic atom* (*blue sphere*) *is subject to a substrate-induced magnetic moment* $\vec{h}$ (*green arrows*). (*b*) *The same atomic chain in the presence of potential and magnetic field disorder. The random heights at which the particles are positioned simulate the irregularity of the substrate surface and thus the disorder on the onsite potential. The random orientations of the field vector represent the disorder in the induced magnetic moment.*(*c*) *Decomposition of the magnetic moment* $\vec{h}$ *onto its spatial coordinates.*

with θ_n and ϕ_n the polar and azimuthal angles, respectively. Through a combination of *local density of states* (LDOS) and transmission probabilities calculations, (B. Pal et al. 2016b) was able to show that the clean Hamiltonian (6.1) could act as a quantum device opening a transmission window only for specific spin components, depending on the energy of the projectile. Interestingly, such a result was shown to hold for arbitrary spin particle ($S = 1/2, 1, 3/2, \dots$).

6.2 Model and methods

In the following, we will provide evidence of the robustness of such spin-filtering effect in the presence of AL, induced by the presence of disorder. We study some modified versions of (6.1), including randomness in the values of the on-site potentials and in the magnitudes as well as in the orientations of the magnetic moments with respect to a preferred axis (See Fig. 6.1 (b) for a visual sketch of the disordered version of the model). More specifically, the onsite energies ϵ_n are chosen as randomly distributed in a box $[-W/2, W/2]$, as in the pure AL model (2.23), and the magnetic moments orientations are determined by random values of the polar angle $\theta_n \in [-W_\theta/2, W_\theta/2]$, and we

fix $\phi = 0$. We perform exhaustive calculations of the *spin-resolved localization lengths*, specifically designed for our purpose, in various disorder scenarios. In order to proceed, it is thus necessary to introduce the main formalism and the related computational techniques employed in the present work.

6.2.1 Transfer Matrix Method

For simplicity, let us start by momentarily neglecting spin components and focusing on a spinless fermionic chain. The TMM has been successfully employed in the past 30 years and imposed itself as one of the best resources to extract localization and transport properties of disordered systems (MacKinnon et al. 1981; Kramer et al. 1993). It allows a direct calculation of the localization length through an iterative formulation of the usual time-independent Schrödinger equation (1.8) for a d-dimensional bar, as

$$t_{n,n+1}\psi_{n+1} = (E - H_n)\psi_n - t_{n,n-1}\psi_{n-1}, \tag{6.4}$$

where ψ_n is the vector of the L^{d-1} wave function amplitudes of the n-th slice of the bar. $t_{n,n+1}$ is the matrix of inter-layer hopping terms between sites on the cross sections n and $n+1$, while H_n is the matrix of intra-layer couplings at n. Equation (6.4) can be explicitly recast in a recursive form through a matrix formalism, [1] i.e.

$$\begin{pmatrix} \psi_{n+1} \\ \psi_n \end{pmatrix} = \begin{pmatrix} \frac{(E-H_n)}{t} & -\mathbf{I} \\ \mathbf{I} & 0 \end{pmatrix} \begin{pmatrix} \psi_n \\ \psi_{n-1} \end{pmatrix} = \mathbf{T}_n \begin{pmatrix} \psi_n \\ \psi_{n-1} \end{pmatrix}, \tag{6.5}$$

defining the symplectic *transfer matrix* $\mathbf{T_n}$. Since the matrix is symplectic, the eigenvalues appear as M^2 pairs of opposite sign. For the whole bar, we thus have

$$\begin{pmatrix} \psi_{L+1} \\ \psi_L \end{pmatrix} = \mathbf{T}_L \mathbf{T}_{L-1} \cdots \mathbf{T}_1 \begin{pmatrix} \psi_1 \\ \psi_0 \end{pmatrix} = \prod_{n=1}^{L} \mathbf{T}_n \begin{pmatrix} \psi_1 \\ \psi_0 \end{pmatrix} = \mathbf{Q}_L \begin{pmatrix} \psi_1 \\ \psi_0 \end{pmatrix}, \tag{6.6}$$

As Q_L is a product of random matrices, one can apply Oseledets's theorem (V. I. Oseledets 1968; Ruelle 1979), which states that the limiting matrix

$$\Omega = \lim_{L\to\infty} (\mathbf{Q}_L \mathbf{Q}_L^\dagger)^{\frac{1}{2L}}, \tag{6.7}$$

has converging eigenvalues e^{γ_i} in the limit of large L and corresponding eigen-

[1] From now on, we set $t_{n,n+1} = t_{n,n-1} = t$.

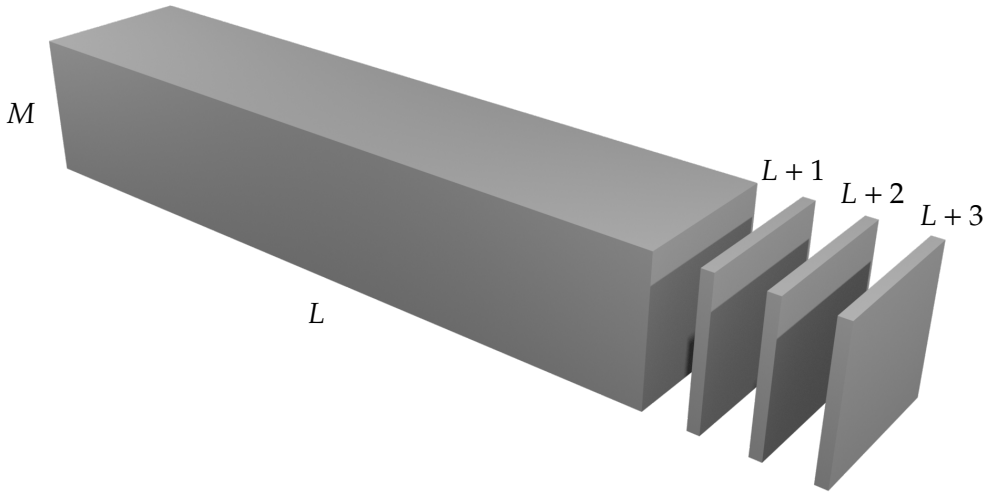

Figure 6.2. *Transfer-matrix bar schematic picture.*

vectors u_i, satisfying

$$\gamma_i = \lim_{L\to\infty} \frac{1}{L} \ln ||\mathbf{Q}_L u_i||. \tag{6.8}$$

The exponents γ_i are called *Lyapunov exponents*[2] and they are directly related to the localization length. Indeed, as the localization length characterizes the largest possible extension of the wavefunction in space, the smallest Lyapunov exponent is the inverse of the localization length λ (MacKinnon et al. 1981):

$$\lambda = \frac{1}{\gamma_{\min}}. \tag{6.9}$$

Choosing an arbitrary starting vector $u^0 = \begin{pmatrix} \psi_1 \\ \psi_0 \end{pmatrix}$ we can iterate equation (6.8) and obtain all the possible Lyapunov exponents. The component of u^0 corresponding to the largest γ_i gets the strongest amplification and leads to γ_{max}. Thus, the first step of the algorithm is the choice of initial condition vectors ψ_1 as the identity matrix and ψ_0 being the null matrix, such that $\{u_i^0\} = \begin{pmatrix} \mathbf{I} \\ 0 \end{pmatrix}$. For $L \to \infty$ the iteration of (6.8) leads to the eigenvalues and eigenvectors of Ω, and one can get the localization length λ. After few multiplications, though, the vectors $\{\tilde{u}_i^0\} = \mathbf{Q}_L u_i^0$ will lose orthogonality, and we have to apply a renormalization routine such as the Gram-Schmidt method to re-establish the orthogonality after

[2]Note that the same terminology refers to the exponent describing the degree of separability of classical trajectories in chaotic systems, see Sec. 1.3.

n_M multiplications.

We can finally get a conclusive expression for the Lyapunov exponents assuming that the vectors u_i^m already converged to the real eigenvectors u_i, thus without changing their direction anymore. Using the norm $a_i^m = ||\tilde{u}_i^m||$ we get

$$\gamma_i = \frac{1}{L} \lim_{n_O \to \infty} \sum_{m=1}^{n_O} \ln ||\tilde{u}_i^m||, \tag{6.10}$$

where n_O is the number of reorthonormalization steps performed during the process and u_i^m are the vectors obtained after the m-th step. Conveniently, it is possible to stop at finite sizes L and obtaining an approximation for γ_i with an error of (Benettin et al. 1980)

$$\frac{\sigma(\gamma_i)}{\gamma_i} = \sqrt{\frac{\sum_{m=1}^{n_O} (\ln a_i^m)^2}{(\sum_{m=1}^{n_O} \ln a_i^m)^2} - \frac{1}{n_O}}. \tag{6.11}$$

With the same spirit, we go back to our model Hamiltonian (6.1). We can write an analytical form of the Schrödinger equation for the two different spin channels ($\uparrow$ and $\downarrow$) at energy E starting from the general time-independent equation $\mathcal{H}\psi = E\psi$, with $\psi = \{\psi_{1,\uparrow}, \psi_{1,\downarrow}, \ldots, \psi_{n,\sigma}, \ldots\}$. We note that the band width is $E_B = 4t + 2h$ for all S in the clean case $W = 0$. Using the Hamiltonian (6.1) we get recursive equations relating the wave function at site n with the neighboring at sites $n \pm 1$. When recast in the transfer matrix formalism, we find

$$\begin{pmatrix} \psi_{n+1,\uparrow} \\ \psi_{n+1,\downarrow} \\ \psi_{n,\uparrow} \\ \psi_{n,\downarrow} \end{pmatrix} = \begin{pmatrix} \frac{(E-\epsilon_{n,\uparrow}+h_n\cos\theta_n)}{t} & \frac{h_n \sin\theta_n}{t} & -1 & 0 \\ \frac{h_n \sin\theta_n}{t} & \frac{(E-\epsilon_{n,\downarrow}-h_n\cos\theta_n)}{t} & 0 & -1 \\ 1 & 0 & 0 & 0 \\ 0 & 1 & 0 & 0 \end{pmatrix} \begin{pmatrix} \psi_{n,\uparrow} \\ \psi_{n,\downarrow} \\ \psi_{n-1,\uparrow} \\ \psi_{n-1,\downarrow} \end{pmatrix} = \mathbf{T}_n \begin{pmatrix} \psi_{n,\uparrow} \\ \psi_{n,\downarrow} \\ \psi_{n-1,\uparrow} \\ \psi_{n-1,\downarrow} \end{pmatrix}, \tag{6.12}$$

where $\mathbf{T}_n$ is the transfer matrix at site n. Thus, we obtain the transfer matrix for the entire linear system as $\mathbf{T_L} = \prod_{n=1}^{L} \mathbf{T}_n$. For spin-1 particles, the generalized spin operator matrices are (Gell-Mann 1962)

$$\boldsymbol{\sigma}_x^{(S=1)} = \frac{1}{\sqrt{2}} \begin{pmatrix} 0 & 1 & 0 \\ 1 & 0 & 1 \\ 0 & 1 & 0 \end{pmatrix}, \quad \boldsymbol{\sigma}_y^{(S=1)} = \frac{1}{\sqrt{2}i} \begin{pmatrix} 0 & 1 & 0 \\ -1 & 0 & 1 \\ 0 & -1 & 0 \end{pmatrix}, \quad \boldsymbol{\sigma}_z^{(S=1)} = \begin{pmatrix} 1 & 0 & 0 \\ 0 & 0 & 0 \\ 0 & 0 & -1 \end{pmatrix}, \tag{6.13}$$

and the interaction term is given by

$$\vec{h}_n \cdot \mathbf{S}_n^{(S=1)} = \begin{pmatrix} h_n \cos\theta_n & \frac{h_n \sin\theta_n}{\sqrt{2}} & 0 \\ \frac{h_n \sin\theta_n}{\sqrt{2}} & 0 & \frac{h_n \sin\theta_n}{\sqrt{2}} \\ 0 & \frac{h_n \sin\theta_n}{\sqrt{2}} & -h_n \cos\theta_n \end{pmatrix}. \tag{6.14}$$

Thus, the transfer matrix at the n-th site for spin-1 particles reads as

$$\mathbf{T}_n^{(S=1)} = \begin{pmatrix} \frac{(E-\epsilon_{n,1}+h_n\cos\theta_n)}{t} & \frac{h_n \sin\theta_n}{\sqrt{2}t} & 0 & -1 & 0 & 0 \\ \frac{h_n \sin\theta_n}{\sqrt{2}t} & \frac{(E-\epsilon_{n,0})}{t} & \frac{h_n \sin\theta_n}{\sqrt{2}t} & 0 & -1 & 0 \\ 0 & \frac{h_n \sin\theta_n}{\sqrt{2}t} & \frac{(E-\epsilon_{n,-1}-h_n\cos\theta_n)}{t} & 0 & 0 & -1 \\ 1 & 0 & 0 & 0 & 0 & 0 \\ 0 & 1 & 0 & 0 & 0 & 0 \\ 0 & 0 & 1 & 0 & 0 & 0 \end{pmatrix}. \tag{6.15}$$

It is worth noting the hidden analogy between the one-dimensional model (6.1) and the relative equations (6.12) with the equations for spinless fermions on a two-strand ladder network (Sil et al. 2008): the system can be imagined as two identical chains coupled laterally, with an effective random onsite potential $\epsilon_{n,\uparrow} - h_n \cos\theta_n$ for the virtual "upper" strand corresponding to the $\uparrow$ component, and $\epsilon_{n,\downarrow} + h_n \cos\theta_n$ for the "lower" strand representing the $\downarrow$ projection. From this point of view, the hopping t is the independent hopping along individual strands in the network, while the off-diagonal terms $h_n \sin\theta_n$ turn on inter-strand hopping channels. This kind of mapping can be generalized to arbitrary spin values, with the number of strands corresponding to the $2S+1$ spin projections. Intuitively, this ladder picture could represent a more immediate way of visualizing the spin filtering phenomenon, imagining that under certain tuning procedures transport is allowed only in one (or some, for $S > 1/2$) strand.

6.2.2 Spin-resolved localization lengths

As described above, the TMM amounts to the diagonalization of the transfer matrix $\mathbf{T}_L = \prod_{n=1}^{L} T_n$,

$$\mathbf{U}^{-1}\mathbf{T}_L^{\dagger}\mathbf{T}_L\mathbf{U} = \mathrm{diag}(e^{-2L/\lambda_1}, e^{-2L/\lambda_2} \ldots, e^{-2L/\lambda_{2S+1}}, e^{2L/\lambda_{2S+1}}, \ldots, e^{2L/\lambda_1}), \tag{6.16}$$

for a suitably large L to achieve the preset accuracy target (Kramer et al. 1993). Each λ_{m_S}, together with its associated eigenvector

$$\left(\psi^{(m_S)}_{L,-S},\ldots,\psi^{(m_S)}_{L,S},\psi^{(m_S)}_{L-1,-S},\ldots,\psi^{(m_S)}_{L-1,S}\right), \tag{6.17}$$

correspond to a transport channel, but not automatically to a spin projection $\sigma = -S,\ldots,S$. Instead, the eigenstate corresponding to the largest localization length, say λ_1, changes its spin content depending on parameters such as E. In Fig. 6.3 (a), we show the computed localization lengths λ_1, λ_2 for $S = 1/2$ with a weak disorder $W = 0.5$. The selection of different values of the fixed magnetic moment strength $h_n = h$ modifies the band structure of the model, opening a clear gap Δ as h increases, as already seen in (B. Pal et al. 2016b) (more details on band structure engineering will be provided in the following Sections). We observe that while λ_1 clearly identifies the two regions with finite transport, λ_2 remains nearly zero throughout the energy band. Nonetheless, by computing the probability amplitudes

$$\begin{aligned}\uparrow^{(i)} &= \left|\psi^{(i)}_{n,\uparrow}\right|^2 + \left|\psi^{(i)}_{n-1,\uparrow}\right|^2\\ \downarrow^{(i)} &= \left|\psi^{(i)}_{n,\downarrow}\right|^2 + \left|\psi^{(i)}_{n-1,\downarrow}\right|^2,\end{aligned} \tag{6.18}$$

with $i = \{1,2\}$ labelling the two transport channels, plotted in Figs. 6.3 (c+e), we see that suitably chosen spin projections can distinguish the spin content of each subband: in (c), the probability of the $\sigma = 1/2$ projection dominates for $E > 0$ while the $\sigma = -1/2$ projection is large for $E < 0$; in (e) the situation is reversed, the $\sigma = 1/2$ projection dominates for $E < 0$ while the $\sigma = -1/2$ projection is large for $E > 0$. At $E = 0$, in both (c) and (e), we find a rapid change. In both figures, we note that the sum of the probabilities adds to 1, due to normalization.

We therefore introduce *spin-resolved localization lengths*, namely,

$$\Lambda_\sigma(n) = \sum_{m_S=1}^{2S+1} \lambda_{m_S}(n)\left(\left|\psi^{(m_S)}_{n,\sigma}\right|^2 + \left|\psi^{(m_S)}_{n-1,\sigma}\right|^2\right), \tag{6.19}$$

for $\sigma = -S, -S+1,\ldots,S$. In Eq. (6.19), the index $m_=1,\ldots,2S+1$ spans all possible spin projections. For $S = 1/2$, the explicit form is

$$\Lambda_\uparrow(n) = \lambda_1(n)\left(\left|\psi^{(1)}_{n,\uparrow}\right|^2 + \left|\psi^{(1)}_{n-1,\uparrow}\right|^2\right) + \lambda_2(n)\left(\left|\psi^{(2)}_{n,\uparrow}\right|^2 + \left|\psi^{(2)}_{n-1,\uparrow}\right|^2\right), \tag{6.20a}$$

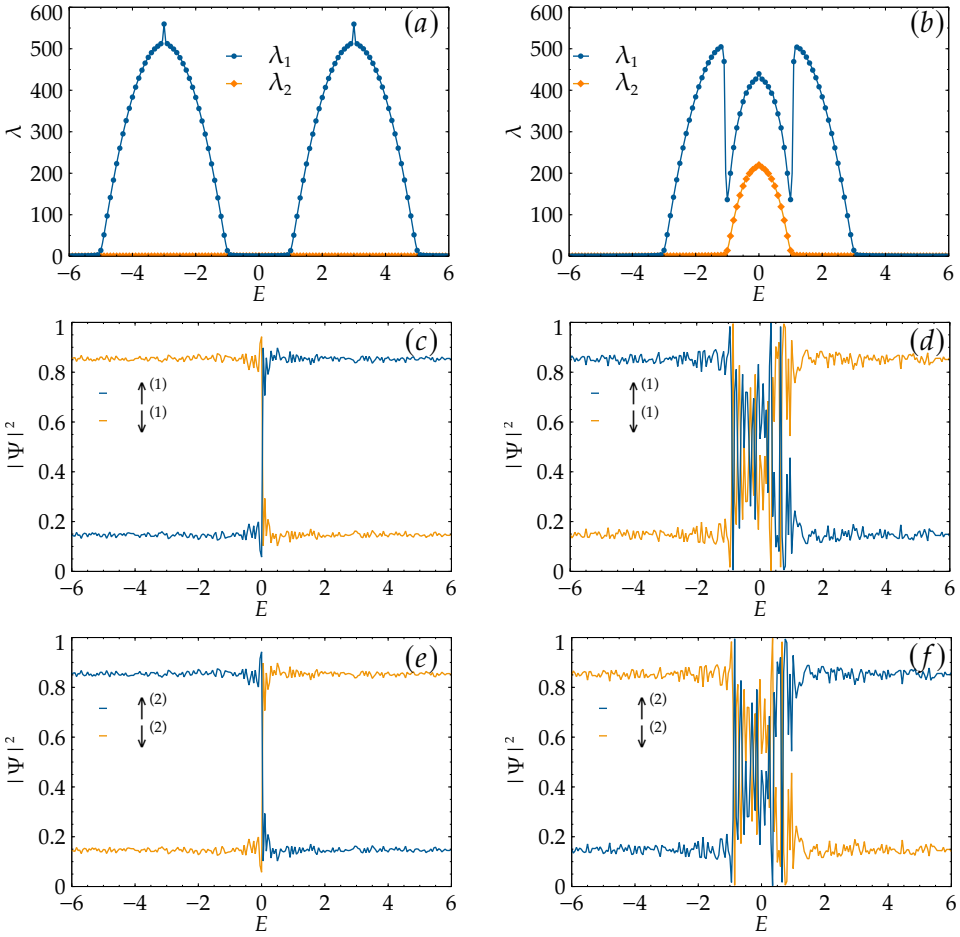

Figure 6.3. *First column (a+c+e): (a) Bare localization length λ_1 and λ_2 from the TMM for $h = 3$ and $\theta = \pi/4$ (d). (c+e) Probability amplitudes $\uparrow^{(i)}$, $\downarrow^{(i)}$ associated with the two transport channels denoted as '1' and '2' for the spin-1/2 case. The results are for $h = 3$ and a polar angle $\theta = \pi/4$. Second column (b+d+f): Same as (a+c+e) for $h = 1$, resulting in band overlapping at the center of the spectrum.*

$$\Lambda_{\downarrow}(n) = \lambda_1(n)\left(\left|\psi^{(1)}_{n,\downarrow}\right|^2 + \left|\psi^{(1)}_{n-1,\downarrow}\right|^2\right) + \lambda_2(n)\left(\left|\psi^{(2)}_{n,\downarrow}\right|^2 + \left|\psi^{(2)}_{n-1,\downarrow}\right|^2\right). \tag{6.20b}$$

We note that $\Lambda_\sigma(n) \leq \lambda_{m_S}(n)$ for all σ and m_S due to the normalization of the $\psi^{(m_S)}_{n,\sigma}$. All the results presented throughout the rest of this Chapter will be in terms of $\Lambda_\sigma(n)$. We note that this interpretation of the eigenvectors in terms of spin projections is very natural also for spatial transport channels in more standard situations (González-Santander et al. 2013). As will be clearer in the following, for smaller values of h the gap Δ between bands corresponding to different spin components vanishes. In such cases, reported for example in Fig. 6.3 (b+d+f) for $h = 1$ and $W = 0.5$, it is much harder to interpret the results beyond the realization of spin mixing in $-1 \leq E \leq 1$. Still, even in this situation, the projected Λ_σ results work well for $|E| > 1$, as we will discuss in 6.3.

Let us comment on the determination of errors for Λ_σ. For the λ_σ, we proceed as usual (Kramer et al. 1993), using the convegence of the Lyapunov exponents ensured by the Oseledet's theorem (6.8) and the fact that they are Gaussian distributed after sufficiently many transfer matrix multiplications (Milde 2000) to compute an error of the mean of at most 0.1%. The $\Psi_{n,\sigma}$, however, are not necessarily Gaussian distributed — indeed, they are mostly not — nor have they "converged" when the Lyapunov exponents already have. This is clearly visible in Fig. 6.3 where the spin projections vary, even for panels (c+e), at the $\sim 5\%$ level while the $\leq 0.1\%$ errors for the λ_σ are well within symbol size. Furthermore, in the overlap regions, e.g. in Fig. 6.3 (d+f), the fluctuations are much larger and represent a systematic source of variation, different from the purely statistical fluctuations of the λ_σ. We therefore show only the errors computed from the λ_σ in the figures of main sections. It may be useful in this context to point out that the computation of the Λ_σ amounts to computing the spatial content of the transport channels for the σ's. This is an even more challenging task than computing the spatial position of a localization center, when given a disorder distribution, which in itself is still an unsolved problem. In the following, we shall use Λ_σ to indicate *converged* estimates for $n \to \infty$, using the usual TMM convergence criteria (Kramer et al. 1993) for the λ_{m_S}'s. For all the calculations, we have set an accuracy threshold of 99.9% (error of the mean at most 0.1% for each λ_{m_S}), corresponding to a system of the order of $n \sim 10^{10}$ sites in the centre of the energy range. Due to normalization of the $\psi^{(m_S)}_{n,\sigma}$, we note that $\Lambda_\sigma \leq \max(\lambda_{m_S}, m_S = 1, \ldots, 2S+1)$ for all σ. Thus, although the Λ_σ are not the direct results of the TMM calculations, they are a proper measure of the localization properties in different spin transport channels. Lastly, we shall

drop the more precise labeling of spin-resolved localization lengths for the Λ_σ and merely call them localization lengths.

6.2.3 Density of States

As shown in (B. Pal et al. 2016b), the tuning of h_n is sufficient for the engineering of the energy bands corresponding to the various spin components, in the absence of magnetic flux. For the sake of simplicity, we restrict ourselves to the $S = 1/2$ case, but the following discussion also holds for particles with higher spin.

In the simplest case of $h_n = h$, $\theta_n = \theta = 0$, the cross terms determining the hybridization of the spin channels in Eq. (6.12) are canceled, and all moments will be parallel to each other, lying along the z-axis. In the limit of $t \to 0$, the energy spectrum will show sharp peaks at $E = \epsilon \pm h$, and the LDOS will correspondingly exhibit two δ-function-like spikes at these energy values. Switching on the hopping t results in a broadening of the spikes, ultimately merging in subbands when $t \sim h$. Hence, for a given value of θ, h can be tuned to open or close a gap in the energy spectrum.

We computed the LDOS for the $\uparrow$ and $\downarrow$ components evaluating the Green's function $\mathbf{G} = (E\mathbf{I} - \mathbf{H})^{-1}$ in the basis $|n, \uparrow (\downarrow)\rangle$. The LDOS is given as (B. Pal et al. 2016b)

$$\rho_{\uparrow\uparrow(\downarrow\downarrow)} = \lim_{\eta \to 0} \langle n, \uparrow (\downarrow) | \mathbf{G}(\mathbf{E} + \mathrm{i}\,\eta) | \mathbf{n}, \uparrow (\downarrow) \rangle \tag{6.21}$$

and the energy gap has the very simple form

$$\Delta = \begin{cases} \frac{h}{S} - 4t & \text{for } \frac{h}{S} > 4t, \\ 0 & \text{otherwise.} \end{cases} \tag{6.22}$$

This gap equation implies the existence of the critical magnetic strength $h_c = 4tS$ at which the bands meet, independently of the choice of θ.

6.3 Spin-filtering robustness

As already stated, we are interested in establishing a spin-filtering device that remains robust in the presence of disorder. In order to do so, we shall choose a small but not negligible onsite disorder $W = 0.5t \ll E_B$. Also, we shall investigate how spatial and random variations in h and θ affect the filtering. In all these cases, we shall take care to retain the connection to the clean case.

Finally, we shall also study the drop in Λ_σ when further increasing disorder. The energy scale is set by $t = 1$.

We obtain the localization lengths $\Lambda_\uparrow$, $\Lambda_\downarrow$ and the LDOS $\rho_\uparrow$, $\rho_\downarrow$ for two different band structure cases: (i) for $h = 1$, we have $\Delta = 0$ and the spectrum shows for $-1 \leq E \leq 1$ an overlapping of the spin-$\uparrow$ and spin-$\downarrow$ bands. (ii) The model develops a gap with growing h, and we chose to set $h = 3$ as the second case of study, representing a clear gap $\Delta = 2$ in the range $-1 \leq E \leq 1$. We also present, in every case, the LDOS for the corresponding 'clean' system without disorder. This is for comparison with the disordered case in order to indicate that the energy range of non-zero localization lengths remains largely in agreement with the clean band structure for the chosen values of W.

6.3.1 Energy dependence

We show in the upper panels of Fig. 6.4 (a+b) the localization length for the case of weak disorder in the on-site potential and $\theta = 0$. Since the off-diagonal terms are zero, we have complete channel separation, i.e. two uncoupled chains. The extent of the non-vanishing Λ_σ values is in good agreement with the span of the LDOS of the corresponding 'clean' system as shown in the LDOS plots in the lower panels of Fig. 6.4 (a+b). We envision that the system obviously exhibits a clear separation into two distinct energy bands for spin-$\uparrow$ and spin-$\downarrow$. This spin filtering effect has already been discussed for the clean version of the system described above (B. Pal et al. 2016b). The effect survives the introduction of randomness in the distribution of the on-site potential: in Fig. 6.4 (a), for $-3 \leq E \leq -1$, only spin-$\uparrow$ electrons get transported through the chain, while they are blocked for $1 \leq E \leq 3$. Conversely, for $1 \leq E \leq 3$, only spin-$\downarrow$ electrons contribute to transport and are blocked for $-3 \leq E \leq -1$. As seen here, the subbands overlap in the range $-1 \leq E \leq 1$, preventing perfect filtering, but allowing a *partial* filtering depending on the value of E. In Fig. 6.4 (b), on the other hand, an obvious gap opens between the subbands, and the spin filtering is complete: only spin-$\uparrow$ electrons get transported in the lower subband and only spin-$\downarrow$ electrons transmit in the upper one.

Of course, one has to be careful when speaking of "transport". Indeed, the finite localization lengths indicate strong localization for any system much larger than the $\Lambda_\uparrow$, $\Lambda_\downarrow$ values found here. Nevertheless, the values of $\Lambda_\uparrow$, $\Lambda_\downarrow$ are of course determined by which value of W was chosen to simulate a disordered environment. Let us assume for a moment that our system would have a finite length L (say, e.g., $L = 200$ in Fig. 6.4 (a+b)). The observation that we can find

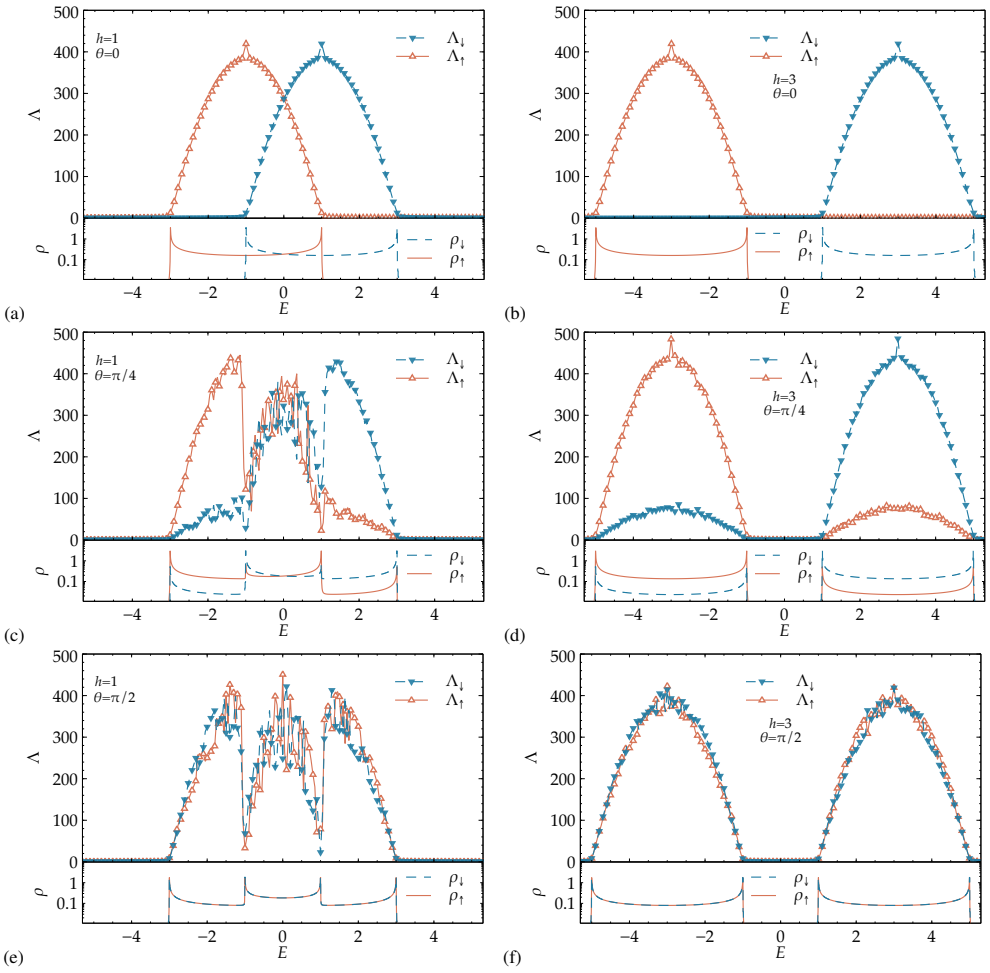

Figure 6.4. *Projected localization lengths* $\Lambda_\sigma = \lambda_\sigma |\Psi^2|$ *for the disordered magnetic chain and LDOS* ρ *for the corresponding pure systems for spin-*$1/2$ *particles, with* (*a*,*c*,*e*) *showing overlapping bands at* $h = 1$ *and* (*b*,*d*,*f*), *the well-separated bands at* $h = 3$. *The value of the polar angle* θ *changes from* (*a*,*b*) $\theta = 0$ *to* (*c*,*d*) $\pi/4$ *and* (*e*,*f*) $\pi/2$. *The strength of the potential disorder is* $W = 0.5$ *in all cases. For clarity, only every second data point is indicated by a symbol, i.e.* $\triangledown$ *for spin-*$\downarrow$ *and* $\triangle$ *for spin-*$\uparrow$. *The LDOS for the corresponding pure systems are shown in the lower part of the panels, corresponding to* $\rho_\downarrow$ (*dashed*) *and* $\rho_\uparrow$ (*solid line*) *for spin-*$\downarrow$ *and spin-*$\uparrow$. *Lines for* Λ_σ *are guides to the eye. The* λ_σ *error bars are within symbol size when not visible.*

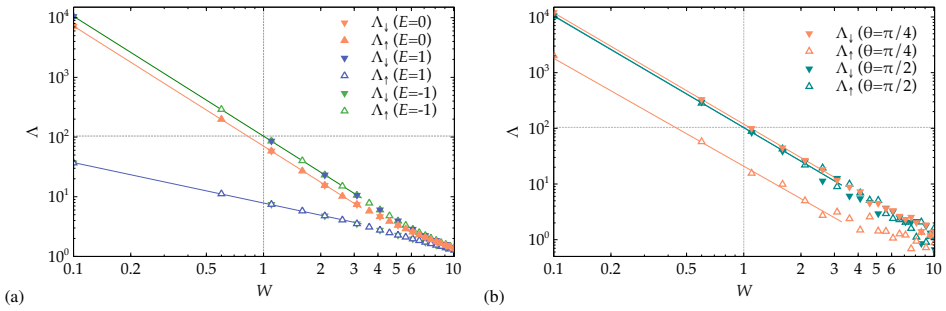

Figure 6.5. *Disorder dependence of spin-resolved localization lengths* Λ_σ *with* (*a*) *overlapping bands at* $h = 1$ *for* $\theta = 0$ *and* (*b*) *well-separated bands at* $h = 3$ *for* $\theta = \pi/2, \pi/4$. *In* (*a*) *different colors correspond to different energy values,* $E = -1$ (*center of the lower subband*), $E = 0$ (*bands crossing point*) *and* $E = 1$ (*center of the higher subband*). *In* (*b*) *the plots show the results for the center of the* $E = 3$ *subband, for different values of the polar angle* θ. *In all panels, the solid lines show fits with Eq.* (6.25) *up to* $W = 4$, *and the crossing point between the horizontal and the vertical dotted lines represents the band center Kappus-Wegner estimate* $\lambda(W = 1) = 104 \pm 1$ (*Kappus et al.* 1981).

broad energy regions with either $\Lambda_\uparrow, \Lambda_\downarrow \gtrsim L$ clearly shows the robustness of the spin filtering to the presence of W. Were we to compute a *spin-resolved* typical, dimensionless conductance by adapting a celebrated relation due to Pichard (Pichard 1984), i.e.

$$G_\sigma(n) = \sum_{m_S=1}^{2S+1} \frac{1}{\cosh^2\left(L/\lambda_{m_S}(n)\right)} \left(\left|\psi_{n,\sigma}^{(m_S)}\right|^2 + \left|\psi_{n-1,\sigma}^{(m_S)}\right|^2 \right), \tag{6.23}$$

we would find $G_\sigma \sim 1$ for energy regions in which $\Lambda_\sigma \gtrsim L$. Conversely, $G_\sigma \sim 0$ when $\Lambda_\sigma < L$. Last, the spikes at $E = -1$ for $\Lambda_\uparrow$, and at $E = 1$ for $\Lambda_\downarrow$ visible in Fig. 6.4 (a+b) are due to the famous Kappus-Wegner degeneracy in 1D Anderson models at the middle of the bands (Kappus et al. 1981).

Switching on the additional hopping between spin-↑ and spin-↓ channels for finite θ has a strong impact on spin filtering. Fig. 6.4 (c+d) show the results for $\theta = \pi/4$, for the same values of h discussed above. One can easily see that *mixing* between spin-↑ and spin-↓ states emerges. Looking at panel (d) for the sake of clarity, spin filtering still exists, but in a weaker sense: in the lower band, the spin-↓'s can travel a distance lower than spin-↑ particles by a factor of ~ 5, resulting in a more pronounced transport of the latter ones. In panel (c) of Fig. 6.4, we find that the spin-filtering for $-1 \leq E \leq 1$ has stopped and neither spin-↑ nor spin-↓ particles dominate. The resulting "transport"

will be spin-unpolarized. Spin filtering disappears for all energies at $\theta = \pi/2$ as expected. Each spin component can be transported through the sample for the same distance for both subbands. The vanishing of spin filtering becomes evident by looking at the complete overlapping of both the $\Lambda_\uparrow$, $\Lambda_\downarrow$ localization lengths and $\rho_\uparrow$, $\rho_\downarrow$ LDOS curves. We can understand the contributions coming from the individual spin projections at finite θ by noting that an SU(2) rotation results in a decoupled basis $\mathbf{\Phi}_n = \mathcal{R}^{-1}_{\mathrm{SU(2)}}\psi_n$ and the relations between the new basis vectors $\{\phi_{n,+}, \phi_{n,-}\}$ and the old $\{\psi_{n,\uparrow}, \psi_{n,\downarrow}\}$ are given by

$$\phi_{n,+} = \cos(\theta/2)\psi_{n,\uparrow} + \sin(\theta/2)\psi_{n,\downarrow}, \qquad \phi_{n,-} = -\sin(\theta/2)\psi_{n,\uparrow} + \cos(\theta/2)\psi_{n,\downarrow}. \tag{6.24}$$

Here, + and − denote the projected spin components after the SU(2) rotation. It is now easy to see that for, e.g., $\theta = \pi/2$ both states $\phi_{n,+}$ and $\phi_{n,-}$ have equally weighted contributions from the old $\psi_{n,\uparrow}$, $\psi_{n,\downarrow}$. The energy bands arising from the transformation (6.24) are centered at $\epsilon - h$ and $\epsilon + h$, and they span the ranges $[\epsilon - h - 2t, \epsilon - h + 2t]$ and $[\epsilon + h - 2t, \epsilon + h + 2t]$, respectively. The spectrum for the original spin states can be obtained through a convolution of the LDOS coming out of Eq. (6.24). Obviously, the numerical results of Fig. 6.4 show exactly this behavior.

Before leaving this discussion of the spin-1/2 case, let us comment on the θ dependence of Λ_σ. Comparing Fig. 6.4 (a+c+e), we see that there is a small increase of the maximal Λ values when θ increases from 0 and $\pi/4$ and $\pi/2$. In these latter situations — including also Fig. 6.4 (b+d+f) —, we are effectively dealing with a coupled quasi-1D system, and it is well-known that this leads to an increase in the localization lengths (Römer et al. 2004).

6.3.2 Disorder dependence

We now study the disorder dependence $\Lambda_\sigma(W)$ at fixed values of E. We focus on some of the most significant energy values in the spectrum, and we present the results in Fig. 6.5. For the gapless case $h = 1$, we study the behavior of Λ_σ for $\theta = 0$ corresponding to the center of the lower subband at $E = -1$, the contact point between the subbands at $E = 0$, and the center of the higher subband at $E = 1$. We find that the standard perturbative small−W Thouless fitting (Thouless 1972b; Czycholl et al. 1981; Kappus et al. 1981)

$$\Lambda(W) = \mathcal{A}\, W^{-\kappa}, \tag{6.25}$$

Table 6.1. *Fit parameters for the $\Lambda_\sigma(W)$ plots in Fig. 6.5 using Eq. (6.25).*

Λ	h	θ	E	$\mathcal{A}$	κ
$\Lambda_\downarrow$	1	0	0	70.4 ± 1.3	2.01 ± 0.02
$\Lambda_\uparrow$	1	0	0	70.5 ± 1.3	2.01 ± 0.02
$\Lambda_\downarrow$	1	0	1	103.4 ± 1.9	2.01 ± 0.02
$\Lambda_\uparrow$	1	0	1	7.9 ± 0.2	0.68 ± 0.02
$\Lambda_\downarrow$	1	0	-1	7.9 ± 0.2	0.68 ± 0.02
$\Lambda_\uparrow$	1	0	-1	103.4 ± 1.9	2.01 ± 0.02
$\Lambda_\downarrow$	3	$\pi/4$	3	118.9 ± 0.1	2.0003 ± 0.0007
$\Lambda_\uparrow$	3	$\pi/4$	3	20.87 ± 0.01	1.9384 ± 0.0006
$\Lambda_\downarrow$	3	$\pi/2$	3	103.7 ± 0.2	2.008 ± 0.001
$\Lambda_\uparrow$	3	$\pi/2$	3	102.64 ± 0.01	2.0004 ± 0.0001

works very well as shown in Table 6.1. We note that for majority states at the center of spin-split bands, even the Kappus-Wegner singularity with $\mathcal{A} = 104 \pm 1$ is well recovered (Kappus et al. 1981). For the mixed states at $E = 0$, the value of $\mathcal{A}$ changes but $\kappa \approx 2$ remains valid. In the tails of the subbands, the behavior is quantitatively different. While the power-law (6.25) still holds, the $\mathcal{A}$ and κ values have changed.

Fig. 6.5 (b) shows the behavior of $\Lambda_\sigma(W)$ for the gapped systems at $h = 3$ for $\theta = \pi/4, \pi/2$ in the center of the higher subband at $E = 3$. There is again good agreement with (6.25) for the κ value. Since we are now effectively dealing with two coupled chains, the value of $\mathcal{A}$ can change (Römer et al. 2004). Again, this is clear from the results of Table 6.1.

6.3.3 The spin-1 case

For $\theta = 0$, it can be seen in Fig. 6.6 (a+b) that the gap appears at higher values of the magnetic strength h, as we expect from Eq. (6.22). For $h = 3$ the subbands corresponding to spin components $m_S = -1, 0, 1$ overlap, and we have a clear gap for $h = 6$. As in the previous $S = 1/2$ scenario, there is perfect filtering for well-separated energy bands, while a partial filtering can be obtained for overlapping bands. The situation becomes quite complex for non zero values of θ, as all three spin channels are coupled. We first again notice the slight increase in maximal Λ_σ values due to the quasi-1D effect. Next, the $m_S = 0$ states have finite Λ_σ in all three subbands for $\theta = \pi/4$ (panels (c) and (d)), while $m_S = -1$ spin states have none-zero Λ_σ values only in the lower and central band and $m_S = 1$ particles only in the upper and central ones. It is worth noting that all components have none-zero Λ_σ values in the central band $-2 \leq E \leq 2$, but the

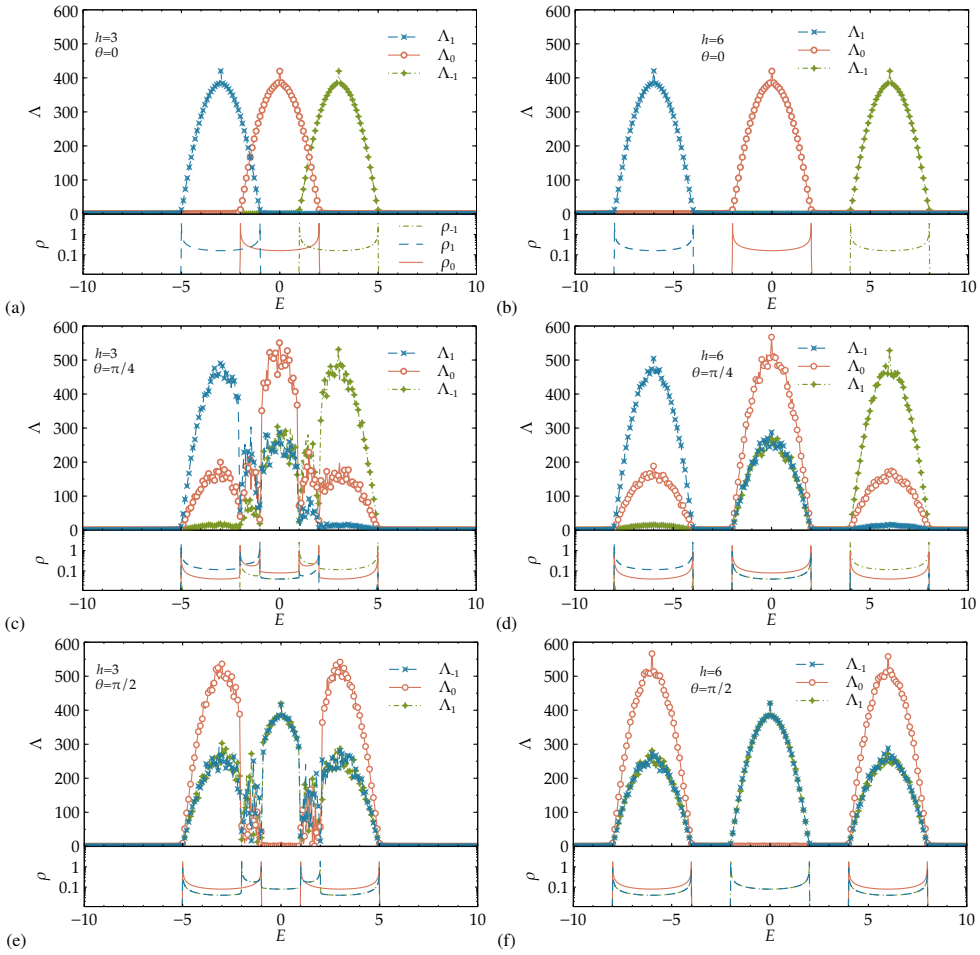

Figure 6.6. *Projected localization lengths Λ_{-1}, Λ_0, Λ_1 and LDOS for spin-1 particles with (a,c,e) overlapping bands at $h = 3$ and (b,d,f) well-separated bands at $h = 6$. The value of the polar angle θ changes from (a,b) $\theta = 0$ to (c,d) $\pi/4$ and (e,f) $\pi/2$. As in Fig. 6.4, we have $W = 0.5$. Symbols and lines for Λ_σ and ρ_σ are as given in the figure legend. Only every second Λ_σ symbol is shown for clarity. Lines for Λ_σ are guides to the eye. The λ_σ error bars are within symbol size when not visible.*

$m_S = 0$ particle states are less localized. Thus, by selecting a system with finite size L comprised between 300 and 500, one can suppress the '-1' and '1' spin states while only the '0' spin-projection survives and contributes to transport in the centre of the band.

A significant difference from the spin-1/2 states appears for spin-1 and $\theta = \pi/2$. Instead of complete mixing of the Λ_σ's and the LDOS curves, we observe that the $m_S = 0$ states spread entirely into the left and right subbands, while they vanish in the central band. An argument analog to the SU(2) rotation for $S = 1/2$ in the context of the band mixing given in the previous section also explains this expulsion of the $m_S = 0$ states from the central part of the spectrum. Also, for $\theta = \pi/2$, there is perfect matching in the behavior of '-1' and '1' spin projections, which cannot be separated for any energy range. Hence, this situation appears significantly peculiar, since we have no possibility for polarization of '1' or '-1' currents, although we have transport of '0' states in the energy regimes that were previously reserved for '1' and '-1' states. We expect similar kind of differences between integer and half-integer spin cases when studying higher spin S states (B. Pal et al. 2016b).

6.3.4 The spin spiral

In (B. Pal et al. 2016a), the authors also explored the choice $\theta_n = 2\pi n P/L$ — a spin *spiral* — for some finite L and $P = 2$, which leads to a spin flip in the transport for clean systems: at $E < 0$ for spin-1/2 and $h = 3$, initial states with spin-↑ emerge after transmitting through the finite system as spin-↓ while for $E > 0$, spin-↓ states emerge as spin-↑. Other states are not transmitting. On the other hand, for $P = 1$, there is no flip and for $E < 0$ ($E > 0$) only spin-↑ (spin-↓) states transmit.

In Fig. 6.7 we show the analogous situation for finite disorder $W = 0.5$. It is immediately clear from the figure that the spin projection fails to separate the spin-↑ and spin-↓ projections in the case of the spiral (see also Sec. 6.2.2). Nevertheless, we still see that the overall localization lengths for $P = 1$, cp. Fig. 6.7 (a), are compatible with previous findings (B. Pal et al. 2016a) as before. In particular, the range of energies with finite Λ_σ values is in excellent agreement. For $P = 2$, however, the Λ_σ values are one order of magnitude lower than for $P = 1$. This indicates that the flip of spin directions is not captured well by the spin-resolved Λ_σ's although the reduction in their values might correctly suggest that direct channels "spin-↑ to spin-↑" (similarly for spin-↓) are indeed suppressed for $P = 2$.

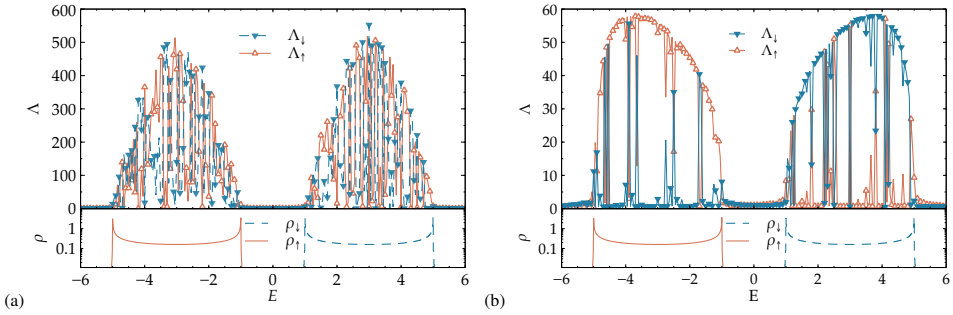

Figure 6.7. *Projected localization lengths $\Lambda_\uparrow$, $\Lambda_\downarrow$ and LDOS for the spin spiral case with $W = 0.5$ for (a) $P = 1$ and (b) $P = 2$ at $h = 3$. Only every second Λ_σ symbol is shown for clarity, lines are guides to the eye.*

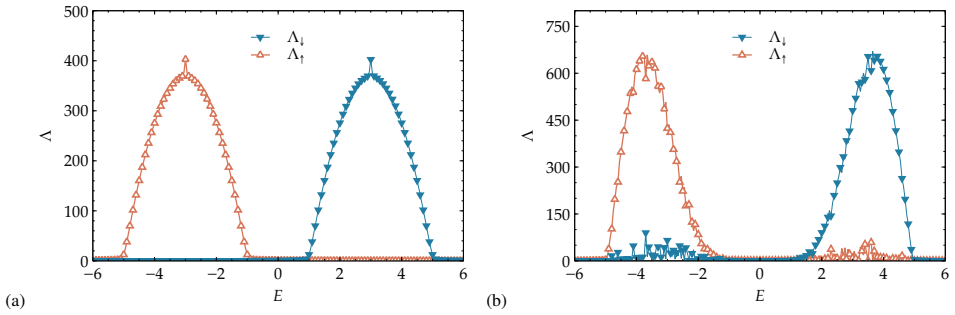

Figure 6.8. *Projected localization lengths $\Lambda_\uparrow$, $\Lambda_\downarrow$ with (a) additional magnetic strength disorder $W_h = 0.5$ and (b) additional magnetic polar angle disorder $W_\theta = 0.25$. In both cases, $W = 0.1$ and $h = 3$. Only every second Λ_σ symbol is shown for clarity, lines are guides to the eye.*

6.3.5 Disorder in magnetic strength and polar angle

Let us also consider other possible sources of disorder to affect the localization and hence spin filtering properties of the system proposed in Fig. 6.1 (b). In Fig. 6.8 we show results for the spin-1/2 case for (a) disorder in h such that at each site n, we have $h_n \in [-W_h/2 + h, h + W_h/2]$ and (b) disorder in θ with local value $\theta_n \in [-\theta_h/2 + \theta, \theta + \theta_h/2]$. Clearly, these situations correspond to (a) changing magnetic field strength or (b) changing field direction. As is clear from Fig. 6.8, at the chosen values $W_h = 0.5$ or $W_\theta = 0.25$, while having a small overall disorder $W = 0.1$, the spin-filtering properties remain as robust as in the previously considered cases of pure onsite disorder with $W = 0.5$.

6.4 Conclusions

Throughout this Chapter, we have investigated the robustness of spin-polarized transport through a linear array of magnetic atoms depicted in a random landscape. Flavor of disorder is introduced in the distributions of the on site potential and in the local magnetic field - in its strength as well as in direction. Band gaps are engineered by controlling the strength of the field, and spin-resolved localization lengths are estimated in every case. We developed a new spin projection transfer matrix method for this purpose, which is also applicable to other multi-channel systems. The calculated localization lengths corroborate the observation of spin filtering in every sub-band, and spin filtering is found to be robust against disorder. The results may be inspiring in experimental realizations in the arena of spintronic devices. The spin-filtering protocol described in this Chapter can be implemented with chains of nanomagnets, i.e. arrays of exchange-coupled atomic magnetic moments engineered at the single atom level by scanning tunnelling microscopy techniques (Serrate et al. 2010; Khajetoorians et al. 2012). In such systems, disorder can be embedded by modulating the morphology of the underlying growing substrate or more general nanoscale modifications of strain and magnetic anisotropy (Nord et al. 2019). The unexpected energy selectivity for the dominant spin projection in the spin-1 case shows that such studies may indeed be particularly interesting for higher spin cases. As the basic difference equations hold equally good for bosons, a parallel experimental study in the field of polarized photonic band gap systems may be just on the cards as well (S. Mukherjee et al. 2015). Such photonic lattices, fabricated with ultrafast laser inscription, represent an alternative to mimic the propagation of the electronic wave function in periodic arrays of optical wave-guides, and the observation of localization effects induced by the implementation of artificial disordered potentials have been multiply reported in the last two decades (Schwartz et al. 2007; Lahini et al. 2008; Martin et al. 2011; Vatnik et al. 2017).

Part IV

Conclusions and outlook

7

Summary and conclusions

Localization is a generic wave phenomena in disordered media, originated from the interference between multiple scattering paths, which ultimately inhibits transport when the disorder is strong enough. In the last two decades, the picture of localization in the quantum regime has been enriched with a renovated interest in the study of the interplay between disorder and strong interactions. In a way, this led to an intriguing encounter between two defining concepts of quantum mechanics itself, namely the wave nature of quantum states, with localization arising from destructive interference phenomena, and entanglement, generally created by direct particle interactions. Localization has wide-ranging implications in many foundational fields of physics, and in particular in the context of statistical mechanics: indeed, MBL of interacting quantum Hamiltonians implies the breakdown of the ergodic hypothesis for a large family of generic (i.e. not fine-tuned) models of quantum matter. In this dissertation, we presented different studies of quantum effects induced by localization in disordered and quasi-periodic systems. In the following, we summarize the main results.

We first considered the manifestation of localization in the short-time dynamics of the paradigmatic XXZ model with random or quasi-periodic potential profiles. We discussed the appearance of a periodic sequence of cusp singularities in the logarithm of the survival probability, which represents a robust feature surviving average over disorder configurations. The observation of such singular dynamics is connected to the fundamental mechanism behind the suppression of transport in the localized regime, i.e. the emergence of a generic form of integrability associated with strong disorder, namely the appearance of an extensive number of local conserved quantities. Such quantities are believed to have the form of dressed S=1/2 operators (l-bits) obtained via a canonical

transformation on the microscopic degrees of freedom and commuting with the many-body Hamiltonian. While AL of non-interacting particles implies the absence of any information transfer between local degrees of freedom, MBL exhibits the novel feature of a slow (logarithmic-in-time) growth of entanglement between any subsystem and its complement, which can be explained in terms of interacting l-bits. In spite of the fundamental importance of l-bits as the central feature of quantum localization in general (and of l-bit interactions as the defining features of many-body localization in particular), their evidence is so far limited to dedicated theoretical studies explicitly constructing local conserved quantities (Ros et al. 2015; Rademaker et al. 2016; Inglis et al. 2016; O'Brien et al. 2016; Pekker et al. 2017a; Kulshreshtha et al. 2018). It is fair to say that none of the experimental studies of quantum localization using quantum simulators (based on cold atoms, trapped ions, superconducting circuits, etc.) have offered direct experimental evidence of the existence of l-bits. The most defining feature of MBL associated with l-bit interactions is represented by the logarithmic growth of entanglement, which is a very challenging experimental task. Even the most advanced experiments in this direction (Lukin et al. 2019) have not achieved so far a conclusive measurement of entanglement entropy growth in the MBL phase, but only a measurement of the growth of correlations among configurations of two subsystems, offering evidence of persistent growth due to interactions.

In Ch. 4, we explain our results by noting that for strong disorder an important subset of the l-bits can be explicitly identified with strongly localized two-level systems (2LS), associated with particles confined on two lattice sites. The existence of such subsystems forming an ensemble of nearly free l-bits is found to dominate the short-time dynamics of the survival probability and of other experimentally relevant quantities, such as the imbalance and the number entropy. Our effective 2LS model is able to predict analytically the existence of the survival probability singularities for an ensemble of non-interacting l-bits, as well as of the power-law decay of their heights, showing a remarkable agreement with ED data for the XXZ spin chain. The failure of the 2LS model to exactly capture the survival probability and imbalance decay at long times represents another important signature. Indeed, a model of free 2LS collectively oscillating clearly cannot capture an essential ingredient of MBL, i.e. l-bits interactions. The l-bits are observed to cross over from an initial regime of decay of their ensemble oscillations (as the inverse of the square root of time) to a regime in which the decay is accelerated by the presence of interactions. The crossover

to the interaction-induced decay corresponds to the time regime in which the half-system entanglement entropy starts to develop its asymptotic logarithmic growth. Hence this crossover stands as a fundamental feature of MBL dynamics, offering an alternative avenue to the experimentally elusive entanglement growth.

We then discussed issues of irreversibility and sensitivity to global perturbations in MBL systems. As the most general class of many-body systems avoiding thermalization, MBL systems have been frequently mentioned as promising candidates for the design of robust quantum memories (R. Nandkishore et al. 2015; Smith et al. 2016) and state transfer protocols (Yao et al. 2015). Indeed, the possibility of encoding information in specific state configurations and avoiding scrambling in the long-time limit due to localization, is the most appealing feature of MBL from a quantum computation perspective. Addressing whether the information stored in a quantum state is robust under the action of external perturbations is thus essential for real applicability considerations. Motivated by such issues we proposed a quench experiment scheme to explore the evolution of the quantum fidelity (or Loschmidt echo) between states evolving with slightly different Hamiltonians in the presence of disorder. Our numerical results suggest a strong dependence of the fidelity decay on both the disorder and the perturbation strength. Indeed, the dynamics of the Loschmidt echo at short times exhibits a parabolic decay which is faster at strong disorders, i.e. in the MBL phase, compared to the ergodic regime. This may appear surprising at first, as the common intuition is that dynamics in the MBL phase should be more stable that in the ETH phase. Nonetheless, simple perturbative arguments provide a clear explanation: the parabolic decay of the Loschmidt echo at short times is a universal feature of quantum dynamics (Goussev et al. 2012) depending only on the dispersion of the perturbation operator, which naturally increases with growing disorder. The advantage yielded by MBL appears at later times, when the decay turns into a power-law, eventually reaching a steady saturation value. The computation of the fidelity steady values in the long-time limit provides another indication of the memory effects characterizing MBL dynamics, as the saturation values grow as one increases the disorder strength, thus confirming the improved stability of quantum evolution due to localization.

Another aspect we investigated in Ch. 5 is the relation between the Loschmidt echo dynamics and the multifractal properties of eigenstates in localized phases. Indeed, perturbative calculations show that the long-time average value of the fidelity in the weak perturbation regime corresponds to the participation ratio

of the chosen initial state over a certain basis. As such, we extracted the fractal dimension governing the anomalous scaling of the inverse participation ratio from the scaling analysis of the fidelity saturation values. Hence, one of the main points of interest of our protocol is the capability of obtaining information about the fractal nature of the spectrum in the MBL phase in an experimentally viable way through the study of long-time quench dynamics of the Loschmidt echo. The appearance of multifractality at disorders below the critical value of the ETH-MBL transition will require further work. The expectation put forward by (Macé et al. 2019) via a refined finite-size scaling analysis, is that multifractal eigenstates should strictly appear only in the MBL phase, i.e. above the critical point. We look forward to improve the statistics of our results and to reach larger system sizes, to explore the possibility of finite-size effects broadening the multifractal region to intermediate disorder values.

A comment on an alternative pathway to experimentally probe the fidelity dynamics is in order. In particular, (Brydges et al. 2019) proposed a new protocol relying on statistical correlations of locally randomized measurements (Elben et al. 2018) for the extraction of the second order Rényi entropy. Such a protocol was successfully tested on a spin model in a trapped-ion quantum simulator, in which the authors managed to monitor the generation of entanglement during quench dynamics. A clear advantage of (Brydges et al. 2019) compared to the interferometry protocol implemented in (Islam et al. 2015) is that it was based only on local operations on individual degrees of freedom of a single quantum state, thus not requiring the preparation of multiple instances of the system of interest. Also, (Elben et al. 2019) elaborated further on the theoretical details behind (Brydges et al. 2019), developing a mathematical toolbox for computing the statistical correlations of repeated local random measurements. Interestingly, the authors explicitly discuss as an example how to adapt their protocol to measure the overlap $\mathrm{Tr}[\rho_1\rho_2]$ and thus the Loschmidt echo, without the need for ancillary degrees of freedom or time-reversal operations (Elben et al. 2019).

Lastly, in Ch. 6 we focused on the influence of disorder in the spin transport properties of a linear array of non-interacting magnetic atoms. The presented results stand at the intersection between two major themes of modern condensed matter physics, such as spintronics and disordered systems. The non-interacting model we studied describes a chain of atoms grafted onto a magnetic substrate, which provides a definite magnetic moment to each individual particle. In a clean scenario, i.e. without disorder, such a simple tight-binding model was shown to exhibit spin-filtering properties, that could be controlled in order to

allow the transmission of injected particles only for selected spin components (B. Pal et al. 2016b). We addressed the robustness of such spin-filtering properties of a magnetized chain in a disordered scenario, introducing randomness in both the strength and orientation of the local magnetic fields, finding evidence of its stability against weak disorder. Our results are based on a variation of the state-of-the-art Transfer Matrix Method for the calculation of localization lengths in random models, which introduces a novel measure that we dubbed "spin-resolved localization length". We note that this new quantity can be of broad interest, as it is suited for the study of generic disordered systems with multiple transport channels. Our numerical results show that the possibility of spin-polarized transport survives the introduction of disorder and our model could be of particular interest for experimental realizations of spin-filtering devices. The exploration of localization effects in more exotic lattice geometries, such as the "spin spiral" we discussed, also represents an exciting future direction.

Despite being a collection of theoretical and numerical results, the motivation behind our work has always been anchored to considerations of experimental relevance. As abundantly mentioned throughout the Thesis, the progress of quantum simulators at the beginning of the century, and more specifically the advent of cold atoms experiment, have offered unprecedented paths to probe quantum phenomena at a fundamental level with a rather spectacular degree of control and precision. In a way, this represented a paradigm shift in the field of modern condensed matter physics, allowing to translate very accurately the plethora of abstract toy models that theorists had been studying for decades into concrete and measurable problems. The extraordinary long coherence time scales of cold atoms platforms also make them ideal for the exploration of peculiar non-equilibrium phenomena, unraveling the mechanisms behind fundamental processes such as equilibration and thermalization, and exploring exotic dynamical behaviors such as the ones discussed throughout this dissertation. The possibilities offered by modern quantum simulators represent a significant part of the future of condensed matter physics, and we look forward to be part of it.

A

Jordan-Wigner transformations

The Jordan-Wigner (JW) transformations are a standard tool in theoretical studies of strongly correlated systems, allowing a direct mapping between a system of N spins to a system of N spinless fermions. [1] In second quantization language, a generic fermionic many-body state can be written as

$$|N_1, N_2, \ldots, N_n\rangle = (c_1^\dagger)^{N_1}(c_2^\dagger)^{N_2}\ldots(c_n^\dagger)^{N_n}\,|\varnothing\rangle\,, \tag{A.1}$$

with $N_i = \{0, 1\}$, $|\varnothing\rangle$ the vacuum state and c_i, $c_i^\dagger$ are fermionic annihilation and creation operators at site i. The state (A.1) is a vector in $(\mathrm{C}^2)^{\otimes n}$, resembling the effective state of a chain of n spins, with $\{0, 1\}$ as the two possible state for each individual spin. The JW transformations allow for an exact mapping between the $c_i(c_i^\dagger)$'s and the spin raising/lowering operators $\sigma^+(\sigma^-)$ as follows:

$$\begin{aligned} c_i^\dagger &= \left(\prod_{j=1}^{i-1}\sigma_j^z\right)\sigma_i^-\,, \\ c_i &= \left(\prod_{j=1}^{i-1}\sigma_j^z\right)\sigma_i^+\,, \end{aligned} \tag{A.2}$$

where

$$\sigma_i^- = \frac{\sigma_i^x - \mathrm{i}\,\sigma_i^y}{2}, \quad \sigma_i^+ = \frac{\sigma_i^x + \mathrm{i}\,\sigma_i^y}{2} \tag{A.3}$$

and σ_i^z is given in (1.4).

[1] A translation from spin language to bosonic creation and annihilation operators can instead be achieved through *Holstein-Primakoff* transformations (Holstein et al. 1940).

B

Scaling theory of localization

The scaling theory of localization was developed by the so-called Gang of four in (Abrahams et al. 1979), based on renormalization group ideas formulated in earlier works (Wilson 1971; Thouless 1974; F. J. Wegner 1976). In particular, (F. J. Wegner 1976) derived, via the Kubo-Greenwood formula (Kubo 1957; Greenwood 1958), the scaling form for the conductivity of a disordered medium as

$$\sigma \sim W^{(d-2)\nu}, \qquad W > 0, \tag{B.1}$$

where W is the disorder strength (following the notation of Chap. 2) and ν is the scaling exponent of the localization length close to criticality, obtained in the same work by Wegner as

$$\xi \sim |W|^{-\nu}. \tag{B.2}$$

Notably, the conductivity critical exponent $s = (d-2)\nu$ represents a case of *hyperscaling*, as it involves the dimensionality d (Cardy 1996) [1], which is usually known to hold up to a upper critical dimension d_c. On the contrary, arguments based on both transport and spectral properties suggest that the critical dimension for Anderson localization is infinite (Tarquini et al. 2017).

Aiming to describe the problem in terms of extensive properties, Thouless focused instead on the conductance (Thouless 1974)

$$G(L) = \sigma L^{d-2}. \tag{B.3}$$

The scaling arguments for G start with a system of size L^d, which is duplicated to obtain a system of size $(2L)^d$, whose eigenstates are simple linear combinations of the eigenstates of the original system. Following the intuition that localized

[1] Also notice that for $d = 3$ the scaling exponents s and ν coincide.

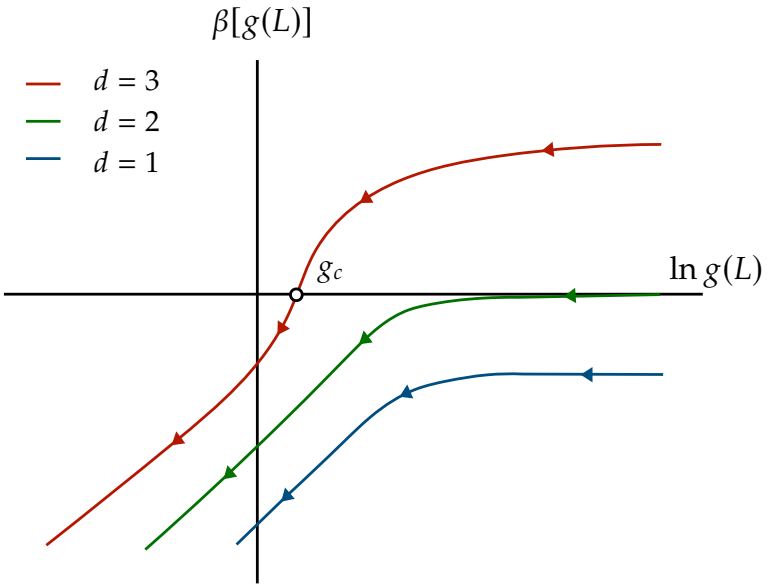

Figure B.1. *Asymptotic behavior of* $\beta[g(L)]$ *for different dimensions* $d = 1, 2, 3$.

states are barely affected by boundary effects, (Edwards et al. 1972) then studied the energy shift ΔE induced by the change of periodic to antiperiodic boundary conditions. Comparing ΔE with the average of the single-energy level spacings $\langle \delta \rangle$ (discussed in Sec. 3.2.1), Thouless and co-workers obtained the *dimensionless conductance*, or *Thouless number* (Edwards et al. 1972; Thouless 1974)

$$g(L) = \frac{\Delta E}{\langle \delta \rangle} = \frac{2\hbar}{e^2} G(L) \propto L^{d-2}, \tag{B.4}$$

which was shown to be exponentially small in the localized phase and large in the metallic phase. It is worth noting that $g(L)$ can also be interpreted as the ratio of two characteristic timescales of the system, i.e. the *Thouless time* t_{Th} and the *Heisenberg time* t_H. The latter is inversely proportional to the average level spacing of the discrete spectrum, and represents the longest time an electron wavepacket can travel inside the system without exploring the same regions twice. On the other hand, t_{Th} is defined as the time scale for a particle to diffuse through the sample and reach its boundaries (Thouless 1974). It is clear that when $t_{Th} > t_H$ a wavepacket is unable to travel through the entire system and remains localized in the bulk. This forms the intuition behind the Thouless criterion of localization, which states that localization occurs when $g < 1$ (Edwards et al. 1972).

The seminal work (Abrahams et al. 1979) stems from the educated guess that the dimensionless conductance (B.4) is the only relevant parameter for a

scaling theory of localization, obeying the scaling form

$$\beta[g(L)] = \frac{d\ln(g(L))}{d\ln L}, \tag{B.5}$$

where β is an analytic function that depends solely on $g(L)$. Although a universal functional form of β is still unknown, the study of its asymptotic behavior, sketched in Fig. B.1 provides significant qualitative insights. In the $g \to \infty$ limit, corresponding to the metallic case, one finds $\beta = d - 2$, thus recovering the usual behavior of a ohmic conductor in Eq. (B.4). In the opposite limit of a localized phase, $g \to -\infty$, the Thouless number becomes exponentially small, i.e. $g \sim \exp(-L/\xi)$, from which one obtains $\beta \sim \ln g$. The critical transition point g_c is identified as the point at which the Thouless number becomes invariant with system size, i.e precisely at $\beta = 0$. From this simple scaling argument, it is immediate to appreciate the existence of a phase transition only for $d > 2$, as β can cross the fixed point from positive to negative values. Indeed, for $d \leq 2$ the dimensionless conductance is always negative and, as a consequence, the eigenstates are fully localized at any disorder strength.

C

Partitioning of the entanglement entropy

We consider a quantum system $\mathcal{S}$ with particle number conservation and we are interested in the EE of a subsystem A. Due to the existence of a global conservation law, the RDM ρ^A of subsystem A is block diagonal, with each block $\rho^{(n)}$ corresponding to a fixed number of particles $n = 0, \ldots, N_A$. This allows to write the EE (1.21) as a sum of factorized blocks

$$S(\rho^A) = \sum_i \rho_{ii} \log \rho_{ii} = \sum_{n=0}^{N_A} \sum_i p_n \rho_{ii}^{(n)} \log \left(p_n \rho_{ii}^{(n)} \right), \tag{C.1}$$

where p_n is the probability of having n particles in subsystem A. The $\rho_{ii}^{(n)}$ are the elements of each block $\rho^{(n)}$, normalized such that

$$\sum_i \rho_{ii}^{(n)} = 1, \tag{C.2}$$

for each n. We can now separate the EE into separate contributions as

$$\begin{aligned} S(\rho^A) &= -\sum_{n=0}^{N_A} p_n \log p_n \sum_i \rho_{ii}^{(n)} - \sum_{n=0}^{N_A} p_n \sum_i \rho_{ii}^{(n)} \log \rho_{ii}^{(n)} \\ &= \underbrace{\sum_{n=0}^{N_A} p_n \log p_n}_{S_{A,n}} \underbrace{- \sum_{n=0}^{N_A} p_n \sum_i \rho_{ii}^{(n)} \log \rho_{ii}^{(n)}}_{S_{A,c}}. \end{aligned} \tag{C.3}$$

The first term $S_{A,n}$, computed in Sec.4.7.2, is called number entropy (also known as charge (Rakovszky et al. 2019) or fluctuation entropy (Bonsignori et al. 2019)) and captures the number fluctuations arising from particles hopping across the partition boundary. The configurational entropy $S_{A,c}$, on the other hand, represents the entropy associated with different configurations of n particles in the subsystem of interest.

Bibliography

Abanin, D. A., E. Altman, I. Bloch, and M. Serbyn (2019). "Colloquium: Many-body localization, thermalization, and entanglement". In: *Rev. Mod. Phys.* 91.2, p. 021001. DOI: 10.1103/RevModPhys.91.021001.

Abrahams, E. (2010). *50 Years of Anderson Localization*. World Scientific.

Abrahams, E., P. W. Anderson, D. C. Licciardello, and T. V. Ramakrishnan (1979). "Scaling Theory of Localization: Absence of Quantum Diffusion in Two Dimensions". In: *Phys. Rev. Lett.* 42.10, pp. 673–676. DOI: 10.1103/PhysRevLett.42.673.

Abramowitz, M. and I. A. Stegun (1964). *Handbook of Mathematical Functions with Formulas, Graphs, and Mathematical Tables*. ninth Dover printing, tenth GPO printing. New York: Dover.

Agarwal, K., E. Altman, E. Demler, S. Gopalakrishnan, D. A. Huse, and M. Knap (2017). "Rare-region effects and dynamics near the many-body localization transition". In: *Annalen der Physik* 529.7, p. 1600326. DOI: https://doi.org/10.1002/andp.201600326. eprint: https://onlinelibrary.wiley.com/doi/pdf/10.1002/andp.201600326.

Agarwal, K., S. Gopalakrishnan, M. Knap, M. Müller, and E. Demler (2015). "Anomalous Diffusion and Griffiths Effects Near the Many-Body Localization Transition". In: *Phys. Rev. Lett.* 114.16, p. 160401. DOI: 10.1103/PhysRevLett.114.160401.

Aharonov, Y. and D. Bohm (1959). "Significance of Electromagnetic Potentials in the Quantum Theory". In: *Physical Review* 115.3, pp. 485–491. ISSN: 0031-899X. DOI: 10.1103/PhysRev.115.485.

Alam, K. M. and S. Pramanik (2015). "Spin Filtering through Single-Wall Carbon Nanotubes Functionalized with Single-Stranded DNA". In: *Advanced Functional Materials* 25.21, pp. 3210–3218. ISSN: 1616301X. DOI: 10.1002/adfm.201500494.

Alet, F. and N. Laflorencie (2018). "Many-body localization: An introduction and selected topics". In: *Comptes Rendus Physique* 19.6, pp. 498–525. ISSN: 16310705. DOI: 10.1016/j.crhy.2018.03.003.

Anderson, P. W. (1958). "Absence of Diffusion in Certain Random Lattices". In: *Physical Review* 109.5, pp. 1492–1505. ISSN: 0031-899X. DOI: 10.1103/PhysRev.109.1492.

Andraschko, F. and J. Sirker (2014). "Dynamical quantum phase transitions and the Loschmidt echo: A transfer matrix approach". In: *Physical Review B* 89.12, p. 125120. ISSN: 10980121. DOI: 10.1103/PhysRevB.89.125120.

Andres, R. P., T. Bein, M. Dorogi, S. Feng, J. I. Henderson, C. P. Kubiak, W. Mahoney, R. G. Osifchin, and R. Reifenberger (1996). “"Coulomb Staircase" at Room Temperature in a Self-Assembled Molecular Nanostructure”. In: *Science* 272.5266, pp. 1323–1325. ISSN: 0036-8075. DOI: 10.1126/science.272.5266.1323.

Arnol'd, V. I. (1963). “Proof of a theorem of A. N. Kolmogorov on the invariance of quasi-periodic motions under small perturbations of the Hamiltonian”. In: *Russian Mathematical Surveys* 18.5, pp. 9–36. DOI: 10.1070/rm1963v018n05abeh004130.

Ashcroft, N. and N. Mermin (1976). *Solid State Physics*. Fort Worth: Saunders College Publishing.

Atas, Y. Y., E. Bogomolny, O. Giraud, and G. Roux (2013). “Distribution of the Ratio of Consecutive Level Spacings in Random Matrix Ensembles”. In: *Phys. Rev. Lett.* 110.8, p. 084101. DOI: 10.1103/PhysRevLett.110.084101.

Aubry, S. and G. André (1980). “Analyticity breaking and Anderson localization in incommensurate lattices”. In: *Ann. Israel Phys. Soc* 3.133, p. 18.

Avishai, Y., J. Richert, and R. Berkovits (2002). “Level statistics in a Heisenberg chain with random magnetic field”. In: *Phys. Rev. B* 66.5, p. 052416. DOI: 10.1103/PhysRevB.66.052416.

Awschalom, D., D. Loss, and N. Samarth (2013). *Semiconductor Spintronics and Quantum Computation*. NanoScience and Technology. Springer Berlin Heidelberg.

Bakr, W. S., J. I. Gillen, A. Peng, S. Fölling, and M. Greiner (2009). “A quantum gas microscope for detecting single atoms in a Hubbard-regime optical lattice”. In: *Nature* 462.7269, pp. 74–77. ISSN: 00280836. DOI: 10.1038/nature08482.

Bar Lev, Y., G. Cohen, and D. R. Reichman (2015). “Absence of Diffusion in an Interacting System of Spinless Fermions on a One-Dimensional Disordered Lattice”. In: *Phys. Rev. Lett.* 114.10, p. 100601. DOI: 10.1103/PhysRevLett.114.100601.

Bar Lev, Y. and D. R. Reichman (2014). “Dynamics of many-body localization”. In: *Phys. Rev. B* 89.22, p. 220201. DOI: 10.1103/PhysRevB.89.220201.

Bardarson, J. H., F. Pollmann, and J. E. Moore (2012). “Unbounded growth of entanglement in models of many-body localization”. In: *Physical Review Letters* 109.1. ISSN: 00319007. DOI: 10.1103/PhysRevLett.109.017202.

Barišič, O. S., J. Kokalj, I. Balog, and P. Prelov šek (2016). “Dynamical conductivity and its fluctuations along the crossover to many-body localization”. In: *Phys. Rev. B* 94.4, p. 045126. DOI: 10.1103/PhysRevB.94.045126.

Basko, D. M., I. L. Aleiner, and B. L. Altshuler (2006). “Metal-insulator transition in a weakly interacting many-electron system with localized single-particle states”. In: *Annals of Physics* 321.5, pp. 1126–1205. ISSN: 00034916. DOI: 10.1016/j.aop.2005.11.014.

Bauer, B. and C. Nayak (2013). “Area laws in a many-body localized state and its implications for topological order”. In: *Journal of Statistical Mechanics: Theory and Experiment* 2013.09, P09005. DOI: 10.1088/1742-5468/2013/09/p09005.

Bell, R. J. (1972). “The dynamics of disordered lattices”. In: *Reports on Progress in Physics* 35.3, pp. 1315–1409. DOI: 10.1088/0034-4885/35/3/306.

Benettin, G., L. Galgani, A. Giorgilli, and J.-M. Strelcyn (1980). "Lyapunov Characteristic Exponents for smooth dynamical systems and for hamiltonian systems; a method for computing all of them. Part 1: Theory". In: *Meccanica* 15.1, pp. 9–20. ISSN: 1572-9648. DOI: 10.1007/BF02128236.

Benini, L., A. Mukherjee, A. Chakrabarti, and R. A. Römer (2019). "Spin-polarized localization in a magnetized chain". In: *Scientific Reports* 9.1, p. 5930. ISSN: 2045-2322. DOI: 10.1038/s41598-019-42316-5.

Benini, L., P. Naldesi, R. A. Römer, and T. Roscilde (2021a). "Loschmidt echo singularities as dynamical signatures of strongly localized phases". In: *New Journal of Physics* 23.2, p. 023030. DOI: 10.1088/1367-2630/abdf9d.

— (2021b). "Quench dynamics of quasi-periodic systems exhibiting Rabi oscillations of two-level integrals of motion". In: *Annals of Physics*, p. 168545. ISSN: 0003-4916. DOI: 10.1016/j.aop.2021.168545.

Bera, S., G. De Tomasi, F. Weiner, and F. Evers (2017). "Density Propagator for Many-Body Localization: Finite-Size Effects, Transient Subdiffusion, and Exponential Decay". In: *Phys. Rev. Lett.* 118.19, p. 196801. DOI: 10.1103/PhysRevLett.118.196801.

Bercioux, D. and P. Lucignano (2015). "Quantum transport in Rashba spin–orbit materials: a review". In: *Reports on Progress in Physics* 78.10, p. 106001. ISSN: 0034-4885. DOI: 10.1088/0034-4885/78/10/106001.

Bernien, H. et al. (2017). "Probing many-body dynamics on a 51-atom quantum simulator". In: *Nature* 551.7682, pp. 579–584. ISSN: 1476-4687. DOI: 10.1038/nature24622.

Berry, M. V. and M. Tabor (1977). "Level Clustering in the Regular Spectrum". In: *Proceedings of the Royal Society of London A: Mathematical, Physical and Engineering Sciences* 356.1686, pp. 375–394. ISSN: 0080-4630. DOI: 10.1098/rspa.1977.0140. eprint: http://rspa.royalsocietypublishing.org/content/356/1686/375.full.pdf.

Bethe, H. (1931). "Zur Theorie der Metalle". In: *Zeitschrift für Physik* 71.3, pp. 205–226. ISSN: 0044-3328. DOI: 10.1007/BF01341708.

Beugeling, W., R. Moessner, and M. Haque (2014). "Finite-size scaling of eigenstate thermalization". In: *Phys. Rev. E* 89.4, p. 042112. DOI: 10.1103/PhysRevE.89.042112.

Billy, J. et al. (2008). "Direct observation of Anderson localization of matter waves in a controlled disorder". In: *Nature* 453.7197, pp. 891–894. ISSN: 1476-4687. DOI: 10.1038/nature07000.

Bloch, I., J. Dalibard, and W. Zwerger (2008). "Many-body physics with ultracold gases". In: *Rev. Mod. Phys.* 80.3, pp. 885–964. DOI: 10.1103/RevModPhys.80.885.

Boltzmann, L. (1872). "Weitere Studien über das Wärmegleichgewicht unter Gasmolekülen". In: *Sitzungs-berichte der Akademie der Wissenschaften zu Wien* 66, p. 275.

Bonsignori, R., P. Ruggiero, and P. Calabrese (2019). "Symmetry resolved entanglement in free fermionic systems". In: *Journal of Physics A: Mathematical and Theoretical* 52.47, p. 475302. DOI: 10.1088/1751-8121/ab4b77.

Bordia, P., H. P. Lüschen, S. S. Hodgman, M. Schreiber, I. Bloch, and U. Schneider (2016). "Coupling Identical 1D Many-Body Localized Systems". In: *Physical Review Letters* 116.14, p. 140401. ISSN: 0031-9007. DOI: 10.1103/PhysRevLett.116.140401.

Brandes, T., B. Huckestein, and L. Schweitzer (1996). "Critical dynamics and multifractal exponents at the Anderson transition in 3d disordered systems". In: *Annalen der Physik* 508.8, pp. 633–651. DOI: https://doi.org/10.1002/andp.2065080803. eprint: https://onlinelibrary.wiley.com/doi/pdf/10.1002/andp.2065080803.

Brandes, T. and S. Ketteman (2003). *Anderson Localization and its Ramifications*. Springer, Berlin.

Brandino, G. P., R. M. Konik, and G. Mussardo (2010). "Energy level distribution of perturbed conformal field theories". In: *Journal of Statistical Mechanics: Theory and Experiment* 2010.07, P07013. DOI: 10.1088/1742-5468/2010/07/p07013.

Brydges, T., A. Elben, P. Jurcevic, B. Vermersch, C. Maier, B. P. Lanyon, P. Zoller, R. Blatt, and C. F. Roos (2019). "Probing Rényi entanglement entropy via randomized measurements". In: *Science* 364.6437, pp. 260–263. ISSN: 0036-8075. DOI: 10.1126/science.aau4963. eprint: https://science.sciencemag.org/content/364/6437/260.full.pdf.

Bull, K., J.-Y. Desaules, and Z. Papić (2020). "Quantum scars as embeddings of weakly broken Lie algebra representations". In: *Phys. Rev. B* 101.16, p. 165139. DOI: 10.1103/PhysRevB.101.165139.

Burin, A. L. (2015). "Localization in a random XY model with long-range interactions: Intermediate case between single-particle and many-body problems". In: *Phys. Rev. B* 92.10, p. 104428. DOI: 10.1103/PhysRevB.92.104428.

Büttiker, M., Y. Imry, and M. Y. Azbel (1984). "Quantum oscillations in one-dimensional normal-metal rings". In: *Physical Review A* 30.4, pp. 1982–1989. ISSN: 0556-2791. DOI: 10.1103/PhysRevA.30.1982.

Bychkov, Y. A. and E. I. Rashba (1984). "Oscillatory effects and the magnetic susceptibility of carriers in inversion layers". In: *Journal of Physics C: Solid State Physics* 17.33, pp. 6039–6045. ISSN: 0022-3719. DOI: 10.1088/0022-3719/17/33/015.

Calabrese, P. and J. Cardy (2004). "Entanglement entropy and quantum field theory". In: *Journal of Statistical Mechanics: Theory and Experiment* 2004.06, P06002. DOI: 10.1088/1742-5468/2004/06/p06002.

Calabrese, P., F. H. L. Essler, and M. Fagotti (2011). "Quantum Quench in the Transverse-Field Ising Chain". In: *Phys. Rev. Lett.* 106.22, p. 227203. DOI: 10.1103/PhysRevLett.106.227203.

Cardy, J. (1996). *Scaling and Renormalization in Statistical Physics*. Cambridge Lecture Notes in Physics. Cambridge University Press. DOI: 10.1017/CBO9781316036440.

Casati, G., B. V. Chirikov, I. Guarneri, and D. L. Shepelyansky (1986). "Dynamical Stability of Quantum "Chaotic" Motion in a Hydrogen Atom". In: *Phys. Rev. Lett.* 56.23, pp. 2437–2440. DOI: 10.1103/PhysRevLett.56.2437.

Cassidy, A. C., C. W. Clark, and M. Rigol (2011). "Generalized Thermalization in an Integrable Lattice System". In: *Phys. Rev. Lett.* 106.14, p. 140405. DOI: 10.1103/PhysRevLett.106.140405.

Caux, J.-S. and F. H. L. Essler (2013). "Time Evolution of Local Observables After Quenching to an Integrable Model". In: *Phys. Rev. Lett.* 110.25, p. 257203. DOI: 10.1103/PhysRevLett.110.257203.

Caux, J.-S. and J. Mossel (2011). "Remarks on the notion of quantum integrability". In: *Journal of Statistical Mechanics: Theory and Experiment* 2011.02, P02023. DOI: 10.1088/1742-5468/2011/02/p02023.

Chabé, J., G. Lemarié, B. Grémaud, D. Delande, P. Szriftgiser, and J. C. Garreau (2008). "Experimental Observation of the Anderson Metal-Insulator Transition with Atomic Matter Waves". In: *Phys. Rev. Lett.* 101.25, p. 255702. DOI: 10.1103/PhysRevLett.101.255702.

Chandran, A., I. H. Kim, G. Vidal, and D. A. Abanin (2015). "Constructing local integrals of motion in the many-body localized phase". In: *Phys. Rev. B* 91.8, p. 085425. DOI: 10.1103/PhysRevB.91.085425.

Cheung, H.-F., Y. Gefen, E. K. Riedel, and W.-H. Shih (1988). "Persistent currents in small one-dimensional metal rings". In: *Physical Review B* 37.11, pp. 6050–6062. ISSN: 0163-1829. DOI: 10.1103/PhysRevB.37.6050.

Chiaro, B. et al. (2020). *Direct measurement of non-local interactions in the many-body localized phase*. arXiv: 1910.06024 [cond-mat.dis-nn].

Choi, J. Y. et al. (2016). "Exploring the many-body localization transition in two dimensions". In: *Science* 352.6293, pp. 1547–1552. ISSN: 0036-8075. DOI: 10.1126/science.aaf8834. eprint: https://science.sciencemag.org/content/352/6293/1547.full.pdf.

Choi, S., C. J. Turner, H. Pichler, W. W. Ho, A. A. Michailidis, Z. Papi ć, M. Serbyn, M. D. Lukin, and D. A. Abanin (2019). "Emergent SU(2) Dynamics and Perfect Quantum Many-Body Scars". In: *Phys. Rev. Lett.* 122.22, p. 220603. DOI: 10.1103/PhysRevLett.122.220603.

Chung, M.-C., A. Iucci, and M. A. Cazalilla (2012). "Thermalization in systems with bipartite eigenmode entanglement". In: *New Journal of Physics* 14.7, p. 075013. DOI: 10.1088/1367-2630/14/7/075013.

Ciobanu, C. V., S.-K. Yip, and T.-L. Ho (2000). "Phase diagrams of FÄ2 spinor Bose-Einstein condensates". In: *Physical Review A - Atomic, Molecular, and Optical Physics* 61.3, p. 033607.

Clément, D., A. F. Varón, J. A. Retter, L. Sanchez-Palencia, A. Aspect, and P. Bouyer (2006). "Experimental study of the transport of coherent interacting matter-waves in a 1D random potential induced by laser speckle". In: *New Journal of Physics* 8.8, pp. 165–165. DOI: 10.1088/1367-2630/8/8/165.

Collura, M., S. Sotiriadis, and P. Calabrese (2013). "Equilibration of a Tonks-Girardeau Gas Following a Trap Release". In: *Phys. Rev. Lett.* 110.24, p. 245301. DOI: 10.1103/PhysRevLett.110.245301.

Cramer, M., C. M. Dawson, J. Eisert, and T. J. Osborne (2008). "Exact Relaxation in a Class of Nonequilibrium Quantum Lattice Systems". In: *Phys. Rev. Lett.* 100.3, p. 030602. DOI: 10.1103/PhysRevLett.100.030602.

Cronenwett, S. M. (1998). "A Tunable Kondo Effect in Quantum Dots". In: *Science* 281.5376, pp. 540–544. ISSN: 1095-9203. DOI: 10.1126/science.281.5376.540.

Cutler, M. and N. F. Mott (1969). "Observation of Anderson Localization in an Electron Gas". In: *Phys. Rev.* 181.3, pp. 1336–1340. DOI: 10.1103/PhysRev.181.1336.

Czycholl, G., B. Kramer, and A. MacKinnon (1981). "Conductivity and localization of electron states in one dimensional disordered systems: Further numerical results". In: *Zeitschrift für Physik B Condensed Matter* 43.1, pp. 5–11. ISSN: 0340-224X. DOI: 10.1007/BF01295469.

D'Alessio, L., Y.Kafri, A.Polkovnikov, and M. Rigol (2016). "From quantum chaos and eigenstate thermalization to statistical mechanics and thermodynamics". In: *Advances in Physics* 65.3, pp. 239–362. DOI: 10.1080/00018732.2016.1198134. eprint: https://doi.org/10.1080/00018732.2016.1198134.

Daley, A. J., H. Pichler, J. Schachenmayer, and P. Zoller (2012). "Measuring entanglement growth in quench dynamics of bosons in an optical lattice". In: *Physical Review Letters* 109.2. ISSN: 00319007. DOI: 10.1103/PhysRevLett.109.020505.

Dalichaouch, R., J. P. Armstrong, S. Schultz, P. M. Platzman, and S. L. McCall (1991). "Microwave localization by two-dimensional random scattering". In: *Nature* 354.6348, pp. 53–55. ISSN: 1476-4687. DOI: 10.1038/354053a0.

De Roeck, W., F. Huveneers, M. Müller, and M. Schiulaz (2016). "Absence of many-body mobility edges". In: *Phys. Rev. B* 93.1, p. 014203. DOI: 10.1103/PhysRevB.93.014203.

De Roeck, W. and J. Z. Imbrie (2017). "Many-body localization: Stability and instability". In: *Philosophical Transactions of the Royal Society A: Mathematical, Physical and Engineering Sciences* 375.2108, p. 20160422. ISSN: 1364503X. DOI: 10.1098/rsta.2016.0422.

Demler, E. and F. Zhou (2002). "Spinor Bosonic Atoms in Optical Lattices: Symmetry Breaking and Fractionalization". In: *Physical Review Letters* 88.16, p. 4. ISSN: 10797114. DOI: 10.1103/PhysRevLett.88.163001.

Desalvo, B. J., M. Yan, P. G. Mickelson, Y. N. Martinez De Escobar, and T. C. Killian (2010). "Degenerate fermi gas of Sr87". In: *Physical Review Letters* 105.3, p. 030402. ISSN: 00319007. DOI: 10.1103/PhysRevLett.105.030402. arXiv: 1005.0668.

Deutsch, J. M. (1991). "Quantum statistical mechanics in a closed system". In: *Phys. Rev. A* 43.4, pp. 2046–2049. DOI: 10.1103/PhysRevA.43.2046.

Devakul, T. and R. R. P. Singh (2015). "Early Breakdown of Area-Law Entanglement at the Many-Body Delocalization Transition". In: *Phys. Rev. Lett.* 115.18, p. 187201. DOI: 10.1103/PhysRevLett.115.187201.

Dey, M., S. K. Maiti, and S. N. Karmakar (2011). "Logical XOR gate response in a quantum interferometer: A spin dependent transport". In: *The European Physical Journal B* 80.1, pp. 105–114. ISSN: 1434-6028. DOI: 10.1140/epjb/e2011-10931-6.

Dirac, P. A. M. and N. H. D. Bohr (1927). "The quantum theory of the emission and absorption of radiation". In: *Proceedings of the Royal Society of London. Series A, Containing Papers of a Mathematical and Physical Character* 114.767, pp. 243–265. DOI: 10.1098/rspa.1927.0039. eprint: https://royalsocietypublishing.org/doi/pdf/10.1098/rspa.1927.0039.

Doggen, E. V. H., I. V. Gornyi, A. D. Mirlin, and D. G. Polyakov (2021). *Many-body localization in large systems: Matrix-product-state approach*. arXiv: 2101.05651 [cond-mat.dis-nn].

Doggen, E. V. H. and A. D. Mirlin (2019). "Many-body delocalization dynamics in long Aubry-André quasiperiodic chains". In: *Phys. Rev. B* 100.10, p. 104203. DOI: 10.1103/PhysRevB.100.104203.

Doggen, E. V. H., F. Schindler, K. S. Tikhonov, A. D. Mirlin, T. Neupert, D. G. Polyakov, and I. V. Gornyi (2018). "Many-body localization and delocalization in large quantum chains". In: *Phys. Rev. B* 98.17, p. 174202. DOI: 10.1103/PhysRevB.98.174202.

Dresselhaus, G. (1955). "Spin-Orbit Coupling Effects in Zinc Blende Structures". In: *Physical Review* 100.2, pp. 580–586. ISSN: 0031-899X. DOI: 10.1103/PhysRev.100.580.

Dyson, F. J. (1962). "Statistical Theory of the Energy Levels of Complex Systems. I". In: *Journal of Mathematical Physics* 3.1, pp. 140–156. DOI: 10.1063/1.1703773.

Edwards, J. T. and D. J. Thouless (1972). "Numerical studies of localization in disordered systems". In: *Journal of Physics C: Solid State Physics* 5.8, pp. 807–820. DOI: 10.1088/0022-3719/5/8/007.

Eisert, J., M. Cramer, and M. B. Plenio (2010). "Colloquium: Area laws for the entanglement entropy". In: *Rev. Mod. Phys.* 82.1, pp. 277–306. DOI: 10.1103/RevModPhys.82.277.

Ekert, A. K., C. M. Alves, D. K. L. Oi, M. Horodecki, P. Horodecki, and L. C. Kwek (2002). "Direct Estimations of Linear and Nonlinear Functionals of a Quantum State". In: *Phys. Rev. Lett.* 88.21, p. 217901. DOI: 10.1103/PhysRevLett.88.217901.

Elben, A., B. Vermersch, M. Dalmonte, J. I. Cirac, and P. Zoller (2018). "Rényi Entropies from Random Quenches in Atomic Hubbard and Spin Models". In: *Phys. Rev. Lett.* 120.5, p. 050406. DOI: 10.1103/PhysRevLett.120.050406.

Elben, A., B. Vermersch, C. F. Roos, and P. Zoller (2019). "Statistical correlations between locally randomized measurements: A toolbox for probing entanglement in many-body quantum states". In: *Phys. Rev. A* 99.5, p. 052323. DOI: 10.1103/PhysRevA.99.052323.

Essler, F. H. L., H. Frahm, F. Göhmann, A. Klümper, and V. E. Korepin (2005). *The One-Dimensional Hubbard Model*. Cambridge University Press. DOI: 10.1017/CBO9780511534843.

Evers, F. and A. D. Mirlin (2008). "Anderson transitions". In: *Rev. Mod. Phys.* 80.4, pp. 1355–1417. DOI: 10.1103/RevModPhys.80.1355.

Fagotti, M., M. Collura, F. H. L. Essler, and P. Calabrese (2014). "Relaxation after quantum quenches in the spin-$\frac{1}{2}$ Heisenberg XXZ chain". In: *Phys. Rev. B* 89.12, p. 125101. DOI: 10.1103/PhysRevB.89.125101.

Fagotti, M. and F. H. L. Essler (2013). "Reduced density matrix after a quantum quench". In: *Phys. Rev. B* 87.24, p. 245107. DOI: 10.1103/PhysRevB.87.245107.

Feher, G., R. C. Fletcher, and E. A. Gere (1955). "Exchange Effects in Spin Resonance of Impurity Atoms in Silicon". In: *Phys. Rev.* 100.6, pp. 1784–1786. DOI: 10.1103/PhysRev.100.1784.2.

Feher, G. and E. A. Gere (1959). "Electron Spin Resonance Experiments on Donors in Silicon. II. Electron Spin Relaxation Effects". In: *Phys. Rev.* 114.5, pp. 1245–1256. DOI: 10.1103/PhysRev.114.1245.

Fermi, E., P. Pasta, S. Ulam, and M. Tsingou (1955). "Studies of Nonlinear Problems". In: *Los Alamos Report No. LA-1940*. DOI: 10.2172/4376203.

Fertig, C. D., K. M. O'Hara, J. H. Huckans, S. L. Rolston, W. D. Phillips, and J. V. Porto (2005). "Strongly Inhibited Transport of a Degenerate 1D Bose Gas in a Lattice". In: *Phys. Rev. Lett.* 94.12, p. 120403. DOI: 10.1103/PhysRevLett.94.120403.

Finkelstein, A. M. (1983). "Influence of coulomb interaction on the properties of disordered metals". In: *Zh. Eksp. Teor. Fiz* 84, pp. 168–169. DOI: http://www.jetp.ac.ru/cgi-bin/dn/e_057_01_0097.pdf.

Fleishman, L. and P. W. Anderson (1980). "Interactions and the Anderson transition". In: *Phys. Rev. B* 21.6, pp. 2366–2377. DOI: 10.1103/PhysRevB.21.2366.

Frustaglia, D., M. Hentschel, and K. Richter (2001). "Quantum Transport in Nonuniform Magnetic Fields: Aharonov-Bohm Ring as a Spin Switch". In: *Physical Review Letters* 87.25, p. 256602. ISSN: 0031-9007. DOI: 10.1103/PhysRevLett.87.256602.

Gärttner, M., J. G. Bohnet, A. Safavi-Naini, M. L. Wall, J. J. Bollinger, and A. M. Rey (2017). "Measuring out-of-time-order correlations and multiple quantum spectra in a trapped-ion quantum magnet". In: *Nature Physics* 13.8, pp. 781–786. ISSN: 1745-2481. DOI: 10.1038/nphys4119.

Gell-Mann, M. (1962). "Symmetries of Baryons and Mesons". In: *Phys. Rev.* 125.3, pp. 1067–1084. DOI: 10.1103/PhysRev.125.1067.

Geng, R., A. Roy, W. Zhao, R. C. Subedi, X. Li, J. Locklin, and T. D. Nguyen (2016). "Engineering of Spin Injection and Spin Transport in Organic Spin Valves Using π-Conjugated Polymer Brushes". In: *Advanced Functional Materials* 26.22, pp. 3999–4006. ISSN: 1616301X. DOI: 10.1002/adfm.201504201.

Giamarchi, T. and H. J. Schulz (1988). "Anderson localization and interactions in one-dimensional metals". In: *Phys. Rev. B* 37.1, pp. 325–340. DOI: 10.1103/PhysRevB.37.325.

Gibbs, J. (1902). *Elementary Principles in Statistical Mechanics: Developed with Especial Reference to the Rational Foundations of Thermodynamics*. C. Scribner's Sons.

Göhler, B., V. Hamelbeck, T. Z. Markus, M. Kettner, G. F. Hanne, Z. Vager, R. Naaman, and H. Zacharias (2011). "Spin selectivity in electron transmission through self-assembled monolayers of double-stranded DNA." In: *Science (New York, N.Y.)* 331.6019, pp. 894–7. ISSN: 1095-9203. DOI: 10.1126/science.1199339.

Goldhaber-Gordon, D., H. Shtrikman, D. Mahalu, D. Abusch-Magder, U. Meirav, and M. A. Kastner (1998). "Kondo effect in a single-electron transistor". In: *Nature* 391.6663, pp. 156–159. ISSN: 0028-0836. DOI: 10.1038/34373.

Goldstein, S., J. L. Lebowitz, R. Tumulka, and N. Zanghì (2010). "Long-time behavior of macroscopic quantum systems". In: *The European Physical Journal H* 35.2, pp. 173–200. ISSN: 2102-6467. DOI: 10.1140/epjh/e2010-00007-7.

Gomez, J. M. G., R. A. Molina, A. Relaño, and J. Retamosa (2002). "Misleading signatures of quantum chaos". In: *Phys. Rev. E* 66.3, p. 036209. DOI: 10.1103/PhysRevE.66.036209.

González-Santander, C., F. Domínguez-Adame, M. Hilke, and R. A. Römer (2013). "Localisation and finite-size effects in graphene flakes". In: *EPL (Europhysics Letters)* 104.1, p. 17012. ISSN: 0295-5075. DOI: 10.1209/0295-5075/104/17012.

Goodman, J. (2007). *Speckle Phenomena in Optics: Theory and Applications*. Roberts & Company.

Gornyi, I. V., A. D. Mirlin, and D. G. Polyakov (2005). "Interacting electrons in disordered wires: Anderson localization and low-T transport". In: *Physical Review Letters* 95.20. ISSN: 00319007. DOI: 10.1103/PhysRevLett.95.206603.

Gorshkov, A. V. et al. (2010). "Two-orbital SU(N) magnetism with ultracold alkaline-earth atoms". In: *Nature Physics* 6.4, pp. 289–295. ISSN: 17452473. DOI: 10.1038/nphys1535.

Goussev, A., R. A. Jalabert, H. M. Pastawski, and D. A. Wisniacki (2012). "Loschmidt echo". In: *Scholarpedia* 7.8. revision #127578, p. 11687. DOI: 10.4249/scholarpedia.11687.

Greenwood, D. A. (1958). "The Boltzmann Equation in the Theory of Electrical Conduction in Metals". In: *Proceedings of the Physical Society* 71.4, pp. 585–596. DOI: 10.1088/0370-1328/71/4/306.

Greiner, M., O. Mandel, T. W. Hänsch, and I. Bloch (2002). "Collapse and revival of the matter wave field of a Bose–Einstein condensate". In: *Nature* 419.6902, pp. 51–54. ISSN: 1476-4687. DOI: 10.1038/nature00968.

Griffiths, D. J. and D. F. Schroeter (2018). *Introduction to Quantum Mechanics*. Cambridge University Press. DOI: 10.1017/9781316995433.

Griffiths, R. B. (1969). "Nonanalytic Behavior Above the Critical Point in a Random Ising Ferromagnet". In: *Phys. Rev. Lett.* 23.1, pp. 17–19. DOI: 10.1103/PhysRevLett.23.17.

Guarrera, V., L. Fallani, J. E. Lye, C. Fort, and M. Inguscio (2007). "Inhomogeneous broadening of a Mott insulator spectrum". In: *New Journal of Physics* 9.4, pp. 107–107. ISSN: 13672630. DOI: 10.1088/1367-2630/9/4/107.

Guo, Q. et al. (2021). "Observation of energy-resolved many-body localization". In: *Nature Physics* 17.2, pp. 234–239. ISSN: 1745-2481. DOI: 10.1038/s41567-020-1035-1.

Guo, X.-Y. et al. (2019). "Observation of a Dynamical Quantum Phase Transition by a Superconducting Qubit Simulation". In: *Phys. Rev. Applied* 11.4, p. 044080. DOI: 10.1103/PhysRevApplied.11.044080.

Halimeh, J. C., N. Yegovtsev, and V. Gurarie (2019). "Dynamical quantum phase transitions in many-body localized systems". In: *arxiv:1903.03109*.

Harper, P. G. (1955). "Single Band Motion of Conduction Electrons in a Uniform Magnetic Field". In: *Proceedings of the Physical Society. Section A* 68.10, pp. 874–878. DOI: 10.1088/0370-1298/68/10/304.

Hastings, M. B. (2007). "An area law for one-dimensional quantum systems". In: *Journal of Statistical Mechanics: Theory and Experiment* 2007.08, P08024–P08024. DOI: 10.1088/1742-5468/2007/08/p08024.

He, K., L. F. Santos, T. M. Wright, and M. Rigol (2013). "Single-particle and many-body analyses of a quasiperiodic integrable system after a quench". In: *Phys. Rev. A* 87.6, p. 063637. DOI: 10.1103/PhysRevA.87.063637.

Heisenberg, W. (1949). *The Physical Principles of the Quantum Theory*. Dover Books on Physics and Chemistry. Dover Publications.

Heller, E. J. (1984). "Bound-state eigenfunctions of classically chaotic Hamiltonian systems: Scars of periodic orbits". In: *Physical Review Letters* 53.16, pp. 1515–1518. ISSN: 00319007. DOI: 10.1103/PhysRevLett.53.1515.

Heyl, M. (2014). "Dynamical quantum phase transitions in systems with broken-symmetry phases". In: *Physical Review Letters* 113.20, p. 205701. ISSN: 10797114. DOI: 10.1103/PhysRevLett.113.205701.

Heyl, M., A. Polkovnikov, and S. Kehrein (2013). "Dynamical Quantum Phase Transitions in the Transverse-Field Ising Model". In: *Physical Review Letters* 110.13, p. 135704. ISSN: 0031-9007. DOI: 10.1103/PhysRevLett.110.135704.

Heyl, M. (2018). "Dynamical quantum phase transitions: a review". In: *Reports on Progress in Physics* 81.5, p. 054001. DOI: 10.1088/1361-6633/aaaf9a.

Ho, T. L. (1998). "Spinor bose condensates in optical traps". In: *Physical Review Letters* 81.4, pp. 742–745. ISSN: 10797114. DOI: 10.1103/PhysRevLett.81.742. arXiv: 9803231 [cond-mat].

Ho, T. L. and S. Yip (1999). "Pairing of fermions with arbitrary spin". In: *Physical Review Letters* 82.2, pp. 247–250. ISSN: 10797114. DOI: 10.1103/PhysRevLett.82.247. arXiv: 9808246 [cond-mat].

Ho, W. W., S. Choi, H. Pichler, and M. D. Lukin (2019). "Periodic Orbits, Entanglement, and Quantum Many-Body Scars in Constrained Models: Matrix Product State Approach". In: *Phys. Rev. Lett.* 122.4, p. 040603. DOI: 10.1103/PhysRevLett.122.040603.

Holstein, T. and H. Primakoff (1940). "Field Dependence of the Intrinsic Domain Magnetization of a Ferromagnet". In: *Phys. Rev.* 58.12, pp. 1098–1113. DOI: 10.1103/PhysRev.58.1098.

Honerkamp, C. and W. Hofstetter (2004). "Ultracold fermions and the SU(N) Hubbard model". In: *Physical Review Letters* 92.17, pp. 170403–170404. ISSN: 00319007. DOI: 10.1103/PhysRevLett.92.170403.

Hong, C. K., Z. Y. Ou, and L. Mandel (1987). "Measurement of subpicosecond time intervals between two photons by interference". In: *Phys. Rev. Lett.* 59.18, pp. 2044–2046. DOI: 10.1103/PhysRevLett.59.2044.

Houck, A. A., H. E. Türeci, and J. Koch (2012). "On-chip quantum simulation with superconducting circuits". In: *Nature Physics* 8.4, pp. 292–299. ISSN: 1745-2481. DOI: 10.1038/nphys2251.

Hu, H., A. Strybulevych, J. H. Page, S. E. Skipetrov, and B. A. van Tiggelen (2008). "Localization of ultrasound in a three-dimensional elastic network". In: *Nature Physics* 4.12, pp. 945–948. ISSN: 1745-2481. DOI: 10.1038/nphys1101.

Huckestein, B. and R. Klesse (1997). "Spatial and spectral multifractality of the local density of states at the mobility edge". In: *Phys. Rev. B* 55.12, R7303–R7306. DOI: 10.1103/PhysRevB.55.R7303.

— (1999). "Wave-packet dynamics at the mobility edge in two- and three-dimensional systems". In: *Phys. Rev. B* 59.15, pp. 9714–9717. DOI: 10.1103/PhysRevB.59.9714.

Huckestein, B. and L. Schweitzer (1994). "Relation between the correlation dimensions of multifractal wave functions and spectral measures in integer quantum Hall systems". In: *Phys. Rev. Lett.* 72.5, pp. 713–716. DOI: 10.1103/PhysRevLett.72.713.

Huse, D. A., R. Nandkishore, and V. Oganesyan (2014). "Phenomenology of fully many-body-localized systems". In: *Phys. Rev. B* 90.17, p. 174202. DOI: 10.1103/PhysRevB.90.174202.

Imbrie, J. Z. (2016). "Diagonalization and Many-Body Localization for a Disordered Quantum Spin Chain". In: *Phys. Rev. Lett.* 117.2, p. 027201. DOI: 10.1103/PhysRevLett.117.027201.

Inglis, S. and L. Pollet (2016). "Accessing Many-Body Localized States through the Generalized Gibbs Ensemble". In: *Phys. Rev. Lett.* 117.12, p. 120402. DOI: 10.1103/PhysRevLett.117.120402.

Islam, R., R. Ma, P. M. Preiss, M. Eric Tai, A. Lukin, M. Rispoli, and M. Greiner (2015). "Measuring entanglement entropy in a quantum many-body system". In: *Nature* 528.7580, pp. 77–83. ISSN: 0028-0836. DOI: 10.1038/nature15750.

Iyer, S., V. Oganesyan, G. Refael, and D. A. Huse (2013). "Many-body localization in a quasiperiodic system". In: *Physical Review B* 87.13, p. 134202. ISSN: 10980121. DOI: 10.1103/PhysRevB.87.134202.

Jacquod, P., İ. Adagideli, and C. W. J. Beenakker (2003). "Anomalous power law of quantum reversibility for classically regular dynamics". In: *Europhysics Letters (EPL)* 61.6, pp. 729–735. DOI: 10.1209/epl/i2003-00289-y.

Janarek, J., D. Delande, and J. Zakrzewski (2018). "Discrete disorder models for many-body localization". In: *Phys. Rev. B* 97.15, p. 155133. DOI: 10.1103/PhysRevB.97.155133.

Janssen, M. (1994). "Multifractal analysis of broadly-distributed observables at criticality". In: *International Journal of Modern Physics B* 08.08, pp. 943–984. DOI: 10.1142/S021797929400049X.

Jordan, P. and E. Wigner (1928). "Über das Paulische Äquivalenzverbot". In: *Zeitschrift für Physik* 47.9, pp. 631–651. ISSN: 0044-3328. DOI: 10.1007/BF01331938.

Jurcevic, P. et al. (2017). "Direct Observation of Dynamical Quantum Phase Transitions in an Interacting Many-Body System". In: *Phys. Rev. Lett.* 119.8, p. 080501. DOI: 10.1103/PhysRevLett.119.080501.

Kappus, M. and F. Wegner (1981). "Anomaly in the Band Centre of the One-Dimensional Anderson Model*". In: *Z. Phys. B -Condensed Matter* 45, pp. 15–21.

Kawaguchi, Y. and M. Ueda (2012). "Spinor Bose–Einstein condensates". In: *Physics Reports* 520.5, pp. 253–381. ISSN: 0370-1573. DOI: 10.1016/J.PHYSREP.2012.07.005.

Khait, I., S. Gazit, N. Y. Yao, and A. Auerbach (2016). "Spin transport of weakly disordered Heisenberg chain at infinite temperature". In: *Phys. Rev. B* 93.22, p. 224205. DOI: 10.1103/PhysRevB.93.224205.

Khajetoorians, A. A., J. Wiebe, B. Chilian, S. Lounis, S. Blügel, and R. Wiesendanger (2012). "Atom-by-atom engineering and magnetometry of tailored nanomagnets". In: *Nature Physics* 8.6, pp. 497–503. ISSN: 1745-2481. DOI: 10.1038/nphys2299.

Khatami, E., G. Pupillo, M. Srednicki, and M. Rigol (2013). "Fluctuation-Dissipation Theorem in an Isolated System of Quantum Dipolar Bosons after a Quench". In: *Phys. Rev. Lett.* 111.5, p. 050403. DOI: 10.1103/PhysRevLett.111.050403.

Khemani, V., C. R. Laumann, and A. Chandran (2019). "Signatures of integrability in the dynamics of Rydberg-blockaded chains". In: *Phys. Rev. B* 99.16, p. 161101. DOI: 10.1103/PhysRevB.99.161101.

Khemani, V., S. P. Lim, D. N. Sheng, and D. A. Huse (2017a). "Critical Properties of the Many-Body Localization Transition". In: *Phys. Rev. X* 7.2, p. 021013. DOI: 10.1103/PhysRevX.7.021013.

Khemani, V., D. Sheng, and D. A. Huse (2017b). "Two Universality Classes for the Many-Body Localization Transition". In: *Physical Review Letters* 119.7, p. 075702. ISSN: 0031-9007. DOI: 10.1103/PhysRevLett.119.075702.

Kiefer-Emmanouilidis, M., R. Unanyan, M. Fleischhauer, and J. Sirker (2020). "Evidence for Unbounded Growth of the Number Entropy in Many-Body Localized Phases". In: *Phys. Rev. Lett.* 124.24, p. 243601. DOI: 10.1103/PhysRevLett.124.243601.

— (2021). "Slow delocalization of particles in many-body localized phases". In: *Phys. Rev. B* 103.2, p. 024203. DOI: 10.1103/PhysRevB.103.024203.

Kim, H., T. N. Ikeda, and D. A. Huse (2014). "Testing whether all eigenstates obey the eigenstate thermalization hypothesis". In: *Phys. Rev. E* 90.5, p. 052105. DOI: 10.1103/PhysRevE.90.052105.

Kim, H. and D. A. Huse (2013). "Ballistic Spreading of Entanglement in a Diffusive Nonintegrable System". In: *Phys. Rev. Lett.* 111.12, p. 127205. DOI: 10.1103/PhysRevLett.111.127205.

Kjäll, J. A., J. H. Bardarson, and F. Pollmann (2014). "Many-Body Localization in a Disordered Quantum Ising Chain". In: *Phys. Rev. Lett.* 113.10, p. 107204. DOI: 10.1103/PhysRevLett.113.107204.

Koga, T., J. Nitta, H. Takayanagi, and S. Datta (2002). "Spin-Filter Device Based on the Rashba Effect Using a Nonmagnetic Resonant Tunneling Diode". In: *Physical Review Letters* 88.12, p. 126601. ISSN: 0031-9007. DOI: 10.1103/PhysRevLett.88.126601.

Kohlert, T., S. Scherg, X. Li, H. P. Lüschen, S. Das Sarma, I. Bloch, and M. Aidelsburger (2019). "Observation of Many-Body Localization in a One-Dimensional System with a Single-Particle Mobility Edge". In: *Physical Review Letters* 122.17. ISSN: 10797114. DOI: 10.1103/PhysRevLett.122.170403.

Kolmogorov, A. N. (1954). "On conservation of conditionally periodic motions for a small change in Hamilton's function". In: *Dokl. Akad. Nauk SSSR* 98, pp. 527–530.

Kramer, B. and A. MacKinnon (1993). "Localization: theory and experiment". In: *Reports on Progress in Physics* 56.12, pp. 1469–1564. DOI: 10.1088/0034-4885/56/12/001.

Krishna, A. and R. N. Bhatt (2018). "Effect of Hilbert space truncation on Anderson localization". In: *Phys. Rev. B* 97.17, p. 174205. DOI: 10.1103/PhysRevB.97.174205.

Kubo, R. (1957). "Statistical-Mechanical Theory of Irreversible Processes. I. General Theory and Simple Applications to Magnetic and Conduction Problems". In: *Journal of the Physical Society of Japan* 12.6, pp. 570–586. DOI: 10.1143/JPSJ.12.570.

Kuhn, C. C., X. W. Guan, A. Foerster, and M. T. Batchelor (2012). "Quantum criticality of spin-1 bosons in a one-dimensional harmonic trap". In: *Physical Review A - Atomic, Molecular, and Optical Physics* 86.1, p. 011605. ISSN: 10502947. DOI: 10.1103/PhysRevA.86.011605.

Kulshreshtha, A. K., A. Pal, T. B. Wahl, and S. H. Simon (2018). "Behavior of l-bits near the many-body localization transition". In: *Phys. Rev. B* 98.18, p. 184201. DOI: 10.1103/PhysRevB.98.184201.

Laflorencie, N., G. Lemarié, and N. Macé (2020). arXiv: 2004.02861 [cond-mat.dis-nn].

Lahini, Y., A. Avidan, F. Pozzi, M. Sorel, R. Morandotti, D. N. Christodoulides, and Y. Silberberg (2008). "Anderson Localization and Nonlinearity in One-Dimensional Disordered Photonic Lattices". In: *Phys. Rev. Lett.* 100.1, p. 013906. DOI: 10.1103/PhysRevLett.100.013906.

Laumann, C. R., A. Pal, and A. Scardicchio (2014). "Many-Body Mobility Edge in a Mean-Field Quantum Spin Glass". In: *Phys. Rev. Lett.* 113.20, p. 200405. DOI: 10.1103/PhysRevLett.113.200405.

Leanhardt, A. E., Y. Shin, D. Kielpinski, D. E. Pritchard, and W. Ketterle (2003). "Coreless Vortex Formation in a Spinor Bose-Einstein Condensate". In: *Physical Review Letters* 90.14, p. 140403. ISSN: 0031-9007. DOI: 10.1103/PhysRevLett.90.140403.

Lee, M., T. R. Look, S. P. Lim, and D. N. Sheng (2017). "Many-body localization in spin chain systems with quasiperiodic fields". In: *Phys. Rev. B* 96.7, p. 075146. DOI: 10.1103/PhysRevB.96.075146.

Lee, M. and C. Bruder (2006). "Spin filter using a semiconductor quantum ring side coupled to a quantum wire". In: *Physical Review B* 73.8, p. 085315. ISSN: 1098-0121. DOI: 10.1103/PhysRevB.73.085315.

Lee, P. A. and T. V. Ramakrishnan (1985). "Disordered electronic systems". In: *Rev. Mod. Phys.* 57.2, pp. 287–337. DOI: 10.1103/RevModPhys.57.287.

Lemarié, G., H. Lignier, D. Delande, P. Szriftgiser, and J. C. Garreau (2010). "Critical State of the Anderson Transition: Between a Metal and an Insulator". In: *Phys. Rev. Lett.* 105.9, p. 090601. DOI: 10.1103/PhysRevLett.105.090601.

Lev, Y. B., D. M. Kennes, C. Klöckner, D. R. Reichman, and C. Karrasch (2017). "Transport in quasiperiodic interacting systems: From superdiffusion to subdiffusion". In: *EPL (Europhysics Letters)* 119.3, p. 37003. DOI: 10.1209/0295-5075/119/37003.

Levitov, L. S. (1990). "Delocalization of vibrational modes caused by electric dipole interaction". In: *Phys. Rev. Lett.* 64.5, pp. 547–550. DOI: 10.1103/PhysRevLett.64.547.

Li, H., J. Wang, X.-J. Liu, and H. Hu (2016). "Many-body localization in Ising models with random long-range interactions". In: *Phys. Rev. A* 94.6, p. 063625. DOI: 10.1103/PhysRevA.94.063625.

Lieb, E., T. Schultz, and D. Mattis (1961). "Two soluble models of an antiferromagnetic chain". In: *Annals of Physics* 16.3, pp. 407–466. ISSN: 0003-4916. DOI: http://dx.doi.org/10.1016/0003-4916(61)90115-4.

Lim, S. P. and D. N. Sheng (2016). "Many-body localization and transition by density matrix renormalization group and exact diagonalization studies". In: *Phys. Rev. B* 94.4, p. 045111. DOI: 10.1103/PhysRevB.94.045111.

Lin, C.-J. and O. I. Motrunich (2019). "Exact Quantum Many-Body Scar States in the Rydberg-Blockaded Atom Chain". In: *Phys. Rev. Lett.* 122.17, p. 173401. DOI: 10.1103/PhysRevLett.122.173401.

Lindinger, J. and A. Rodriguez (2017). "Multifractal finite-size scaling at the Anderson transition in the unitary symmetry class". In: *Phys. Rev. B* 96.13, p. 134202. DOI: 10.1103/PhysRevB.96.134202.

Lopez, M., J.-F. ç. Clément, P. Szriftgiser, J. C. Garreau, and D. Delande (2012). "Experimental Test of Universality of the Anderson Transition". In: *Phys. Rev. Lett.* 108.9, p. 095701. DOI: 10.1103/PhysRevLett.108.095701.

Lorenz, E. N. (1963). "Deterministic Nonperiodic Flow". In: *Journal of Atmospheric Sciences* 20.2, pp. 130–141. DOI: 10.1175/1520-0469(1963)020<0130:DNF>2.0.CO;2.

Loschmidt, J. (1876). "Über den Zustand des Wärmegleichgewichtes eines Systems von Körpern mit Rücksicht auf die Schwerkraft". In: *Sitzungs-berichte der Akademie der Wissenschaften zu Wien* 73, p. 128.

Lü, H.-F. and Y. Guo (2007). "Pure spin current in a three-terminal spin device in the presence of Rashba spin-orbit interaction". In: *Applied Physics Letters* 91.9, p. 092128. ISSN: 0003-6951. DOI: 10.1063/1.2777149.

Luitz, D. J., N. Laflorencie, and F. Alet (2014a). "Participation spectroscopy and entanglement Hamiltonian of quantum spin models". In: *Journal of Statistical Mechanics: Theory and Experiment* 2014.8, P08007. DOI: 10.1088/1742-5468/2014/08/p08007.

— (2016a). "Extended slow dynamical regime close to the many-body localization transition". In: *Physical Review B* 93.6. ISSN: 24699969. DOI: 10.1103/PhysRevB.93.060201.

Luitz, D. J. (2016). "Long tail distributions near the many-body localization transition". In: *Phys. Rev. B* 93.13, p. 134201. DOI: 10.1103/PhysRevB.93.134201.

Luitz, D. J., F. Alet, and N. Laflorencie (2014b). "Universal Behavior beyond Multifractality in Quantum Many-Body Systems". In: *Phys. Rev. Lett.* 112.5, p. 057203. DOI: 10.1103/PhysRevLett.112.057203.

Luitz, D. J. and Y. Bar Lev (2016b). "Anomalous Thermalization in Ergodic Systems". In: *Phys. Rev. Lett.* 117.17, p. 170404. DOI: 10.1103/PhysRevLett.117.170404.

Luitz, D. J., I. M. Khaymovich, and Y. B. Lev (2020a). "Multifractality and its role in anomalous transport in the disordered XXZ spin-chain". In: *SciPost Phys. Core* 2.2, p. 6. DOI: 10.21468/SciPostPhysCore.2.2.006.

Luitz, D. J., N. Laflorencie, and F. Alet (2015). "Many-body localization edge in the random-field Heisenberg chain". In: *Physical Review B* 91.8, p. 81103. ISSN: 1550235X. DOI: 10.1103/PhysRevB.91.081103.

Luitz, D. J. and Y. B. Lev (2017). "The ergodic side of the many-body localization transition". In: *Annalen der Physik* 529.7, p. 1600350. DOI: https://doi.org/10.1002/andp.201600350. eprint: https://onlinelibrary.wiley.com/doi/pdf/10.1002/andp.201600350.

— (2020b). "Absence of slow particle transport in the many-body localized phase". In: *Phys. Rev. B* 102.10, p. 100202. DOI: 10.1103/PhysRevB.102.100202.

Lukin, A., M. Rispoli, R. Schittko, M. E. Tai, A. M. Kaufman, S. Choi, V. Khemani, J. Léonard, and M. Greiner (2019). "Probing entanglement in a many-body-localized system." In: *Science* 364.6437, pp. 256–260. ISSN: 1095-9203. DOI: 10.1126/science.aau0818.

Lüschen, H. P. et al. (2017). "Signatures of many-body localization in a controlled open quantum system". In: *Physical Review X* 7.1, p. 011034. ISSN: 21603308. DOI: 10.1103/PhysRevX.7.011034.

Lye, J. E., L. Fallani, C. Fort, V. Guarrera, M. Modugno, D. S. Wiersma, and M. Inguscio (2007). "Effect of interactions on the localization of a Bose-Einstein condensate in a quasiperiodic lattice". In: *Phys. Rev. A* 75.6, p. 061603. DOI: 10.1103/PhysRevA.75.061603.

M. Schreiber, S. S. Hodgman, P. Bordia, H. P. Lüschen, M. H. Fischer, R. Vosk, E. Altman, U. Schneider, and I. Bloch (2015). "Observation of many-body localization of interacting fermions in a quasirandom optical lattice". In: *Science* 349.6250, pp. 842–845. DOI: 10.1126/science.aaa7432.

Macé, N., F. Alet, and N. Laflorencie (2019). "Multifractal Scalings Across the Many-Body Localization Transition". In: *Phys. Rev. Lett.* 123.18, p. 180601. DOI: 10.1103/PhysRevLett.123.180601.

MacKinnon, A. and B. Kramer (1981). "One-Parameter Scaling of Localization Length and Conductance in Disordered Systems". In: *Phys. Rev. Lett.* 47.21, pp. 1546–1549. DOI: 10.1103/PhysRevLett.47.1546.

Manai, I., J.-F. ç. Clément, R. Chicireanu, C. Hainaut, J. C. Garreau, P. Szriftgiser, and D. Delande (2015). "Experimental Observation of Two-Dimensional Anderson Localization with the Atomic Kicked Rotor". In: *Phys. Rev. Lett.* 115.24, p. 240603. DOI: 10.1103/PhysRevLett.115.240603.

Mandelbrot, B. B. (1974). "Intermittent turbulence in self-similar cascades: divergence of high moments and dimension of the carrier". In: *Journal of Fluid Mechanics* 62.2, pp. 331–358. DOI: 10.1017/S0022112074000711.

Mardaani, M. and A. A. Shokri (2006). "Theoretical approach on spin-dependent conductance in a magnetic-quantum wire". In: *Chemical Physics* 324.2-3, pp. 541–546. ISSN: 03010104. DOI: 10.1016/j.chemphys.2005.11.041.

Martin, L. et al. (2011). "Anderson localization in optical waveguide arrays with off-diagonal coupling disorder". In: *Opt. Express* 19.14, pp. 13636–13646. DOI: 10.1364/OE.19.013636.

Mathew, S. P., P. C. Mondal, H. Moshe, Y. Mastai, and R. Naaman (2014). "Non-magnetic organic/inorganic spin injector at room temperature". In: *Applied Physics Letters* 105.24, p. 242408. ISSN: 0003-6951. DOI: 10.1063/1.4904941.

Matityahu, S., A. Aharony, O. Entin-Wohlman, and S. Tarucha (2013). "Spin filtering in a Rashba–Dresselhaus–Aharonov–Bohm double-dot interferometer". In: *New Journal of Physics* 15.12, p. 125017. ISSN: 1367-2630. DOI: 10.1088/1367-2630/15/12/125017.

McCoy, B. M. (1969). "Incompleteness of the Critical Exponent Description for Ferromagnetic Systems Containing Random Impurities". In: *Phys. Rev. Lett.* 23.7, pp. 383–386. DOI: 10.1103/PhysRevLett.23.383.

Messiah, A. (2014). *Quantum Mechanics*. Dover Books on Physics. Dover Publications.

Milde, F. (2000). "Disorder-induced metal-insulator transition in anisotropic systems". PhD thesis. TU Chemnitz, p. 105.

Mildenberger, A., F. Evers, and A. D. Mirlin (2002). "Dimensionality dependence of the wave-function statistics at the Anderson transition". In: *Phys. Rev. B* 66.3, p. 033109. DOI: 10.1103/PhysRevB.66.033109.

Modak, R., S. Mukerjee, E. A. Yuzbashyan, and B. S. Shastry (2016). "Integrals of motion for one-dimensional Anderson localized systems". In: *New Journal of Physics* 18.3, p. 033010. DOI: 10.1088/1367-2630/18/3/033010.

Modugno, G. (2010). "Anderson localization in Bose–Einstein condensates". In: *Reports on Progress in Physics* 73.10, p. 102401. DOI: 10.1088/0034-4885/73/10/102401.

Montambaux, G., D. Poilblanc, J. Bellissard, and C. Sire (1993). "Quantum chaos in spin-fermion models". In: *Phys. Rev. Lett.* 70.4, pp. 497–500. DOI: 10.1103/PhysRevLett.70.497.

Moser, J. (1962). "On invariant curves of area-preserving mappings of an annulus". In: *Nachr. Akad. Wiss. Göttingen, II*, pp. 1–20.

Mott, N. F. (1967). "Electrons in disordered structures". In: *Advances in Physics* 16, pp. 49–144. DOI: 10.1080/00018736700101265.

Moudgalya, S., N. Regnault, and B. A. Bernevig (2018). "Entanglement of exact excited states of Affleck-Kennedy-Lieb-Tasaki models: Exact results, many-body scars, and violation of the strong eigenstate thermalization hypothesis". In: *Phys. Rev. B* 98.23, p. 235156. DOI: 10.1103/PhysRevB.98.235156.

Moudgalya, S., N. Regnault, and B. A. Bernevig (2020). "η-pairing in Hubbard models: From spectrum generating algebras to quantum many-body scars". In: *Phys. Rev. B* 102.8, p. 085140. DOI: 10.1103/PhysRevB.102.085140.

Mukherjee, A., A. Chakrabarti, and R. A. Römer (2018). "Flux-driven and geometry-controlled spin filtering for arbitrary spins in aperiodic quantum networks". In: *Physical Review B* 98.7, p. 075415. ISSN: 2469-9950. DOI: 10.1103/PhysRevB.98.075415.

Mukherjee, S. and R. R. Thomson (2015). "Observation of localized flat-band modes in a quasi-one-dimensional photonic rhombic lattice". In: *Optics Letters* 40.23, p. 5443. ISSN: 0146-9592. DOI: 10.1364/OL.40.005443.

Naldesi, P., E. Ercolessi, and T. Roscilde (2016). "Detecting a many-body mobility edge with quantum quenches". In: *SciPost Phys* 1.1, p. 10. ISSN: 2542-4653. DOI: 10.21468/SciPostPhys.1.1.010.

Nandkishore, R. and D. A. Huse (2015). "Many-Body Localization and Thermalization in Quantum Statistical Mechanics". In: *Annual Review of Condensed Matter Physics* 6.1, pp. 15–38. DOI: 10.1146/annurev-conmatphys-031214-014726.

Nandkishore, R. M. and S. L. Sondhi (2017). "Many-Body Localization with Long-Range Interactions". In: *Phys. Rev. X* 7.4, p. 041021. DOI: 10.1103/PhysRevX.7.041021.

Neuenhahn, C. and F. Marquardt (2012). "Thermalization of interacting fermions and delocalization in Fock space". In: *Phys. Rev. E* 85.6, p. 060101. DOI: 10.1103/PhysRevE.85.060101.

Neumann, J. von (1929). "Beweis des Ergodensatzes und desH-Theorems in der neuen Mechanik". In: *Zeitschrift für Physik* 57.1, pp. 30–70. ISSN: 0044-3328. DOI: 10.1007/BF01339852.

Ng, G. S., J. Bodyfelt, and T. Kottos (2006). "Critical Fidelity at the Metal-Insulator Transition". In: *Phys. Rev. Lett.* 97.25, p. 256404. DOI: 10.1103/PhysRevLett.97.256404.

Nielsen, M. A. and I. L. Chuang (2010). *Quantum Computation and Quantum Information: 10th Anniversary Edition*. Cambridge University Press.

Nord, M. et al. (2019). "Strain Anisotropy and Magnetic Domains in Embedded Nanomagnets". In: *Small* 15.52, p. 1904738. DOI: https://doi.org/10.1002/smll.201904738. eprint: https://onlinelibrary.wiley.com/doi/pdf/10.1002/smll.201904738.

O'Brien, T. E., D. A. Abanin, G. Vidal, and Z. Papi ć (2016). "Explicit construction of local conserved operators in disordered many-body systems". In: *Phys. Rev. B* 94.14, p. 144208. DOI: 10.1103/PhysRevB.94.144208.

Oganesyan, V. and D. A. Huse (2007). "Localization of interacting fermions at high temperature". In: *Physical Review B* 75.15. ISSN: 10980121. DOI: 10.1103/PhysRevB.75.155111.

Ono, Y., T. Ohtsuki, and B. Kramer (1989). "Inverse Participation Number and Fractal Dimensionality of Electronic States in a Two Dimensional System in Strong Per-

pendicular Magnetic Field". In: *Journal of the Physical Society of Japan* 58.5, pp. 1705–1716. DOI: 10.1143/JPSJ.58.1705.

Ott, H., E. de Mirandes, F. Ferlaino, G. Roati, G. Modugno, and M. Inguscio (2004). "Collisionally Induced Transport in Periodic Potentials". In: *Phys. Rev. Lett.* 92.16, p. 160601. DOI: 10.1103/PhysRevLett.92.160601.

Pagano, G. et al. (2014). "A one-dimensional liquid of fermions with tunable spin". In: *Nature Physics* 10.3, pp. 198–201. ISSN: 17452473. DOI: 10.1038/nphys2878.

Page, D. N. (1993). "Average entropy of a subsystem". In: *Phys. Rev. Lett.* 71.9, pp. 1291–1294. DOI: 10.1103/PhysRevLett.71.1291.

Pal, A. and D. A. Huse (2010). "Many-body localization phase transition". In: *Physical Review B* 82.17. ISSN: 10980121. DOI: 10.1103/PhysRevB.82.174411.

Pal, B. and P. Dutta (2016a). "Spin filtering and switching action in a diamond network with magnetic-nonmagnetic atomic distribution". In: *Scientific Reports* 6.1, p. 32543. ISSN: 2045-2322. DOI: 10.1038/srep32543.

Pal, B., R. A. Römer, and A. Chakrabarti (2016b). "Spin filter for arbitrary spins by substrate engineering". In: *Journal of Physics: Condensed Matter* 28.33, p. 335301. ISSN: 0953-8984. DOI: 10.1088/0953-8984/28/33/335301.

Parameswaran, S. A. and R. Vasseur (2018). "Many-body localization, symmetry and topology". In: *Reports on Progress in Physics* 81.8, p. 082501. DOI: 10.1088/1361-6633/aac9ed.

Pareek, T. P. and P. Bruno (2002). "Spin and charge transport in the presence of spin-orbit interaction". In: *Pramana* 58.2, pp. 293–311. ISSN: 0304-4289. DOI: 10.1007/s12043-002-0015-z.

Parshin, D. A. and H. R. Schober (1999). "Distribution of Fractal Dimensions at the Anderson Transition". In: *Phys. Rev. Lett.* 83.22, pp. 4590–4593. DOI: 10.1103/PhysRevLett.83.4590.

Pekker, D., B. K. Clark, V. Oganesyan, and G. Refael (2017a). "Fixed Points of Wegner-Wilson Flows and Many-Body Localization". In: *Phys. Rev. Lett.* 119.7, p. 075701. DOI: 10.1103/PhysRevLett.119.075701.

— (2017b). "Fixed Points of Wegner-Wilson Flows and Many-Body Localization". In: *Phys. Rev. Lett.* 119.7, p. 075701. DOI: 10.1103/PhysRevLett.119.075701.

Peres, A. (1984). "Stability of quantum motion in chaotic and regular systems". In: *Physical Review A* 30.4, pp. 1610–1615. ISSN: 10502947. DOI: 10.1103/PhysRevA.30.1610.

Pichard, J.-L. (1984). "Contribution à une théorie quantique des phénomènes de transport par études numériques de systèmes désordonnés: localisation d'Anderson". PhD thesis. Orsay.

Pietracaprina, F. and N. Laflorencie (2021). "Hilbert-space fragmentation, multifractality, and many-body localization". In: *Annals of Physics*, p. 168502. ISSN: 0003-4916. DOI: https://doi.org/10.1016/j.aop.2021.168502.

Poilblanc, D., T. Ziman, J. Bellissard, F. Mila, and G. Montambaux (1993). "Poisson vs. GOE Statistics in Integrable and Non-Integrable Quantum Hamiltonians". In: *Europhysics Letters (EPL)* 22.7, pp. 537–542. DOI: 10.1209/0295-5075/22/7/010.

Potter, A. C., R. Vasseur, and S. A. Parameswaran (2015). "Universal Properties of Many-Body Delocalization Transitions". In: *Phys. Rev. X* 5.3, p. 031033. DOI: 10.1103/PhysRevX.5.031033.

Prelovšek, P., M. Mierzejewski, O. Barišić, and J. Herbrych (2017). "Density correlations and transport in models of many-body localization". In: *Annalen der Physik* 529.7, p. 1600362. DOI: https://doi.org/10.1002/andp.201600362. eprint: https://onlinelibrary.wiley.com/doi/pdf/10.1002/andp.201600362.

Prinz, G. A. (1998). "Magnetoelectronics". In: *Science* 282.5394, pp. 1660–1663. ISSN: 00368075. DOI: 10.1126/science.282.5394.1660.

Prosen, T. (2002). "General relation between quantum ergodicity and fidelity of quantum dynamics". In: *Phys. Rev. E* 65.3, p. 036208. DOI: 10.1103/PhysRevE.65.036208.

Prosen, T. and M. Znidaric (2002). "Stability of quantum motion and correlation decay". In: *Journal of Physics A: Mathematical and General* 35.6, pp. 1455–1481. DOI: 10.1088/0305-4470/35/6/309.

Prosen, T., T. H. Seligman, and M. Žnidarič (2003). "Theory of Quantum Loschmidt Echoes". In: *Progress of Theoretical Physics Supplement* 150, pp. 200–228. ISSN: 0375-9687. DOI: 10.1143/PTPS.150.200. eprint: https://academic.oup.com/ptps/article-pdf/doi/10.1143/PTPS.150.200/5243181/150-200.pdf.

Rademaker, L. and M. Ortuño (2016). "Explicit Local Integrals of Motion for the Many-Body Localized State". In: *Phys. Rev. Lett.* 116.1, p. 010404. DOI: 10.1103/PhysRevLett.116.010404.

Rakovszky, T., C. W. von Keyserlingk, and F. Pollmann (2019). "Entanglement growth after inhomogenous quenches". In: *Phys. Rev. B* 100.12, p. 125139. DOI: 10.1103/PhysRevB.100.125139.

Relaño, A., J. Dukelsky, J. M. G. Gómez, and J. Retamosa (2004). "Stringent numerical test of the Poisson distribution for finite quantum integrable Hamiltonians". In: *Phys. Rev. E* 70.2, p. 026208. DOI: 10.1103/PhysRevE.70.026208.

Richardella, A., P. Roushan, S. Mack, B. Zhou, D. A. Huse, D. D. Awschalom, and A. Yazdani (2010). "Visualizing Critical Correlations Near the Metal-Insulator Transition in Ga1-xMnxAs". In: *Science* 327.5966, pp. 665–669. ISSN: 0036-8075. DOI: 10.1126/science.1183640. eprint: https://science.sciencemag.org/content/327/5966/665.full.pdf.

Rigol, M. (2009a). "Breakdown of Thermalization in Finite One-Dimensional Systems". In: *Phys. Rev. Lett.* 103.10, p. 100403. DOI: 10.1103/PhysRevLett.103.100403.

— (2009b). "Quantum quenches and thermalization in one-dimensional fermionic systems". In: *Phys. Rev. A* 80.5, p. 053607. DOI: 10.1103/PhysRevA.80.053607.

Rigol, M., V. Dunjko, and M. Olshanii (2008). "Thermalization and its mechanism for generic isolated quantum systems". In: *Nature* 452.7189, pp. 854–858. ISSN: 1476-4687. DOI: 10.1038/nature06838.

Rigol, M., V. Dunjko, V. Yurovsky, and M. Olshanii (2007). "Relaxation in a Completely Integrable Many-Body Quantum System: An Ab Initio Study of the Dynamics of the Highly Excited States of 1D Lattice Hard-Core Bosons". In: *Phys. Rev. Lett.* 98.5, p. 050405. DOI: 10.1103/PhysRevLett.98.050405.

Rigol, M. and L. F. Santos (2010). "Quantum chaos and thermalization in gapped systems". In: *Phys. Rev. A* 82.1, p. 011604. DOI: 10.1103/PhysRevA.82.011604.

Rispoli, M., A. Lukin, R. Schittko, S. Kim, M. E. Tai, J. Léonard, and M. Greiner (2019). "Quantum critical behaviour at the many-body localization transition". In: *Nature* 573.7774, pp. 385–389. ISSN: 1476-4687. DOI: 10.1038/s41586-019-1527-2.

Roati, G., C. D'Errico, L. Fallani, M. Fattori, C. Fort, M. Zaccanti, G. Modugno, M. Modugno, and M. Inguscio (2008). "Anderson localization of a non-interacting Bose–Einstein condensate". In: *Nature* 453.7197, pp. 895–898. ISSN: 1476-4687. DOI: 10.1038/nature07071.

Rodriguez, A., L. J. Vasquez, and R. A. Römer (2009). "Optimisation of multifractal analysis at the 3D Anderson transition using box-size scaling". In: *The European Physical Journal B* 67.1, pp. 77–82. ISSN: 1434-6036. DOI: 10.1140/epjb/e2009-00009-7.

Rodriguez, A., L. J. Vasquez, K. Slevin, and R. A. Römer (2011). "Multifractal finite-size scaling and universality at the Anderson transition". In: *Phys. Rev. B* 84.13, p. 134209. DOI: 10.1103/PhysRevB.84.134209.

Römer, R. A. and H. Schulz-Baldes (2004). "Weak-disorder expansion for localization lengths of quasi-1D systems". In: *Europhysics Letters (EPL)* 68.2, pp. 247–253. ISSN: 0295-5075. DOI: 10.1209/epl/i2004-10190-9. arXiv: 0405125v1 [cond-mat].

Ronzheimer, J. P., M. Schreiber, S. Braun, S. S. Hodgman, S. Langer, I. P. McCulloch, F. Heidrich-Meisner, I. Bloch, and U. Schneider (2013). "Expansion Dynamics of Interacting Bosons in Homogeneous Lattices in One and Two Dimensions". In: *Phys. Rev. Lett.* 110.20, p. 205301. DOI: 10.1103/PhysRevLett.110.205301.

Ros, V., M. Müller, and A. Scardicchio (2015). "Integrals of motion in the many-body localized phase". In: *Nuclear Physics B* 891, pp. 420–465. ISSN: 0550-3213. DOI: https://doi.org/10.1016/j.nuclphysb.2014.12.014.

Roushan, P. et al. (2017). "Spectroscopic signatures of localization with interacting photons in superconducting qubits". In: *Science* 358.6367, pp. 1175–1179. ISSN: 0036-8075. DOI: 10.1126/science.aao1401.

Ruelle, D. (1979). "Ergodic theory of differentiable dynamical systems". In: *Publications Mathématiques de l'Institut des Hautes Études Scientifiques* 50.1, pp. 27–58. ISSN: 1618-1913. DOI: 10.1007/BF02684768.

Sagi, Y., M. Brook, I. Almog, and N. Davidson (2012). "Observation of Anomalous Diffusion and Fractional Self-Similarity in One Dimension". In: *Phys. Rev. Lett.* 108.9, p. 093002. DOI: 10.1103/PhysRevLett.108.093002.

Sahoo, S., T. Kontos, C. Schönenberger, and C. Sürgers (2005). "Electrical spin injection in multiwall carbon nanotubes with transparent ferromagnetic contacts". In: *Applied Physics Letters* 86.11, p. 112109. ISSN: 0003-6951. DOI: 10.1063/1.1882761.

Santos, L. F. and M. Rigol (2010). "Localization and the effects of symmetries in the thermalization properties of one-dimensional quantum systems". In: *Phys. Rev. E* 82.3, p. 031130. DOI: 10.1103/PhysRevE.82.031130.

Scardicchio, A. and T. Thiery (2017). *Perturbation theory approaches to Anderson and Many-Body Localization: some lecture notes*. arXiv: 1710.01234 [cond-mat.dis-nn].

Schneider, U. et al. (2012). "Fermionic transport and out-of-equilibrium dynamics in a homogeneous Hubbard model with ultracold atoms". In: *Nature Physics* 8.3, pp. 213–218. ISSN: 1745-2481. DOI: 10.1038/nphys2205.

Schreiber, M. (1985). "Fractal character of eigenstates in weakly disordered three dimensional systems". In: *Phys. Rev. B* 31.9, pp. 6146–6149. DOI: 10.1103/PhysRevB.31.6146.

Schreiber, M. and H. Grussbach (1991). "Multifractal wave functions at the Anderson transition". In: *Phys. Rev. Lett.* 67.5, pp. 607–610. DOI: 10.1103/PhysRevLett.67.607.

Schulz, M., S. R. Taylor, A. Scardicchio, and M. Žnidarič (2020). "Phenomenology of anomalous transport in disordered one-dimensional systems". In: *Journal of Statistical Mechanics: Theory and Experiment* 2020.2, p. 023107. DOI: 10.1088/1742-5468/ab6de0.

Schulz, M., S. R. Taylor, C. A. Hooley, and A. Scardicchio (2018). "Energy transport in a disordered spin chain with broken U(1) symmetry: Diffusion, subdiffusion, and many-body localization". In: *Phys. Rev. B* 98.18, p. 180201. DOI: 10.1103/PhysRevB.98.180201.

Schuster, C., R. A. Römer, and M. Schreiber (2002). "Interacting particles at a metal-insulator transition". In: *Phys. Rev. B* 65.11, p. 115114. DOI: 10.1103/PhysRevB.65.115114.

Schwartz, T., G. Bartal, S. Fishman, and M. Segev (2007). "Transport and Anderson localization in disordered two-dimensional photonic lattices". In: *Nature* 446.7131, pp. 52–55. ISSN: 1476-4687. DOI: 10.1038/nature05623.

Scully, M. O. and M. Zubairy (1997). *Quantum Optics*. Cambridge University Press.

Serbyn, M. and J. E. Moore (2016). "Spectral statistics across the many-body localization transition". In: *Phys. Rev. B* 93.4, p. 041424. DOI: 10.1103/PhysRevB.93.041424.

Serbyn, M., Z. Papic, and D. A. Abanin (2015). "Criterion for Many-Body Localization-Delocalization Phase Transition". In: *Phys. Rev. X* 5.4, p. 041047. DOI: 10.1103/PhysRevX.5.041047.

— (2017). "Thouless energy and multifractality across the many-body localization transition". In: *Phys. Rev. B* 96.10, p. 104201. DOI: 10.1103/PhysRevB.96.104201.

Serbyn, M., Z. Papič, and D. A. Abanin (2014). "Quantum quenches in the many-body localized phase". In: *Phys. Rev. B* 90.17, p. 174302. DOI: 10.1103/PhysRevB.90.174302.

Serbyn, M., Z. Papić, and D. A. Abanin (2013a). "Universal slow growth of entanglement in interacting strongly disordered systems". In: *Physical Review Letters* 110.26, pp. 1–5. ISSN: 00319007. DOI: 10.1103/PhysRevLett.110.260601.

Serbyn, M., Z. Papič, and D. A. Abanin (2013b). "Local Conservation Laws and the Structure of the Many-Body Localized States". In: *Phys. Rev. Lett.* 111.12, p. 127201. DOI: 10.1103/PhysRevLett.111.127201.

Serrate, D., P. Ferriani, Y. Yoshida, S.-W. Hla, M. Menzel, K. von Bergmann, S. Heinze, A. Kubetzka, and R. Wiesendanger (2010). "Imaging and manipulating the spin direction of individual atoms". In: *Nature Nanotechnology* 5.5, pp. 350–353. ISSN: 1748-3395. DOI: 10.1038/nnano.2010.64.

Sharp, K. and F. Matschinsky (2015). "Translation of Ludwig Boltzmann's Paper "On the Relationship between the Second Fundamental Theorem of the Mechanical Theory of Heat and Probability Calculations Regarding the Conditions for Thermal Equilibrium" Sitzungberichte der Kaiserlichen Akademie der Wissenschaften. Mathematisch-Naturwissen Classe. Abt. II, LXXVI 1877, pp 373-435 (Wien. Ber. 1877, 76:373-435). Reprinted in Wiss. Abhandlungen, Vol. II, reprint 42, p. 164-223, Barth, Leipzig, 1909". In: *Entropy* 17.4, pp. 1971–2009. ISSN: 1099-4300. DOI: 10.3390/e17041971.

Shokri, A. A. and M. Mardaani (2006). "Spin-flip effect on electrical transport in magnetic quantum wire systems". In: *Solid State Communications* 137.1-2, pp. 53–58. ISSN: 00381098. DOI: 10.1016/j.ssc.2005.10.011.

Shokri, A. A., M. Mardaani, and K. Esfarjani (2005). "Spin filtering and spin diode devices in quantum wire systems". In: *Physica E: Low-dimensional Systems and Nanostructures* 27.3, pp. 325–331. ISSN: 13869477. DOI: 10.1016/j.physe.2004.12.008.

Sierant, P., D. Delande, and J. Zakrzewski (2017a). "Many-body localization due to random interactions". In: *Phys. Rev. A* 95.2, p. 021601. DOI: 10.1103/PhysRevA.95.021601.

— (2017b). "Many-Body Localization for Randomly Interacting Bosons". In: *Acta Physica Polonica A* 132. DOI: 10.12693/APhysPolA.132.1707.

Sierant, P., M. Lewenstein, and J. Zakrzewski (2020). arXiv: 2005.09534 [cond-mat.dis-nn].

Sil, S., S. K. Maiti, and A. Chakrabarti (2008). "Metal-Insulator Transition in an Aperiodic Ladder Network: An Exact Result". In: *Physical Review Letters* 101.7, p. 076803. ISSN: 0031-9007. DOI: 10.1103/PhysRevLett.101.076803.

Smith, J., A. Lee, P. Richerme, B. Neyenhuis, P. W. Hess, P. Hauke, M. Heyl, D. A. Huse, and C. Monroe (2016). "Many-body localization in a quantum simulator with programmable random disorder". In: *Nature Physics* 12.10, pp. 907–911. ISSN: 17452481. DOI: 10.1038/nphys3783.

Solórzano, A., L. F. Santos, and E. J. Torres-Herrera (2021). *Multifractality and self-averaging at the many-body localization transition*. arXiv: 2102.02824 [cond-mat.dis-nn].

Sperling, T., W. Bührer, C. M. Aegerter, and G. Maret (2013). "Direct determination of the transition to localization of light in three dimensions". In: *Nature Photonics* 7.1, pp. 48–52. ISSN: 1749-4893. DOI: 10.1038/nphoton.2012.313.

Srednicki, M. (1994). "Chaos and quantum thermalization". In: *Phys. Rev. E* 50.2, pp. 888–901. DOI: 10.1103/PhysRevE.50.888.

Stagraczyński, S., L. Chotorlishvili, M. Schüler, M. Mierzejewski, and J. Berakdar (2017). "Many-body localization phase in a spin-driven chiral multiferroic chain". In: *Phys. Rev. B* 96.5, p. 054440. DOI: 10.1103/PhysRevB.96.054440.

Stamper-Kurn, D. M., H.-J. Miesner, A. P. Chikkatur, S. Inouye, J. Stenger, and W. Ketterle (1999). "Quantum Tunneling across Spin Domains in a Bose-Einstein Condensate". In: *Physical Review Letters* 83.4, pp. 661–665. ISSN: 0031-9007. DOI: 10.1103/PhysRevLett.83.661.

Steinigeweg, R., J. Herbrych, and P. Prelov šek (2013). "Eigenstate thermalization within isolated spin-chain systems". In: *Phys. Rev. E* 87.1, p. 012118. DOI: 10.1103/PhysRevE.87.012118.

Steinigeweg, R., A. Khodja, H. Niemeyer, C. Gogolin, and J. Gemmer (2014). "Pushing the Limits of the Eigenstate Thermalization Hypothesis towards Mesoscopic Quantum Systems". In: *Phys. Rev. Lett.* 112.13, p. 130403. DOI: 10.1103/PhysRevLett.112.130403.

Stenger, J., S. Inouye, D. M. Stamper-Kurn, H.-J. Miesner, A. P. Chikkatur, and W. Ketterle (1998). "Spin domains in ground-state Bose–Einstein condensates". In: *Nature* 396.6709, pp. 345–348. ISSN: 0028-0836. DOI: 10.1038/24567.

Stepanov, V. V., G. Müller, and J. Stolze (2008). "Quantum integrability and nonintegrability in the spin-boson model". In: *Phys. Rev. E* 77.6, p. 066202. DOI: 10.1103/PhysRevE.77.066202.

Störzer, M., P. Gross, C. M. Aegerter, and G. Maret (2006). "Observation of the Critical Regime Near Anderson Localization of Light". In: *Phys. Rev. Lett.* 96.6, p. 063904. DOI: 10.1103/PhysRevLett.96.063904.

Stoytchev, M. and A. Z. Genack (1997). "Microwave transmission through a periodic three-dimensional metal-wire network containing random scatterers". In: *Phys. Rev. B* 55.14, R8617–R8621. DOI: 10.1103/PhysRevB.55.R8617.

Strohmaier, N., Y. Takasu, K. Günter, R. Jördens, M. Köhl, H. Moritz, and T. Esslinger (2007). "Interaction-Controlled Transport of an Ultracold Fermi Gas". In: *Phys. Rev. Lett.* 99.22, p. 220601. DOI: 10.1103/PhysRevLett.99.220601.

Sutherland, B. (2004). *Beautiful Models*. World Scientific. DOI: 10.1142/5552. eprint: https://www.worldscientific.com/doi/pdf/10.1142/5552.

Taie, S., Y. Takasu, S. Sugawa, R. Yamazaki, T. Tsujimoto, R. Murakami, and Y. Takahashi (2010). "Realization of a SU(2)×SU(6) system of fermions in a cold atomic gas". In: *Physical Review Letters* 105.19, p. 190401. ISSN: 00319007. DOI: 10.1103/PhysRevLett.105.190401.

Tarquini, E., G. Biroli, and M. Tarzia (2017). "Critical properties of the Anderson localization transition and the high-dimensional limit". In: *Phys. Rev. B* 95.9, p. 094204. DOI: 10.1103/PhysRevB.95.094204.

Thomson, S. J. and M. Schiró (2018). "Time evolution of many-body localized systems with the flow equation approach". In: *Phys. Rev. B* 97.6, p. 060201. DOI: 10.1103/PhysRevB.97.060201.

Thouless, D. J. (1972a). "A relation between the density of states and range of localization for one dimensional random systems". In: *Journal of Physics C: Solid State Physics* 5.1, pp. 77–81. DOI: 10.1088/0022-3719/5/1/010.

— (1972b). "A relation between the density of states and range of localization for one dimensional random systems". In: *Journal of Physics C: Solid State Physics* 5.1, pp. 77–81. ISSN: 0022-3719. DOI: 10.1088/0022-3719/5/1/010.

— (1974). "Electrons in disordered systems and the theory of localization". In: *Physics Reports* 13.3, pp. 93–142. ISSN: 0370-1573. DOI: https://doi.org/10.1016/0370-1573(74)90029-5.

Thouless, D. J. and Q. Niu (1983). "Wavefunction scaling in a quasi-periodic potential". In: *Journal of Physics A: Mathematical and General* 16.9, pp. 1911–1919. DOI: 10.1088/0305-4470/16/9/015.

Torres-Herrera, E. J. and L. F. Santos (2013). "Effects of the interplay between initial state and Hamiltonian on the thermalization of isolated quantum many-body systems". In: *Phys. Rev. E* 88.4, p. 042121. DOI: 10.1103/PhysRevE.88.042121.

— (2015). "Dynamics at the many-body localization transition". In: *Phys. Rev. B* 92.1, p. 014208. DOI: 10.1103/PhysRevB.92.014208.

— (2017). "Extended nonergodic states in disordered many-body quantum systems". In: *Annalen der Physik* 529.7, p. 1600284. DOI: https://doi.org/10.1002/andp.201600284. eprint: https://onlinelibrary.wiley.com/doi/pdf/10.1002/andp.201600284.

Torres-Herrera, E. J., G. De Tomasi, M. Schiulaz, F. Pérez-Bernal, and L. F. Santos (2020). "Self-averaging in many-body quantum systems out of equilibrium: Approach to the localized phase". In: *Phys. Rev. B* 102.9, p. 094310. DOI: 10.1103/PhysRevB.102.094310.

Torres-Herrera, E. J., J. A. Mendez-Bermudez, and L. F. Santos (2019). "Level repulsion and dynamics in the finite one-dimensional Anderson model". In: *Phys. Rev. E* 100.2, p. 022142. DOI: 10.1103/PhysRevE.100.022142.

Torres-Herrera, E. J., J. Karp, M. Távora, and L. F. Santos (2016). "Realistic Many-Body Quantum Systems vs. Full Random Matrices: Static and Dynamical Properties". In: *Entropy* 18.10. ISSN: 1099-4300. DOI: 10.3390/e18100359.

Trotzky, S., Y.-A. Chen, A. Flesch, I. P. McCulloch, U. Schollwöck, J. Eisert, and I. Bloch (2012). "Probing the relaxation towards equilibrium in an isolated strongly correlated one-dimensional Bose gas". In: *Nature Physics* 8.4, pp. 325–330. ISSN: 1745-2481. DOI: 10.1038/nphys2232.

Turner, C. J., A. A. Michailidis, D. A. Abanin, M. Serbyn, and Z. Papić (2018a). "Quantum scarred eigenstates in a Rydberg atom chain: Entanglement, breakdown of thermalization, and stability to perturbations". In: *Physical Review B* 94.15, p. 155134. ISSN: 24699969. DOI: 10.1103/PhysRevB.98.155134.

— (2018b). "Weak ergodicity breaking from quantum many-body scars". In: *Nature Physics* 14.7, pp. 745–749. ISSN: 17452481. DOI: 10.1038/s41567-018-0137-5.

V. I. Oseledets (1968). "A multiplicative ergodic theorem: characteristic Ljapunov exponents of dynamical systems". In: *Tr. Mosk. Mat. Obs.* 19, pp. 179–210.

Varela, S., V. Mujica, and E. Medina (2016). "Effective spin-orbit couplings in an analytical tight-binding model of DNA: Spin filtering and chiral spin transport". In: *Physical Review B* 93.15, p. 155436. ISSN: 2469-9950. DOI: 10.1103/PhysRevB.93.155436.

Vatnik, I. D., A. Tikan, G. Onishchukov, D. V. Churkin, and A. A. Sukhorukov (2017). "Anderson localization in synthetic photonic lattices". In: *Scientific Reports* 7.1, p. 4301. ISSN: 2045-2322. DOI: 10.1038/s41598-017-04059-z.

Vázquez, J. C. and D. Jou (2003). "Temperature in non-equilibrium states: a review of open problems and current proposals". In: *Reports on Progress in Physics* 66.11, pp. 1937–2023. DOI: 10.1088/0034-4885/66/11/r03.

Vidmar, L. and M. Rigol (2016). "Generalized Gibbs ensemble in integrable lattice models". In: *Journal of Statistical Mechanics: Theory and Experiment* 2016.6, p. 064007. DOI: 10.1088/1742-5468/2016/06/064007.

Vogtmann, K., A. Weinstein, and V. Arnol'd (1997). *Mathematical Methods of Classical Mechanics*. Graduate Texts in Mathematics. Springer New York.

Vosk, R., D. A. Huse, and E. Altman (2015). "Theory of the Many-Body Localization Transition in One-Dimensional Systems". In: *Phys. Rev. X* 5.3, p. 031032. DOI: 10.1103/PhysRevX.5.031032.

Wang, M. and K. Chang (2008). "Anisotropic spin transport in two-terminal mesoscopic rings: Rashba and Dresselhaus spin-orbit interactions". In: *Physical Review B* 77.12, p. 125330. ISSN: 1098-0121. DOI: 10.1103/PhysRevB.77.125330.

Weaver, R. (1990). "Anderson localization of ultrasound". In: *Wave Motion* 12.2, pp. 129–142. ISSN: 0165-2125. DOI: https://doi.org/10.1016/0165-2125(90)90034-2.

Wegner, F. (1980). "Inverse participation ratio in 2+ϵ dimensions". In: *Zeitschrift für Physik B Condensed Matter* 36.3, pp. 209–214. ISSN: 1431-584X. DOI: 10.1007/BF01325284.

Wegner, F. J. (1976). "Electrons in disordered systems. Scaling near the mobility edge". In: *Zeitschrift für Physik B Condensed Matter* 25.4, pp. 327–337. ISSN: 1431-584X. DOI: 10.1007/BF01315248.

Weiner, F., F. Evers, and S. Bera (2019). "Slow dynamics and strong finite-size effects in many-body localization with random and quasiperiodic potentials". In: *Phys. Rev. B* 100.10, p. 104204. DOI: 10.1103/PhysRevB.100.104204.

Wiersma, D. S., P. Bartolini, A. Lagendijk, and R. Righini (1997). "Localization of light in a disordered medium". In: *Nature* 390.6661, pp. 671–673. ISSN: 1476-4687. DOI: 10.1038/37757.

Wigner, E. P. (1955). "Characteristic Vectors of Bordered Matrices With Infinite Dimensions". In: *The Annals of Mathematics* 62.3, pp. 548–564.

Wigner, E. P. (1958). "On the Distribution of the Roots of Certain Symmetric Matrices". In: *Annals of Mathematics* 67.2, pp. 325–327. ISSN: 0003486X.

Will, S., T. Best, U. Schneider, L. Hackermüller, D.-S. Lühmann, and I. Bloch (2010). "Time-resolved observation of coherent multi-body interactions in quantum phase revivals". In: *Nature* 465.7295, pp. 197–201. ISSN: 1476-4687. DOI: 10.1038/nature09036.

Will, S., D. Iyer, and M. Rigol (2015). "Observation of coherent quench dynamics in a metallic many-body state of fermionic atoms". In: *Nature Communications* 6.1, p. 6009. ISSN: 2041-1723. DOI: 10.1038/ncomms7009.

Wilson, K. G. (1971). "Renormalization Group and Critical Phenomena. II. Phase-Space Cell Analysis of Critical Behavior". In: *Phys. Rev. B* 4.9, pp. 3184–3205. DOI: 10.1103/PhysRevB.4.3184.

Wright, T. M., M. Rigol, M. J. Davis, and K. V. Kheruntsyan (2014). "Nonequilibrium Dynamics of One-Dimensional Hard-Core Anyons Following a Quench: Complete Relaxation of One-Body Observables". In: *Phys. Rev. Lett.* 113.5, p. 050601. DOI: 10.1103/PhysRevLett.113.050601.

Wu, C., J.-p. Hu, and S.-c. Zhang (2003). " Exact SO(5) Symmetry in the Spin- 3/2 Fermionic System ". In: *Physical Review Letters* 91.18, p. 186402. ISSN: 0031-9007. DOI: 10.1103/physrevlett.91.186402.

Xia, L., L. A. Zundel, J. Carrasquilla, A. Reinhard, J. M. Wilson, M. Rigol, and D. S. Weiss (2015). "Quantum distillation and confinement of vacancies in a doublon sea". In: *Nature Physics* 11.4, pp. 316–320. ISSN: 1745-2481. DOI: 10.1038/nphys3244.

Xie, Z., T. Z. Markus, S. R. Cohen, Z. Vager, R. Gutierrez, and R. Naaman (2011). "Spin Specific Electron Conduction through DNA Oligomers". In: *Nano Letters* 11.11, pp. 4652–4655. ISSN: 1530-6984. DOI: 10.1021/nl2021637.

Yang, C., Y. Wang, P. Wang, X. Gao, and S. Chen (2017). "Dynamical signature of localization-delocalization transition in a one-dimensional incommensurate lattice". In: *Physical Review B* 95.18. ISSN: 24699969. DOI: 10.1103/PhysRevB.95.184201.

Yao, N. Y., C. R. Laumann, S. Gopalakrishnan, M. Knap, M. Müller, E. A. Demler, and M. D. Lukin (2014). "Many-Body Localization in Dipolar Systems". In: *Phys. Rev. Lett.* 113.24, p. 243002. DOI: 10.1103/PhysRevLett.113.243002.

Yao, N. Y., C. R. Laumann, and A. Vishwanath (2015). *Many-body localization protected quantum state transfer*. arXiv: 1508.06995 [quant-ph].

Yin, H., S. Chen, X. Gao, and P. Wang (2018). "Zeros of Loschmidt echo in the presence of Anderson localization". In: *Physical Review A* 97.3, p. 033624. ISSN: 2469-9926. DOI: 10.1103/PhysRevA.97.033624.

Ying, T., Y. Gu, X. Chen, X. Wang, S. Jin, L. Zhao, W. Zhang, and X. Chen (2016). "Anderson localization of electrons in single crystals: LixFe7Se8". In: *Science Advances* 2.2. DOI: 10.1126/sciadv.1501283. eprint: https://advances.sciencemag.org/content/2/2/e1501283.full.pdf.

Yip, S. K. and T. L. Ho (1999). "Zero sound modes of dilute Fermi gases with arbitrary spin". In: *Physical Review A - Atomic, Molecular, and Optical Physics* 59.6, pp. 4653–4656. ISSN: 10941622. DOI: 10.1103/PhysRevA.59.4653. arXiv: 9810064v1 [cond-mat].

Yu, H. and J.-Q. Liang (2005). "Spin current and shot noise in single-molecule quantum dots with a phonon mode". In: *Physical Review B* 72.7, p. 075351. ISSN: 1098-0121. DOI: 10.1103/PhysRevB.72.075351.

Yuzbashyan, E. A., B. L. Altshuler, and B. S. Shastry (2002). "The origin of degeneracies and crossings in the 1d Hubbard model". In: *Journal of Physics A: Mathematical and General* 35.34, pp. 7525–7547. DOI: 10.1088/0305-4470/35/34/319.

Zabusky, N. J. and M. D. Kruskal (1965). "Interaction of "Solitons" in a Collisionless Plasma and the Recurrence of Initial States". In: *Phys. Rev. Lett.* 15.6, pp. 240–243. DOI: 10.1103/PhysRevLett.15.240.

Zelevinsky, V., B. Brown, N. Frazier, and M. Horoi (1996). "The nuclear shell model as a testing ground for many-body quantum chaos". In: *Physics Reports* 276.2, pp. 85–176. ISSN: 0370-1573. DOI: https://doi.org/10.1016/S0370-1573(96)00007-5.

Zhang, X., M. Bishof, S. L. Bromley, C. V. Kraus, P. Zoller, A. M. Rey, and J. Ye (2014). "Spectroscopic observation of SU (N) - symmetric interactions in Sr orbital magnetism". In: *Science* 345, p. 1467.

Zhou, F. (2001). "Spin correlation and discrete symmetry in spinor bose-einstein condensates". In: *Physical Review Letters* 87.8, pp. 80401–1. ISSN: 10797114. DOI: 10.1103/PhysRevLett.87.080401.

Znidaric, M. and T. Prosen (2003). "Fidelity and purity decay in weakly coupled composite systems". In: *Journal of Physics A: Mathematical and General* 36.10, pp. 2463–2481. DOI: 10.1088/0305-4470/36/10/307.

Žnidarič, M., T. Prosen, and P. Prelovšek (2008). "Many-body localization in the Heisenberg XXZ magnet in a random field". In: *Physical Review B* 77.6. ISSN: 10980121. DOI: 10.1103/PhysRevB.77.064426.

Žnidarič, M., A. Scardicchio, and V. K. Varma (2016). "Diffusive and Subdiffusive Spin Transport in the Ergodic Phase of a Many-Body Localizable System". In: *Phys. Rev. Lett.* 117.4, p. 040601. DOI: 10.1103/PhysRevLett.117.040601.

Žutić, I., J. Fabian, and S. Das Sarma (2004). "Spintronics: Fundamentals and applications". In: *Reviews of Modern Physics* 76.2, pp. 323–410. ISSN: 0034-6861. DOI: 10.1103/RevModPhys.76.323.